Untersuchungen zur Struktur-Eigenschafts-Beziehung und Reaktivität von *N*-heterozyklischen Chinodimethanen

Inauguraldissertation zur Erlangung des Doktorgrades der naturwissenschaftlichen Fachbereiche im Fachgebiet Organische Chemie der Justus-Liebig-Universität Gießen

vorgelegt von

Jama Ariai

aus Fulda

Betreuer: Prof. Dr. Urs Gellrich

Gießen 2024

Selbstständigkeitserklärung

Hiermit versichere ich, die vorgelegte Thesis selbstständig und ohne unerlaubte fremde Hilfe und nur mit den Hilfen angefertigt zu haben, die ich in der Thesis angegeben habe. Alle Textstellen, die wörtlich oder sinngemäß aus veröffentlichten Schriften entnommen sind, und alle Angaben die auf mündlichen Auskünften beruhen, sind als solche kenntlich gemacht. Bei den von mir durchgeführten und in der Thesis erwähnten Untersuchungen habe ich die Grundsätze guter wissenschaftlicher Praxis, wie sie in der ‚Satzung der Justus-Liebig-Universität zur Sicherung guter wissenschaftlicher Praxis' niedergelegt sind, eingehalten. Entsprechend §22 Abs. 2 der Allgemeinen Bestimmungen für modularisierte Studiengänge dulde ich eine Überprüfung der Thesis mittels Anti-Plagiatssoftware.

Datum	Unterschrift

Erstgutachter: Prof. Dr. Urs Gellrich

Zweitgutachter: Prof. Dr. Peter R. Schreiner, PhD

Inhaltsverzeichnis

1 Abstract

In the course of this work a new class of *N*-heterocyclic olefins (NHOs) was developed. The so-called *N*-heterocyclic quinodimethanes (NHQs) represent phenylene-extended *N*-heterocyclic carbenes (NHCs) with dual reactivity. Using the prototypical representative **1**, it was demonstrated that the aromatization of the C_6H_4-linker as an additional driving force causes NHQs to be more basic than their NHO analogues. Additionally, **1** reacts as a diradical via a dehydrogenative head-to-head dimerization to form a stable bis-quinodimethane **2**, a super-electron donor (SED) with a small singlet–triplet gap.

Moreover, the covalent linker in the NHQ is further polarized upon acceptor-substitution. Using the *ortho*-acceptor-substituted NHQ **3**, the fundamental question is addressed if charge separation occurs in a conjugated organic system or if **3** is a non-aromatic quinodimethane. Extensive investigations of the structural and electronic properties in the solid state, in solution, and in the gas phase suggest that an aromatic zwitterion provides the most accurate description of the electronic structure. As a consequence, **3** reacts as an ambiphile analogous to frustrated Lewis pairs (FLPs) such as **4**, demonstrated by the dehydrogenation of ammonia borane and the addition of phenylacetylene via C−H bond cleavage.

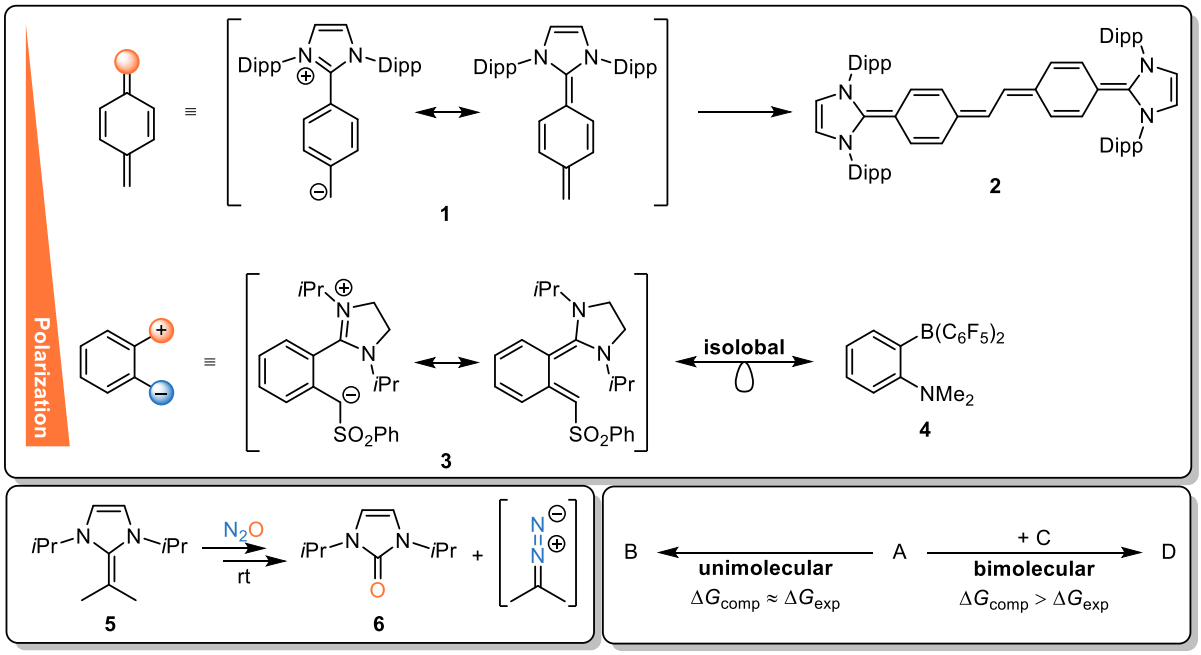

Furthermore, the reaction mechanism of a *gem*-dimethylated NHO **5** with N_2O has been elucidated. Eyring-analysis and quantum mechanical (QM) calculations utilizing density functional theory (DFT) suggest that a sequence of cycloaddition–cycloreversion occurs at room temperature and releases 2-diazopropane and imidazolone **6**.

In a theoretical study, the "entropic penalty" was outlined, i.e., the systematic penalization of associative reactions in solution by classic computations of Gibbs energies due to the overestimation of gas phase entropic contributions despite employing an implicit solvent model. Based on Garza's entropy formalism, an additive correction was developed to counteract the overestimation of Gibbs energies of bimolecular reactions.

2 Zusammenfassung

Im Zuge dieser Arbeit wurde eine neue Verbindungsklasse der *N*-heterozyklischen Olefine (NHOs) entwickelt. Bei den sogenannten *N*-heterozyklischen Chinodimethanen (engl. *N-heterocyclic quinodimethanes*, NHQs) handelt es sich um Phenylen-erweiterte *N*-heterozyklische Carbene (NHCs) mit dualer Reaktivität. Anhand des prototypischen Vertreters **1** wurde gezeigt, dass die Aromatisierung des C_6H_4-Linkers als zusätzliche Triebkraft bewirkt, dass NHQs basischer als ihre NHO-Analoga sind. Außerdem reagiert **1** als Diradikal über eine dehydrogenative Kopf–Kopf-Dimerisierung zu einem stabilen Bis-Chinodimethan **2**, einem Super-Elektronendonor (SED) mit kleiner Singulett–Triplett-Lücke.

Außerdem wird der kovalente Linker des NHQs bei Akzeptor-Substitution weiter polarisiert. Am Beispiel des *ortho*-Akzeptor-substituierten NHQs **3** wird die fundamentale Frage diskutiert, ob Ladungstrennung in einem konjugierten organischen System vorliegt oder ob es sich um ein nicht-aromatisches Chinodimethan handelt. Ausgiebige Untersuchungen der Struktureigenschaften im Festkörper, in Lösung und in der Gasphase legen nahe, dass ein aromatisches Zwitterion die elektronische Struktur am besten beschreibt. Eine Konsequenz ist die ambiphile Reaktivität von **3**, die der von frustrierten Lewis-Paaren (FLPs) wie **4** entspricht, was anhand der Dehydrierung von Amminboran und der Addition von Phenylacetylen unter C–H-Bindungsspaltung gezeigt wurde.

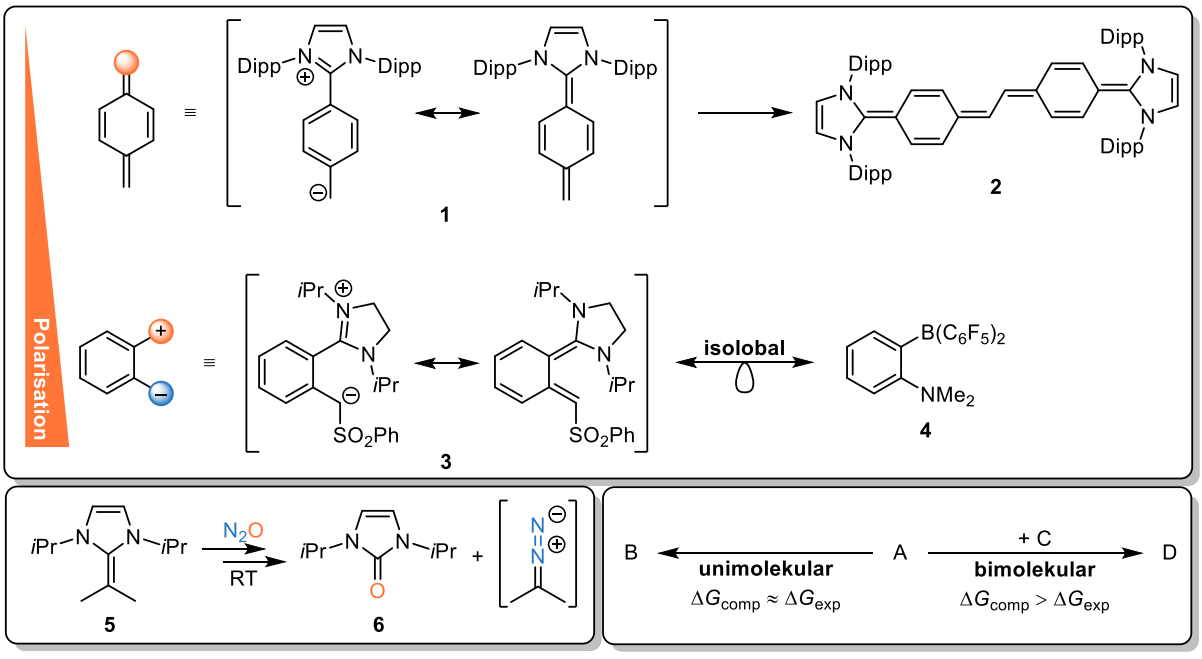

Weiterhin wurde die Reaktion eines *gem*-dimethylierten NHOs **5** mit N_2O mechanistisch aufgeklärt. Wie durch eine Eyring-Analyse und durch quantenmechanische (QM) Berechnungen mittels Dichtefunktionaltheorie (DFT) gezeigt werden konnte, findet bereits bei Raumtemperatur eine Sequenz aus Cycloaddition–Cycloreversion statt und setzt 2-Diazopropan und Imidazolon **6** frei.

In einer theoretischen Arbeit wurde zudem gezeigt, dass auf klassische Weise berechnete Gibbs-Energien für Assoziationsreaktionen in Lösung diese systematisch benachteiligen, weil Beiträge der Gasphasen-Entropie trotz impliziter Lösungsmittelmodelle überschätzt werden („Entropie-Fehler“). Basierend auf Garzas Formalismus zur Berechnung der Entropie wurde ein additiver Korrekturterm entwickelt, der der Überschätzung der Gibbs-Energien bimolekularer Reaktionen entgegenwirkt.

3 Einleitung

Die Entwicklung neuartiger Verbindungsklassen zur Bindungsaktivierung stellt einen fundamentalen Schlüsselschritt in der Katalyseforschung dar. Diese neuen Systeme sind von entscheidender Bedeutung, um komplexe chemische Transformationen energieeffizient und nachhaltig durchzuführen. Lange Zeit galt die Annahme, dass hierzu Übergangsmetalle oder Enzyme zwingend erforderlich seien. Die edlen 4*d*-Übergangsmetalle, die für die Katalyse von besonderer Relevanz sind, sind jedoch selten und oft toxisch.[1] Enzyme, die als hochspezifische Katalysatoren in biologischen Systemen fungieren, zeichnen sich durch ihre strukturelle Komplexität aus, was ihre Anwendung in der chemischen Synthese einschränkt. Mit der Verleihung des Nobelpreises 2021 für die *asymmetrische Organokatalyse* an List und MacMillan wurde der Paradigmenwechsel gewürdigt, dass selbst vermeintlich einfache organische Verbindungen zur Bindungsaktivierung und effizienten Katalyse geeignet sind.[2]

Vor diesem Hintergrund nehmen frustrierte Lewis-Paare (FLPs) und *N*-heterozyklische Olefine (NHOs) eine besondere Rolle ein. Bei FLPs handelt es sich um ein bedeutendes Konzept zur Bindungsaktivierung, bei dem die Synergie komplementärer Reaktivitäten entscheidend ist. Die Reaktivität von NHOs erregte vor allem in jüngster Zeit besondere Aufmerksamkeit. Die im Zuge dieser Promotion behandelten Projekte beschäftigen sich mit den Untersuchungen zur Struktur-Eigenschafts-Beziehung verschiedener NHOs und der Entwicklung konzeptionell neuartiger NHOs zur Bindungsaktivierung, die von FLPs inspiriert sind. Im ersten Kapitel soll zunächst das Konzept der FLPs vorgestellt werden, worauf im nächsten Kapitel NHOs folgen. Anschließend werden im dritten Kapitel die beiden Themenfelder vereint, und es werden die Grundgedanken hinter dem Konzept eines organischen Zwitterions als kohlenstoffbasiertes FLP dargelegt. Im letzten Kapitel werden kurz die Formalismen zur Bestimmung der Entropie in der Gasphase bzw. in Lösung vorgestellt und die damit verbundenen Herausforderungen bei quantenmechanischen (QM) Untersuchungen zur Bindungsaktivierung diskutiert.

3.1 Frustrierte Lewis-Paare

Vor etwa 100 Jahren führte Gilbert Newton Lewis das Konzept der Lewis-Säuren (engl. *Lewis acids*, LAs) und Lewis-Basen (engl. *Lewis bases*, LBs) ein und erkannte, dass sie in Kombination typischerweise ein sogenanntes Lewis-Addukt bilden. Dabei dient die LA als Elektronenpaarakzeptor und die LB als Elektronenpaardonor.[3]

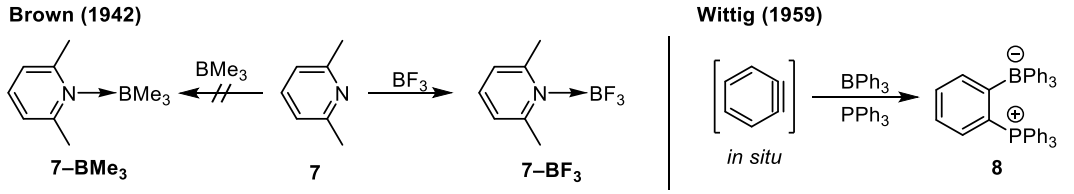

Schema 1: Arbeiten zu sterisch gehinderten Lewis-Säuren/-Basen von Brown (links) und von Wittig beobachtete 1,2-Addition von BPh_3/PPh_3 an 1,2-Didehydrobenzol (rechts). Hier und im Folgenden wird für die Lewis-Struktur klassischer LA–LB-Addukte wie **7**–$\mathbf{BF_3}$ die Notation nach Haaland verwendet.[4]

Als Brown 1942 den Einfluss sterischer Spannung auf die relative Stabilität verschiedener klassischer B/N-Lewis-Addukte untersuchte, stellte er jedoch fest, dass 2,6-Lutidin **7** ein Lewis-Addukt mit BF_3 aber nicht mit BMe_3 bildet (Schema 1).[5] Pyridin hingegen verdrängt die stärkere Base **7** aus seinem

Lewis-Addukt (**7**−**BF**$_3$) und bildet außerdem ein Addukt mit BMe_3. Weiterhin berichtete Wittig, dass BPh_3 und PPh_3 mit *in situ* gebildetem Arin eine Phosphoniumborat-Spezies **8** bilden, aber BPh_3 und PPh_3 selbst nicht miteinander reagieren (Schema 1).[6] Tochtermann beobachtete 1966 die 1,2-Addition des Trityl-Anions (Ph_3C^-) und BPh_3 an 1,3-Butadien anstelle der Bildung eines klassischen Lewis-Addukts und prägte den Begriff „antagonistisches Paar“ (siehe Kapitel 3.1.3).[7] Piers und Parks untersuchten bereits 1996 den „ungewöhnlichen nukleophilen/elektrophilen Mechanismus“ der $B(C_6F_5)$-katalysierte Hydrosilylierung von Ketonen.[8] Diese Beobachtungen ebneten den Weg für das Konzept der frustrierten Lewis-Paare. Im Jahr 2006 berichteten Stephan und Mitarbeiter über die erste reversible, metallfreie Aktivierung von molekularem Wasserstoff unter milden Bedingungen durch das Phosphin–Boran **9** (Schema 2).[9]

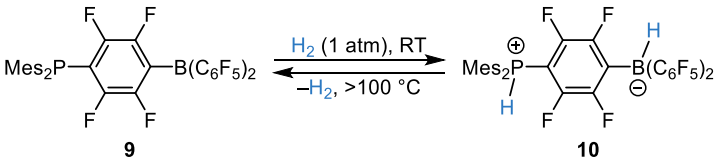

Schema 2: Metallfreie Heterolyse und Freisetzung von molekularem Wasserstoff durch ein Phosphin–Boran (Mes = 2,4,6-Trimethylphenylgruppe).

Schnell folgte die Entwicklung weiterer intra- und auch intermolekularer Kombinationen sterisch gehinderter Lewis-Paare, die H_2 heterolytisch spalten, wie z.B. $B(C_6F_5)_3/PR_3$ (R = *t*Bu und Mes; Mes = 2,4,6-Trimethylphenylgruppe).[10] Der Begriff „frustrierte Lewis-Paare" wurde von Stephan geprägt, um den Umstand zu beschreiben, dass die Reaktivität der einzelnen Komponenten des Lewis-Paars nicht durch eine Addukt-Bildung annuliert wird.[11] Stattdessen bleibt die individuelle LA- und LB-Reaktivität erhalten und aktiviert ein Substrat durch die kooperative Wechselwirkung der komplementären Reaktionszentren (Schema 3).

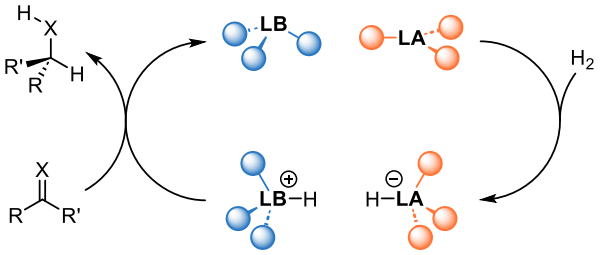

Schema 3: Veranschaulichung des FLP-Konzepts am Beispiel der Bindungsaktivierung von H_2 (typisch: LB = P oder N und LA = B oder Al): Heterolyse von H_2 gefolgt von der Hydrierung ungesättigter Systeme (X = CR_2, NR oder O).

Die reversible Bindungsaktivierung von molekularem Wasserstoff durch FLPs, d.h. die kontrollierte Spaltung/Rekombination der H−H-Bindung bzw. die H_2-Übertragung auf ein anderes Substrat, stellt einen Meilenstein dar, weil diese Reaktivität bis zu diesem Zeitpunkt nur für Übergangsmetallkomplexe bekannt war.[12] Die Wasserstoffspaltung ist herausfordernd, da die σ-Bindung in H_2 die stärkste homoatomare Bindung und im Vergleich zu π-Bindungen (z.B. in CO_2) kaum polarisierbar ist. Vor der Entwicklung der FLP-Chemie waren nur vereinzelte übergangsmetallfreie Systeme zur H_2-Spaltung unter milden Bedingungen befähigt, wobei dies irreversibel erfolgte.[13] Entsprechend waren Berichte über Hydrierungen mit H_2 in Abwesenheit von Übergangsmetallen selten und geprägt von speziellen Substraten und/oder harschen Reaktionsbedingungen.[14] Mit der Entdeckung des speziellen Phosphin–Borans **8** ist ein fundamentales Konzept für die Bindungsaktivierung und metallfreien Katalyse entstanden, das über die bloße H_2-Aktivierung weit hinausgeht. Beispielhaft sei neben der C−H-Aktivierung[15] die Fixierung umweltrelevanter kleiner Moleküle, wie CO_2,[16] N_2O[17] und SO_2,[18] sowie deren chemische

Transformation erwähnt.[19] Von besonderer Bedeutung ist die Verwendung von CO_2 als C1-Ressource durch Reduktion zu Methanol oder weiteren organisch-synthetischen Bausteinen.[20] Außerdem werden FLPs zusammen mit Amminboran (NH_3BH_3) als potentielle Energiespeicher diskutiert.[21] Darüber hinaus eignen sich zahlreiche FLPs als potente (enantioselektive) Hydrierungskatalysatoren.[22]

Für einen umfassenden Überblick wird auf die Vielzahl an Übersichtsartikeln zur FLP-Chemie von Stephan und weiteren Autoren verwiesen.[23] Im weiteren Verlauf dieses Kapitels soll der konzeptionelle Grundgedanke der FLP-Chemie näher beleuchtet werden. Hierzu wird zunächst der Begegnungskomplex (engl. *encounter complex*) diskutiert, gefolgt vom FLP-basierten Mechanismus der Bindungsaktivierung am Beispiel der H_2-Heterolyse. Abschließend werden kohlenstoffbasierte LA- und LB-Komponenten (bezogen auf das reaktive Zentrum) vorgestellt.

3.1.1 Begegnungskomplex

Die Spaltung von H_2 durch die kooperative Interaktion von LA und LB entspricht formal einer Reaktion mit drei Komponenten. Trotz vorhandener Beispiele für termolekulare Reaktionen sind diese äußerst unwahrscheinlich, da hierzu alle Reaktionsteilnehmer gleichzeitig in geeigneter Orientierung zusammenstoßen müssen.[24] Daher wurde von Pápai und Mitarbeitern die initiale Assoziation von LA und LB zu einem Begegnungskomplex [LA]···[LB] postuliert, von dem ausgehend eine bimolekulare Reaktion mit einem geeigneten Substrat erfolgt.[25]

Eine Strategie zur Verbesserung der Präorganisation zu einem reaktiven Konformer ist die Verknüpfung der LA- und LB-Einheit über einen kovalenten Linker. Erkers Ethylen-verbrücktes B/P-FLP **11** gilt als Prototyp für diese sogenannten intramolekularen FLPs; es folgten weitere Beispiele verschiedener Arbeitsgruppen (Schema 4).[26,27]

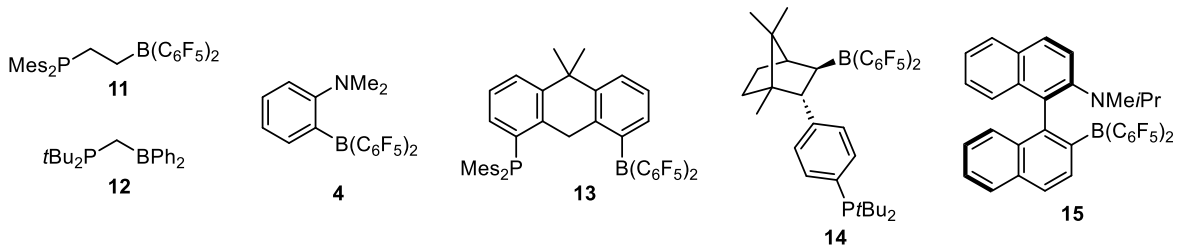

Schema 4: Auswahl repräsentativer intramolekularer FLPs der Arbeitsgruppen von Erker (**11**), Slootweg und Lammertsma (**12**), Repo (**4**), Aldridge (**13**), Klankermayer (**14**) und Pápai und Repo (**15**).

Außerdem sind auch FLPs bekannt, die als klassisches Lewis-Addukt vorliegen, aber deren dissoziierte Form im Gleichgewicht zugänglich ist (z.B. $B(C_6F_5)_3$ mit 2,6-Lutidin, Diethylether oder 1,4-Dioxan).[28] Die Struktur-Reaktivitäts-Beziehung unter Berücksichtigung der intramolekularen Assoziation/Dissoziation wurde von Erker und Mitarbeitern am Beispiel zahlreicher B/P- und B/N-FLPs untersucht.[29]

Im Folgenden wird der Begegnungskomplex intermolekularer FLPs am Beispiel von $B(C_6F_5)_3/PR_3$ diskutiert (R = Mes und *t*Bu). Für Details sei auf Übersichtsartikel verwiesen.[30] Die erste Untersuchung zu $[B(C_6F_5)_3]\cdots[PtBu_3]$ wurde von Pápai und Mitarbeitern präsentiert und durch QM Berechnungen auf SCS-MP2- und B3LYP-Niveau gestützt (Abbildung 1).[25]

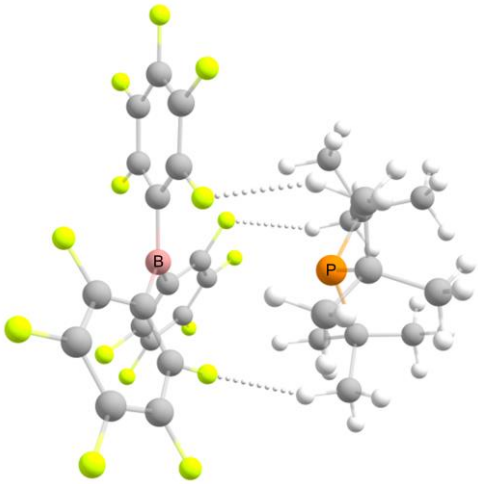

Abbildung 1: Von Pápai und Mitarbeitern berechnete Minimumsstruktur des $[B(C_6F_5)_3]\cdots[PtBu_3]$ Begegnungskomplexes in der Gasphase (SCS-MP2/cc-pVTZ). Ausgewählte Abstände: B−P: 4.16 Å, F−H: 2.39 Å.[25]

Neben der planaren BC_3-Einheit fällt auf, dass der P···B-Abstand von 4.16 Å (SCS-MP2) die Summe der kovalenten Radien von Phosphor und Bor (1.96 Å) übersteigt.[31] Daraus schlussfolgern die Autoren, dass die Assoziation (ΔE = −11.5 kcal mol^{-1}) nicht auf eine dative P→B-Interaktion, sondern auf C−H···F-Interaktionen und London-Dispersion zurückzuführen ist.[25,32] Durch diese langreichweitigen nicht-kovalenten Wechselwirkungen weist der Begegnungskomplex die nötige strukturelle Flexibilität auf, d.h. einen geringen Energieaufwand zur Variation des P···B-Abstandes, um in einer „reaktive Tasche" in geeigneter Orientierung mit einem Substrat zu interagieren. Theoretische Untersuchungen von Vankova und Mitarbeitern zu weiteren B/P-FLPs stützen diese Erkenntnisse und deuten außerdem darauf hin, dass ein P···B-Abstand von 3−5 Å im Begegnungskomplex ideal für die synergistische LA–LB-Interaktion zur H_2-Spaltung ist. Außerdem berechneten die Autoren eine exotherme aber endergone Bildungsenergie der Begegnungskomplexe in Toluol bei Raumtemperatur (5−7 kcal mol^{-1}), was vor allem auf Entropie-Effekte zurückzuführen ist.[33] Mit Hilfe von Molekulardynamik-Simulationen (MD-Simulationen) in Toluol untersuchten Pápai und Mitarbeiter die Konformationen von $B(C_6F_5)_3/PtBu_3$. Daraus folgt, dass die Bildung von $[B(C_6F_5)_3]\cdots[PtBu_3]$ energetisch ungünstig ist (1.2 kcal mol^{-1} über dem Dissoziationslimit) und der Assoziationsgrad 2% für eine beliebige Konformation (P···B-Abstand kleiner 6 Å) bzw. 0.5% für einen reaktiven P···B-Abstand von etwa. 4.5 Å beträgt.[34]

Erste experimentelle Untersuchungen basierend auf temperaturabhängiger NMR-Spektroskopie (^1H, ^{11}B, ^{19}F und ^{31}P Kerne) äquimolarer Toluol-Lösungen der beiden FLPs $(B(C_6F_5)_3/PR_3$, R = Mes und *t*Bu) lieferten zunächst keine Hinweise für eine Phosphin–Boran-Interaktion (NMR: engl. *nuclear magnetic resonance*, Kernspinresonanz).[10] Diese Ergebnisse decken sich mit denen einer umfassenden NMR-spektroskopischen Studie von Rocchigiani und Mitarbeitern.[35] Diese nutzten allerdings zusätzlich $^{19}F,^1H$-HOESY NMR-Experimente für $B(C_6F_5)_3/PMes_3$ (HOESY: engl. *heteronuclear Overhauser enhancement spectroscopy*) und beobachteten Korrelationssignale, was eine räumliche Nähe zwischen Boran und Phosphin impliziert (genauer zwischen $C_6H_2(CH_3)_3$ und C_6F_5). Zeitabhängige NOE-Messungen deuten auf eine zufällige Orientierung von Boran und Phosphin zueinander hin (NOE: engl. *nuclear Overhauser effect*, Kern-Overhauser-Effekt). Die Assoziationskonstante in Benzol-d_6 beträgt K_{298} = 0.5(2) M^{-1}, was einer endergonen Assoziation entspricht ($\Delta G°$(298 K) = 0.4(2) kcal mol^{-1}) und im Einklang mit den vorangegangenen theoretischen Berechnungen ist. Swadźba-Kwaśny und Mitarbeiter untersuchten $[B(C_6F_5)_3]\cdots[PtBu_3]$ in Benzol mittels Neutronenstreuung und ermittelten eine Population von <1% für einen P···B-Abstand von 5.7 Å bzw. 4.9% für einen P···B-Abstand von bis zu 8 Å.[36] Weiterhin stellten die Autoren anhand von

Veränderungen der ^{19}F- und ^{31}P-NMR-Verschiebungen in Bezug auf die individuellen Komponenten des Lewis-Paares fest, dass der Assoziationsgrad in ionischen Flüssigkeiten wie 1-Decyl-3-methylimidazolium Bis(trifluoromethansulfonyl)amid [C_{10}mim][NTf_2] höher als in Benzol ist.

Welch und Stephan beobachteten bereits 2007 die violette Farbe äquimolarer Toluol-Lösungen von $B(C_6F_5)_3$/$PMes_3$ und vermuteten π-π-Wechselwirkungen als Ursache.[10] Zehn Jahre später untersuchten Stephan und Mitarbeiter dieses System erneut und konnten $[PMes]^{\bullet+}$ in Lösung über Elektronenspinresonanz (ESR, engl. *electron paramagnetic resonance*, EPR) nachweisen.[37] Gestützt durch spektroskopische Messungen und QM Berechnungen zeigten Slootweg und Mitarbeiter, dass $[B(C_6F_5)_3]\cdots[PMes_3]$ als Elektronen–Donor–Akzeptor-Komplex (EDA-Komplex) mit einer Absorptionsbande für die Ladungsübertragung (*charge transfer*) bei 534 nm aufgefasst werden kann. Entsprechend führt die Absorption eines Photons zum Einelektronentransfer (engl. *single-electron transfer*, SET) vom Phosphin zum Boran und zur Bildung eines frustrierten Radikalpaars (engl. *frustrated radical pairs*, FRPs) mit einer Lebenszeit von 237 ps.[38]

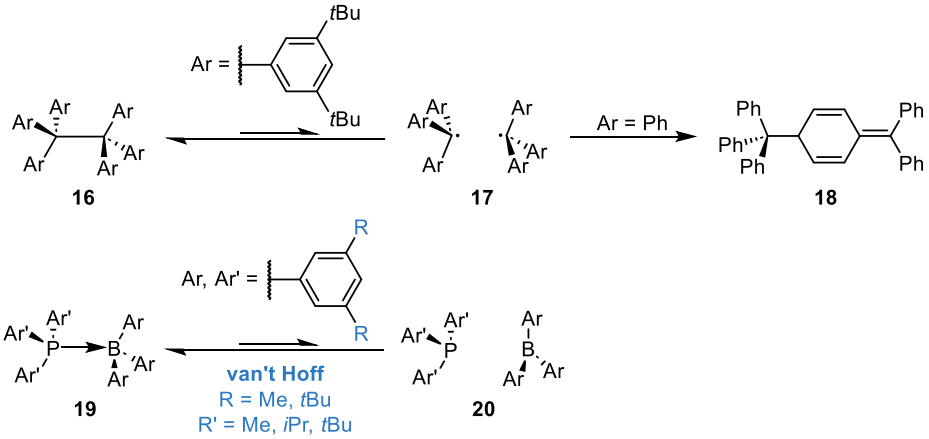

Schema 5: Analogie zwischen Gombergs Hexaphenylethan-System und der Bildung von FLPs.

Insbesondere das FLP bestehend aus $B(C_6F_5)_3$/$PMes_3$ erinnert an Gombergs Hexaphenylethan (HPE).[39] Während unsubstituiertes HPE instabil ist und nach Dissoziation zum Trityl-Radikal **17** schließlich zum chinoiden Addukt **18** (Jacobsen–Nauta-Struktur) rekombiniert,[40] lassen sich HPE-Derivate **16** durch London-Dispersion[41] stabilisieren und damit isolieren (Schema 5). Hierfür ist vor allem die *meta*-Substitution mit DEDs (engl. *dispersion energy donors*) wie *tert*-Butylgruppen von zentraler Bedeutung.[42] FLPs können als eine ionische Variante der DED-stabilisierten Radikalpaare **17** angesehen werden. Kürzlich vereinten Paradies, Hansen und Mitarbeiter die beiden Konzepte und untersuchten isostrukturelle B/P-Lewis-Paare **19** mittels NMR-Spektroskopie und QM Berechnungen (Schema 5).[43] Analog zu **16** beobachteten die Autoren eine reversible Bildung von Lewis-Addukten. Die Assoziation **20**→**19** wird mit zunehmender Größe der DEDs exergoner (−0.2(6) kcal mol^{-1} bis zu −3.6(6) kcal mol^{-1}). Außerdem bewirkt die DED-Substitution in **19** eine kürzere P−B-Bindungslänge verglichen mit unsubstituierten Derivaten.

Kürzlich berichteten Liu und Gabbaï von einem intramolekularen LA/LB-Paar, das es erstmals ermöglichte, sowohl das Lewis-Addukt $\mathbf{21_I}$ als auch den zugehörigen Begegnungskomplex $\mathbf{21_O}$ zu isolieren und kristallographisch zu charakterisieren (Schema 6).[44] Außerdem wurde das analoge Gleichgewicht isostruktureller Acenaphthenyl-verbrückter C/O-Paare, bestehend aus einem Xanthylium- und einem Phosphinoxid-Fragment, mittels Infrarot- (IR-) und ^{13}C-NMR-Spektroskopie analysiert.

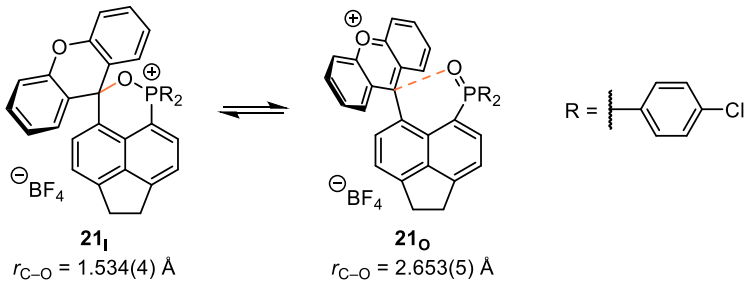

Schema 6: Strukturchemische Analyse eines intramolekularen C/O-Lewis-Paares **21I** und seinem Begegnungskomplex **21O** mittels SCXRD und DFT. Die orange dargestellten C−O-Bindungspfade weisen einen bindungskritischen Punkt auf [**21I** (in a.u.): $\rho(r) = 2.0\cdot10^{-1}$, $\nabla^2\rho(r) = -2.6\cdot10^{-1}$; **21O** (in a.u.): $\rho(r) = 0.2\cdot10^{-1}$, $\nabla^2\rho(r) = +0.8\cdot10^{-1}$; berechnet auf B97M-V/def2-mTZVP Niveau].

3.1.2 Mechanismus der Bindungsaktivierung

Am Beispiel des prototypischen $B(C_6F_5)_3/P\mathit{t}Bu_3$ FLPs soll der Mechanismus der heterolytischen Spaltung von H_2 diskutiert werden (Schema 7).

Das Elektronentransfermodell (ET-Modell) von Pápai basiert auf der gleichzeitigen Orbitalwechselwirkung von LA und LB mit dem Substrat.[25,45,46] Die individuellen $\sigma\rightarrow p_{LA}$- und $n_{LB}\rightarrow\sigma^*$-Interaktionen allein sind nicht ausreichend, um die H−H-Bindung ausreichend zu polarisieren und schlussendlich zu spalten. Jedoch ist ausgehend vom Begegnungskomplex [LA]···[LB] eine konzertierte $n_{LB}\rightarrow\sigma^*$- und $\sigma\rightarrow p_{LA}$-Wechselwirkung möglich. Dieser synergistische Elektronentransfer führt zu einer amphoteren H_2-Spezies und zur Elongation der H−H-Bindung im Übergangszustand. Die Orientierung des Wasserstoffs entspricht hierbei einem Kompromiss aus der seitlichen η^2-H_2−LA-Koordination (*side-on*) und der endständigen η^1-H_2−LB-Koordination (*end-on*).

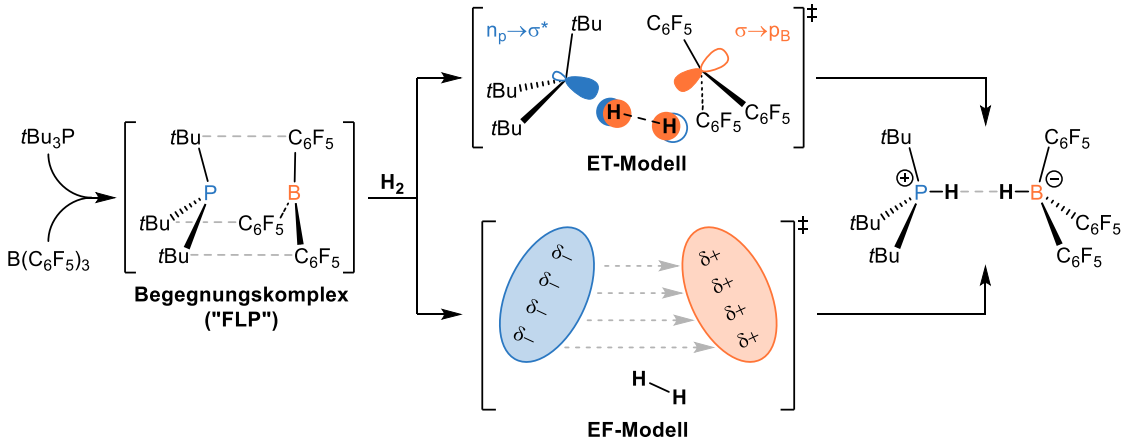

Schema 7: Exemplarischer Mechanismus der H_2-Heterolyse nach Pápais ET-Modell und Grimmes EF-Modell.

Das elektrische Feldmodell (EF-Modell) von Grimme berücksichtigt keine spezifischen Orbitalwechselwirkungen sondern die elektrostatische Wechselwirkung im Begegnungskomplex [LA]···[LB].[47] Demnach erzeugt die Frustration, also das Ausbleiben der LA−LB-Bindung trotz vorhandener intrinsischer Reaktivität, ein elektrisches Feld innerhalb des FLPs. Die Barriere der H_2-Heterolyse wird der Präorganisation des FLPs und dem Eintritt des molekularen Wasserstoffs in die „reaktive Tasche“ zugeschrieben. Gemäß des EF-Modells polarisiert das elektrische Feld im FLP die H−H-Bindung, was zur heterolytischen Spaltung führt, wobei umstritten ist, ob die durch FLPs erzeugten elektrischen Felder ausreichend stark sind.[46]

Die beiden Modelle haben grundlegend gemeinsam, dass sie die Präorganisation von LA und LB zum Begegnungskomplex [LA]···[LB] annehmen. Was den Übergangszustand der H_2-Aktivierung betrifft, lassen sich die beiden Modelle nicht scharf voneinander trennen und können als theoretische Grenzfälle für einen frühen (EF-Modell) bzw. späten (ET-Modell) Übergangszustand entlang der Reaktionskoordinate betrachtet werden.[48]

Die Bindungsaktivierung durch intramolekulare FLPs erfordert im Allgemeinen eine geringere kumulative Stärke der LA und LB als bei intermolekularen FLPs, da die Reaktion des bereits präorganisierten intramolekularen Lewis-Paares mit einem Subtrat entropisch weniger benachteiligt ist.[49] Es ist jedoch zu beachten, dass intramolekulare FLPs abhängig vom Substitutionsmuster auch intermolekular reagieren können.[50] Darüber hinaus wurde die Struktur-Reaktivitäts-Beziehung von FLPs intensiv untersucht, wobei vor allem die Beiträge von Pápai und Mitarbeitern, basierend auf umfangreichen QM Berechnungen,[49] und von Paradies und Mitarbeitern, basierend auf Hammett-Analysen,[51] hervorzuheben sind. Für Details bezüglich radikalische Bindungsaktivierung in FRPs sei auf Übersichtsartikel verwiesen.[52]

3.1.3 Kohlenstoffbasierte FLPs

In diesem Kapitel werden ausgewählte FLPs vorgestellt, die mindestens ein Kohlenstoffatom als reaktives Zentrum aufweisen. Für weitere Beispiele sei auf Übersichtsartikel verwiesen.[53]

Noch bevor das Konzept der FLPs entwickelt wurde, beobachtete Tochtermann, dass das sogenannte „antagonistische Paar“ aus BPh_3 und dem Trityl-Anion **22** mit 1,3-Butadien eine 1,2-Addition unter Bildung von **23** eingeht anstelle der zu erwartenden anionischen Polymerisation bzw. Bildung eines Lewis-Addukts (Schema 8).

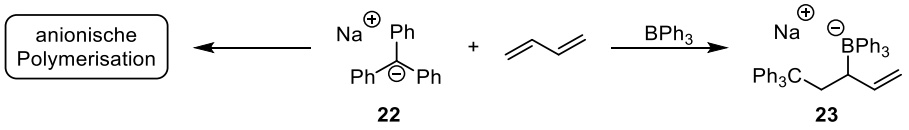

Schema 8: Frühe Arbeiten von Tochtermann zu einem formalen B/C-FLP („antagonistisches Paar“).

Nach Stephans Entdeckung der H_2-Aktivierung durch Kombinationen von $B(C_6F_5)_3$ mit sterisch gehinderten Phosphinen bzw. Aminen folgte die Untersuchung von *N*-heterozyklischen Carbenen (NHCs) als kohlenstoffbasierte LBs, wovon Stephan und Tamm unabhängig voneinander zeitgleich berichteten (Schema 9).[54]

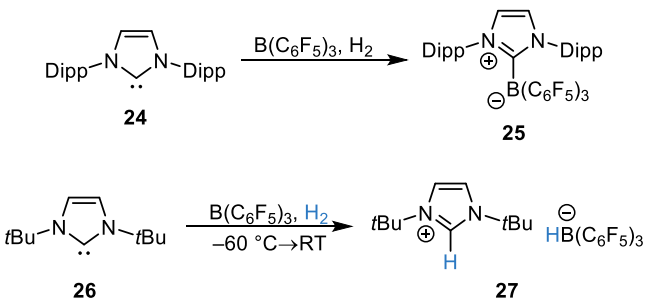

Schema 9: B/C-FLPs aus $B(C_6F_5)_3$ und NHCs zur Spaltung von H_2 (Dipp = 2,6-Diisopropylphenylgruppe).

Eine äquimolare Mischung aus **24** und $B(C_6F_5)_3$ bildet irreversibel das NHC−$B(C_6F_5)_3$-Addukt **25**. Wird der Dipp-Substituent gegen eine *tert*-Butylgruppe ausgetauscht, bildet sich bei Raumtemperatur

nur langsam ein aNHC−B(C_6F_5)$_3$-Addukt (aNHC: abnormales NHC, d.h. Koordination über die C4-Position).[55,56] Bei −60 °C hingegen bildet sich kein Lewis-Addukt und stattdessen spaltet das B(C_6F_5)$_3$/**26** FLP H_2. Das gleiche Produkt (**27**) wird beobachtet, wenn die Reaktion zügig bei Raumtemperatur durchgeführt wird. Das Carbodiphosphoran C(PPh_3)$_2$ bildet bei −78 °C ebenfalls ein FLP mit B(C_6F_5)$_3$, welches H_2 spaltet und mit Si−H- bzw. C(sp)−H-Bindungen reagiert.[57]

Die Kombination elektronenarmer Allene mit geeigneten NHCs stellt ein organisches C/C-FLP dar, das von Alcarazo und Mitarbeitern erstmalig 2010 beschrieben wurde (Schema 10).[58] Anders als mit B(C_6F_5)$_3$ führt hierbei die Kombination aus Allen **28** und NHC **26** zu einem Lewis-Addukt **29**, während **28** und NHC **24** ein FLP bilden, welches aromatische Disulfide heterolytisch spaltet (**30**).

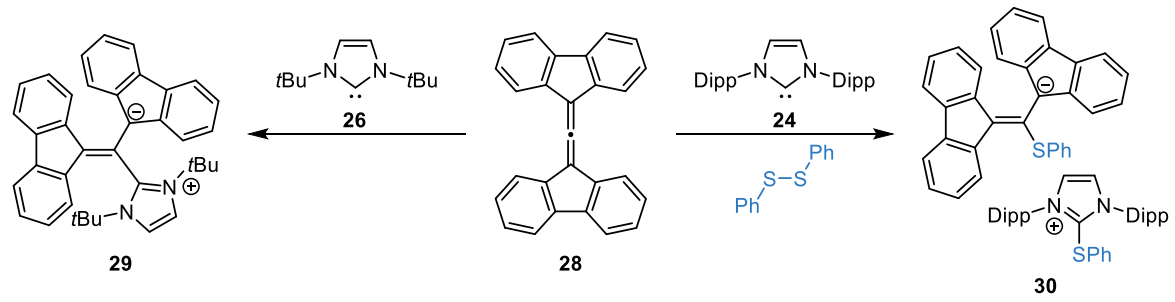

Schema 10: Erstes organisches C/C-FLP zur Spaltung von Disulfiden von Alcarazo und Mitarbeitern (Dipp = 2,6-Diisopropylphenylgruppe).

Ein naheliegender Gedanke, um ein C/C-FLP zu erhalten, ist die Verwendung des Trityl-Kations **31**, welches sich isolobal zu B(C_6F_5)$_3$ verhält. Diesen Ansatz verfolgten Arduengo und Mitarbeiter und berichteten von der irreversiblen H_2-Heterolyse bei −60 °C zu **32** und Ph_3CH (Schema 11).[59]

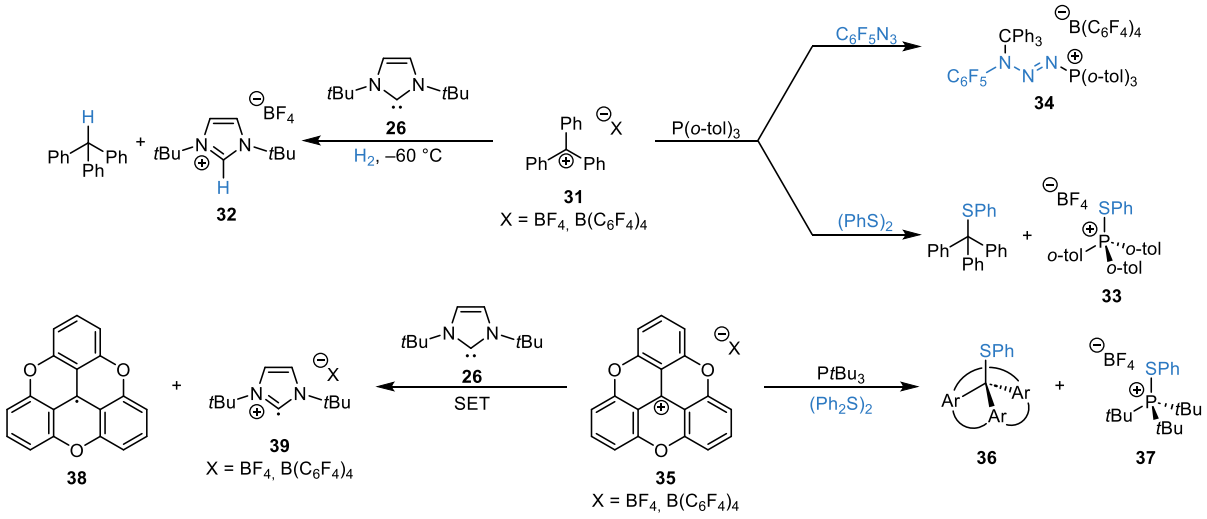

Schema 11: FLP-Reaktivität tritylbasierter LAs mit Phosphinen und NHCs als LBs (*o*-tol = 2-Methylphenylgruppe).

Die Gruppen von Stephan und Berionni untersuchten die Reaktivität des Trityl-Kations **31** mit verschiedenen Phosphinen.[60] Dabei bilden PPh_3, PMe_3, PCy_3 und P*t*Bu$_3$ irreversibel ein Lewis-Addukt (Cy = Cyclohexylgruppe), wobei PCy_3 und P*t*Bu$_3$ an die *para*-Position des Trityl-Kations binden und ein zur Jacobsen–Nauta Struktur **18** analoges chinoides Addukt bilden. Im Fall von P(*o*-tol)$_3$ entsteht ein FLP (*o*-tol: 2-Methylphenylgruppe), welches Diphenyldisulfid $(PhS)_2$ spaltet (**33**+Ph_3CSPh), 1,4-Cyclohexadien dehydriert und Azide fixiert (**34**) (Schema 11). Ähnliche FLP-Reaktivität beobachteten Gianetti und Mitarbeiter, die ein strukturell eingeschränktes Trityl-Derivat

35, das sogenannte *trioxatriangulenium* (TOTA$^+$), verwendeten.[61] Abhängig vom Phosphin beobachteten sie die reversible Bildung von Lewis-Addukten, die verschiedene Disulfide heterolytisch spalten (z.B. zu **36**+**37**). In Kombination mit P*t*Bu$_3$ lässt sich außerdem 1,4-Cyclohexadien dehydrieren und Benzylazid sowie Formaldehyd aus Paraformaldehyd fixieren. Wird das Phosphin durch das NHC **26** ersetzt, so bildet sich ein Radikalpaar (**38**+**39**), das zu einem Addukt equilibriert.

Meyer und Mitarbeiter präsentierten einen biomimetischen Ansatz und modellierten die [Fe]-Hydrogenase, indem sie das Imidazolinium **40** als LA und ein Rutheniummetallat **41** als LB zur Modellierung von Methenyl-H$_4$MPT$^+$ bzw. des FeGP-Cofaktors verwendeten (Schema 12).[62] Stephan und Boone berichteten von einem außergewöhnlichen C/P-FLP **44**. Hierbei fungiert ein kationischer Ru-η^6-Komplex **45** als kohlenstoffbasierte LA in *ortho*- bzw. *para*-Position (Schema 12). Das PCy$_3$-Addukt **44** dissoziiert bei 45 °C und spaltet H$_2$, was zur ersten FLP-katalysierten Hydrierung von Iminen mittels kohlenstoffbasierter LAs führte (102 atm H$_2$).[63]

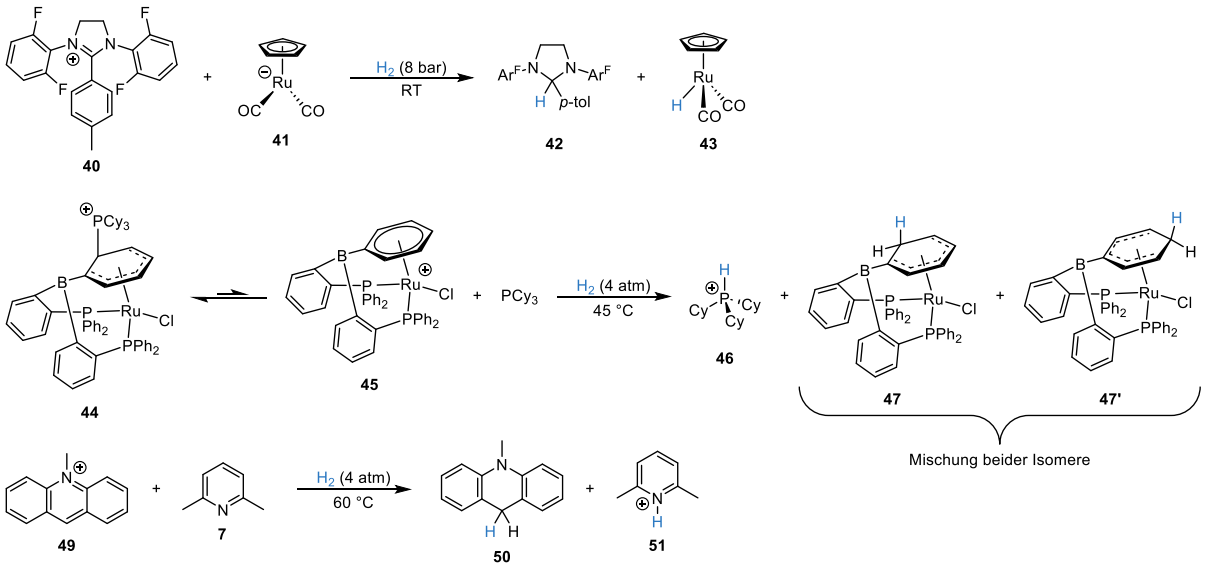

Schema 12: Ausgewählte Beispiele kohlenstoffbasierter LAs in FLPs zur Heterolyse von H$_2$ (*p*-tol = 4-Methylphenylgruppe, Cy = Cyclohexylgruppe). Die Gegenionen sind zur besseren Übersicht ausgelassen (**40**: Br$^-$, **41**: K$^+$, **44**, **45**, **46**: B(C$_6$F$_5$)$_4^-$, **49**, **51**: B(C$_6$H$_3$(*m*-Cl)$_2$)$_4^-$).

Ingleson und Clark verwendeten das *N*-Methylacridinium **49** als LA und beobachteten in Kombination mit 2,6-Lutidin als LB bei 60 °C eine langsame Heterolyse von H$_2$ (4 atm) zu **50**+**51** (Schema 12). Wegen der geringeren Elektrophilie des Acridiniums **49** im Vergleich zu B(C$_6$F$_5$)$_3$ toleriert dieses FLP (**49**/**7**) die Anwesenheit von H$_2$O und ermöglicht die katalytische Transferhydrierung und Hydrosilylierung sterisch ungehinderter Imine.[64]

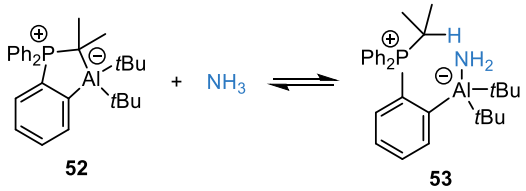

Schema 13: Reversible NH-Aktivierung von Ammoniak durch ein intramolekulares Al/C-FLP bei Raumtemperatur.

Kürzlich berichteten Breher und Mitarbeiter von einem intramolekularen Al/C-FLP **52**, das die erste katalytische N−H Aktivierung von Ammoniak durch eine Hauptgruppenelement-Verbindung ermöglichte (Schema 13).[65] Das FLP liegt als stabiles Al−C-Addukt **52** vor und dessen aktive Spezies, bestehend aus einem Phosphor-Ylid und einer Al-basierten LA, konnte nicht direkt

experimentell beobachtet werden. Bei Umsetzung mit NH_3 (1.1 bar) bildet sich reversibel das Phosphoniumalanat **53**, welches außerdem das Amid (NH_2^-) auf geeignete organische Substrate übertragen kann.

3.2 *N*-Heterozyklische Olefine

N-Heterozyklische Carbene, die ein Kohlenstoffatom mit einem Elektronensextett enthalten, sind etablierte organische σ-Donoren und Lewis-Basen, die weitreichende Anwendungen in den Materialwissenschaften und in der (Organo)Katalyse finden.[56,66] Die Erweiterung von NHCs durch ein Alkylidenfragment führt zu *N*-heterozyklischen Olefinen, die früher als Deoxy-Breslow-Intermediate[67] bzw. als Ketenaminale klassifiziert wurden. Diese Verbindungsklasse zeichnet sich durch eine stark polarisierte C=C-Doppelbindung aus. Die deutliche Akkumulation von Elektronendichte am exozyklischen Kohlenstoff kann durch eine dipolare Resonanzstruktur ausgedrückt werden (Schema 14).

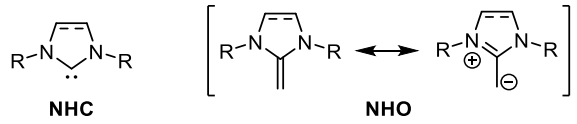

Schema 14: Generische Lewis-Struktur üblicher *N*-heterozyklischer Carbene (NHCs) und *N*-heterozyklischer Olefine (NHOs) basierend auf einem Imidazolin- bzw. Imidazolidin-Grundgerüst.

Imidazolbasierte NHOs, die im Zuge der Addition eines Elektrophils bzw. einer LA am exozyklischen Kohlenstoff aromatisieren, sind besonders reaktiv (Schema 15).[68] Ähnlich zu NHCs gelten NHOs als superbasisch und sind starke σ-Donoren. Die Protonenaffinitäten (PAs), d.h. die berechneten Enthalpien $\Delta_r H_g$ der Dissoziation eines Protons in der Gasphase $[LB{-}H]^+ \rightarrow LB + H^+$, von NHOs übersteigen die von ihren NHC-Analoga.[69] Cheng und Ji verglichen experimentelle pK_S-Werte und Mayrs Nukleophilie-Parameter *N* von NHOs mit denen ihrer NHC-Analoga (Schema 15).[70]

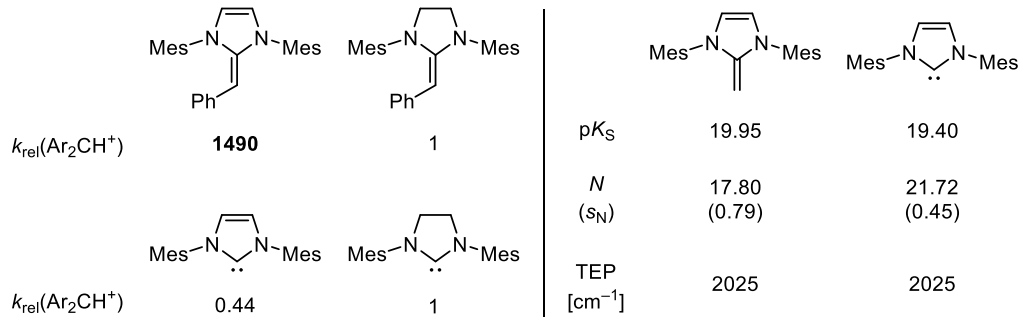

Schema 15: Exemplarischer Vergleich zwischen NHOs und NHCs anhand experimenteller Parameter (Mes = 2,4,6-Trimethylphenylgruppe):[68,70–72] Links: Relative Geschwindigkeitskonstanten der Addition von Benzhydrolium-Kationen an NHOs bzw. *p*-Chinonmethiden an NHCs (THF, 20 °C). Rechts: pK_S-Werte in DMSO, Mayrs Nukleophilie-Parameter *N* bzw. Sensitivitätsparameter s_N in THF und anhand von $[RhCl(CO)_2L]$ (L = NHO oder NHC) bestimmten Tolmans elektronischen Parameter (TEP). Für einen umfassenderen Vergleich sei auf Übersichtsartikel verwiesen.[73]

Ungesättigte NHOs sind basischer als ihre NHC-Analoga, aber das Gegenteil gilt für die gesättigten Derivate. Was die Nukleophilie betrifft, reagieren NHCs schneller als ihre NHO-Analoga mit Michael-Akzeptoren in THF, wobei alle untersuchten NHOs nukleophiler als Ph_3P, 4-(Dimethylamino)pyridin (DMAP) und 1,8-Diazabicyclo[5.4.0]undec-7-en (DBU) sind. Die von Hansmann und Mitarbeitern kürzlich etablierten mesoionischen NHOs (mNHOs) sind noch nukleophiler und diesbezüglich vergleichbar mit Akzeptor-substituierten Carbanionen.[74]

Es sei darauf hingewiesen, dass der Vergleich der Nukleophilie-Parameter zwischen NHOs und NHCs täuschen kann, da sich die Sensitivitätsparameter s_N teilweise deutlich unterscheiden. Das impliziert, dass die relative Nukleophilie stark vom Elektrophil abhängt [$\log k = s_N(N + E)$].[70] Ähnlich trügerisch ist die Korrelation von Basizität und Nukleophilie, wenn aromatisierende und nicht-aromatisierende NHOs miteinander verglichen werden. Ein weniger basisches Derivat muss nicht zwangsläufig langsamer mit einem Elektrophil reagieren, da der Übergangszustand der Addition durch partielle Aromatizität stabilisiert wird, was sich nicht unbedingt in der Basizität widerspiegelt.[70]

Aufgrund ihrer ausgeprägten σ-Donorfähigkeit sind NHOs vielversprechende Liganden, die zahlreich Anwendung in der Hauptgruppenchemie und Übergangsmetallkatalyse finden.[71,75,76] Die Besonderheit hierbei ist, dass NHOs wegen ihrer starken Polarisation endständig über den exozyklischen Kohlenstoff koordinieren (η^1-Koordination), während Olefine für gewöhnlich eine seitliche η^2-Koordination bevorzugen, was in Schema 16 beispielhaft dargestellt ist.[77] Daher können NHOs als latente Carbanionen angesehen werden, die im Zuge der Koordination die formal negative Ladung auf das Metallzentrum übertragen, was mit einer formalen sp^3-Hybridisierung des exozyklischen Kohlenstoffs und positiven Ladungsverteilung im Heterozyklus einhergeht. Außerdem gehen NHOs im Gegensatz zu NHCs keine π-Rückbindung mit dem Metallzentrum ein.

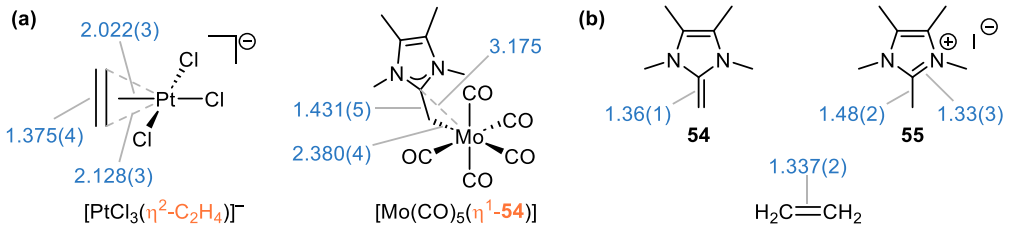

Schema 16: Vergleich experimenteller Strukturparameter zwischen η^2-Olefin-Koordination und η^1-NHO-Koordination am Beispiel von Zeise-Salz $K[PtCl_3(C_2H_4)]$ und einem NHO–Molybdän(0)-Komplex (a).[78,79] Als Referenz dienen Bindungslängen ohne Koordinationspartner (b).[80,81] Alle Bindungslängen (in Å) wurden mittels Röntgen- bzw. Neutronen- und Elektronenbeugung bestimmt.

Die Donorfähigkeit eines Liganden L lässt sich mittels IR-Spektroskopie der Carbonyl-Streckschwingung $\nu_{Rh}(CO)$ des Rhodium-Komplexes $[RhCl(CO)_2L]$ bestimmen, womit dann der sogenannte *Tolman electronic parameter* (TEP) berechnet wird (früher anhand von Ni(0)-Komplexen):[71,82] Je stärker die donierenden Eigenschaften des Liganden L sind, desto ausgeprägter ist die π-Rückbindung des Metalls an den CO-Liganden, was eine Verringerung der Carbonyl-Schwingungsfrequenz und damit des TEPs bewirkt. Daran bemessen sind NHOs typischerweise stärkere Donoren als NHCs. Allerdings zeigen Liganden-Austauschexperimente, dass NHCs die thermodynamisch stabileren Komplexe bilden und NHOs aus diesen verdrängen, was auf das Zwischenspiel aus σ-Donation und π-Rückbindung zurückzuführen ist.[71,72,83]

Im Folgenden wird die Historie von NHOs chronologisch vorgestellt, die zwar seit den 1960er Jahren bekannt sind, aber erst in jüngster Zeit besondere Popularität genießen (Schema 17).[73,84] Abschließend werden Anwendungen in der Bindungsaktivierung und Katalyse mit besonderem Fokus auf die Aktivierung von CO_2 und N_2O diskutiert. Für zusätzliche Informationen zu NHO-katalysierten Polymerisationen, von unter anderem Propylenoxid und Laktonen, sei auf die Arbeiten von Naumann verwiesen.[85] Für Details zur Koordinationschemie sei auf die Arbeiten von Rivard verwiesen.[86]

3.2.1 Historische Entwicklung

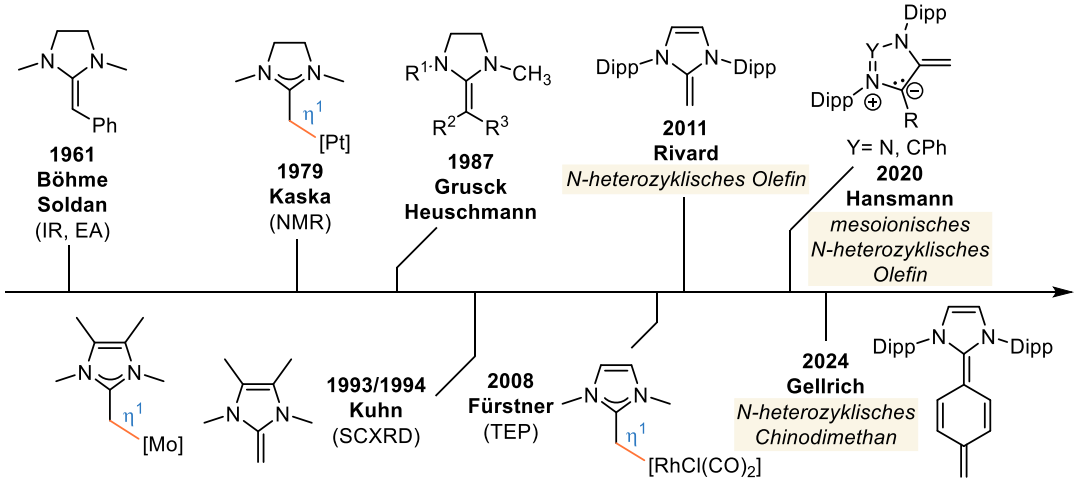

Schema 17: Chronologie ausgewählter Errungenschaften in der Entwicklung des Konzepts von *N*-heterozyklischen Olefinen (Dipp = 2,6-Diisopropylphenylgruppe).

Die erste Synthese eines NHO-Derivats wurde 1961 von Böhme und Soldan berichtet, die 2-Benzyliden-1,3-dimethylimidazolidin isoliert und mittels Elementaranalyse (EA) und IR-Spektroskopie charakterisiert haben.[87] Im Jahr 1979 beobachteten Kaska und Mitarbeiter in NMR-Experimenten die endständige η^1-Koordination eines NHOs an einen von Zeise-Salz $K[PtCl_3(C_2H_4)]$ abgeleiteten dimeren Platin-Komplex.[88] Jahre später untersuchten Gruseck und Heuschmann gezielt diverse 2-Alkylidenimidazolidine.[89] Dabei diskutierten sie die für Olefine ungewöhnlichen chemischen Verschiebungen der Alkylidenfragmente im ^{1}H- und ^{13}C-NMR-Spektrum und setzten ihre NHOs in Diels–Alder-Reaktionen mit inversem Elektronenbedarf ein. Im Jahr 1993 erfolgten umfangreiche Synthesen und spektroskopische Untersuchungen zur Olefin-Polarisation anhand von NHO-Derivaten mit verschiedenen heterozyklischen Grundgerüsten.[90] Im selben Jahr isolierten Kuhn und Mitarbeiter das prototypische 1,3,4,5-Tetramethyl-2-methylidenimidazolin **54** und bestimmten erstmals die Molekülstruktur eines NHOs und seines η^1-koordinierten Komplexes am Beispiel von $[Mo(CO)_5(\eta^1$–**54**$)]$ mittels Einkristall-Röntgenstrukturanalyse (engl. *single-crystal X-ray diffraction*, SCXRD).[79,81] Im Jahr 2008 untersuchten Fürstner und Mitarbeiter systematisch die Koordination von NHOs und zeigten, dass selbst das simple 1,3-Dimethyl-2-methylidenimidazolin ein potenterer σ-Donor als typische NHCs ist.[72] Schließlich synthetisierten Rivard und Mitarbeiter 2011 das populäre Dipp-substituierte NHO **58** ausgehend vom NHC und prägten erstmals den Begriff „*N*-heterozyklisches Olefin“.[76] Kürzlich erweiterten Hansmann und Mitarbeiter das Konzept der NHOs und stellten mesoionische NHOs, wie **56** und **57**, als noch stärkere σ-Donoren bzw. Lewis-Basen vor, die sich nicht mit einer ladungsneutralen Lewis-Struktur darstellen lassen (Schema 18).[83,91] Während sich NHOs aus NHCs ableiten lassen, handelt es sich bei mNHOs um die analoge Erweiterung mesoionischer Carbene (MICs) bzw. aNHCs.

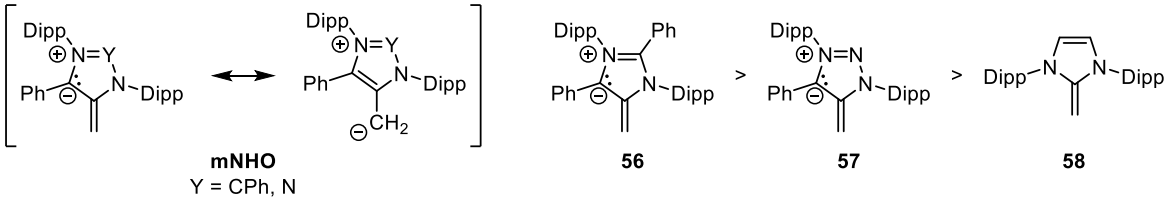

Schema 18: Mesoionische NHOs (mNHOs) sind reaktiver als herkömmliche NHOs in Bezug auf Nukleophilie, Basizität und Donorstärke (Dipp = 2,6-Diisopropylphenylgruppe).

Im Zuge dieser Arbeit wurde eine neuartige Klasse der NHOs entwickelt. Charakteristisch für das sogenannte *N*-heterozyklische Chinodimethan **1** (engl. *N-heterocyclic quinodimethane*, NHQ) ist der C_6H_4-Linker zwischen der NHC-Einheit und der Methylidengruppe (Schema 19). Die Aromatisierung des Linkers liefert eine zusätzliche Triebkraft für die Reaktion mit Elektrophilen. Das NHQ **1** ist aber dadurch nicht nur basischer als übliche NHOs wie **58**, es zeigt außerdem radikalische Reaktivität und equilibriert über eine dehydrogenative Kopf–Kopf-Dimerisierung, die über einen offenschaligen Singulett-Reaktionspfad verläuft, zum Super-Elektronendonor (SED) **2** (siehe Kapitel 5.2).

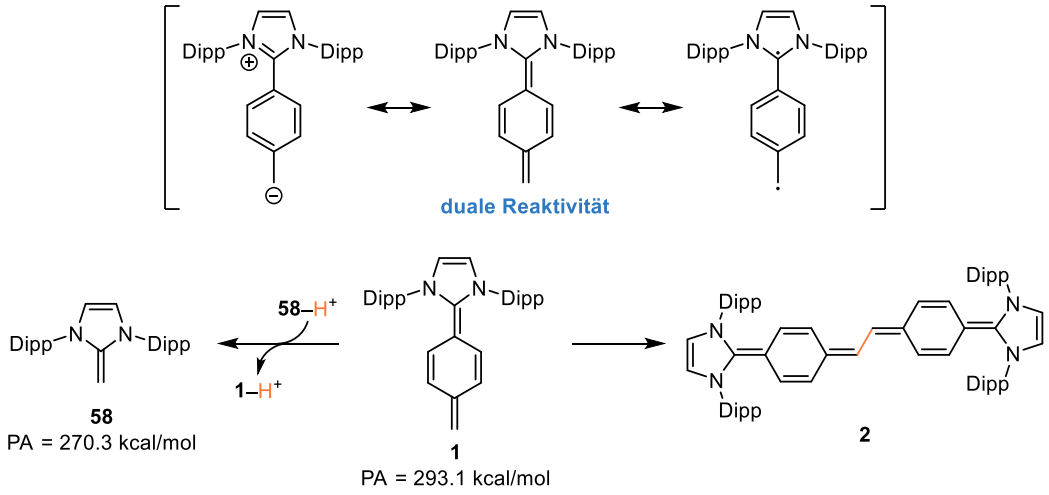

Schema 19: Duale Reaktivität des *N*-heterozyklischen Chinodimethans **1** als starke Base und als Diradikal (Dipp = 2,6-Diisopropylphenylgruppe). Protonenaffinitäten (PAs) wurden auf ωB97X-D4/def2-QZVPP//PBEh-3c Niveau berechnet. Das Iodid-Gegenion von **58**−H^+ und **1**−H^+ ist zur besseren Übersicht ausgelassen.

3.2.2 Anwendung zur Bindungsaktivierung

In diesem Kapitel werden NHOs zur Bindungsaktivierung von CO_2 und N_2O diskutiert. Für weitere Beispiele von NHOs in organokatalytischen Reaktionen sei auf Übersichtsartikel verwiesen.[73]

Lu und Mitarbeiter untersuchten die reversible CO_2-Aktivierung durch verschiedene NHOs (Schema 20a).[92] Temperaturabhängige kinetische Untersuchungen zur CO_2-Freisetzung deuten auf eine höhere Aktivität von NHOs im Vergleich zu NHCs hin, was am Beispiel der NHO-/NHC-katalysierten carboxylativen Zyklisierung von Propargylalkoholen zu Carbonaten bekräftigt wurde (Schema 20b).

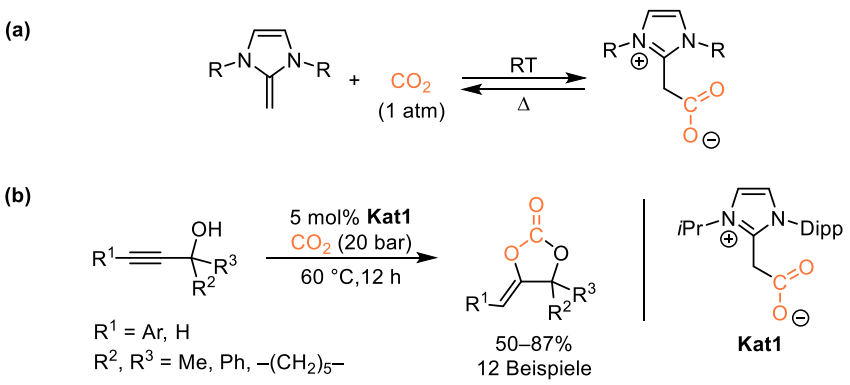

Schema 20: Allgemeine Reaktionsgleichung zur reversiblen CO_2-Aktivierung durch NHOs (a) und NHO-katalysierte carboxylative Zyklisierung von Propargylalkoholen zu Carbonaten (Dipp = 2,6-Diisopropylphenylgruppe) (b).

Theoretische Untersuchungen zur CO_2-Aktivierung verallgemeinerten die höhere Aktivität von NHOs verglichen mit NHCs.[93] Gleichermaßen bindet auch das basischere NHQ **1** unter milden Bedingungen CO_2. Weiterhin katalysieren NHOs die Carboxylierung von Aziridinen und Epoxiden sowie die Formylierung von Aminen unter reduzierenden Bedingungen.[94]

Kürzlich präsentierten Mandal und Mitarbeiter eine mNHO-katalysierte (5 mol%), metallfreie *S*-Formylierung aliphatischer Thiole zu **63** mit CO_2 (1 atm) und Phenylsilan (2 äquiv. $PhSiH_3$) als Reduktionsmittel (Schema 21).[95] Dabei erzielten sie für 48 Beispiele Ausbeuten von 69−92%. Darüber hinaus eignet sich die Reaktion zur Darstellung pharmazeutisch relevanter Isotopologe und zur Synthese von *E*-Vinylsulfiden **64** über eine Eintopf-Wittig-Reaktion.

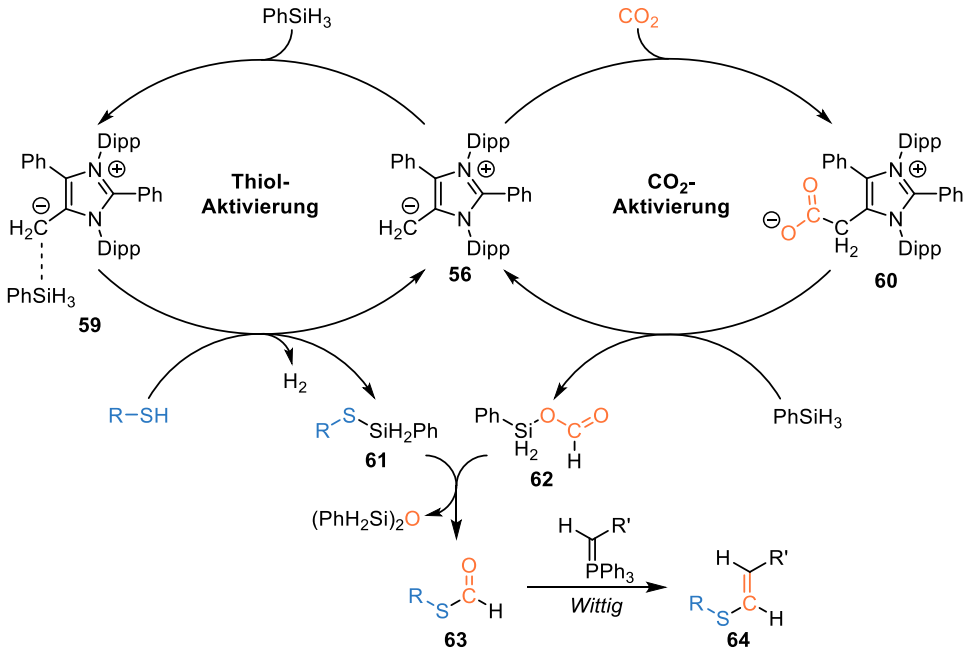

Schema 21: Eine mNHO-katalysierte, metallfreie *S*-Formylierung von Thiolen mit CO_2 und optionaler Eintopf-Wittig-Olefinierung zu *E*-Vinylsulfiden (Dipp = 2,6-Diisopropylphenylgruppe).

Das Entscheidende hierbei ist, dass das mNHO **56** erst CO_2 fixiert (**60**) und dieses dann in die Si−H-Bindung des Phenylsilans insertiert, wodurch **62** entsteht. Gleichzeitig katalysiert **56** die dehydrogenative Kupplung zwischen Thiol und Phenylsilan, wodurch **61** und H_2 entsteht. Eine Limitation der Reaktion sind aromatische Thiole, die geringe Ausbeuten erzielen (30−35%).

Severin und Mitarbeiter zeigten, dass N_2O an NHCs bindet und isolierbare NHC−N_2O-Addukte bildet, die thermisch unter Freisetzung von N_2 zum Harnstoff als Oxidationsprodukt zerfallen.[96] NHOs reagieren ebenfalls mit N_2O unter milden Bedingungen. In Acetonitril bilden sie Azo-verbrückte NHO-Dimere **65a−c**, die als SEDs gelten (Schema 22).[97] Überraschenderweise führt die Reaktion in DMF oder THF zur Bildung von Diazoolefinen **66a−d**.[98] Gleichzeitig berichteten Hansmann und Mitarbeiter ebenfalls von der Isolierung und Charakterisierung des Diazoolefins **69** ausgehend vom imidazolbasierten mNHO **56** und erweiterten den Geltungsbereich der Reaktion in einer darauf folgenden Arbeit für weitere mNHOs wie unter anderem **57** (Schema 22).[99] Die Bildung des Diazoolefins **69** verläuft über eine Sequenz aus Addition von N_2O an das mNHO (**67**), gefolgt von einer Tautomerisierung zu **68**, und der Eliminierung von Wasser. Im Fall von mNHO **56** wurde das azyklische Amid **70** als stöchiometrisches Nebenprodukt detektiert. Diese Limitation lässt sich für **57** in Anwesenheit von 4 Å Molsieb umgehen.

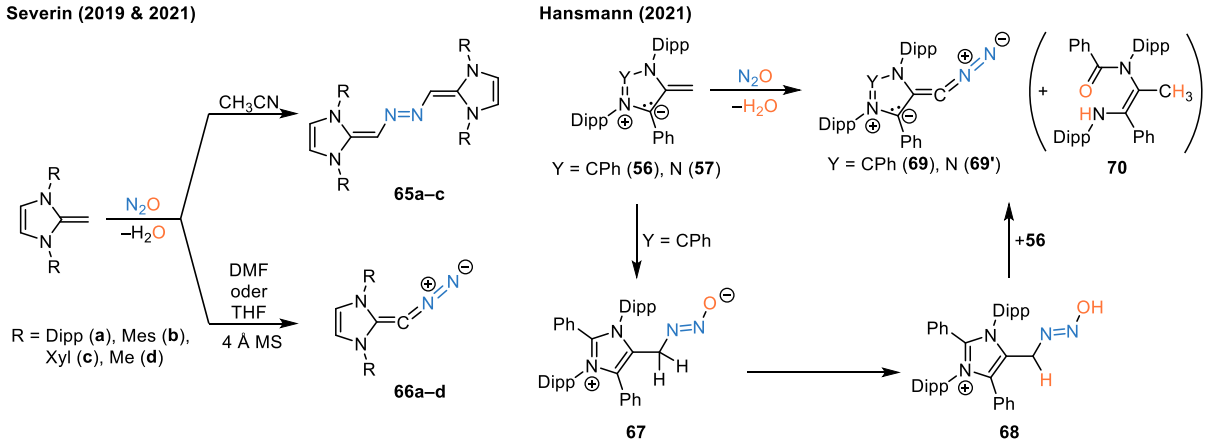

Schema 22: Ausgewählte Reaktionen von NHOs mit N_2O (Dipp = 2,6-Diisopropylphenylgruppe, Mes = 2,4,6-Trimethylphenylgruppe, Xyl = 2,6-Dimethylphenylgruppe, MS = Molsieb).

Damit konnten die beiden Arbeitsgruppen von Hansmann und Severin unabhängig voneinander erstmalig 2021 die Stabilität von Diazoalkenen bei Raumtemperatur nachweisen, welche zuvor nur indirekt oder unter kryogenen Bedingungen nachgewiesen wurden.[100] Dieses Beispiel verdeutlicht, wie die reaktive Methylidengruppe der NHOs neuartige Reaktionspfade eröffnet, die für NHCs unzugänglich sind.

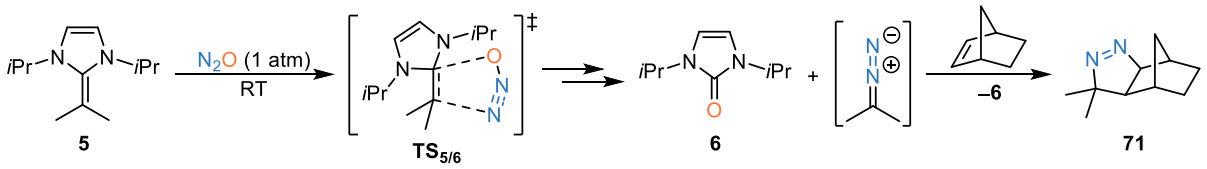

Schema 23: Freisetzung von 2-Diazopropan durch eine Sequenz aus 1,3-dipolarer Cycloaddition und Cycloreversion zwischen dem *gem*-dimethylierten NHO **5** und N_2O.

Im Zuge dieser Arbeit wurde die Reaktion eines *gem*-dimethylierten NHOs **5** mit N_2O untersucht. Durch das Fehlen der reaktiven CH_2-Einheit ist kein Additions–Eliminierungs-Mechanismus zugänglich. Stattdessen findet bereits bei Raumtemperatur eine 1,3-dipolare Cycloaddition mit N_2O statt (Schema 23). Eine anschließende Cycloreversion setzt Imidazolon **6** und 2-Diazopropan frei, welches in einer Folgereaktion mit Norbornen abgefangen wurde (**71**). Eine Eyring-Analyse und QM Berechnungen mittels Dichtefunktionaltheorie (DFT) legen nahe, dass die initiale Cycloaddition zwischen **5** und N_2O geschwindigkeitsbestimmend ist (siehe Kapitel 5.3).

3.3 Konzept eines organischen C/C−Zwitterions

In dieser Arbeit sollte die Reaktivität von NHOs genutzt werden, um ein kohlenstoffbasiertes FLP zu entwickeln. Aus der isolobalen Transformation des B/P-FLPs **11** von Erker folgt ein intramolekulares Carbokation/Carbanion-Paar (Schema 24a).[26,101] Eine Herausforderung hierbei liegt darin, der intrinsischen Reaktivität entgegen zu wirken, das heißt zu vermeiden, dass eine $C(sp^3)$−$C(sp^3)$-σ-Bindung irreversibel geknüpft wird, wie es für organische Verbindungen zu erwarten ist. Um die Neutralisation der reaktiven Zentren zu verhindern, wurde die formale C−C-Bindung durch geeignete Substituenten polarisiert und zusätzlich Ringspannung eingeführt (Ringspannung in Cyclobutan: 26.5 kcal mol^{-1}).[102] Konkret wurde als LB ein α-Sulfonylcarbanion verwendet, da Sulfongruppen im Unterschied zu den meisten gängigen elektronenziehenden Gruppen die negative Ladung in α-Position durch Hyperkonjugation statt durch Resonanz stabilisieren.[103] Als LA wurde eine Imidazol(in)ium-

Einheit verwendet. Es sei erwähnt, dass die positive Formalladung in der Lewis-Schreibweise zwar dem Stickstoff zugeschrieben wird, aber der größte Orbitalkoeffizient des niedrigsten unbesetzten Molekülorbitals (engl. *lowest unoccuppied molecular orbital*, LUMO) am zentralen C2-Kohlenstoff zu finden ist. Die Synthese eines organischen Zwitterions erfolgt über eine Michael-artige 1,4-Addition zwischen einem NHO und α-Phenylvinylsulfon **72**.

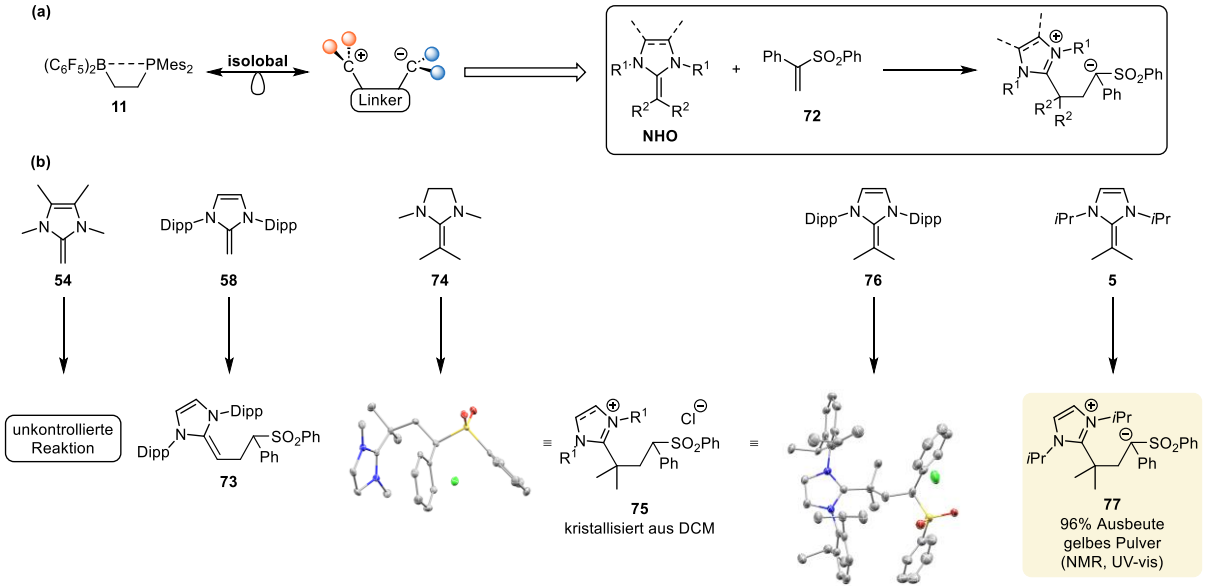

Schema 24: Konzept der isolobalen Transformation des prototypischen B/P-FLPs **11** von Erker zum Design intramolekularer C/C-FLPs über eine 1,4-Addition zwischen einem NHO und α-Phenylvinylsulfon **72** (Mes = 2,4,6-Trimethylphenylgruppe) (a). Diverse eingesetzte NHOs und zugehörige Reaktionsprodukte (Dipp = 2,6-Diisopropylphenylgruppe) (b). Durch SCXRD ermittelte Molekülstrukturen sind mit 50% Wahrscheinlichkeitsellipsoiden dargestellt (Wasserstoffatome sind zur besseren Übersicht ausgelassen). Die hier dargestellten Ergebnisse sind nicht publiziert.

Gängige literaturbekannte NHOs erwiesen sich hierbei als ungeeignet (Schema 24b). Das reaktivste der berücksichtigten NHOs (**54**) reagiert unkontrolliert ab. Das geläufige Dipp-substituierte NHO **58** bildet die gewünschte C–C-Bindung aus, aber tautomerisiert schließlich zu **73**. Im Fall des entsprechenden gesättigten NHCs (SIPr) wurde die Eliminierung von Phenylsulfinat $PhSO_2^-$ nach analog verlaufender Addition und Tautomerisierung beobachtet.[104] Um die Tautomerisierung zu verhindern und die zwitterionische Struktur zu stabilisieren, wurden *gem*-dimethylierte NHOs für die 1,4-Addition verwendet. Hierzu wurde ein literaturbekanntes, gesättigtes NHO **74** berücksichtigt und neuartige reaktivere NHOs **76** und **5** synthetisiert. Das reaktionsträgere NHO **74** führt nicht zum gewünschten C/C-Zwitterion, sondern zum Imidazolinium **75**, dessen Molekülstruktur nach Kristallisation aus DCM über SCXRD bestätigt wurde. Nach Deprotonierung mit KHMDS oder KO*t*Bu wurde die Dissoziation zu den Edukten (**72**+**74**) beobachtet. Ein ähnliches Addukt wurde für das NHO **76** isoliert und kristallisiert. Das NHO **5** bildet nahezu quantitativ das gewünschte Zwitterion **77**, welches als gelbes Pulver isoliert wurde. Versuche **77** zu kristallisieren, wurden jedoch durch die Dissoziation zu **78** in Lösung erschwert (Schema 25). Nichtsdestotrotz wurde **77** mittels ^{1}H- und ^{13}C-NMR-Spekroskopie sowie UV-vis-Spektroskopie charakterisiert. Die Molekülstruktur wurde zusätzlich indirekt nachgewiesen, indem identische ^{1}H- und ^{13}C-NMR-Verschiebungen nach Deprotonierung des HBF_4-Salzes **79**, dessen Molekülstruktur mittels SCXRD bestätigt werden konnte, beobachtet wurden.

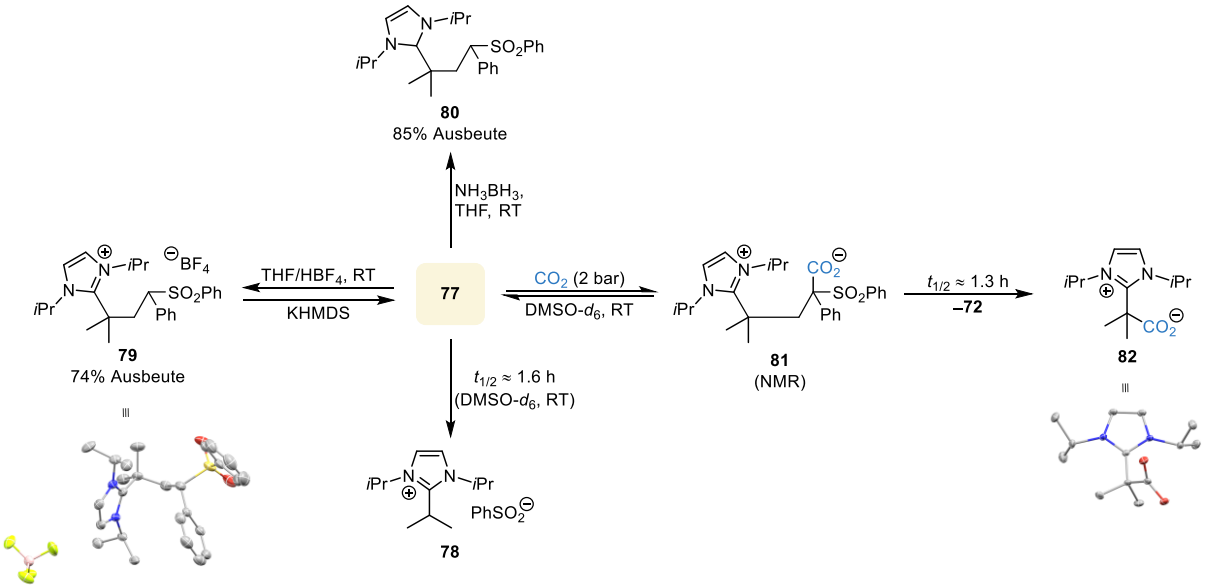

Schema 25: Reaktivität eines Ethylen-verbrückten organischen Zwitterions **77**. Durch SCXRD ermittelte Molekülstrukturen sind mit 50% Wahrscheinlichkeitsellipsoiden dargestellt (Wasserstoffatome sind zur besseren Übersicht ausgelassen). Die hier dargestellten Ergebnisse sind nicht publiziert.

Die Lebenszeit von **77** in Lösung reicht aus, um Amminboran bei Raumtemperatur zu dehydrieren (**80**) und CO_2 zu binden. Allerdings konnte das CO_2-Addukt **81** nur NMR-spektroskopisch untersucht werden, weil es zum NHO−CO_2-Addukt **82** weiter reagiert, was auf eine reversible CO_2-Aktivierung schließen lässt. Aufgrund der mangelnden Stabilität des Systems wurde das zum B/N-FLP **4** von Repo isolobale Zwitterion **3** entwickelt (Schema 26). Im Gegensatz zu **77** ist dieses System kompatibel mit einer reaktiveren Imidazolinium-Einheit als LA.

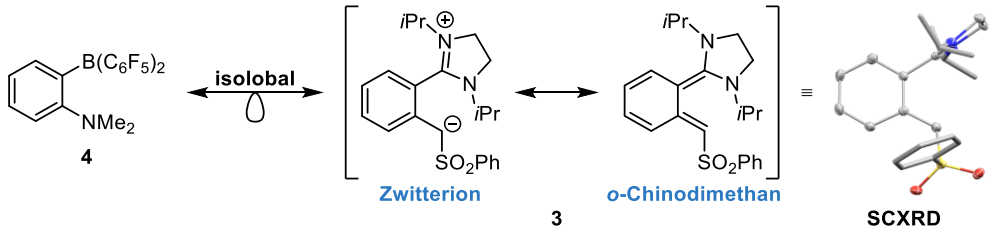

Schema 26: Konzept eines Akzeptor-substituierten NHQs **3** und mittels SCXRD ermittelte Molekülstruktur mit 50% Wahrscheinlichkeitsellipsoiden (zur besseren Übersicht sind *i*Pr- und Ph-Substituenten im Stäbchenmodell dargestellt und Wasserstoffatome weggelassen).

Eine mögliche Konsequenz des C_6H_4-Linkers in **3** ist die Neutralisation der reaktiven Zentren über Resonanzstabilisierung. Eine genauere Betrachtung der mesomeren Grenzformeln wirft zudem die fundamentale Frage auf, welche Lewis-Schreibweise die elektronische Struktur von **3** besser repräsentiert: Ein aromatisches Zwitterion trotz in Konjugation stehender Ladungszentren, was gängigen Regeln zur Formulierung von Lewis-Schreibweisen organischer Verbindungen widerspricht,[105] oder ein neutrales *ortho*-Chinodimethan-Derivat? Im Hinblick auf optoelektronische Anwendungen wurde diese Frage am Beispiel Donor–Akzeptor-substituierter *para*-Chinodimethane diskutiert und die Struktur-Eigenschafts-Beziehung verschiedener Derivate untersucht, die meistens aus 1,3-Benzodithiol-2-yliden als Donor und Dicyanomethylen als Akzeptor zusammengesetzt sind (Schema 27). Abhängig vom π-Linker lassen sich verschiedene elektronische Zustände stabilisieren, was den intramolekularen Ladungstransfer und das Absorptionsverhalten beeinflusst.

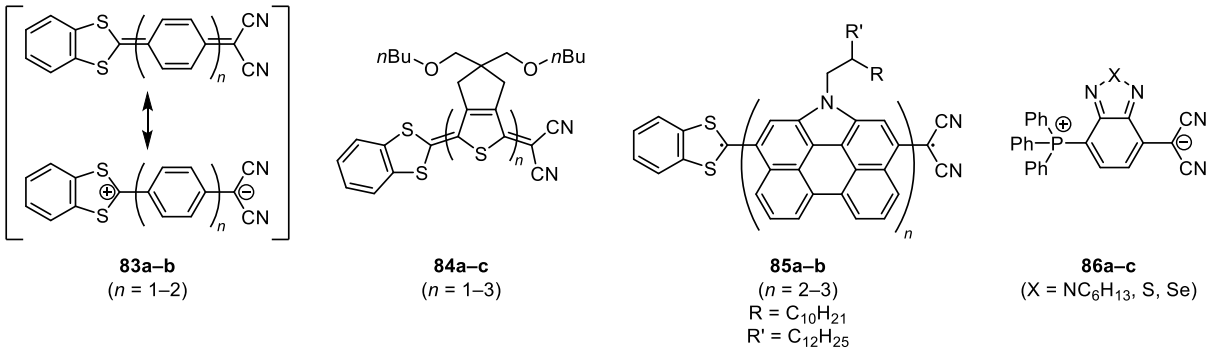

Schema 27: Ausgewählte Beispiele von Donor–Akzeptor-substituierten *para*-Chinodimethanen und Derivaten davon.

Otsubo und Mitarbeiter erweiterten das von Gompper eingeführte Stammsystem **83a**[106] um einen zweiten Phenyl-Linker. Diese zusätzliche Aromatisierung in **83b** stabilisiert anteilig den zwitterionischen Zustand, was IR-spektroskopisch gestützt wurde.[107] Die Thiophen-verbrückten Derivate hingegen liegen als Chinone vor, wobei die Polarisation mit der Anzahl an Linkern zunimmt **84c** > **84b** > **84a**.[108] Anderson und Mitarbeiter untersuchten analoge Porphyrin-verbrückte Systeme und beobachteten einen insignifikanten Beitrag der zwitterionischen Resonanzstruktur.[109] Die Arbeitsgruppen von Wu, Kim, Nakano, Casado und Ding berichteten 2015 erstmalig von stabilen Donor–Akzeptor-substituierten Diradikalen **85a−b** mit einem offenschaligen Singulett-Grundzustand.[110] Kürzlich diskutierten Zhang und Mitarbeiter die aromatische, zwitterionische Struktur und das Absorptionsverhalten von **86a−c** mit einem PPh_3-Donor.[111]

Die im Zuge dieser Arbeit erlangten Ergebnisse, basierend auf SCXRD, ^{1}H-/^{13}C-/^{15}N-NMR- und UV-vis-Spektroskopie, zyklischer Voltammetrie und DFT-Berechnungen, zeigen, dass aufgrund der Donor–Akzeptor-Substitution in **3** die Polarisation des π-Systems so ausgeprägt ist, dass Ladungsseparation entlang des konjugierten *ortho*-Phenyl-Linkers vorliegt. Dementsprechend beschreibt die Lewis-Schreibweise als aromatisches Zwitterion die elektronische Struktur besser als die chinoide Darstellung. DFT-Berechnungen zu Derivaten von **3** legen außerdem nahe, dass elektronische Effekte hauptverantwortlich für die Polarisation sind. Zusätzlich führt der sterische Anspruch der Imidazolinium-Einheit in **3** dazu, dass sich der Heterozyklus aus der Ringebene des C_6H_4-Linkers dreht, was die Konjugation einschränkt und den zwitterionischen Charakter verstärkt. Zudem dehydriert **3** Amminboran unter Bildung von **87** und addiert an Phenylacetylen unter C−H-Bindungsspaltung (**88**), was an die Reaktivität von FLPs erinnert (Schema 28). Daher kann **3** als intramolekulares kohlenstoffbasiertes FLP betrachtet werden kann (siehe Kapitel 5.4).

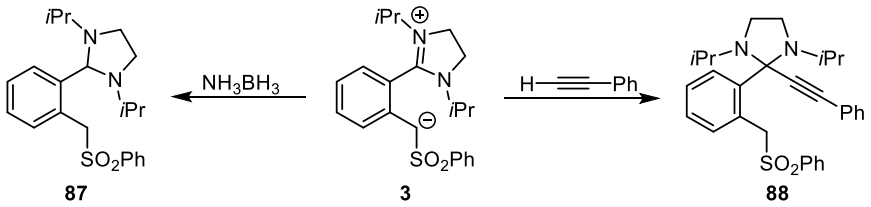

Schema 28: Ambiphile Reaktivität des Akzeptor-substituierten NHQs.

3.4 Entropie

Die Berechnung von Aktivierungsbarrieren ($\Delta^{\ddagger}G_{soln}$) und freien Reaktionsenthalpien ($\Delta_r G_{soln}$) in Lösung war ein essentieller Bestandteil der im Rahmen der vorliegenden Arbeit durchgeführten Forschungsprojekte und erfordert typischerweise drei quantenmechanische Berechnungen:[112] (*i*) Zunächst erfolgt die Optimierung der Atomkoordinaten und Bestimmung der Schwingungsfrequenzen. (*ii*) Anschließend werden präzisere elektronische Energien auf einem höheren theoretischen Niveau berechnet. (*iii*) Schließlich werden implizite Lösungsmittelmodelle verwendet, um die Solvatation in kondensierter Phase zu berücksichtigen. Während enorme Fortschritte bei der Methodenentwicklung zur Bestimmung präziser elektronischer Energien erzielt wurden, sind Entropie-Effekte aufgrund ihrer Komplexität verhältnismäßig rudimentär beschrieben.[112,113] Es ist bekannt, dass insbesondere für Reaktionen, bei denen sich die Zahl der Reaktanten verändert (z.B. Assoziations- und Dissoziationsprozesse), die unzureichende Berücksichtigung von Entropie-Effekten für ungenaue Ergebnisse verantwortlich ist. Im Jahr 2019 präsentierte Garza einen physikalisch fundierten Formalismus für die Berechnung der Entropie in Lösung $S°_{soln}$.[114] Dieser Formalismus wurde im Zuge dieser Arbeit in den klassischen Arbeitsablauf integriert und derart automatisiert, dass $S°_{soln}$ nutzerfreundlich berechnet werden kann. Außerdem wurde überprüft, wie allgemeingültig und wie groß der systematische „Entropie-Fehler" ist, und ob der neue Formalismus diesen korrigiert (siehe Kapitel 5.1). Im Folgenden wird kurz der Entropie-Formalismus in der Gasphase erläutert und darauf aufbauend der neue Formalismus von Garza für $S°_{soln}$ präsentiert. Für die Vibrationsentropie, die von den Schwingungsfrequenzen ν_i abhängt, wird angenommen, dass sie in der Gasphase und in Lösung gleich ist ($S_{soln,vib} \approx S_{g,vib}$).

3.4.1 Formalismus in der Gasphase

Die Gasphasen-Entropie (S_{gas}) setzt sich aus den Beiträgen der Translation ($S_{gas,trans}$), Rotation ($S_{gas,rot}$) und Vibration ($S_{gas,vib}$) zusammen (Gl. 1).

$$S_{\mathrm{gas}} = S_{\mathrm{gas,trans}} + S_{\mathrm{gas,rot}} + S_{\mathrm{gas,vib}} \tag{1}$$

Unter der Annahme eines idealen Gases, des starren Rotators und des harmonischen Oszillators (engl. *rigid-rotor-harmonic-oscillator approximation*) lassen sich die einzelnen Terme berechnen.[115]

$$S_{\mathrm{gas,trans}} = R\left[\frac{3}{2}\ln\left(\frac{2\pi m k_{\mathrm{B}} T}{h^2}\right) + \ln V_{\mathrm{gas,ideal}} + \frac{5}{2}\right] \tag{2}$$

$$S_{\mathrm{gas,rot}} = R\ln\left(\frac{8\pi^2}{\sigma}\left(\frac{2\pi k_{\mathrm{B}} T \mathrm{e}}{h^2}\right)^{\frac{3}{2}}\left(I_{\mathrm{x}} I_{\mathrm{y}} I_{\mathrm{z}}\right)^{\frac{1}{2}}\right) \tag{3}$$

Was die stoffspezifischen Variablen betrifft, ist die Translationsentropie eine Funktion der Masse m (Gl. 2) und die Rotationsentropie eine Funktion der Symmetriezahl σ und des Trägheitsmoments I (Gl. 3). Das ideale Gasvolumen $V_{gas,ideal}$ hängt nur von Temperatur und Druck und nicht von stoffspezifischen Größen ab.

3.4.2 Formalismus in Lösung nach Garza

Die Entropie eines Moleküls in Lösung $S°_{soln}$ lässt sich analog zur Gasphasen-Entropie in ihre Bestandteile aufteilen (Gl. 4). Hierbei muss neben der Translation, Rotation und Vibration auch die

Kavitätsbildung des Lösungsmittels (S_{cav}) berücksichtigt werden. Da sich die Standardbedingungen in der Gasphase (1 bar) und in Lösung (1 mol L^{-1}) unterscheiden, ist noch eine Korrektur für die unterschiedlichen Konzentrationen notwendig ($\Delta S°_{conc}$). Bei 25 °C folgt damit $-T\Delta S°_{conc}$ = 1.894 kcal mol^{-1}.

$$S°_{soln} = S_{soln,trans} + S_{soln,rot} + S_{soln,vib} + S_{cav} + \Delta S°_{conc} \quad (4)$$

Typischerweise führt die Solvatation eines beliebigen gasförmigen Moleküls A_g zu einem Verlust seiner Freiheitsgrade und damit auch seiner Entropie ($\Delta_r S < 0$ für $A_{gas} \rightarrow A_{soln}$). Bei der Translation zeigt sich das darin, dass für die Molekülbewegung in x-, y- und z-Richtung in Lösung nicht mehr das ideale Gasvolumen $V_{gas,ideal}$ sondern das stoffspezifische Kavitätsvolumen $N_{cav}V_{cav}$ zur Verfügung steht (Gl. 5). Das Kavitätsvolumen ist eine Funktion des molekularen Volumens des Lösungsmittels und des solvatisierten Moleküls A_{soln} und außerdem eine Funktion der molaren Masse M_{LM} und Dichte ρ_{LM} des Lösungsmittels. Für die Rotation muss berücksichtigt werden, dass diese im Gegensatz zur Gasphase nicht mehr frei sondern aufgrund der Lösungsmittelkavität nur noch gehindert erfolgt (Gl. 6). Hierbei ist das Verhältnis aus dem Streumassenradius des gelösten Moleküls r_{gyr} (engl. *radius of gyration*) und dem Radius der Lösungsmittelkavität r_{cav} von Bedeutung. Der Streumassenradius ist definiert als der mittlere quadratische Abstand der einzelnen Atome zum Schwerpunkt des Moleküls.

$$S_{soln,trans} = S_{gas,trans} + R \ln\left(\frac{N_{cav}V_{cav}}{V_{gas,ideal}}\right) \quad (5)$$

$$S_{soln,rot} = S_{gas,rot} + 3R \ln\left(1 - \frac{r_{gyr}}{r_{cav}}\right) \quad (6)$$

Die Entropie der Kavitätsbildung lässt sich aus der sogenannten *scaled particle theory* (SPT) ableiten (Gl. 7). Zur Berechnung wird das Verhältnis der Radien des solvatisierten Moleküls A_{soln} und des Lösungsmittels ($X = r_A/r_{LM}$) sowie die relative Permittivität ε_r des Lösungsmittels (Gl. 8) benötigt.

$$S_{cav} = -R\left[-\ln(1-y) + \frac{3y}{1-y}X + X^2\left(\frac{3y}{1-y} + \frac{9}{2}\left(\frac{y}{1-y}\right)^2\right)\right] \quad (7)$$

$$y = \frac{3}{4\pi}\left(\frac{\varepsilon_r - 1}{\varepsilon_r + 2}\right) \quad (8)$$

Die Gasphasen-Entropie nach Gl. 1 wird als gegeben angenommen, da diese standardmäßig im Zuge QM Untersuchungen nach der Bestimmung der Schwingungsfrequenzen berechnet wird. Bei Kenntnis der Solvatationsentropie $\Delta_{solv}S°$ lässt sich damit direkt die Entropie in Lösung $S°_{soln}$ bestimmen. Bildet man die Differenz aus Gl. 4 und Gl. 1 folgt ein verhältnismäßig simpler Ausdruck für die Solvatationsentropie $\Delta_{solv}S°$ eines beliebigen gasförmigen Moleküls A_{gas} (Gl. 9). Alle benötigten Größen lassen sich entweder aus den Atomkoordinaten der optimierten Molekülstruktur berechnen (V_A, V_{LM}, r_{gyr}) oder aus vorhandenen Tabellenwerken entnehmen (M_{LM}, ρ_{LM}, ε_r). Somit kann diese Methode ohne erheblichen zusätzlichen Rechenaufwand routinemäßig durchgeführt werden (siehe Kapitel 5.1)

$$\Delta_{solv}S° = R \ln\left(\frac{N_{cav}V_{cav}}{V_{g,ideal}}\right) + 3R \ln\left(1 - \frac{r_{gyr}}{r_{cav}}\right) + S_{cav} + \Delta S°_{conc} \quad (9)$$

4 Literaturverzeichnis

[1] P. T. Anastas, J. B. Zimmerman, *Green Chem.* **2019**, *21*, 6545.

[2] a) B. List, *Chem. Rev.* **2007**, *107*, 5413; b) B. List, R. A. Lerner, C. F. Barbas, *J. Am. Chem. Soc.* **2000**, *122*, 2395; c) K. A. Ahrendt, C. J. Borths, D. W. C. MacMillan, *J. Am. Chem. Soc.* **2000**, *122*, 4243; d) NobelPrize.org, "The Nobel Prize in Chemistry 2021", abrufbar unter https://www.nobelprize.org/prizes/chemistry/2021/summary/, **2021** (aufgerufen am 17.11.2024).

[3] G. N. Lewis, *Valence and the Structure of Atoms and Molecules*, Chemical Catalog Company, Inc., New York, **1923**.

[4] A. Haaland, *Angew. Chem. Int. Ed. Engl.* **1989**, *28*, 992.

[5] H. C. Brown, H. I. Schlesinger, S. Z. Cardon, *J. Am. Chem. Soc.* **1942**, *64*, 325.

[6] G. Wittig, E. Benz, *Chem. Ber.* **1959**, *92*, 1999.

[7] W. Tochtermann, *Angew. Chem. Int. Ed. Engl.* **1966**, *5*, 351.

[8] D. J. Parks, W. E. Piers, *J. Am. Chem. Soc.* **1996**, *118*, 9440.

[9] G. C. Welch, R. R. San Juan, J. D. Masuda, D. W. Stephan, *Science* **2006**, *314*, 1124.

[10] G. C. Welch, D. W. Stephan, *J. Am. Chem. Soc.* **2007**, *129*, 1880.

[11] J. S. J. McCahill, G. C. Welch, D. W. Stephan, *Angew. Chem. Int. Ed.* **2007**, *46*, 4968.

[12] G. J. Kubas, *Science* **2006**, *314*, 1096.

[13] a) G. H. Spikes, J. C. Fettinger, P. P. Power, *J. Am. Chem. Soc.* **2005**, *127*, 12232; b) G. D. Frey, V. Lavallo, B. Donnadieu, W. W. Schoeller, G. Bertrand, *Science* **2007**, *316*, 439.

[14] a) J. Wristers, *J. Am. Chem. Soc.* **1975**, *97*, 4312; b) E. J. DeWitt, F. L. Ramp, L. E. Trapasso, *J. Am. Chem. Soc.* **1961**, *83*, 4672; c) F. L. Ramp, E. J. DeWitt, L. E. Trapasso, *J. Org. Chem.* **1962**, *27*, 4368; d) M. Yalpani, R. Köster, *Chem. Ber.* **1990**, *123*, 719; e) M. Yalpani, T. Lunow, R. Köster, *Chem. Ber.* **1989**, *122*, 687; f) M. W. Haenel, J. Narangerel, U.-B. Richter, A. Rufińska, *Angew. Chem. Int. Ed.* **2006**, *45*, 1061; g) C. Walling, L. Bollyky, *J. Am. Chem. Soc.* **1961**, *83*, 2968; h) C. Walling, L. Bollky, *J. Am. Chem. Soc.* **1964**, *86*, 3750; i) A. Berkessel, T. J. S. Schubert, T. N. Müller, *J. Am. Chem. Soc.* **2002**, *124*, 8693.

[15] a) M. A. Dureen, D. W. Stephan, *J. Am. Chem. Soc.* **2009**, *131*, 8396; b) M.-A. Légaré, M.-A. Courtemanche, É. Rochette, F.-G. Fontaine, *Science* **2015**, *349*, 513; c) K. Chernichenko, M. Lindqvist, B. Kótai, M. Nieger, K. Sorochkina, I. Pápai, T. Repo, *J. Am. Chem. Soc.* **2016**, *138*, 4860.

[16] C. M. Mömming, E. Otten, G. Kehr, R. Fröhlich, S. Grimme, D. W. Stephan, G. Erker, *Angew. Chem. Int. Ed.* **2009**, *48*, 6643.

[17] a) E. Otten, R. C. Neu, D. W. Stephan, *J. Am. Chem. Soc.* **2009**, *131*, 9918; b) R. C. Neu, E. Otten, D. W. Stephan, *Angew. Chem. Int. Ed.* **2009**, *48*, 9709; c) R. C. Neu, E. Otten, A. Lough, D. W. Stephan, *Chem. Sci.* **2011**, *2*, 170.

[18] M. Sajid, A. Klose, B. Birkmann, L. Liang, B. Schirmer, T. Wiegand, H. Eckert, A. J. Lough, R. Fröhlich, C. G. Daniliuc et al., *Chem. Sci.* **2013**, *4*, 213.

[19] D. W. Stephan, G. Erker, *Chem. Sci.* **2014**, *5*, 2625.

[20] a) A. E. Ashley, A. L. Thompson, D. O'Hare, *Angew. Chem. Int. Ed.* **2009**, *48*, 9839; b) A. Berkefeld, W. E. Piers, M. Parvez, *J. Am. Chem. Soc.* **2010**, *132*, 10660; c) G. Ménard, D. W. Stephan, *J. Am. Chem. Soc.* **2010**, *132*, 1796; d) M.-A. Courtemanche, M.-A. Légaré, L. Maron, F.-G. Fontaine, *J. Am. Chem. Soc.* **2013**, *135*, 9326; e) M.-A. Courtemanche, M.-A. Légaré, L. Maron, F.-G. Fontaine, *J. Am. Chem. Soc.* **2014**, *136*, 10708.

[21] a) Z. Mo, A. Rit, J. Campos, E. L. Kolychev, S. Aldridge, *J. Am. Chem. Soc.* **2016**, *138*, 3306; b) D. H. A. Boom, E. J. J. de Boed, E. Nicolas, M. Nieger, A. W. Ehlers, A. R. Jupp, J. C. Slootweg,

Z. Anorg. Allg. Chem. **2020**, *646*, 586; c) V. Sumerin, F. Schulz, M. Nieger, M. Atsumi, C. Wang, M. Leskelä, P. Pyykkö, T. Repo, B. Rieger, *J. Organomet. Chem.* **2009**, *694*, 2654.

[22] a) L. J. Hounjet, D. W. Stephan, *Org. Process Res. Dev.* **2014**, *18*, 385; b) J. Lam, K. M. Szkop, E. Mosaferi, D. W. Stephan, *Chem. Soc. Rev.* **2019**, *48*, 3592; c) D. W. Stephan, *Org. Biomol. Chem.* **2012**, *10*, 5740; d) D. J. Scott, M. J. Fuchter, A. E. Ashley, *Chem. Soc. Rev.* **2017**, *46*, 5689; e) W. Meng, X. Feng, H. Du, *Acc. Chem. Res.* **2018**, *51*, 191; f) D. W. Stephan, *J. Am. Chem. Soc.* **2021**, *143*, 20002; g) P. A. Chase, T. Jurca, D. W. Stephan, *Chem. Commun.* **2008**, *0*, 1701; h) K. Chernichenko, Á. Madarász, I. Pápai, M. Nieger, M. Leskelä, T. Repo, *Nat. Chem.* **2013**, *5*, 718-723.

[23] a) D. W. Stephan, *Org. Biomol. Chem.* **2008**, *6*, 1535; b) D. W. Stephan, *Acc. Chem. Res.* **2015**, *48*, 306; c) D. W. Stephan, *J. Am. Chem. Soc.* **2015**, *137*, 10018; d) D. W. Stephan, G. Erker, *Angew. Chem. Int. Ed.* **2015**, *54*, 6400; e) D. W. Stephan, *Science* **2016**, *354*, aaf7229; f) F.-G. Fontaine, D. W. Stephan, *Phil. Trans. R. Soc. A* **2017**, *375*, 20170004.

[24] a) M. P. Burke, S. J. Klippenstein, *Nat. Chem.* **2017**, *9*, 1078; b) R. T. Skodje, *Nat. Chem.* **2017**, *9*, 1038.

[25] T. A. Rokob, A. Hamza, A. Stirling, T. Soós, I. Pápai, *Angew. Chem. Int. Ed.* **2008**, *47*, 2435.

[26] P. Spies, G. Erker, G. Kehr, K. Bergander, R. Fröhlich, S. Grimme, D. W. Stephan, *Chem. Commun.* **2007**, *76*, 5072.

[27] a) F. Bertini, V. Lyaskovskyy, B. J. J. Timmer, F. J. J. de Kanter, M. Lutz, A. W. Ehlers, J. C. Slootweg, K. Lammertsma, *J. Am. Chem. Soc.* **2012**, *134*, 201; b) K. Chernichenko, M. Nieger, M. Leskelä, T. Repo, *Dalton Trans.* **2012**, *41*, 9029; c) Z. Mo, E. L. Kolychev, A. Rit, J. Campos, H. Niu, S. Aldridge, *J. Am. Chem. Soc.* **2015**, *137*, 12227; d) G. Ghattas, D. Chen, F. Pan, J. Klankermayer, *Dalton Trans.* **2012**, *41*, 9026; e) M. Lindqvist, K. Borre, K. Axenov, B. Kótai, M. Nieger, M. Leskelä, I. Pápai, T. Repo, *J. Am. Chem. Soc.* **2015**, *137*, 4038.

[28] a) S. J. Geier, D. W. Stephan, *J. Am. Chem. Soc.* **2009**, *131*, 3476; b) D. J. Scott, M. J. Fuchter, A. E. Ashley, *J. Am. Chem. Soc.* **2014**, *136*, 15813; c) T. Mahdi, D. W. Stephan, *J. Am. Chem. Soc.* **2014**, *136*, 15809.

[29] a) K. V. Axenov, C. M. Mömming, G. Kehr, R. Fröhlich, G. Erker, *Chem. Eur. J.* **2010**, *16*, 14069; b) T. Özgün, K.-Y. Ye, C. G. Daniliuc, B. Wibbeling, L. Liu, S. Grimme, G. Kehr, G. Erker, *Chem. Eur. J.* **2016**, *22*, 5988; c) P. Spies, G. Kehr, K. Bergander, B. Wibbeling, R. Fröhlich, G. Erker, *Dalton Trans.* **2009**, *0*, 1534; d) K.-Y. Ye, C. G. Daniliuc, S. Dong, G. Kehr, G. Erker, *Organometallics* **2017**, *36*, 5003; e) S. Schwendemann, R. Fröhlich, G. Kehr, G. Erker, *Chem. Sci.* **2011**, *2*, 1842.

[30] A. R. Jupp, *Dalton Trans.* **2022**, *51*, 10681.

[31] P. Pyykkö, M. Atsumi, *Chem. Eur. J.* **2009**, *15*, 186.

[32] G. Bistoni, A. A. Auer, F. Neese, *Chem. Eur. J.* **2017**, *23*, 865.

[33] L. L. Zeonjuk, N. Vankova, A. Mavrandonakis, T. Heine, G.-V. Röschenthaler, J. Eicher, *Chem. Eur. J.* **2013**, *19*, 17413.

[34] I. Bakó, A. Stirling, S. Bálint, I. Pápai, *Dalton Trans.* **2012**, *41*, 9023.

[35] L. Rocchigiani, G. Ciancaleoni, C. Zuccaccia, A. Macchioni, *J. Am. Chem. Soc.* **2014**, *136*, 112.

[36] L. C. Brown, J. M. Hogg, M. Gilmore, L. Moura, S. Imberti, S. Gärtner, H. Q. N. Gunaratne, R. J. O'Donnell, N. Artioli, J. D. Holbrey et al., *Chem. Commun.* **2018**, *54*, 8689.

[37] L. Liu, L. L. Cao, Y. Shao, G. Ménard, D. W. Stephan, *Chem* **2017**, *3*, 259.

[38] F. Holtrop, A. R. Jupp, N. P. van Leest, M. Paradiz Dominguez, R. M. Williams, A. M. Brouwer, B. de Bruin, A. W. Ehlers, J. C. Slootweg, *Chem. Eur. J.* **2020**, *26*, 9005.

[39] a) M. Gomberg, *J. Am. Chem. Soc.* **1900**, *22*, 757; b) M. Gomberg, *Ber. Dtsch. Chem. Ges.* **1900**, *33*, 3150; c) S. Rösel, P. R. Schreiner, *Isr. J. Chem.* **2022**, *62*, e202200002.

[40] a) P. Jacobson, *Ber. Dtsch. Chem. Ges.* **1905**, *38*, 196; b) H. Lankamp, W.T. Nauta, C. MacLean, *Tetrahedron Lett.* **1968**, *9*, 249; c) J. M. McBride, *Tetrahedron* **1974**, *30*, 2009.
[41] a) J. P. Wagner, P. R. Schreiner, *Angew. Chem. Int. Ed.* **2015**, *54*, 12274; b) L. Rummel, P. R. Schreiner, *Angew. Chem. Int. Ed.* **2024**, *63*, e202316364.
[42] a) S. Rösel, H. Quanz, C. Logemann, J. Becker, E. Mossou, L. Cañadillas-Delgado, E. Caldeweyher, S. Grimme, P. R. Schreiner, *J. Am. Chem. Soc.* **2017**, *139*, 7428; b) B. Kahr, D. van Engen, K. Mislow, *J. Am. Chem. Soc.* **1986**, *108*, 8305; c) S. Grimme, P. R. Schreiner, *Angew. Chem. Int. Ed.* **2011**, *50*, 12639; d) S. Rösel, C. Balestrieri, P. R. Schreiner, *Chem. Sci.* **2017**, *8*, 405; e) S. Rösel, J. Becker, W. D. Allen, P. R. Schreiner, *J. Am. Chem. Soc.* **2018**, *140*, 14421; f) D. Maué, P. H. Strebert, D. Bernhard, S. Rösel, P. R. Schreiner, M. Gerhards, *Angew. Chem. Int. Ed.* **2021**, *60*, 11305.
[43] B. Sieland, M. Stahn, R. Schoch, C. Daniliuc, S. Spicher, S. Grimme, A. Hansen, J. Paradies, *Angew. Chem. Int. Ed.* **2023**, *62*, e202308752.
[44] a) W.-C. Liu, F. P. Gabbaï, *Science* **2024**, *385*, 1184; b) A. R. Jupp, *Science* **2024**, *385*, 1165.
[45] A. Hamza, A. Stirling, T. A. Rokob, I. Pápai, *Int. J. Quantum Chem.* **2009**, *109*, 2416.
[46] T. A. Rokob, I. Bakó, A. Stirling, A. Hamza, I. Pápai, *J. Am. Chem. Soc.* **2013**, *135*, 4425.
[47] a) S. Grimme, H. Kruse, L. Goerigk, G. Erker, *Angew. Chem. Int. Ed.* **2010**, *49*, 1402; b) B. Schirmer, S. Grimme, *Chem. Commun.* **2010**, *46*, 7942.
[48] G. Skara, F. de Vleeschouwer, P. Geerlings, F. de Proft, B. Pinter, *Sci. Rep.* **2017**, *7*, 16024.
[49] T. A. Rokob, A. Hamza, I. Pápai, *J. Am. Chem. Soc.* **2009**, *131*, 10701.
[50] L. Liu Zeonjuk, P. St. Petkov, T. Heine, G.-V. Röschenthaler, J. Eicher, N. Vankova, *Phys. Chem. Chem. Phys.* **2015**, *17*, 10687.
[51] a) J. Paradies, *Acc. Chem. Res.* **2023**, *56*, 821; b) J. Paradies, *Eur. J. Org. Chem.* **2019**, *2019*, 283.
[52] a) H. B. Hamilton, D. F. Wass, *Chem* **2017**, *3*, 198; b) L. J. C. van der Zee, S. Pahar, E. Richards, R. L. Melen, J. C. Slootweg, *Chem. Rev.* **2023**, *123*, 9653; c) L. L. Liu, D. W. Stephan, *Chem. Soc. Rev.* **2019**, *48*, 3454; d) M. Ju, Z. Lu, L. F. T. Novaes, J. I. Martinez Alvarado, S. Lin, *J. Am. Chem. Soc.* **2023**, *145*, 19478.
[53] S. A. Weicker, D. W. Stephan, *Bull. Chem. Soc. Jpn.* **2015**, *88*, 1003.
[54] a) P. A. Chase, D. W. Stephan, *Angew. Chem. Int. Ed.* **2008**, *47*, 7433; b) D. Holschumacher, T. Bannenberg, C. G. Hrib, P. G. Jones, M. Tamm, *Angew. Chem. Int. Ed.* **2008**, *47*, 7428; c) P. A. Chase, A. L. Gille, T. M. Gilbert, D. W. Stephan, *Dalton Trans.* **2009**, 7179.
[55] E. Aldeco-Perez, A. J. Rosenthal, B. Donnadieu, P. Parameswaran, G. Frenking, G. Bertrand, *Science* **2009**, *326*, 556.
[56] S. C. Sau, P. K. Hota, S. K. Mandal, M. Soleilhavoup, G. Bertrand, *Chem. Soc. Rev.* **2020**, *49*, 1233.
[57] a) M. Alcarazo, C. Gomez, S. Holle, R. Goddard, *Angew. Chem. Int. Ed.* **2010**, *49*, 5788; b) M. Alcarazo, C. Gomez, S. Holle, R. Goddard, *Angew. Chem. Int. Ed.* **2010**, *49*, 5597.
[58] a) B. Inés, S. Holle, R. Goddard, M. Alcarazo, *Angew. Chem. Int. Ed.* **2010**, *49*, 8389; b) D. Palomas, S. Holle, B. Inés, H. Bruns, R. Goddard, M. Alcarazo, *Dalton Trans.* **2012**, *41*, 9073.
[59] J. W. Runyon, O. Steinhof, H. V. R. Dias, J. C. Calabrese, W. J. Marshall, A. J. Arduengo, *Aust. J. Chem.* **2011**, *64*, 1165.
[60] a) L. Cabrera, G. C. Welch, J. D. Masuda, P. Wei, D. W. Stephan, *Inorg. Chim. Acta* **2006**, *359*, 3066; b) J. Zhou, L. L. Cao, L. L. Liu, D. W. Stephan, *Dalton Trans.* **2017**, *46*, 9334; c) E. Follet, P. Mayer, D. S. Stephenson, A. R. Ofial, G. Berionni, *Chem. Eur. J.* **2017**, *23*, 7422.
[61] A. C. Shaikh, J. M. Veleta, J. Moutet, T. L. Gianetti, *Chem. Sci.* **2021**, *12*, 4841.
[62] K. F. Kalz, A. Brinkmeier, S. Dechert, R. A. Mata, F. Meyer, *J. Am. Chem. Soc.* **2014**, *136*, 16626.

[63] a) M. P. Boone, D. W. Stephan, *J. Am. Chem. Soc.* **2013**, *135*, 8508; b) M. P. Boone, D. W. Stephan, *Chem. Eur. J.* **2014**, *20*, 3333.
[64] E. R. Clark, M. J. Ingleson, *Angew. Chem. Int. Ed.* **2014**, *53*, 11306.
[65] F. Krämer, J. Paradies, I. Fernández, F. Breher, *Nat. Chem.* **2024**, *16*, 63.
[66] a) P. Bellotti, M. Koy, M. N. Hopkinson, F. Glorius, *Nat. Rev. Chem.* **2021**, *5*, 711; b) M. N. Hopkinson, C. Richter, M. Schedler, F. Glorius, *Nature* **2014**, *510*, 485; c) A. J. Arduengo III, R. L. Harlow, M. Kline, *J. Am. Chem. Soc.* **1991**, *113*, 361; d) D. Enders, O. Niemeier, A. Henseler, *Chem. Rev.* **2007**, *107*, 5606.
[67] a) R. Breslow, *J. Am. Chem. Soc.* **1957**, *79*, 1762; b) R. Breslow, *J. Am. Chem. Soc.* **1958**, *80*, 3719; c) A. Berkessel, S. Elfert, V. R. Yatham, J.-M. Neudörfl, N. E. Schlörer, J. H. Teles, *Angew. Chem. Int. Ed.* **2012**, *51*, 12370; d) A. Berkessel, V. R. Yatham, S. Elfert, J.-M. Neudörfl, *Angew. Chem. Int. Ed.* **2013**, *52*, 11158; e) M. Paul, P. Sudkaow, A. Wessels, N. E. Schlörer, J.-M. Neudörfl, A. Berkessel, *Angew. Chem. Int. Ed.* **2018**, *57*, 8310; f) A. Wessels, M. Klussmann, M. Breugst, N. E. Schlörer, A. Berkessel, *Angew. Chem. Int. Ed.* **2022**, *61*, e202117682; g) M. Pareek, Y. Reddi, R. B. Sunoj, *Chem. Sci.* **2021**, *12*, 7973.
[68] B. Maji, M. Horn, H. Mayr, *Angew. Chem. Int. Ed.* **2012**, *51*, 6231.
[69] R. Schuldt, J. Kästner, S. Naumann, *J. Org. Chem.* **2019**, *84*, 2209.
[70] Z. Li, P. Ji, J.-P. Cheng, *J. Org. Chem.* **2021**, *86*, 2974.
[71] K. Powers, C. Hering-Junghans, R. McDonald, M. J. Ferguson, E. Rivard, *Polyhedron* **2016**, *108*, 8.
[72] A. Fürstner, M. Alcarazo, R. Goddard, C. W. Lehmann, *Angew. Chem. Int. Ed.* **2008**, *47*, 3210.
[73] M. G, D. Sharma, R. Dandela, V. Dhayalan, *Chem. Eur. J.* **2023**, *29*, e202302106.
[74] A. Eitzinger, J. Reitz, P. W. Antoni, H. Mayr, A. R. Ofial, M. M. Hansmann, *Angew. Chem. Int. Ed.* **2023**, *62*, e202309790.
[75] a) S. Kronig, P. G. Jones, M. Tamm, *Eur. J. Inorg. Chem.* **2013**, *2013*, 2301; b) A. Causero, H. Elsen, J. Pahl, S. Harder, *Angew. Chem. Int. Ed.* **2017**, *56*, 6906; c) R. S. Ghadwal, C. J. Schürmann, F. Engelhardt, C. Steinmetzger, *Eur. J. Inorg. Chem.* **2014**, *2014*, 4921; d) A. Dumrath, X.-F. Wu, H. Neumann, A. Spannenberg, R. Jackstell, M. Beller, *Angew. Chem. Int. Ed.* **2010**, *49*, 8988; e) D. Rottschäfer, M. K. Sharma, B. Neumann, H.-G. Stammler, D. M. Andrada, R. S. Ghadwal, *Chem. Eur. J.* **2019**, *25*, 8127; f) M. R. Buchmeiser, D. Imbrich, D. Wang, S. Naumann, *J. Organomet. Chem.* **2023**, *991*, 122674; g) A. Iturmendi, N. García, E. A. Jaseer, J. Munárriz, P. J. Sanz Miguel, V. Polo, M. Iglesias, L. A. Oro, *Dalton Trans.* **2016**, *45*, 12835; h) I. C. Watson, A. Schumann, H. Yu, E. C. Davy, R. McDonald, M. J. Ferguson, C. Hering-Junghans, E. Rivard, *Chem. Eur. J.* **2019**, *25*, 9678; i) A. Schumann, C. Hering-Junghans, *Eur. J. Inorg. Chem.* **2018**, *2018*, 2584; j) L. Körner, L. Yang, D. Bockfeld, M. Tamm, *J. Organomet. Chem.* **2023**, *984*, 122572.
[76] S. M. Ibrahim Al-Rafia, A. C. Malcolm, S. K. Liew, M. J. Ferguson, R. McDonald, E. Rivard, *Chem. Commun.* **2011**, *47*, 6987.
[77] a) M. J. S. Dewar, *Bull. Soc. Chim. Fr.* **1951**, *18*, C79; b) J. Chatt, L. A. Duncanson, *J. Chem. Soc.* **1953**, 2939; c) G. Frenking, N. Fröhlich, *Chem. Rev.* **2000**, *100*, 717; d) G. J. Kubas, *J. Organomet. Chem.* **2001**, *635*, 37.
[78] a) W. C. Zeise, *Ann. Phys.* **1831**, *97*, 497; b) R. A. Love, T. F. Koetzle, G. J. B. Williams, L. C. Andrews, R. Bau, *Inorg. Chem.* **1975**, *14*, 2653.
[79] N. Kuhn, H. Bohnen, D. Bläser, R. Boese, *Chem. Ber.* **1994**, *127*, 1405.
[80] a) L. S. Bartell, E. A. Roth, C. D. Hollowell, K. Kuchitsu, Young, J. E., Jr., *J. Chem. Phys.* **1965**, *42*, 2683; b) N. Kuhn, G. Henkel, J. Kreutzberg, *Z. Naturforsch. B* **1991**, *46*, 1706.
[81] N. Kuhn, H. Bohnen, J. Kreutzberg, D. Bläser, R. Boese, *J. Chem. Soc., Chem. Commun.* **1993**, 1136.

[82] a) C. A. Tolman, *Chem. Rev.* **1977**, *77*, 313; b) R. Tonner, G. Frenking, *Organometallics* **2009**, *28*, 3901; c) H. V. Huynh, *Chem. Rev.* **2018**, *118*, 9457; d) W. A. Herrmann, J. Schütz, G. D. Frey, E. Herdtweck, *Organometallics* **2006**, *25*, 2437.
[83] M. M. Hansmann, P. W. Antoni, H. Pesch, *Angew. Chem. Int. Ed.* **2020**, *59*, 5782.
[84] R. D. Crocker, T. V. Nguyen, *Chem. Eur. J.* **2016**, *22*, 2208.
[85] a) S. Naumann, A. W. Thomas, A. P. Dove, *Angew. Chem. Int. Ed.* **2015**, *54*, 9550; b) P. Walther, A. Krauß, S. Naumann, *Angew. Chem. Int. Ed.* **2019**, *58*, 10737; c) S. Naumann, A. W. Thomas, A. P. Dove, *ACS Macro Lett.* **2016**, *5*, 134; d) P. Walther, W. Frey, S. Naumann, *Polym. Chem.* **2018**, *9*, 3674; e) S. Naumann, *Chem. Commun.* **2019**, *55*, 11658.
[86] M. M. D. Roy, E. Rivard, *Acc. Chem. Res.* **2017**, *50*, 2017.
[87] H. Böhme, F. Soldan, *Chem. Ber.* **1961**, *94*, 3109.
[88] P. P. Ponti, J. C. Baldwin, W. C. Kaska, *Inorg. Chem.* **1979**, *18*, 873.
[89] a) U. Gruseck, M. Heuschmann, *Chem. Ber.* **1987**, *120*, 2053; b) U. Gruseck, M. Heuschmann, *Chem. Ber.* **1987**, *120*, 2065.
[90] H. Quast, M. Ach, M. K. Kindermann, P. Rademacher, M. Schindler, *Chem. Ber.* **1993**, *126*, 503.
[91] a) Q. Sun, A. Eitzinger, R. Esken, P. W. Antoni, R. J. Mayer, A. R. Ofial, M. M. Hansmann, *Angew. Chem. Int. Ed.* **2024**, *63*, e202318283; b) Q. Liang, D. Song, *Dalton Trans.* **2022**, *51*, 9191.
[92] Y.-B. Wang, Y.-M. Wang, W.-Z. Zhang, X.-B. Lu, *J. Am. Chem. Soc.* **2013**, *135*, 11996.
[93] Z. Wang, Q.-H. Niu, X.-S. Xue, P. Ji, *J. Org. Chem.* **2020**, *85*, 13204.
[94] a) V. B. Saptal, B. M. Bhanage, *ChemSusChem* **2016**, *9*, 1980; b) Y.-B. Wang, D.-S. Sun, H. Zhou, W.-Z. Zhang, X.-B. Lu, *Green Chem.* **2015**, *17*, 4009.
[95] S. Maji, A. Das, M. M. Bhatt, S. K. Mandal, *Nat. Catal.* **2024**, *7*, 375.
[96] a) A. G. Tskhovrebov, E. Solari, M. D. Wodrich, R. Scopelliti, K. Severin, *Angew. Chem. Int. Ed.* **2012**, *51*, 232; b) A. G. Tskhovrebov, B. Vuichoud, E. Solari, R. Scopelliti, K. Severin, *J. Am. Chem. Soc.* **2013**, *135*, 9486.
[97] a) Eymann, L. Y. M., P. Varava, A. M. Shved, B. F. E. Curchod, Y. Liu, O. M. Planes, A. Sienkiewicz, R. Scopelliti, F. Fadaei Tirani, K. Severin, *J. Am. Chem. Soc.* **2019**, *141*, 17112; b) L. Y. M. Eymann, P. Varava, A. M. Shved, B. F. E. Curchod, Y. Liu, O. M. Planes, A. Sienkiewicz, R. Scopelliti, F. Fadaei Tirani, K. Severin, *J. Am. Chem. Soc.* **2020**, *142*, 1112.
[98] P. Varava, Z. Dong, R. Scopelliti, F. Fadaei-Tirani, K. Severin, *Nat. Chem.* **2021**, *13*, 1055.
[99] a) P. W. Antoni, C. Golz, J. J. Holstein, D. A. Pantazis, M. M. Hansmann, *Nat. Chem.* **2021**, *13*, 587; b) P. W. Antoni, J. Reitz, M. M. Hansmann, *J. Am. Chem. Soc.* **2021**, *143*, 12878.
[100] M. M. Hansmann, *Angew. Chem. Int. Ed.* **2023**, *62*, e202304574.
[101] R. Hoffmann, *Angew. Chem. Int. Ed. Engl.* **1982**, *21*, 711.
[102] K. B. Wiberg, *Angew. Chem. Int. Ed. Engl.* **1986**, *25*, 312.
[103] a) G. Raabe, H.-J. Gais, J. Fleischhauer, *J. Am. Chem. Soc.* **1996**, *118*, 4622; b) S. Wolfe, A. Rauk, I. G. Csizmadia, *J. Am. Chem. Soc.* **1969**, *91*, 1567; c) J. S. Grossert, J. Hoyle, T. S. Cameron, S. P. Roe, B. R. Vincent, *Can. J. Chem.* **1987**, *65*, 1407; d) I. V. Alabugin, K. M. Gilmore, P. W. Peterson, *WIREs Comput. Mol. Sci.* **2011**, *1*, 109.
[104] a) R. L. Atienza, K. A. Scheidt, *Aust. J. Chem.* **2011**, *64*, 1158; b) X.-Y. Chen, S. Ye, *Org. Biomol. Chem.* **2013**, *11*, 7991.
[105] a) W.-Y. Ahmad, S. Omar, *J. Chem. Educ.* **1992**, *69*, 791; b) I. Kaufmann, K. M. Hamza, C.-J. Rundgren, L. Eriksson, *Int. J. Sci. Educ.* **2017**, *39*, 1601; c) J. Q. Pardo, *J. Chem. Educ.* **1989**, *66*, 456; d) L. Suidan, J. K. Badenhoop, E. D. Glendening, F. Weinhold, *J. Chem. Educ.* **1995**, *72*, 583; e) A. B. P. Lever, *J. Chem. Educ.* **1972**, *49*, 819.
[106] a) R. Gompper, H.-U. Wagner, E. Kutter, *Chem. Ber.* **1968**, *101*, 4123; b) R. Gompper, H.-U. Wagner, *Tetrahedron Lett.* **1968**, *9*, 165.

[107] S. Inoue, Y. Aso, T. Otsubo, *Chem. Commun.* **1997**, 1105.
[108] T. Takahashi, K. Takimiya, T. Otsubo, Y. Aso, *Org. Lett.* **2005**, *7*, 4313.
[109] M. J. Smith, W. Clegg, K. A. Nguyen, J. E. Rogers, R. Pachter, P. A. Fleitz, H. L. Anderson, *Chem. Commun.* **2005**, 2433.
[110] Z. Zeng, S. Lee, M. Son, K. Fukuda, P. M. Burrezo, X. Zhu, Q. Qi, R.-W. Li, J. T. L. Navarrete, J. Ding et al., *J. Am. Chem. Soc.* **2015**, *137*, 8572.
[111] W. Shang, W. Meng, L. Chen, Z. Shangguan, Y. Huang, X.-S. Zhang, C. Li, S. Bai, G. Zhang, D. Zhang, *Angew. Chem. Int. Ed.* **2024**, *63*, e202412704.
[112] M. Bursch, J.-M. Mewes, A. Hansen, S. Grimme, *Angew. Chem. Int. Ed.* **2022**, *61*, e202205735.
[113] a) S. Grimme, P. R. Schreiner, *Angew. Chem. Int. Ed.* **2018**, *57*, 4170; b) A. M. Teale, T. Helgaker, A. Savin, C. Adamo, B. Aradi, A. V. Arbuznikov, P. W. Ayers, E. J. Baerends, V. Barone, P. Calaminici et al., *Phys. Chem. Chem. Phys.* **2022**, *24*, 28700; c) S. Kozuch, S. Shaik, *Acc. Chem. Res.* **2011**, *44*, 101; d) D. J. Tantillo, *J. Am. Chem. Soc.* **2022**, *144*, 13996; e) J. N. Harvey, F. Himo, F. Maseras, L. Perrin, *ACS Catal.* **2019**, *9*, 6803; f) D. Ardura, R. López, T. L. Sordo, *J. Phys. Chem. B* **2005**, *109*, 23618.
[114] A. J. Garza, *J. Chem. Theory Comput.* **2019**, *15*, 3204.
[115] S. Grimme, *Chem. Eur. J.* **2012**, *18*, 9955.

5 Veröffentlichte Projekte

5.1 The entropic penalty for associative reactions and their physical treatment during routine computations

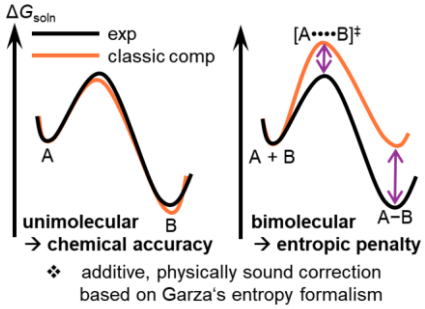

Eine systematische Untersuchung der entropischen Benachteiligung assoziativer Reaktionen wird vorgestellt. Es wird gezeigt, dass freie Enthalpien in Lösung ΔG_{soln} häufig die entropischen Beiträge überschätzen. Dieser „Entropie-Fehler“ für assoziative Reaktionen in Lösung, d.h., wenn die Anzahl der Teilchen entlang der Reaktionskoordinate abnimmt (Summe der Stöchiometriezahlen $\sum \nu_i < 0$), entsteht durch die unzureichende Behandlung entropischer Effekte durch implizite Lösungsmittelmodelle. Wir stellen ein additives Korrekturschema für die freien Enthalpien vor, das für Routineanwendungen geeignet ist. Diese Korrektur basiert auf Garzas physikalisch fundiertem Formalismus zur Berechnung der Entropie in Lösung S_{soln} [A. J. Garza, *J. Chem. Theory Comput.* **2019**, *15*, 3204.], der in einen effizienten Blackbox-Algorithmus eingebettet ist. Um den „Entropie-Fehler“ und die vorgeschlagene Korrektur kritisch zu bewerten, haben wir einen experimentellen Benchmark-Datensatz von 31 Reaktionsenergien und 22 Aktivierungsbarrieren in 15 verschiedenen Lösungsmitteln zusammengestellt. Unter Verwendung eines repräsentativen Arbeitsablaufes (auf Basis der Wellenfunktionstheorie (WFT) mit DLPNO-CCSD(T) und der Dichtefunktionaltheorie (DFT) mit revDSD-PBEP86-D4 sowie einem impliziten Lösungsmittelmodell) wurde ein beträchtlicher systematischer „Entropie-Fehler“ von 2–11 kcal mol^{-1} bestimmt. Mit dem hier vorgestellten Korrekturschema wird die entropische Benachteiligung auf eine chemische Genauigkeit von ≤1 kcal mol^{-1} (WFT und DFT) korrigiert. Gleiches gilt für die Barrieren auf WFT-Niveau. Barrieren auf DFT-Niveau werden in der klassischen Berechnung um 2 kcal mol^{-1} überschätzt und nach der Korrektur um 2 kcal mol^{-1} unterschätzt. Dieser Effekt wird darauf zurückgeführt, dass Barrieren, die auf DFT-Niveau berechnet werden, systematisch 2–3 kcal mol^{-1} niedriger liegen als die mit WFT erhaltenen Barrieren.

Referenz:

J. Ariai, U. Gellrich, *Phys. Chem. Chem. Phys.* **2023**, *25*, 14005.

DOI: 10.1039/D3CP00970J

Akzeptiertes Manuskript online: 29. April 2023

Final veröffentlichte Version online: 2. Mai 2023

PCCP

ROYAL SOCIETY OF CHEMISTRY

PAPER

View Article Online
View Journal | View Issue

Cite this: *Phys. Chem. Chem. Phys.*, 2023, **25**, 14005

The entropic penalty for associative reactions and their physical treatment during routine computations†

Jama Ariai * and Urs Gellrich *

Received 2nd March 2023,
Accepted 29th April 2023

DOI: 10.1039/d3cp00970j

rsc.li/pccp

A systematic study of the entropic penalty for associative reactions is presented. It is shown that computed solution-phase Gibbs free energies typically overestimate entropic contributions. This entropic penalty for associative reactions in solution, *i.e.*, if the number of particles decreases along the reaction coordinate (sum of stoichiometric numbers $\sum \nu_i < 0$), originates from the insufficient treatment of entropic effects by implicit solvent models. We propose an additive correction scheme to Gibbs free energies that is suitable for routine applications by non-expert users. This correction is based on Garza's formalism for the solution-phase entropy [A. J. Garza, *J. Chem. Theory Comput.*, 2019, **15**, 3204.] that is physically sound and embedded into an efficient black-box type algorithm. To critically evaluate the entropic penalty and its proposed treatment, we compiled an experimental benchmark set of 31 $\Delta_r G$ and 22 $\Delta^{\ddagger} G$ in 15 different solvents. Using a representative best-practice computational protocol (at wave function theory (WFT) based DLPNO-CCSD(T) and density functional theory (DFT) based revDSD-PBEP86-D4 level with an implicit solvent model), we determined a sizeable entropic penalty ranging from 2–11 kcal mol^{-1}. Using the correction scheme presented herein, the entropic penalty is corrected to the chemical accuracy of $\leq$1 kcal mol^{-1} (WFT and DFT). The same applies to $\Delta^{\ddagger} G$ at the WFT level. Barriers at the DFT level are overestimated by 2 kcal mol^{-1} (classic) and underestimated by 2 kcal mol^{-1} (corrected). This effect is attributed to the finding that barriers computed at the DFT level are systematically 2–3 kcal mol^{-1} lower than barriers obtained with WFT.

Introduction

The last decades have witnessed tremendous progress in electronic structure computations.[1,2] Nowadays, sophisticated DFT methods[3–15] and efficient implementations of coupled cluster theory[16–21] are affordable for even complex/large molecular systems and thereby allow to compute the electronic structure with high accuracy. When it comes to the computational study of (bio)chemical reactions (*e.g.*, catalysis, bond activation, binding affinities of proteins/drugs, *etc.*), the change of the Gibbs free energy during the course of the reaction is of particular interest. Since the partition functions that are needed to calculate the thermochemistry of an ideal gas are also known, the Gibbs free energy of a chemical reaction in the gas-phase ΔG_g can be calculated accurately.[22–27] However, most chemical reactions that are relevant for synthetic chemistry and chemical biology take place in solution. An analytical treatment of the thermochemistry for chemical reactions in solution is not routinely possible. Thus, the classic computational protocol for that purpose is as follows: Applying Hess' law, the solution-phase Gibbs free energy ΔG_{soln} is calculated from the corresponding gas-phase Gibbs free energy ΔG_g and the individual Gibbs free solvation energies $\Delta_{solv} G$ (Fig. 1). The latter is routinely obtained from continuum solvent models (CSMs), *i.e.*, an implicit solvent treatment.[9,28,29] Consequently, the accuracy of computed ΔG_{soln} values depends on the precision of their contributions from ΔG_g and $\Delta_{solv} G$. It is well recognized that the treatment of entropy in solution is fundamentally difficult, which can severely diminish the predictive applications of computational chemistry.[1,2,9,30–35] CSMs are parametrized to reproduce Gibbs free solvation energies of individual species without chemical transformations being taken into account.[29,36–48] When the number of particles changes during the course of the reaction (*e.g.* bimolecular reactions), entropic contributions become particularly important. In these cases, the classic computational protocol tends to overestimate the gas-phase entropic contributions which manifests itself in an entropic penalty that systematically disfavors bimolecular reactions (or generally speaking associative reaction pathways with decreasing particle number). Various treatments of this so-called entropic penalty have

Institute of Organic Chemistry, Justus Liebig University, Heinrich-Buff-Ring 17, 35392 Giessen, Germany. E-mail: urs.gellrich@org.chemie.uni-giessen.de, jama.ariai@org.chemie.uni-giessen.de

† Electronic supplementary information (ESI) available: Derivation of mathematical expressions, statistical analysis, comprehensive lists of computed quantities, documentation on the black-box algorithm, and numerical examples. See DOI: https://doi.org/10.1039/d3cp00970j

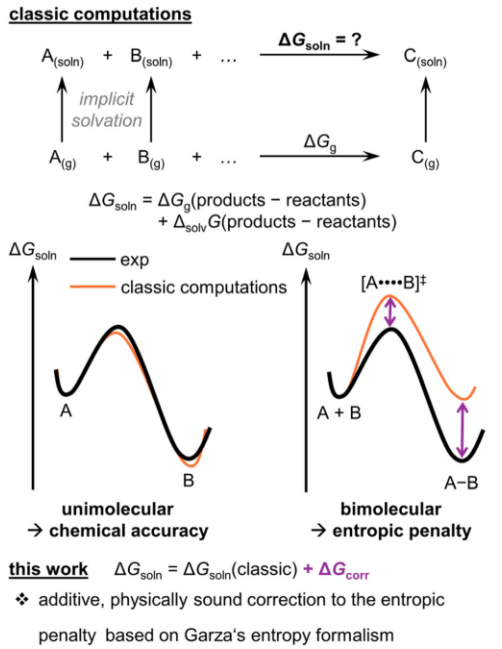

Fig. 1 Schematic presentation of a classic best-practise workflow to determine the solution-phase Gibbs free energy ΔG_{soln}. The implications for bimolecular reactions that suffer from an entropic penalty (in contrast to unimolecular reactions) are illustrated. This work quantifies the entropic penalty and proposes a correction.

already been proposed and debated in literature.[30,35,48–79] However, these are mostly case-specific, empirical, or costly so that they cannot be embedded into a general computational protocol. Thus, to the best of our knowledge, there is no physically sound correction scheme to the entropic penalty that is universally applicable for routine computations.

In 2019, Garza introduced a nonempirical formalism to approximate the solution-phase entropy based on physical arguments and properties of the solvent.[80] According to this approach, the solution-phase entropy is calculated as the sum of translational, rotational, vibrational, and cavitation entropy. The solution-phase expressions are derived from the gas-phase formalism with appropriate adjustments to the condensed phase (*vide infra*). The solvation entropies calculated this way reached chemical accuracy as demonstrated by Garza.

However, is it possible to obtain corrected (regarding the entropic penalty) reaction/activation Gibbs free energies by calculating $\Delta_{solv}H$ independently using an existing CSM as suggested by Garza but not demonstrated? And how is the accuracy for a broader scope of chemical reactions in a variety of solvents? To answer these questions, we compiled a benchmark set that covers 31 experimental solution-phase Gibbs free reaction energies $\Delta_r G_{soln}$ in 5 solvents and 22 activation free energies $\Delta^{\ddagger}G_{soln}$ in 13 solvents (including enthalpic and entropic components for each entry) for a diverse set of bimolecular chemical reactions. Existing benchmark sets do not serve our purpose of determining the entropic penalty because they typically consider electronic energies or gas-phase energies. Among the reactions that we considered are cycloadditions, dimerizations, hydrogen bonding, and coordination. Thus, it is possible to systematically investigate the entropic penalty and to quantify it for both, $\Delta_r G_{soln}$ and $\Delta^{\ddagger}G_{soln}$, employing DFT and domain-based local pair natural orbital coupled cluster theory (DLPNO-CCSD(T)). Based on these findings, we examine if Garza's formalism can compete with the common computational protocol. To elaborate on a useful computational protocol suitable for routine non-expert applications, we define the following criteria. The computational effort should be as low as possible, preferably similar to the gas-phase entropy so that it does not require an additional QM computation or software. Furthermore, the protocol should be reliable for $\Delta_r G_{soln}$ and $\Delta^{\ddagger}G_{soln}$ independent from the solvent and the molecularity of the reaction to be suitable in predictive applications.

For this purpose, we combined Garza's solution-phase entropy formalism with the existing gas-phase formalism to obtain simple expressions for the solvation entropy. We implemented these into a universal black-box algorithm feasible for routine applications that calculates the solvation entropy of any species within seconds on the command line using a regular desktop computer requiring no more than the atomic coordinates of the solute and specification of the solvent. Putting all together, we propose an additive correction to the entropic penalty that meets all our criteria.

This article is organized as follows: First, we outline the theoretical background that includes common usage of CSMs, Garza's formalism of the solution-phase entropy, and the origin of the entropic penalty. Secondly, we comment on the computational protocol and compiled benchmark set. The results are summarized and critically discussed in the main section. After a demonstration of the entropic penalty and a proposed correction, we conclude this investigation with a summary and outlook.

Theoretical background

Commonly, solution-phase Gibbs free energies

$$\Delta_r G_{soln} = \Delta_r G_{gas} + \Delta_r \Delta_{solv} G \quad (1)$$

are calculated as the sum of gas-phase and solvation energies according to Hess' law (eqn (1)). The solvation free energy is calculated from CSMs. We will consider the SMD model hereafter as a representative because it belongs to the best-performing CSMs with broad availability, scope, and high accuracy.[40] However, most CSMs operate similarly and therefore the conclusion is not exclusively limited to this particular solvent model.[46] The solvation free energy

$$\Delta_r \Delta_{solv} G = \Delta_r E_{elst} + \Delta_r G_{nes} \quad (2)$$

includes electrostatic ($\Delta_r E_{elst} < 0$) and non-electrostatic ($\Delta_r G_{nes}$) contributions (eqn (2)). $\Delta_r G_{nes}$ is parametrized to

reproduce $\Delta_{solv}G$ from a training set and to cover apolar interactions, cavity formation, and entropic contributions. Entropic contributions are particularly sensitive to changes in particle number but this was not considered during parametrization, so these effects are not covered by CSMs.

We propose a correction scheme that is based on the formalism presented by Garza.[80] Accordingly, the solution-phase entropy is treated similarly to the gas-phase entropy but corrected for cavity formation and thereby reduced translational and rotational entropy. Thus, reformulation of the solvation entropy

$$\Delta_{solv}S = \Delta_{solv}S^{trans} + \Delta_{solv}S^{rot} + S^{cav} \quad (3)$$

with

$$\Delta_{solv}S^{trans} = R\ln\left(\frac{N_{cav}V_{cav}}{V_{gas}^{ideal}}\right) \quad (4)$$

$$\Delta_{solv}S^{rot} = 3R\ln\left(1-\frac{r_{gyr}}{r_{cav}}\right) \quad (5)$$

$$S_{cav} = -R\left[-\ln(1-y)+\frac{3y}{1-y}X+y'X^2\right] \quad (6)$$

requires the number of accessible cavities (N_{cav}), their volume (V_{cav}) and radius (r_{cav}), the radius of gyration (r_{gyr}), the (modified) reduced number density of the solvent (y' and y), and the ratio of the radii of solute to solvent (X).[80] For the calculation of these expressions, tabulated physical bulk properties of the solvent (molar mass, density, permittivity), optimized atomic coordinates of the solute, and the molecular volume of both the solute and solvent are required. The molecular volume is derived from the atomic coordinates by considering overlapping atomic spheres based on the van der Waals (vdW) radii.[81] Thus, we optimized the molecular structures of common solvents at the PBEh-3c level and computed the vdW volume. Together with the aforementioned physical bulk properties, we compiled a solvent library comprising 187 entries. With this in hand, the computational effort to determine the solvation entropy is further reduced. It is comparable to the gas-phase formalism as it requires no more than the radius of gyration and the vdW volume of the solute. Both quantities are derived from optimized atomic coordinates.

Entropic penalty

If we consider a chemical reaction rather than just a solvation process of a single particle, we obtain

$$\Delta_r\Delta_{solv}S^{trans} = R\Delta_r\ln(V_r) \quad (7)$$

$$\Delta_r\Delta_{solv}S^{rot} = 3R\Delta_r\ln(r_r') \quad (8)$$

$$\Delta_rS_{cav} = -R\left[-\sum\nu_i\ln(1-y)+\frac{3y}{1-y}\Delta_rX+y'\Delta_r(X^2)\right] \quad (9)$$

where the ratio of the multiplied product terms to the multiplied reactant terms

$$\Delta_r\ln(V_r) = \ln\left(\prod_i\left(\frac{N_{cav}V_{cav}}{V_{ideal}^{gas}}\right)^{\nu_i}\right) \quad (10)$$

$$\Delta_r\ln(r_r') = \ln\left(\prod_i\left(1-\frac{r_{gyr}}{r_{cav}}\right)^{\nu_i}\right) \quad (11)$$

are condensed for brevity (eqn (10) and (11)). Now, the entropic contributions do not depend on the properties of the solute but on the properties that change during the chemical reaction. The translational entropy (eqn (7)) depends on the relative reaction volume V_r(products)/V_r(reactants). The rotational entropy (eqn (8)) and cavitation entropy (eqn (9)) are also functions of the change in molecular volume or shape during the chemical reaction but are expressed here in terms of r_{gyr}/r_{cav} and Δ_rX, respectively. Comparison of eqn (4)–(6) *versus* eqn (7)–(9) reveals the drawback of current CSMs: the solvation entropy (eqn (3)) is parametrized into G_{nes} by considering a unimolecular process $A_{(g)} \rightarrow A_{(soln)}$ with constant particle number ($\sum\nu_i = 0$, shown for an arbitrary solute A). This implies no change in molecular shape and volume $\Delta V = 0$. Thus, G_{nes} cannot account for effects associated with changes in ΔV because its variation has not been considered during parametrization and entropic effects caused by changes in ΔV cannot be described by CSMs. This is illustrated by considering eqn (7)–(9) under the conditions of parametrization of CSMs, *i.e.*, $\sum\nu_i = 0$ and no change in molecular volume/shape. They individually add up to 0. In bimolecular reactions ($\sum\nu_i = -1$), however, these effects are significant because the particle number, volume, and shape change that is neglected in CSMs. To provide and estimate, we considered a dimerization reaction of a hypothetical monomer and assume $V_{mon} = 10^3$ Å^3 and $V_{dim} = 2V_{mon}$. Thus, $\Delta_r\Delta_{solv}S^{trans}$ contributes about $+4R$ (note: $V_{ideal} \approx 40 \times 10^3$ Å^3). For $\Delta_r\Delta_{solv}S^{rot}$, we obtain about $+2R$ assuming typical values for $r_{gyr}/r_{cav} \approx 0.5$. Lastly, the cavitation term contributes to about $+2R$ for apolar solvents (*n*-hexane, benzene) and about $+5R$ for polar solvents (DCM, THF, water) assuming $X = 1.3$, *i.e.*, the vdW volume of the monomer is twice the vdW volume of the solvent. Overall, this results in an estimate of up to $11R$ neglected entropic contributions for a hypothetical dimerization reaction (> -7 kcal mol^{-1} at room temperature). In other words, bimolecular reactions, *i.e.*, reactions with decreasing particle number along the reaction coordinate ($\sum\nu_i = -1$), suffer from an entropic penalty. The overestimation of the gas-phase entropic contributions arises from an inadequate description of the loss of degrees of freedom upon solvation. To correct this systematic error, we build on the limitations of G_{nes}. With $\Delta_r\Delta_{solv}S(\sum\nu_i = 0) = 0$ in hand (*vide supra*), going from a unimolecular reaction to a bimolecular reaction requires explicit consideration of eqn (7)–(9) to account for entropic effects due to changes in volume, *i.e.*, $\Delta_r\Delta_{solv}S^{trans}$ ($V_r \neq 1$), $\Delta_r\Delta_{solv}S^{rot}$($r_r' \neq 1$), and Δ_rS^{cav}($\Delta_rX \neq 0$). This leads to

$$\Delta_r\Delta_{solv}G = \Delta_rE_{elst} + \Delta_r\Delta_{solv}S(+\Delta_rG_{nes}) \quad (12)$$

where $\Delta_r\Delta_{solv}S$ can be regarded as an entropy-correction to $\Delta_r\Delta_{solv}G$ (eqn (12)). In other words, this expression corrects the solution-phase Gibbs free energy obtained by a classic computational protocol. The term $\Delta_r\Delta_{solv}S$ explicitly accounts for the changes that are not covered by G_{nes}. Furthermore, tests indicate that $\Delta_r\Delta_{solv}S$ is better used as a replacement for Δ_rG_{nes}, rather than being added to it, possibly due to double counting

and/or negligible apolar attractive interactions (*vide infra*). To substantiate the reliability of this approach, we compare it with the classic protocol for unimolecular reactions as a sanity check. According to our hypothesis, the correction term should vanish for unimolecular reactions, *i.e.*, $\Delta_r\Delta_{solv}S(\sum \nu_i = 0) \approx 0$ and $\Delta_r G_{nes}(\sum \nu_i = 0) \approx 0$.

Computational methods

All computations were performed with the ORCA software package (versions 4.2.0 and 4.2.1)[82,83] with tight SCF convergence criteria. For structure optimizations and analytical harmonic vibrational frequencies, we employed the PBEh-3c level of theory.[84] This hybrid DFT variant gives reliable structures and is feasible for routine computations. For the PBEh-3c computations, we used the grid4 integration grid as implemented in ORCA. Minima and transition states were characterized by the absence and presence of one imaginary frequency, respectively. Zero-point vibrational energies (ZPVEs) and thermal corrections were derived from unscaled harmonic frequencies and Grimme's quasi-rigid-rotor-harmonic-oscillator (qRRHO) approximation at the given temperatures as implemented in ORCA by default (cutoff frequency 100 cm^{-1}).[28] The rotational symmetry number was manually corrected if it had not been determined correctly by ORCA. When available, input structures were taken from a previous study.[66]

Implicit solvation

Bulk solvation was considered implicitly with the SMD model.[40] Thus, solvation free energies $\Delta_{solv}G$ were obtained at the PBE0[85] /def2-SVP level (grid4, finalgrid5) using gas-phase optimized structures. We point out that the accuracy of $\Delta_{solv}G$ will be highest if its computation is performed in comparable rigor as the parametrization of the particular solvent model.[29,43] All values are corrected for standard-state conditions at the given temperature unless otherwise noted. The solvents 1-methoxy-2-(2-methoxyethoxy)ethane (diglyme) and 1-decene are not included in the SMD model by default. We set their parameters manually (ε = 7.23,[86] n = 1.4097,[86] γ/γ_0 = 28.3,[87] β = 0.45 (assumed from dibutyl ether) for diglyme, and ε = 2.136,[86] n = 1.4215,[86] γ/γ_0 = 34.54,[88] for 1-decene).

Electronic energies

Highly accurate electronic energies are crucial to determine the entropic penalty reliably. Therefore, we employed representative top-tier DFT and WFT methods for single-point energy (SPE) computations.

For WFT, we utilized the domain-based local pair natural orbital coupled cluster theory with single, double, and perturbative triple excitations (DLPNO-CCSD(T)) with its default settings (NormalPNO).[17,18,20,89] Compared to the canonical CCSD(T) that is considered as the gold standard, the DLPNO approach covers up to 99.6% correlation energy. Thus, DLPNO-CCSD(T) is a highly efficient method for benchmarks[7] and general (bio)chemical applications.[16,19]

For DFT, we utilized a revised dispersion-corrected (D4),[90,91] spin-component-scaled (revDSD), double-hybrid functional (DHF) based on PBE exchange[92,93] and Perdew correlation (P86)[94,95] developed by Martin.[5,12] The so-called revDSD-PBEP86-D4 functional belongs to the best-performing double-hybrid methods within the highest rung of Jacob's ladder with a weighted mean absolute deviation over GMTKN55 (WTMAD2) of 2.33 kcal mol^{-1}. For integration, grid6 together with the chain-of-spheres approximation (RIJCOSX) was used as implemented in ORCA.[96]

All SPE computations utilize an Ahlrichs-type basis set with quadruple-zeta valence quality (def2-QZVPP)[97] and the appropriate auxiliary basis sets.[98,99]

Solvation entropies

We developed a script executable in a black-box type fashion on the command line to calculate the solvation entropy within seconds for any minimum/transition state structure following Garza's formalism.[80] This script is available from the authors upon request. Molecular volumes, converged to 10^{-4} $Å^3$, were computed analytically using Petitjean's algorithm (EPSTAB = 5×10^{-5}, NPERM = 7).[81] Details of the implementation are outlined in the ESI.† We validated our script by reproducing $\Delta_{solv}S$ of Garza's work. In agreement with that we obtained for 108 solvation entropies (excluding iodine and methyl ether as solvents) a mean error of −0.3 (−0.5) cal mol^{-1} K^{-1} and MAE of 2.4 (2.3) cal mol^{-1} K^{-1} (values in parentheses refer to Garza's work).

Results and discussion

Experimental benchmark set

For this study, we compiled an experimental benchmark set composed of solution-phase Gibbs free reaction/activation energies considering different solvents (Scheme 1). The benchmark set is structured as follows. First, we divided the set into unimolecular and bimolecular reactions. The former are required for a sanity check and the latter are used to determine the entropic penalty. Every reaction is assigned a reaction number (unimolecular 1–6, bimolecular 7a–15). Then, we further divided the set into reaction energies ($\Delta_r G$) and activation energies ($\Delta^{\ddagger}G$). We assigned every individual Gibbs free energy a number depending on the solvent (Table 1). Thus, to determine the entropic penalty, we considered 31 $\Delta_r G$ values in five different solvents (entries 9–39) and 22 $\Delta^{\ddagger}G$ values in 13 different solvents (entries 40–61). The entry number (first column of Table 1) and the reaction number (second column of Table 1) differ because for some reactions either multiple solvents or both activation and reaction parameters are considered.

To successfully quantify the entropic penalty by comparison of experimental Gibbs free energies with computed ones, we must ensure that our values are reliable and accurate. Otherwise, artefacts and/or propagated errors could be mistaken for the entropic penalty. Accordingly, appropriate reactions must be considered that meet certain requirements. To minimize the errors of the computed values, all reactants/products are neutral in net charge and exhibit a closed shell singlet state as the only

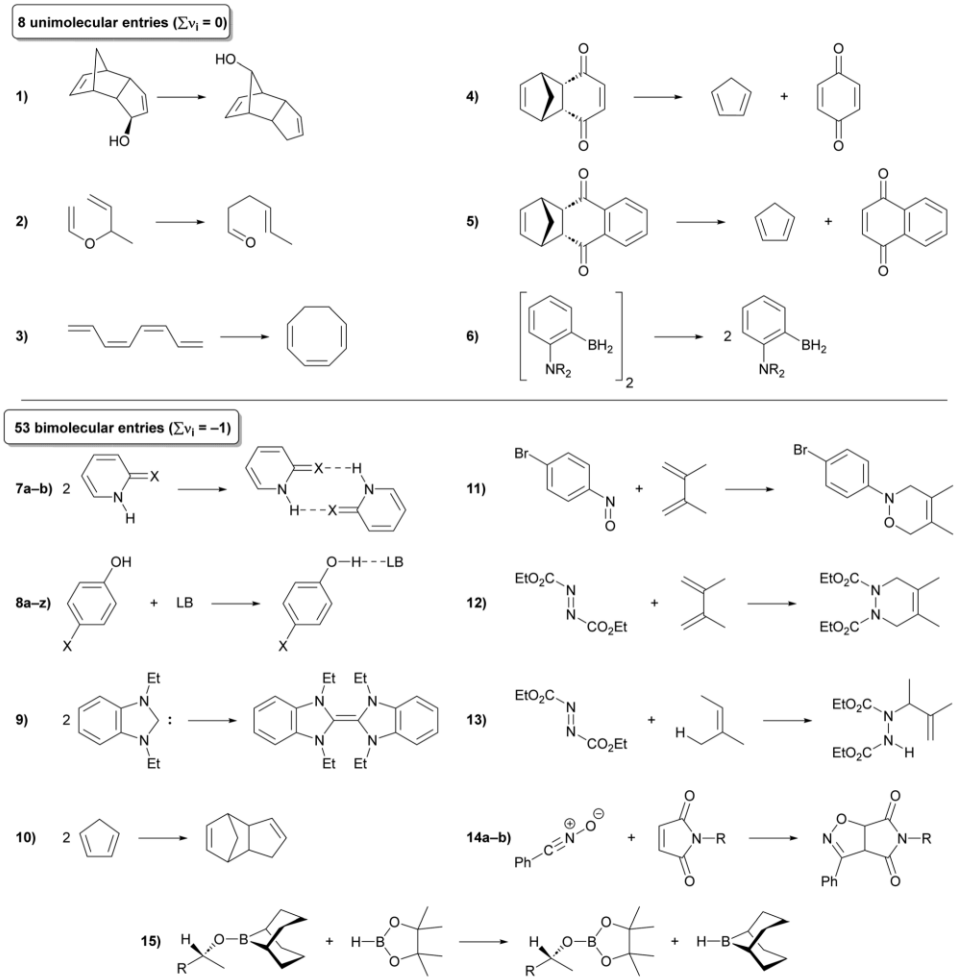

Scheme 1 Reactions included in the experimental benchmark set: 8 entries for unimolecular reactions, among them 7 barriers and 6 different solvents; and 53 entries for bimolecular reactions, among them 22 barriers and 15 different solvents. The solvents for each reaction are given in Table 1. Annotations: reaction 6: R = piperidyl; reaction 7: X = O (a), S (b); reaction 8: X = F, LB = Ph_2O (a), PhOMe (b), Et_2O (c), EtOAc (d), butanone (e), 3-(dimethylamino)propionitrile (f), anthrone (g), THF (h), 3-bromopyridine (i), cyclohexanone (j), quinoline (k), pyridine (l), Et_3N (m), *N*-methylformamide (n), Ph_2SO (o), 4-picoline (p), DMF (q), *N*,*N*-dimethylacetamide (r), DMSO (s), $Ph_3P{=}O$ (t), HMPA (u), $CypNH_2$ (v); X = H, LB = THF (w), butanone (x), DMF (y), pyridine (z); reaction 14: R = Et (a), *n*-Bu (b); reaction 15: R = C≡C–(*o*-tol).

relevant electronic ground state configuration. Furthermore, we chose reactions involving rather rigid molecules to minimize the conformational complexity.[100,101] Nevertheless, our benchmark set covers a variety of chemical reactions ranging from hydrogen bonding (entries 9–38), carbene-dimerization (entry 39), Diels–Alder reactions (entries 40–48), Alder-ene reactions (entries 49–51), 1,3-dipolar cycloadditions (entries 52–60) to a transfer borylation (entry 61). As proof of concept, we also investigated similar unimolecular reactions, *i.e.*, Cope rearrangements (entries 1–2), Claisen rearrangements (entries 3–4), electrocyclization (entry 5), retro-Diels-Alder reactions (entries 6–7), and a dissociation reaction of a dimeric borane (entry 8). Concerning the solvents, virtually any class is considered, *i.e.*, apolar/aprotic (*e.g.* ether, aliphatic/aromatic hydrocarbons), and polar/protic (water, alcohols).

Table 1 Experimental solution-phase reaction/activation energies and entropies (in kcal mol^{-1}) at the given temperature compiled from the literature. DCM and THF refer to dichloromethane and tetrahydrofuran, respectively. Note that the entry number (first column) and the reaction number (second column) differ because for some reactions either multiple solvents or both activation and reaction parameters are considered. The chemical reactions are depicted in Scheme 1

Unimolecular ($\sum \nu_i = 0$)

Entry	Reaction	Solvent	$\Delta_r G_{exp}$	$\Delta_r H_{exp}$	$-T\Delta_r S_{exp}$	T/K	Ref.
1	1	Decalin	−0.5 ± 1.1	−2.1 ± 0.5	1.6 ± 0.5	411	102

Entry	Reaction	Solvent	$\Delta^{\ddagger} G_{exp}$	$\Delta^{\ddagger} H_{exp}$	$-T\Delta^{\ddagger} S_{exp}$	T/K	Ref.
2	1	Decalin	31.6 ± 0.8	33.3 ± 0.4	−1.8 ± 0.4	411	102
3	2	1-Decene	29.6 ± 0.1	24.9 ± 0.1	4.7 ± 0.1	396	103
4	2	Benzonitrile	28.8 ± 0.3	24.5 ± 0.1	4.3 ± 0.1	383	103
5	3	*n*-Hexane	19.4	16.4	3.0	303	104
6	4	Benzene	29.3 ± 4.2	28.1 ± 2.1	1.2 ± 2.1	340	105
7	5	Benzene	28.8 ± 2.0	26.1 ± 1.0	2.7 ± 1.0	337	105
8	6	Chloroform	21.1 ± 5.4	18.4 ± 2.7	2.6 ± 2.7	329	106

Bimolecular ($\sum \nu_i = -1$)

Entry	Reaction	Solvent	$\Delta_r G_{exp}$	$\Delta_r H_{exp}$	$-T\Delta_r S_{exp}$	T/K	Ref.
9	7a	DCM	−4.1	−7.3	3.2	270	107
10	7b	Benzene	−2.8 ± 0.8	−6.9 ± 0.4	4.1 ± 0.4	314	52
11	8a	CCl_4	−0.4 ± 0.1	−1.9 ± 0.4	1.5 ± 0.4	298	108
12	8b	CCl_4	−0.5 ± 0.1	−3.1 ± 0.2	2.6 ± 0.2	298	108
13	8c	CCl_4	−1.4 ± 0.1	−5.6 ± 0.1	4.2 ± 0.1	298	108
14	8d	CCl_4	−1.5 ± 0.0	−4.7 ± 0.1	3.2 ± 0.1	298	108
15	8e	CCl_4	−1.6 ± 0.0	−5.2 ± 0.1	3.6 ± 0.1	298	108
16	8f	CCl_4	−1.7 ± 0.0	−5.8 ± 0.1	4.1 ± 0.1	298	108
17	8g	CCl_4	−1.7 ± 0.0	−5.6 ± 0.4	3.9 ± 0.4	298	108
18	8h	CCl_4	−1.7 ± 0.0	−5.6 ± 0.1	3.9 ± 0.1	298	108
19	8i	CCl_4	−1.8 ± 0.0	−6.2 ± 0.2	4.4 ± 0.2	298	108
20	8j	CCl_4	−1.8 ± 0.0	−5.8 ± 0.2	4.0 ± 0.2	298	108
21	8k	CCl_4	−2.5 ± 0.0	−7.4 ± 0.1	4.8 ± 0.1	298	108
22	8l	CCl_4	−2.6 ± 0.0	−7.1 ± 0.1	4.5 ± 0.1	298	108
23	8m	CCl_4	−2.6 ± 0.0	−8.9 ± 0.1	6.3 ± 0.1	298	108
24	8n	CCl_4	−2.7 ± 0.0	−5.5 ± 0.1	2.8 ± 0.1	298	108
25	8o	CCl_4	−2.8 ± 0.0	−6.3 ± 0.3	3.5 ± 0.3	298	108
26	8p	CCl_4	−2.8 ± 0.0	−7.3 ± 0.1	4.5 ± 0.1	298	108
27	8q	CCl_4	−2.8 ± 0.0	−6.6 ± 0.1	3.8 ± 0.1	298	108
28	8r	CCl_4	−3.3 ± 0.0	−7.4 ± 0.1	4.1 ± 0.1	298	108
29	8s	CCl_4	−3.5 ± 0.0	−6.6 ± 0.1	3.2 ± 0.1	298	108
30	8t	CCl_4	−4.3 ± 0.0	−7.4 ± 0.1	3.1 ± 0.1	298	108
31	8u	CCl_4	−4.9 ± 0.0	−8.0 ± 0.1	3.2 ± 0.4	298	108
32	8v	CCl_4	−2.2 ± 0.0	−7.5 ± 0.3	5.2 ± 0.3	298	108
33	8w	CCl_4	−1.6 ± 0.4	−5.6 ± 0.2	4.0 ± 0.2	298	108
34	8x	CCl_4	−1.4 ± 0.2	−5.2 ± 0.1	3.8 ± 0.1	298	108
35	8y	CCl_4	−2.8 ± 0.2	−6.9 ± 0.1	4.1 ± 0.1	298	108
36	8z	CCl_4	−2.3 ± 0.2	−7.0 ± 0.2	4.7 ± 0.2	298	108
37	8z	Benzene	−2.1 ± 0.1	−6.0 ± 0.1	3.9 ± 0.2	298	109
38	8z	Cyclohexane	−2.5 ± 0.0	−7.8 ± 0.1	5.3 ± 0.1	298	109
39	9	Diglyme	−3.1 ± 1.2	−13.7 ± 0.6	10.6 ± 0.6	348	110

Entry	Reaction	Solvent	$\Delta^{\ddagger} G_{exp}$	$\Delta^{\ddagger} H_{exp}$	$-T\Delta^{\ddagger} S_{exp}$	T/K	Ref.
40	10	CCl_4	23.2 ± 0.4	16.3 ± 0.2	6.9 ± 0.2	301	111
41	11	Cyclohexane	20.9 ± 1.7	10.7 ± 0.8	10.2 ± 0.9	301	112
42	11	Benzene	20.8 ± 1.4	10.0 ± 0.8	10.8 ± 0.6	301	112
43	11	1,4-Dioxane	20.3 ± 1.4	10.7 ± 0.8	9.6 ± 0.6	301	112
44	11	2-Propanol	20.5 ± 1.4	9.7 ± 0.8	10.8 ± 0.6	301	112
45	11	Methanol	20.4 ± 1.1	11.1 ± 0.6	9.3 ± 0.3	301	112
46	12	Cyclohexane	22.7 ± 1.3	10.7 ± 0.7	12.0 ± 0.6	301	112
47	12	Benzene	22.5 ± 1.0	9.9 ± 0.5	12.6 ± 0.5	301	112
48	12	1,4-Dioxane	22.4 ± 1.0	9.9 ± 0.5	12.5 ± 0.5	301	112
49	13	Cyclohexane	27.3 ± 1.0	12.7 ± 0.5	14.6 ± 0.5	348	113
50	13	Benzene	27.2 ± 0.7	12.6 ± 0.4	14.6 ± 0.3	348	113
51	13	Acetone	27.2 ± 0.4	12.4 ± 0.2	14.8 ± 0.2	348	113
52	14a	*n*-Hexane	18.1 ± 2.1	10.2 ± 1.6	8.0 ± 0.5	303	114
53	14a	Chloroform	19.1 ± 2.1	12.4 ± 1.6	6.7 ± 0.5	303	114
54	14a	1-Propanol	18.1 ± 2.1	10.2 ± 1.6	7.9 ± 0.5	303	114

Table 1 (*continued*)

Entry	Reaction	Solvent	$\Delta^{\ddagger}G_{exp}$	$\Delta^{\ddagger}H_{exp}$	$-T\Delta^{\ddagger}S_{exp}$	T/K	Ref.
55	14a	Water	18.1 ± 2.1	12.0 ± 1.6	6.1 ± 0.5	303	114
56	14a	Trifluoroethanol	19.1 ± 1.3	8.2 ± 0.8	10.9 ± 0.5	303	114
57	14b	*n*-Hexane	18.0 ± 1.0	9.8 ± 0.8	8.3 ± 0.2	303	114
58	14b	1-Propanol	18.0 ± 1.0	9.7 ± 0.8	8.3 ± 0.2	303	114
59	14b	Trifluoroethanol	19.0 ± 1.0	7.9 ± 0.8	11.1 ± 0.2	303	114
60	14b	Water	17.8 ± 1.0	11.5 ± 0.8	6.4 ± 0.2	303	114
61	15	THF	22.9 ± 4.3	16.3 ± 2.1	6.6 ± 2.2	308	115

Table 2 Comparison of experimental and computed Gibbs free energies for unimolecular reactions in six different solvents. Bulk solvation was considered implicitly with the SMD model. All energies in kcal mol^{-1}

			comp–exp	
Entry[a]	Reaction/Solvent	Δ_rG_{exp}	WFT[b]	DHF[c]
1	1/Decalin	−0.5 ± 1.1	−0.4	−0.4

			comp–exp	
Entry[a]	Reaction/Solvent	$\Delta^{\ddagger}G_{exp}$	WFT[b]	DHF[c]
2	1/Decalin	31.6 ± 0.8	3.0	1.1
3	2/1-Decene	29.6 ± 0.1	−0.1	0.3
4	2/Benzonitrile	28.8 ± 0.3	0.3	−1.6
5	3/*n*-Hexane	19.4[d]	0.0	−1.0
6	4/Benzene	29.3 ± 4.2	2.6	−0.4
7	5/Benzene	28.8 ± 2.0	2.2	−0.6
8	6/Chloroform	21.1 ± 5.4	0.0	0.1

[a] Refers to Table 1. [b] DLPNO-CCSD(T)/def2-QZVPP//PBEh-3c. [c] revDSD-PBEP86-D4/def2-QZVPP//PBEh-3c. [d] No experimental error given.

Sanity check (unimolecular: A → B)

To validate our concept and demonstrate its general purpose, we first consider unimolecular reactions (entries 1–8) comprising pericyclic reactions and a dissociation reaction (Table 2). Accordingly, we expect that the classic ΔG_{comp} is accurate because of the missing entropic penalty. Moreover, we expect a negligible contribution from our proposed correction (eqn (12)). Indeed, the ΔG_{comp} results are in excellent agreement with the experiments. We note that the DHF results are slightly superior to WFT. We further note that the computed barrier heights at DHF level are lower than the barriers at WFT by about 2–4 kcal mol^{-1}. Moreover, the entropy-related corrections to $\Delta^{\ddagger}\Delta_{solv}G$ according to eqn (12) are insignificant with $\lesssim$1.1 kcal mol^{-1} (see ESI†). Overall, our sanity check is successful.

Entropic penalty (bimolecular: A + B → C)

First, we will systematically determine the entropic penalty. For this purpose, we compare the experimental Gibbs free energies with the computed ones obtained by the classic computational protocol. We begin with the discussion of Δ_rG for bimolecular reactions (Fig. 2a). Visual inspection already shows an excellent agreement between WFT and DHF. Furthermore, the classic reaction energies are systematically overestimated by *ca.* 4 kcal mol^{-1}, which is attributed to the entropic penalty. Regarding the hydrogen-bonded adducts with Δ_rG_{exp} between −0.4 and −4.9 kcal mol^{-1} (entries 9–38), only three out of the 30 reaction energies are correctly calculated to be exergonic. Thus, the entropic penalty overcompensates weak interactions that are responsible for association in solution. It is noteworthy that hydrogen-bond formations were carried out in an apolar solvent that does not participate in explicit solvent interactions (CCl_4), and therefore these reactions should supposedly be well mimicked by classic implicit solvent models. Most significantly, the dimerization of the N-heterocyclic carbene (NHC) is overestimated by 19.4 and 17.7 kcal mol^{-1} at WFT and DHF level, respectively (entry 39). Thus, a slightly exergonic reaction (−3.1 kcal mol^{-1}) is predicted to be highly endergonic. These findings already demonstrate that the classic approach without any special attention to entropy has significant disadvantages that might produce misleading results when it comes to predictive applications or *in silico* design.

Next, we examined the entropic penalty of barrier heights (Fig. 2b). Opposed to reaction energies, the entropic penalty in

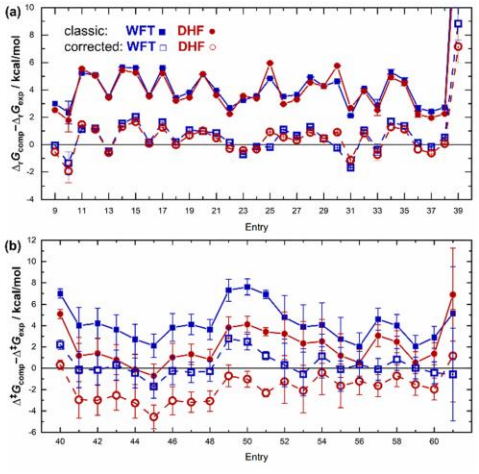

Fig. 2 Comparison of computed Gibbs free reaction energies (a) and Gibbs free activation energies (b) with experimental values and error bars for bimolecular reactions. Blue squares and red circles indicate computations at DLPNO-CCSD(T) and revDSD-PBEP86-D4 levels, respectively. Filled symbols refer to the classic approach without any correction. Hollow symbols include the entropy correction according to eqn (14) (*vide infra*). Connecting lines serve for clarity. Entries along the *x*-axis refer to Table 1.

barrier heights potentially depends on the reaction coordinate of the transition state. Following Hammond's postulate and Bell–Evans–Polanyi principle,[116–118] transition state structures appear "earlier", *i.e.*, are more strongly resembled by the reactant state, with increased exergonicity. This effect potentially counteracts the molecularity of a reaction. Visual inspection already confirms that the situation is not as clear as for the reaction energies. While there is a sizeable entropic penalty for barriers at the WFT level that is comparable to that of reaction energies (*ca.* 4 kcal mol^{-1}), the trend is different for DHF. We observe a systematic underestimation of the barrier heights by DHF compared to WFT (by *ca.* 2–3 kcal mol^{-1}). This seemingly counteracts the entropic penalty resulting in (partial) error compensation.

Correction of the entropic penalty

From a theoretical perspective, it is unclear if $\Delta_r G_{nes}$ plays a crucial role in eqn (12). All contributions other than electrostatic interactions $\Delta_r E_{elst}$ are parametrized into $\Delta_r G_{nes}$. Among them are most importantly apolar interactions and entropic contributions. Thus, considering $\Delta_r G_{nes}$ comes with the danger of double counting entropic contributions. Therefore, we tested the performance of both options

$$\Delta_r\Delta_{solv}G = \Delta_r E_{elst} + \Delta_r\Delta_{solv}S + \Delta_r G_{nes} \quad (13)$$

and

$$\Delta_r\Delta_{solv}G = \Delta_r E_{elst} + \Delta_r\Delta_{solv}S \quad (14)$$

to calculate $\Delta_r G_{soln}$. Then, we compared the results with the classic (uncorrected) $\Delta_r\Delta_{solv}G$ from SMD model (Fig. 3). We found that the correction according to eqn (14) is superior to eqn (13) in any scenario. This indicates that electrostatic interactions and entropic contributions alone cover the most dominant parts of the solvation process for chemical reactions. Apparently, remaining effects, *e.g.* apolar interactions, included in G_{nes} change hardly during chemical reactions and therefore vanish in $\Delta_r G_{nes}$ for the given benchmark set. Regarding the uncorrected values, we recognize that MAE $\approx$ MSE which reflects that the error due to the entropic penalty is a systematic effect. This situation changes for the corrected values causing MSEs $\leq$ 0.

Regarding the reaction energies, the entropy-correction greatly improves the accuracy for both WFT and DHF from $>$4 kcal mol^{-1} error to chemical accuracy (Fig. 3). The differences between the corrections based on eqn (13) and eqn (14) are subtle compared to the overall improvements. However, eqn (14) is superior (MAE $\leq$ 1 kcal mol^{-1}). This indicates problematic double counting of $\Delta_{solv}S$ and G_{nes} in eqn (13). We point out that all $\Delta_r G$ values benefit from the entropy-correction (Fig. 2a) and that 27 out of 30 hydrogen-bonded associates are accurately calculated to be exergonic. The dimerization of the NHC, however, is still endergonic with 5.7 kcal mol^{-1} (WFT) and 4.0 kcal mol^{-1} (DHF).

The situation for WFT barriers is similar to WFT reaction energies. Likewise, all WFT barriers benefit from entropy-correction that reduces the error from $>$4 kcal mol^{-1} to chemical accuracy (MAE $\leq$ 1 kcal mol^{-1}, eqn (14)).

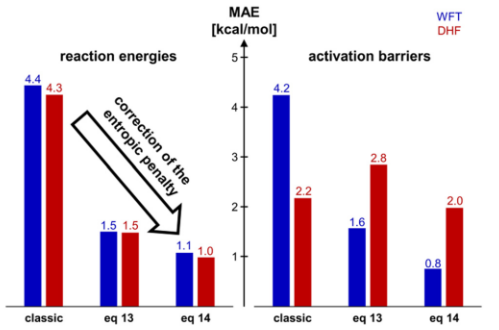

Fig. 3 Mean absolute errors (kcal mol^{-1}) of Gibbs free reaction energies (left) and Gibbs free activation barriers (right) for bimolecular reactions. Bulk solvation was considered implicitly with the SMD model according to the given equations. The classic SMD approach refers to eqn (2). WFT (blue) and DHF (red) refer to DLPNO-CCSD(T)/def2-QZVPP//PBEh-3c and revDSD-PBEP86-D4/def2-QZVPP//PBEh-3c level, respectively.

The situation is different in the case of barriers at the DHF level. Entropy-correction causes a shift from 2 kcal mol^{-1} overestimation to 2 kcal mol^{-1} underestimation (MAE $\approx$ $-$MSE). Thus, the correction scheme might imbalance the putative error cancellation between self-interaction and entropic penalty for DHF barriers. This suggests that uncorrected Gibbs free activation energies at the DHF level can be regarded as upper limit values and corrected energies as lower limit values.

Finally, we reformulate the proposed entropy-correction (eqn (14)) to

$$\Delta G_{corr} = \Delta_r\Delta_{solv}S - \Delta_r G_{nes} \quad (15)$$

so that it can be applied additively to the Gibbs free energy afterwards (eqn (16)).

$$\Delta G_{soln} = \Delta G_{soln}(\text{classic}) + \Delta G_{corr} \quad (16)$$

Conclusions

We compiled an experimental benchmark to quantify the entropic penalty for associative reaction pathways. We studied 53 bimolecular reactions (hydrogen bonding, NHC dimerization, Diels–Alder reactions, Alder-ene reactions, 1,3-dipolar cycloadditions, transfer borylation) in 15 different solvents computationally using state-of-the-art WFT (DLPNO-CCSD(T)) and DFT at a double-hybrid density functional level (revDSD-PBEP86-D4) together with an implicit solvent model. By comparison with 31 experimental Gibbs free reaction energies and 22 activation energies, we demonstrated that bimolecular reactions suffer from a sizeable entropic penalty resulting in an overestimation of the computed Gibbs free energies. This is because implicit solvent models were not trained on chemical transformations and cannot account for the loss of degrees of freedom upon solvation properly. Instead, gas-phase entropic contributions are overestimated causing errors of

2–11 kcal mol^{-1}. We note that reaction energies are more susceptible to the entropic penalty compared to barrier heights.

We proposed a universal, simple additive correction suitable for routine non-expert applications. This is based on Garza's physically sound formalism of the solvation entropy. Thus, it is possible to obtain accurate reaction and activation energies by calculating $\Delta_{solv}H$ independently using an existing implicit solvent model. As demonstrated with the SMD model, the purely electrostatic component suffices to approximate the enthalpy of solvation ($\Delta_r E_{elst} \approx \Delta_r\Delta_{solv}H$). Combined with $\Delta_r\Delta_{solv}S$, the resulting $\Delta_r\Delta_{solv}G$ comes virtually at the same computational cost as the classic expression but now correctly accounts for the change in molecularity during a reaction. We emphasize that the correction improved the accuracy of all reaction energies and all barriers at DLPNO-CCSD(T) level compared to the classic approach.

To conclude, we propose recommendations for the protocol presented in this work. For computations of solution-phase Gibbs free reaction energies $\Delta_r G_{soln}$ and activation barriers $\Delta^{\ddagger}G_{soln}$ at DLPNO-CCSD(T) level we recommend calculating the solvation energy using Garza's formalism for the entropy and only the electrostatic contribution from an implicit solvent model (eqn (14)). Especially equilibria of weakly bound associates, *e.g.* hydrogen bonding, or reactions with changes in particle number larger than 1, *e.g.* resting states in catalysis, are otherwise prone to false predictions. For barriers at the DFT level, we recommend using the presented approach to estimate the extent of entropic penalty. The obtained results may be regarded as a lower limit of the barrier height.

We expect this work to stimulate the development of further methodologies that address the treatment effects in condensed phases, in particular entropy. With highly accurate computational protocols for routine applications in gas-phase reactions in hand, special attention to entropic contributions in solution is vital.

Conflicts of interest

There are no conflicts to declare.

Acknowledgements

We thank the German research foundation (DFG, GE 3117/1-1), the Aventis Foundation, and the Fonds of the Chemical Industry for financial support. We would like to thank Dr Alejandro J. Garza for kind support during reproduction of the solvation entropies. We would also like to thank Tizian Müller for assistance with the development of the black-box algorithm. Continuous support by Prof. Dr Peter R. Schreiner, Prof. Dr Richard Göttlich, and Prof. Dr Hermann A. Wegner is acknowledged.

References

1 S. Grimme and P. R. Schreiner, *Angew. Chem., Int. Ed.*, 2018, **57**, 4170.
2 A. M. Teale, T. Helgaker, A. Savin, C. Adamo, B. Aradi, A. V. Arbuznikov, P. W. Ayers, E. J. Baerends, V. Barone, P. Calaminici, E. Cancès, E. A. Carter, P. K. Chattaraj, H. Chermette, I. Ciofini, T. D. Crawford, F. de Proft, J. F. Dobson, C. Draxl, T. Frauenheim, E. Fromager, P. Fuentealba, L. Gagliardi, G. Galli, J. Gao, P. Geerlings, N. Gidopoulos, P. M. W. Gill, P. Gori-Giorgi, A. Görling, T. Gould, S. Grimme, O. Gritsenko, H. J. A. Jensen, E. R. Johnson, R. O. Jones, M. Kaupp, A. M. Köster, L. Kronik, A. I. Krylov, S. Kvaal, A. Laestadius, M. Levy, M. Lewin, S. Liu, P.-F. Loos, N. T. Maitra, F. Neese, J. P. Perdew, K. Pernal, P. Pernot, P. Piecuch, E. Rebolini, L. Reining, P. Romaniello, A. Ruzsinszky, D. R. Salahub, M. Scheffler, P. Schwerdtfeger, V. N. Staroverov, J. Sun, E. Tellgren, D. J. Tozer, S. B. Trickey, C. A. Ullrich, A. Vela, G. Vignale, T. A. Wesolowski, X. Xu and W. Yang, *Phys. Chem. Chem. Phys.*, 2022, **24**, 28700.
3 A. J. Cohen, P. Mori-Sánchez and W. Yang, *Science*, 2008, **321**, 792.
4 R. Peverati and D. G. Truhlar, *Philos. Trans. R. Soc., A*, 2014, **372**, 20120476.
5 G. Santra and J. M. L. Martin, *Isr. J. Chem.*, 2020, **60**, 787.
6 P. Verma and D. G. Truhlar, *Trends Chem.*, 2020, **2**, 302.
7 L. Goerigk, A. Hansen, C. Bauer, S. Ehrlich, A. Najibi and S. Grimme, *Phys. Chem. Chem. Phys.*, 2017, **19**, 32184.
8 L. Goerigk and N. Mehta, *Aust. J. Chem.*, 2019, **72**, 563.
9 M. Bursch, J.-M. Mewes, A. Hansen and S. Grimme, *Angew. Chem., Int. Ed.*, 2022, **61**, e202205735.
10 Y.-S. Lin, G.-D. Li, S.-P. Mao and J.-D. Chai, *J. Chem. Theory Comput.*, 2013, **9**, 263.
11 N. Mardirossian and M. Head-Gordon, *Phys. Chem. Chem. Phys.*, 2014, **16**, 9904.
12 G. Santra, N. Sylvetsky and J. M. L. Martin, *J. Phys. Chem. A*, 2019, **123**, 5129.
13 J.-D. Chai and M. Head-Gordon, *J. Chem. Phys.*, 2009, **131**, 174105.
14 J. C. Sancho-García and C. Adamo, *Phys. Chem. Chem. Phys.*, 2013, **15**, 14581.
15 L. Goerigk and S. Grimme, *Wiley Interdiscip. Rev.: Comput. Mol. Sci.*, 2014, **4**, 576.
16 G. Bistoni, I. Polyak, M. Sparta, W. Thiel and F. Neese, *J. Chem. Theory Comput.*, 2018, **14**, 3524.
17 D. G. Liakos and F. Neese, *J. Chem. Theory Comput.*, 2015, **11**, 4054.
18 D. G. Liakos, M. Sparta, M. K. Kesharwani, J. M. L. Martin and F. Neese, *J. Chem. Theory Comput.*, 2015, **11**, 1525.
19 E. Paulechka and A. Kazakov, *J. Phys. Chem. A*, 2017, **121**, 4379.
20 C. Riplinger, B. Sandhoefer, A. Hansen and F. Neese, *J. Chem. Phys.*, 2013, **139**, 134101.
21 C. Riplinger, P. Pinski, U. Becker, E. F. Valeev and F. Neese, *J. Chem. Phys.*, 2016, **144**, 24109.
22 N. O. B. Lüttschwager, T. N. Wassermann, R. A. Mata and M. A. Suhm, *Angew. Chem., Int. Ed.*, 2013, **52**, 463.
23 J. N. Byrd, R. J. Bartlett and J. A. Montgomery, *J. Phys. Chem. A*, 2014, **118**, 1706.
24 D. G. Liakos and F. Neese, *J. Chem. Theory Comput.*, 2015, **11**, 2137.

25 X. He, L. Fusti-Molnar and K. M. Merz, *J. Phys. Chem. A*, 2009, **113**, 10096.
26 K. Range, D. Riccardi, Q. Cui, M. Elstner and D. M. York, *Phys. Chem. Chem. Phys.*, 2005, **7**, 3070.
27 O. Isayev, L. Gorb and J. Leszczynski, *J. Comput. Chem.*, 2007, **28**, 1598.
28 S. Grimme, *Chem. Eur. J.*, 2012, **18**, 9955.
29 J. Ho, A. Klamt and M. L. Coote, *J. Phys. Chem. A*, 2010, **114**, 13442.
30 S. Kozuch and S. Shaik, *Acc. Chem. Res.*, 2011, **44**, 101.
31 Q. Peng, F. Duarte and R. S. Paton, *Chem. Soc. Rev.*, 2016, **45**, 6093.
32 O. J. Conquest, T. Roman, A. Marianov, A. Kochubei, Y. Jiang and C. Stampfl, *J. Chem. Theory Comput.*, 2021, **17**, 7753.
33 S. Spicher, C. Plett, P. Pracht, A. Hansen and S. Grimme, *J. Chem. Theory Comput.*, 2022, **18**, 3174.
34 D. J. Tantillo, *J. Am. Chem. Soc.*, 2022, **144**, 13996.
35 J. N. Harvey, F. Himo, F. Maseras and L. Perrin, *ACS Catal.*, 2019, **9**, 6803.
36 A. Klamt, *J. Phys. Chem.*, 1995, **99**, 2224.
37 V. Barone and M. Cossi, *J. Phys. Chem. A*, 1998, **102**, 1995.
38 A. Klamt and G. Schüürmann, *J. Chem. Soc., Perkin Trans. 2*, 1993, 799.
39 F. Eckert and A. Klamt, *AIChE J.*, 2002, **48**, 369.
40 A. V. Marenich, C. J. Cramer and D. G. Truhlar, *J. Phys. Chem. B*, 2009, **113**, 6378.
41 M. Cossi, N. Rega, G. Scalmani and V. Barone, *J. Comput. Chem.*, 2003, **24**, 669.
42 C. J. Cramer and D. G. Truhlar, *Acc. Chem. Res.*, 2008, **41**, 760.
43 A. Klamt, B. Mennucci, J. Tomasi, V. Barone, C. Curutchet, M. Orozco and F. J. Luque, *Acc. Chem. Res.*, 2009, **42**, 489.
44 C. J. Cramer and D. G. Truhlar, *Acc. Chem. Res.*, 2009, **42**, 493.
45 J. Tomasi and M. Persico, *Chem. Rev.*, 1994, **94**, 2027.
46 J. Tomasi, B. Mennucci and R. Cammi, *Chem. Rev.*, 2005, **105**, 2999.
47 J. Zhang, H. Zhang, T. Wu, Q. Wang and D. van der Spoel, *J. Chem. Theory Comput.*, 2017, **13**, 1034.
48 J. Tomasi, *Theor. Chem. Acc.*, 2004, **112**, 184.
49 B. O. Leung, D. L. Reid, D. A. Armstrong and A. Rauk, *J. Phys. Chem. A*, 2004, **108**, 2720.
50 D. Ardura, R. López and T. L. Sordo, *J. Phys. Chem. B*, 2005, **109**, 23618.
51 B. Mondal, F. Neese and S. Ye, *Inorg. Chem.*, 2015, **54**, 7192.
52 D. Moran, K. Sukcharoenphon, R. Puchta, H. F. Schaefer, P. V. R. Schleyer and C. D. Hoff, *J. Org. Chem.*, 2002, **67**, 9061.
53 S. Kozuch, S. E. Lee and S. Shaik, *Organometallics*, 2009, **28**, 1303.
54 H. Ryu, J. Park, H. K. Kim, J. Y. Park, S.-T. Kim and M.-H. Baik, *Organometallics*, 2018, **37**, 3228.
55 U. Ryde and P. Söderhjelm, *Chem. Rev.*, 2016, **116**, 5520.
56 J. Cooper and T. Ziegler, *Inorg. Chem.*, 2002, **41**, 6614.
57 A. A. C. Braga, G. Ujaque and F. Maseras, *Organometallics*, 2006, **25**, 3647.
58 P. A. Dub and R. Poli, *J. Mol. Catal. A: Chem.*, 2010, **324**, 89.
59 N. Singh and A. Warshel, *J. Phys. Chem. B*, 2009, **113**, 7372.
60 D. H. Wertz, *J. Am. Chem. Soc.*, 1980, **102**, 5316.
61 H. Tamura, H. Yamazaki, H. Sato and S. Sakaki, *J. Am. Chem. Soc.*, 2003, **125**, 16114.
62 Z. Alassad, A. Nandi, S. Kozuch and A. Milo, *J. Am. Chem. Soc.*, 2023, **145**, 89.
63 S. Sakaki, T. Takayama, M. Sumimoto and M. Sugimoto, *J. Am. Chem. Soc.*, 2004, **126**, 3332.
64 M. Sumimoto, N. Iwane, T. Takahama and S. Sakaki, *J. Am. Chem. Soc.*, 2004, **126**, 10457.
65 R. E. Plata and D. A. Singleton, *J. Am. Chem. Soc.*, 2015, **137**, 3811.
66 S.-J. Li and D.-C. Fang, *Phys. Chem. Chem. Phys.*, 2016, **18**, 30815.
67 Z.-X. Yu and K. N. Houk, *J. Am. Chem. Soc.*, 2003, **125**, 13825.
68 C. T. Liu, C. I. Maxwell, D. R. Edwards, A. A. Neverov, N. J. Mosey and R. S. Brown, *J. Am. Chem. Soc.*, 2010, **132**, 16599.
69 L. M. Amzel, *Proteins*, 1997, **28**, 144.
70 M. Strajbl, Y. Y. Sham, J. Villà, Z.-T. Chu and A. Warshel, *J. Phys. Chem. B*, 2000, **104**, 4578.
71 J. González-Fabra, F. Castro-Gómez, W. M. C. Sameera, G. Nyman, A. W. Kleij and C. Bo, *Catal. Sci. Technol.*, 2019, **9**, 5433.
72 M. Tarrago, S. Ye and F. Neese, *Chem. Sci.*, 2022, **13**, 10029.
73 J. Song, E. L. Klein, F. Neese and S. Ye, *Inorg. Chem.*, 2014, **53**, 7500.
74 G. Xue, C. Geng, S. Ye, A. T. Fiedler, F. Neese and L. Que, *Inorg. Chem.*, 2013, **52**, 3976.
75 L. Watson and O. Eisenstein, *J. Chem. Educ.*, 2002, **79**, 1269.
76 G. Morales, R. Martínez and T. Ziegler, *J. Phys. Chem. A*, 2008, **112**, 3192.
77 R. L. Martin, P. J. Hay and L. R. Pratt, *J. Phys. Chem. A*, 1998, **102**, 3565.
78 R. Tanaka, M. Yamashita, L. W. Chung, K. Morokuma and K. Nozaki, *Organometallics*, 2011, **30**, 6742.
79 J. Hermans and L. Wang, *J. Am. Chem. Soc.*, 1997, **119**, 2707.
80 A. J. Garza, *J. Chem. Theory Comput.*, 2019, **15**, 3204.
81 M. Petitjean, *J. Comput. Chem.*, 1994, **15**, 507.
82 F. Neese, *Wiley Interdiscip. Rev.: Comput. Mol. Sci.*, 2012, **2**, 73.
83 F. Neese, *Wiley Interdiscip. Rev.: Comput. Mol. Sci.*, 2018, **8**, e1327.
84 S. Grimme, J. G. Brandenburg, C. Bannwarth and A. Hansen, *J. Chem. Phys.*, 2015, **143**, 54107.
85 C. Adamo and V. Barone, *J. Chem. Phys.*, 1999, **110**, 6158.
86 D. R. Lide, *CRC Handbook of Chemistry and Physics, Internet Version 2005*, CRC Press, Boca Raton, FL, 2005.
87 Y. Ren, F. Wang and Z. Huang, *Energy Fuels*, 2007, **21**, 1628.
88 J. J. Jasper and E. V. Kring, *J. Phys. Chem.*, 1955, **59**, 1019.
89 M. Saitow, U. Becker, C. Riplinger, E. F. Valeev and F. Neese, *J. Chem. Phys.*, 2017, **146**, 164105.

90 E. Caldeweyher, C. Bannwarth and S. Grimme, *J. Chem. Phys.*, 2017, **147**, 34112.
91 E. Caldeweyher, S. Ehlert, A. Hansen, H. Neugebauer, S. Spicher, C. Bannwarth and S. Grimme, *J. Chem. Phys.*, 2019, **150**, 154122.
92 J. P. Perdew, K. Burke and M. Ernzerhof, *Phys. Rev. Lett.*, 1996, **77**, 3865.
93 J. P. Perdew, K. Burke and M. Ernzerhof, *Phys. Rev. Lett.*, 1997, **78**, 1396.
94 J. P. Perdew, *Phys. Rev. B: Condens. Matter Mater. Phys.*, 1986, **33**, 8822.
95 J. P. Perdew, *Phys. Rev. B: Condens. Matter Mater. Phys.*, 1986, **34**, 7406.
96 R. Izsák and F. Neese, *J. Chem. Phys.*, 2011, **135**, 144105.
97 F. Weigend and R. Ahlrichs, *Phys. Chem. Chem. Phys.*, 2005, **7**, 3297.
98 F. Weigend, *Phys. Chem. Chem. Phys.*, 2006, **8**, 1057.
99 A. Hellweg, C. Hättig, S. Höfener and W. Klopper, *Theor. Chem. Acc.*, 2007, **117**, 587.
100 P. Pracht and S. Grimme, *Chem. Sci.*, 2021, **12**, 6551.
101 J. Gorges, S. Grimme, A. Hansen and P. Pracht, *Phys. Chem. Chem. Phys.*, 2022, **24**, 12249.
102 I. R. Bellobono, P. Beltrame, M. G. Cattania and M. Simonetta, *Tetrahedron*, 1970, **26**, 4407.
103 H. M. Frey and D. C. Montague, *Trans. Faraday Soc.*, 1968, **64**, 2369.
104 T. D. Goldfarb and L. Lindqvist, *J. Am. Chem. Soc.*, 1967, **89**, 4588.
105 B. S. Khambata and A. Wassermann, *J. Chem. Soc.*, 1939, 375.
106 J. Légaré Lavergne, A. Jayaraman, L. C. Misal Castro, É. Rochette and F.-G. Fontaine, *J. Am. Chem. Soc.*, 2017, **139**, 14714.
107 L. Szyc, J. Guo, M. Yang, J. Dreyer, P. M. Tolstoy, E. T. J. Nibbering, B. Czarnik-Matusewicz, T. Elsaesser and H.-H. Limbach, *J. Phys. Chem. A*, 2010, **114**, 7749.
108 E. M. Arnett, L. Joris, E. Mitchell, T. S. Murty, T. M. Gorrie and P. V. Schleyer, *J. Am. Chem. Soc.*, 1970, **92**, 2365.
109 J. N. Spencer, J. C. Andrefsky, A. Grushow, J. Naghdi, L. M. Patti and J. F. Trader, *J. Phys. Chem.*, 1987, **91**, 1673.
110 Y. Liu, P. E. Lindner and D. M. Lemal, *J. Am. Chem. Soc.*, 1999, **121**, 10626.
111 G. A. Benford, H. Kaufmann, B. S. Khambata and A. Wassermann, *J. Chem. Soc.*, 1939, 381.
112 G. Desimoni, G. Faita, P. P. Righetti and L. Toma, *Tetrahedron*, 1990, **46**, 7951.
113 G. Desimoni, G. Faita, P. P. Righetti, A. Sfulcini and D. Tsyganov, *Tetrahedron*, 1994, **50**, 1821.
114 T. Rispens and J. B. Engberts, *J. Phys. Org. Chem.*, 2005, **18**, 908.
115 K. Nicholson, J. Dunne, P. DaBell, A. B. Garcia, A. D. Bage, J. H. Docherty, T. A. Hunt, T. Langer and S. P. Thomas, *ACS Catal.*, 2021, **11**, 2034.
116 G. S. Hammond, *J. Am. Chem. Soc.*, 1955, **77**, 334.
117 R. P. Bell, *Proc. R. Soc. London, Ser. A*, 1936, **154**, 414.
118 M. G. Evans and M. Polanyi, *J. Chem. Soc., Faraday Trans.*, 1937, **33**, 448.

5.2 An *N*-Heterocyclic Quinodimethane: A Strong Organic Lewis Base Exhibiting Diradical Reactivity

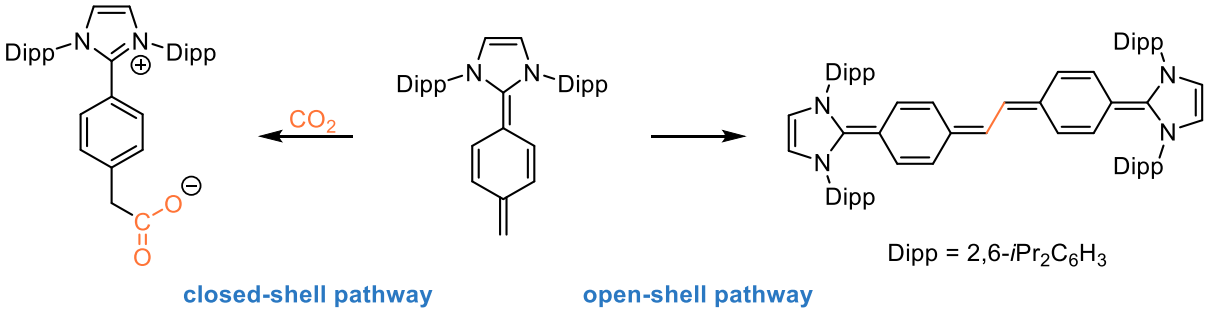

Wir berichten über die Darstellung eines neuen organischen σ-Donors mit einem C_6H_4-Linker zwischen einem *N*-heterozyklischen Carben (NHC) und einer exozyklischen Methylidengruppe, den wir als *N*-heterozyklisches Chinodimethan (engl. *N-heterocyclic quinodimethane*, NHQ) bezeichnen. Die Aromatisierung des C_6H_4-Linkers liefert eine entscheidende Triebkraft für die Reaktion des NHQs mit einem Elektrophil und macht das NHQ deutlich basischer als analoge NHCs und *N*-heterozyklische Olefine (NHOs), wie durch DFT-Berechnungen und Konkurrenzexperimente gezeigt werden konnte. In Lösung findet eine unerwartete Kopf–Kopf-Dimerisierung des NHQs unter formaler Wasserstofffreisetzung durch C−C-Kupplung der Methylidengruppen statt. DFT-Berechnungen zeigen, dass diese Reaktion über einen offenschaligen Singulettpfad verläuft, was auf einen diradikalischen Charakter des NHQs hinweist. Das Produkt dieser Dimerisierung kann als konjugiertes *N*-heterozyklisches Bis-Chinodimethan beschrieben werden, das laut zyklischer Voltammetrie ein starkes organisches Reduktionsmittel ist ($E_{1/2}$ = −1.71 V vs. Fc/Fc^+) und eine bemerkenswert kleine Singulett–Triplett-Lücke von $\Delta E_{S\rightarrow T}$ = 4.4 kcal mol^{-1} aufweist.

Referenz:

J. Ariai, M. Ziegler, C. Würtele, U. Gellrich, *Angew. Chem. Int. Ed.* **2024**, *63*, e202316720; *Angew. Chem.* **2024**, *136*, e202316720.

DOI (englische Fassung): 10.1002/anie.202316720

DOI (deutsche Fassung): 10.1002/ange.202316720

Akzeptiertes Manuskript online: 13. Dezember 2023

Final veröffentlichte Version online: 18. Januar 2024

How to cite: *Angew. Chem. Int. Ed.* **2024**, *63*, e202316720
doi.org/10.1002/anie.202316720

Organic Chemistry

An *N*-Heterocyclic Quinodimethane: A Strong Organic Lewis Base Exhibiting Diradical Reactivity

*Jama Ariai, Maya Ziegler, Christian Würtele, and Urs Gellrich**

Abstract: We report the preparation of a new organic σ-donor with a C_6H_4-linker between an *N*-heterocyclic carbene (NHC) and an exocyclic methylidene group, which we term *N*-heterocyclic quinodimethane (NHQ). The aromatization of the C_6H_4-linker provides a decisive driving force for the reaction of the NHQ with an electrophile and renders the NHQ significantly more basic than analogous NHCs or *N*-heterocyclic olefins (NHOs), as shown by DFT computations and competition experiments. In solution, the NHQ undergoes an unprecedented dehydrogenative head-to-head dimerization by C–C coupling of the methylidene groups. DFT computations indicate that this reaction proceeds via an open-shell singlet pathway revealing the diradical character of the NHQ. The product of this dimerization can be described as conjugated *N*-heterocyclic bis-quinodimethane, which according to cyclic voltammetry is a strong organic reducing agent ($E_{1/2} = -1.71$ V vs. Fc/Fc^+) and exhibits a remarkable small singlet–triplet gap of $\Delta E_{S-T} = 4.4$ kcal mol^{-1}.

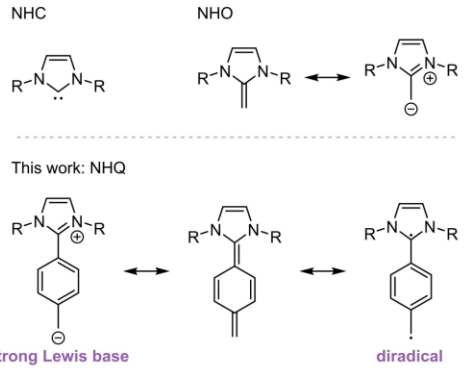

Scheme 1. The concept of this study: The insertion of a C_6H_4-linker between the NHC and the alkylidene group of an NHO should result in an NHQ that is a strong Lewis base with radical reactivity (NHC = *N*-heterocyclic carbene, NHO = *N*-heterocyclic olefin, NHQ = *N*-heterocyclic quinodimethane).

Introduction

N-heterocyclic carbenes (NHCs, Scheme 1, top left), which initially attracted attention as stable representatives of a compound class containing a carbon atom with an electron sextet, have since then found applications as organic σ-donors in catalysis, materials science, and medicine.[1] The extension of NHCs by an alkylidene group leads to *N*-heterocyclic olefins (NHO) that contain a strongly polarized C–C double bond (Scheme 1, top right).[2] When the association of imidazolium-based NHOs with an electrophile leads to aromatization of the *N*-heterocycle, the σ-donor capacity and the relative nucleophilicity of the NHOs exceed that of the corresponding NHCs.[3] In 2020, Hansmann et al. introduced mesoionic NHOs that cannot be described by a charge-neutral Lewis structure and represent the strongest donors and Lewis bases within the class of NHOs.[4] Due to their ability to act as strong σ-donors, NHOs have also been used as ligands in main group chemistry and transition metal catalysis.[5] In addition, their nucleophilicity has been exploited for applications in organocatalysis and polymer chemistry.[6] Furthermore, NHOs bind small molecules such as CO_2 and N_2O.[7] Binding of CO_2 enables its catalytic valorization while the reaction of NHOs with N_2O is of particular interest as it leads to organic super electron donors and diazoolefins. Since aromatization of the imidazoline system during the reaction of the NHO with an electrophile increases the σ-donor strength and the nucleophilicity of the NHO, we expected that a second aromatization would provide an additional driving force to the reaction with an electrophile. This assumption prompted us to investigate an NHO with a C_6H_4-linker between the NHC and the alkylidene group. (Scheme 1, lower panel).

Following the nomenclature of NHCs and NHOs, such a system could be denoted as *N*-heterocyclic quinodimethane (NHQ). Coordination of the NHQ to a Lewis acid (or protonation of the NHQ) would not only lead to aromatiza-

[*] J. Ariai, M. Ziegler, Dr. U. Gellrich
Institut für Organische Chemie, Justus-Liebig-Universität Gießen
Heinrich-Buff-Ring 17, 35392 Gießen (Germany)
E-mail: urs.gellrich@org.chemie.uni-giessen.de
Dr. C. Würtele
Institut für Anorganische und Analytische Chemie, Justus-Liebig-Universität Gießen
Heinrich-Buff-Ring 17, 35392 Gießen (Germany)

tion of the imidazoline ring but also of the C_6H_4-linker. Recent work by Coote, Sherburn and co-workers has confirmed that quinodimethanes (QDMs) exhibit the reactivity of a diradical.[8] Moreover, Ghadwal and co-workers showed that NHC-substituents are well suited to stabilize C-centered radicals.[9] Thus, the question further arises to what extent NHQs might exhibit radical reactivity.

Results and Discussion

We began our study with a computational evaluation of the effects of the C_6H_4-linker on the proton affinity (PA) of NHQ **1** with a Dipp-substituted (Dipp = 2,6-iPr$_2$C$_6$H$_3$) imidazolium backbone, through a comparison to the PAs of NHC **2** and NHO **3**; both of which are iconic examples of their respective compound classes. We chose the ωB97X functional together with the recent D4 correction, a combination which has been shown to be reliable for thermodynamics and kinetics, for this study.[10] For structure optimization, we used the efficient PBEh-3c composite method.[11] The comparison of the computed PAs shows that the PA of **3** is 2.8 kcal mol^{-1} higher than that of **2**. As hypothesized, the incorporation of a C_6H_4-linker at the C2 position has indeed a decisive effect on the basicity of **3**; the PA of NHQ **1** exceeds that of **3** by 22.9 kcal mol^{-1} (Figure 1).

NHQs with phenyl or cyano substituents at the exocyclic ylidene carbon have been reported previously.[12] However, their computed PAs are significantly lower than that of **1** (Figure S15), presumably as a consequence of the –I-effect of these substituents. Encouraged by the computed basicity of **1**, we turned to the synthesis of an imidazolium precursor that would allow us to generate **1** by deprotonation. To this end, imidazolium iodide **4** was synthesized by coupling **2** with 4-iodotoluene according to a procedure described by Ghadwal et al.[13] Treatment of **4** with KHMDS in THF-d_8 resulted in quantitative conversion to **1** (Scheme 2).

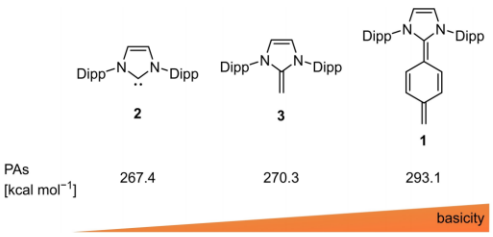

Figure 1. Proton affinities (PAs) of NHQ **1** in comparison to the structurally related NHC **2** and NHO **3** computed at ωB97X-D4/def2-QZVPP//PBEh-3c (Dipp = 2,6-iPr$_2$C$_6$H$_3$).

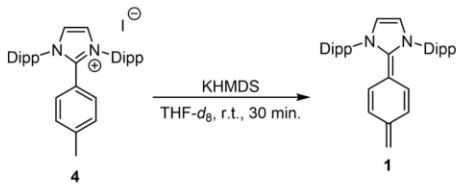

Scheme 2. In situ formation of **1** by deprotonation of **4** with KHMDS.

Diagnostic of the formation of **1** is a pronounced high-field shift in the signals attributable to the C_6H_4-linker in the ^{1}H NMR spectrum, indicating partial de-aromatization and the formation of a quinoidal structure (Figure S26). The CH_2 group appears in the ^{1}H NMR as a singlet at 3.46 ppm. Thus, the signal that can be assigned to this group is slightly low-field shifted compared to the signal of the methylidene group of NHO **3**, but significantly shifted to higher field than the signal of the methylidene group of the parent QDM *p*-xylylene.[14] Likewise, the ^{13}C NMR signal of the CH_2 group at 87.9 ppm is low-field shifted compared to **3** but high-field shifted compared to the signal of the exocyclic carbon of *p*-xylylene. In the course of deprotonation with KHMDS, the color of the reaction mixture turned dark green. UV/Vis spectra of **1** recorded in THF at various concentrations show an intense, sharp absorption band at 330 nm ($\varepsilon = 6.7(2)\cdot10^3$ cm^{-1}M^{-1}) and a broad band of low intensity at about 525 nm ($\varepsilon = 132(5)$ cm^{-1}M^{-1}) (Figure S8). TD-DFT calculations at the ωB97X-D4/def2-QZVPP//PBEh-3c level of theory allowed us to assign the excitation in the UV region to a π→π* transition (computed absorption at 363 nm) from the highest occupied molecular orbital (HOMO) to the lowest unoccupied molecular orbital (LUMO). The broad band in the visible region at 525 nm is almost undetectable when deprotonation is performed with NaHMDS while the HOMO→LUMO transition remains comparable, indicating that the color of the solution is caused by potassium adducts or traces of impurities (Figure S8 and Table S2). The calculations show that the largest coefficient of the HOMO of **1** in the closed-shell singlet state is indeed at the exocyclic methylidene group, as is the spin density of the triplet state of **1** (Figure 2).

We then turned our attention to an experimental assessment of the basicity of **1** by competition experiments. Therefore, imidazolium iodide **5** was added to a solution of **1**, which afforded NHO **3** in near quantitative yield

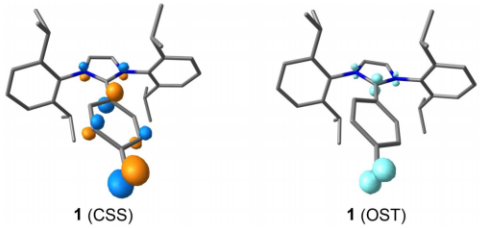

Figure 2. The HOMO of the closed-shell singlet state of **1** (left) and the total spin density of the triplet state of **1** (right). (CSS = closed-shell singlet, OST = open-shell triplet). Hydrogens are omitted for clarity.

supporting the computational result that the PA of NHQ **1** is higher than that of the analogous NHO **3** (Scheme 3).

To explore whether **1** acts not only as Brønsted but also as Lewis base, tris(pentafluoro)phenylborane $B(C_6F_5)_3$ was added to a solution of **1**, which allowed us to isolate the air- and moisture-stable $B(C_6F_5)_3$-adduct **6** in 41 % yield by column chromatography (Scheme 4). NMR analysis of **6** indicates that the formation of the Lewis adduct is accompanied by re-aromatization of the C_6H_4-linker (Figure S36). The C–C bond lengths of the C_6H_4-linker determined by single crystal X-ray diffraction (SCXRD) analysis of **6** support this assumption (Figure 3).[15]

When a THF solution of **1** was exposed to a CO_2-atmosphere, the immediate formation of a precipitate was observed. Filtration and crystallization of the solid from DCM/*n*-hexane allowed us to isolate the carboxylate **7**, which was characterized by NMR, IR, and ESI-MS, in 58 % yield (Scheme 5). The formation of the $B(C_6F_5)_3$-adduct **6** and carboxylate **7** shows that the lifetime of **1** allows its use as a Lewis base. However, attempts to isolate **1** are prevented by its slow conversion to new species in solution. We have followed the progress of this transformation by ^{1}H NMR spectroscopy (Scheme 6).

Already after one day, the appearance of a new set of signals is observed, indicating the emergence of a species with a quinoidal phenylene unit. This is evident from the appearance of two doublets at 5.60 and 5.41 ppm with a coupling constant of 10.3 Hz. In addition, a sharp singlet at 5.03 ppm indicates the formation of a new methylidene group. Within 20 days, the conversion of **1** is complete. When a THF-solution of the new species was overlaid with *n*-pentane and stored at −36 °C for several days, dark orange crystals formed. SCXRD analysis revealed that these crystals consist of the dimer **8**, which was isolated in 36 % yield (Figure 4). Significant alternation of the C–C bond lengths in the C_6H_4-linker of **8** revealed by SCXRD support that **8** is indeed best described as quinoidal structure. The NMR spectrum obtained upon dissolution of the crystals in THF-d_8 proves that the new species into which **1** converts in solution is indeed dimer **8** (Scheme 6). Apparently, **8** is formed by a C–C coupling between the methylidene groups of **1**. This reactivity seems to contradict the ground state polarity of **1**, as two nucleophilic centers react with each

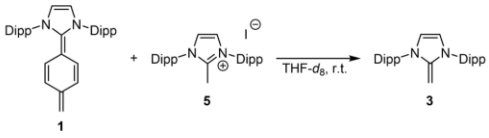

Scheme 3. Deprotonation of imidazolium iodide **5** by NHQ **1**.

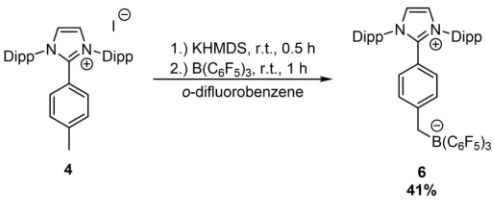

Scheme 4. Synthesis of the NHQ–$B(C_6F_5)_3$-adduct **6**.

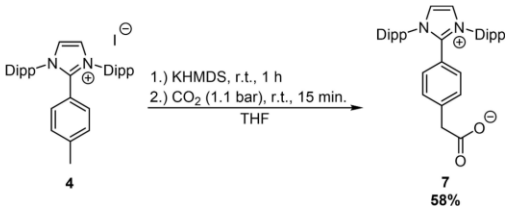

Scheme 5. Synthesis of carboxylate **7** by deprotonation of **4** and exposure to CO_2.

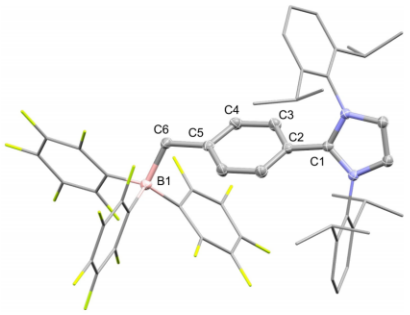

Figure 3. Molecular structure of **6** derived from SCXRD (50% probability ellipsoids, all hydrogens attached to carbons are omitted, Dipp-groups and C_6F_5-rings are shown in stick representation for clarity). Selected bond lengths: C1–C2: 1.466(4) Å, C2–C3: 1.391(4) Å, C3–C4: 1.389(4) Å, C4–C5: 1.401(4) Å, C5–C6: 1.506(4) Å, C6–B1: 1.660(4) Å.

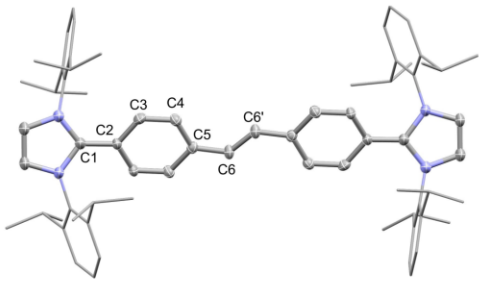

Figure 4. Molecular structure of **8** derived from SCXRD (50% probability ellipsoids, all hydrogens attached to carbons are omitted and Dipp-groups are shown in stick representation for clarity). Selected bond lengths and angles: C1–C2: 1.424(5) Å, C2–C3: 1.420(6) Å, C3–C4: 1.368(6) Å, C4–C5: 1.435(4) Å, C5–C6: 1.397(4) Å, C6–C6′: 1.400(5) Å, C5–C6–C6′: 127.7(3)°.

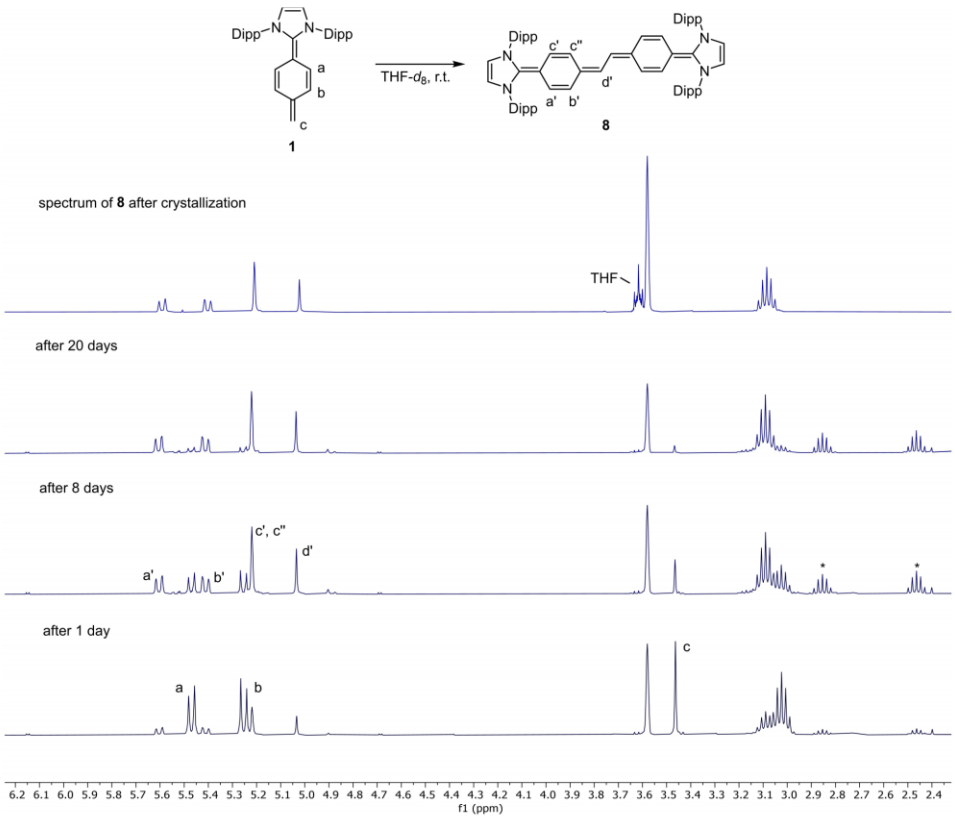

Scheme 6. Monitoring of the conversion of NHQ **1** to dimer **8** by ^{1}H NMR (400 MHz, 0.1 M in THF-d_8) and the ^{1}H NMR spectrum of dimer **8** isolated by crystallization. Signals marked with an asterisk can be assigned to imidazole **10** and 1,3-di(isopropyl)benzene.

other. However, the dimerization of QDMs such as *p*-xylylene is known, and recent computational and experimental studies provided conclusive evidence that this process is initiated by a C–C coupling between the exocyclic methylene carbons along an open-shell diradical pathway.[8,16,14] In addition, the dimerization of heteroatom-containing QDMs has been reported.[17] It is therefore reasonable to attribute the formation of **8** to such diradical coupling as well. We investigated this hypothesis with DFT calculations (Figure 5).

Consistent with the computational study by Sherburn and Coote, dimerization via an open-shell singlet (OSS) state is clearly preferred over the triplet pathway.[8] The calculated barrier of 21.5 kcal mol^{-1} agrees well with the experimental observation that dimerization proceeds, albeit slowly, at r.t. We observed experimentally an acceleration of the formation of **8** at high concentrations (Table S1), which, in agreement with the lack of a detectable intermediate, suggests that the initial C–C coupling is rate-limiting. In the OSS transition state structure, the NHQs are oriented *syn* to each other, presumably due to an attractive dispersive interaction between the bulky Dipp substituents. The product of the coupling, diradical **9**, is more stable in the triplet state, although the energetic preference over the open-shell singlet state is not significant. A feature of NHQ **1** dimerization that distinguishes it from QDM dimerization is that one equivalent of hydrogen is formally released upon formation of **8**. By ^{1}H NMR spectroscopy we observed signals appearing at 2.46 ppm and 2.85 ppm that could be assigned to the formation of by-products during the dimerization of **1**, in a ratio of 1:1 (Scheme 6). From the mother liquor of a crystallization of **8**, we were able to isolate imidazole **10** by column chromatography, thus unambiguously identifying it as one of these by-products. Based on the computational study and the experimental observations, we propose the following mechanism for the formation of dimer **8** and imidazole **10** (Scheme 7): An initial C–C coupling between the methylidene groups of NHQ **1** gives

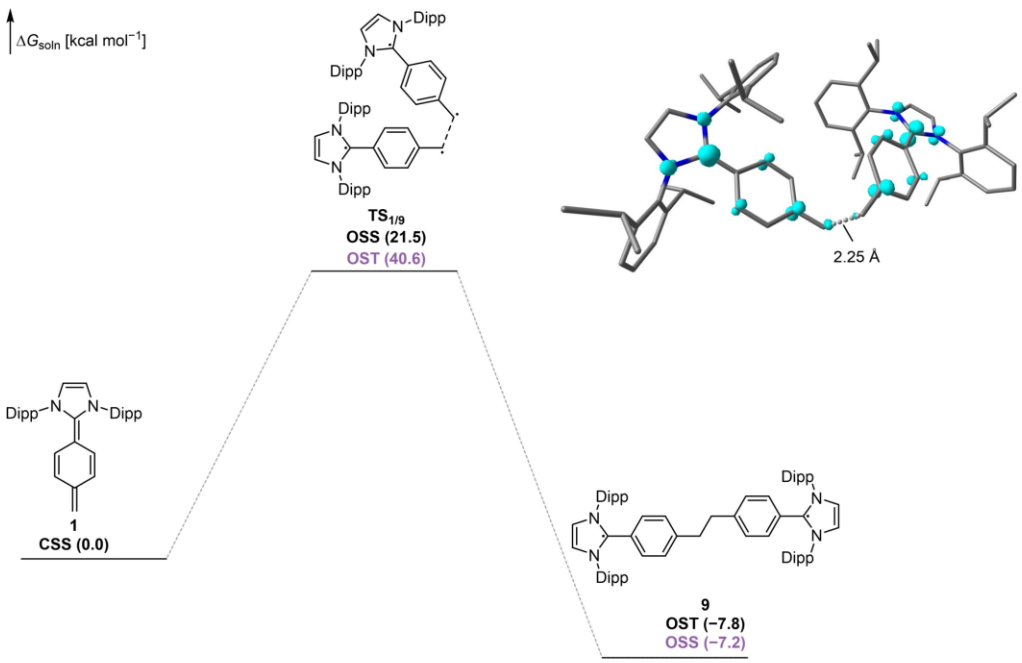

Figure 5. Gibbs free energies for the dimerization of **1** computed at ωB97X-D4/def2-TZVPP//PBEh-3c (CSS = closed-shell singlet, OSS = open-shell singlet, OST = open-shell triplet). Bulk solvation was considered implicitly with the SMD model for THF.[18] The inset shows the open-shell singlet state transition state structure of the C–C bond formation with the spin density.

rise to the diradical **9**. Hydrogen atom transfer (HAT) from diradical **9** to NHQ **1** yields **11** and radical **12**, a reaction that further substantiates the diradical character of **1**. The formation of imidazole **10** under the reaction conditions indicates that radical **12** is not stable and fragments by C–N scission. This mechanistic hypothesis is further supported by the experimental observation that treatment of imidazolium iodide **4** with one-electron reducing agent KC_8 leads directly to the formation of **10** (Figure S4). The radical fragmentation releases an aryl radical that can abstract a second hydrogen atom from **11**. This reaction step then leads to the formation of the dimer **8** and 1,3-di(isopropyl)benzene, the formation of which was experimentally secured by spiking the reaction solution with an authentic sample and analyzing it by ^{1}H NMR spectroscopy (Figure S3).

Dimer **8** constitutes a rare example of a conjugated bis-quinodimethane. For the related Wittig hydrocarbon and the parent bis(*p*-xylylene), which has been prepared in noble-gas matrices at cryogenic temperatures, a diradical character was discussed.[19] This prompted us to investigate the electronic properties of **8** in more detail. To assess the diradical character, we determined the singlet–triplet gap of **8** computationally at the ωB97X-D4/def2-QZVPP/PBEh-3c level of theory. The calculations show that **8** indeed has a remarkably small singlet–triplet gap of only $\Delta E_{S\rightarrow T} =$ 4.4 kcal mol^{-1}. This small energy gap and the intense blue color of **8** in solution indicate possible excitation with visible light. Therefore, we recorded UV/Vis absorption spectra at different concentrations of **8** in THF (Figure 6). We observed an intense absorption band over the entire visible range (400–800 nm) with a maximum at 650 nm ($\varepsilon = 3.8\text{-}(3)\cdot10^4$ cm^{-1} M^{-1}). Analogous to **1**, this is assigned to a HOMO→LUMO transition corresponding to a π→π* excitation, for which an absorption at 581 nm was computed at

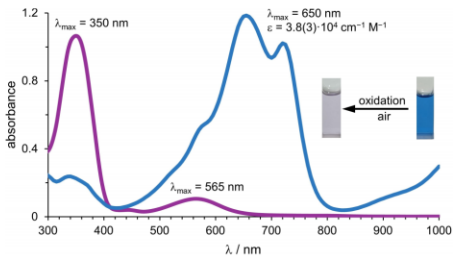

Figure 6. UV/Vis spectrum of **8** in THF (blue, $4\cdot10^{-5}$ mol/L). Upon placing the unmodified sample onto a bench, the color changes from blue to fade purple within minutes due to oxidation (purple).

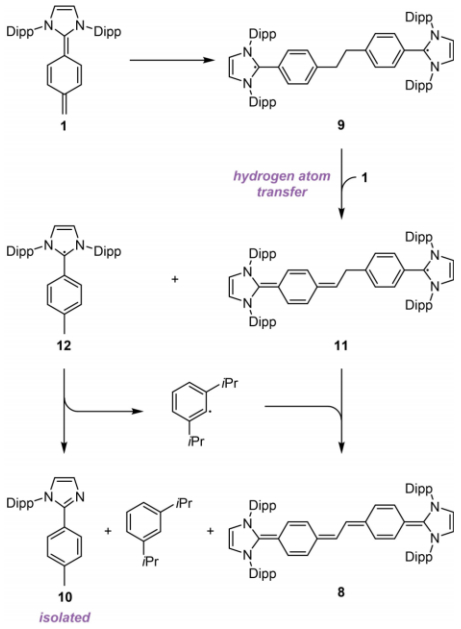

Scheme 7. Proposed mechanism for the formation of **8** and imidazole **10** by a sequence of C–C coupling, hydrogen atom transfer, and radical fragmentation.

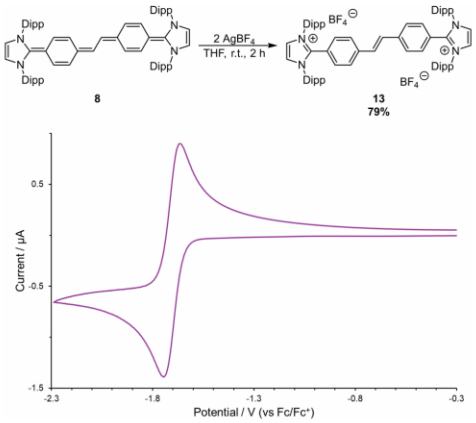

Figure 7. Oxidation of **8** with two equivalents $AgBF_4$ to afford **13** and its cyclic voltammogram ($E_{1/2} = -1.71$ V (vs Fc/Fc^+), 250 mV/s, CH_3CN (0.1 M nBu_4NPF_6)).

the ωB97X-D4/def2-TZVPP//PBEh-3c level by TD-DFT. The bathochromic shift of 320 nm and the greater intensity compared to **1** is likely caused by the extension of π-conjugation in **8** that lowers the HOMO–LUMO gap from 7.0 eV (**1**) to 5.0 eV (**8**). Exposure of **8** to air results in immediate color change from blue to purple. The oxidized species exhibits a broad band in the visible area with low intensity (565 nm) and an intense absorption in the UV region at 350 nm.

We assume that re-aromatization of the two quinoidal rings causes the facile oxidation of **8**. Consequently, we expect a sizeable reducing power from **8** driven by re-aromatization of the entire π-system. To elucidate the redox reactivity of **8** further, we oxidized **8** chemically with two equivalents $AgBF_4$ to obtain the dication **13** in 79 % yield, which was then used to study the redox reactivity of **8** by cyclic voltammetry (Figure 7). We observed a reversible redox event at $E_{1/2} = -1.71$ V (vs Fc/Fc^+) with constant anodic and cathodic peak potentials at scan rates of 50–500 mV/s (Figure S11). These results indicate that **8** is indeed a strong organic electron donor.[20]

Conclusion

In summary, we have prepared an NHQ and documented its dual reactivity: In its closed-shell form, it acts as a comparatively strong organic base with a proton affinity exceeding that of analogous NHCs and NHOs. However, it also exhibits diradical reactivity, as demonstrated by its head-to-head dimerization via an open-shell singlet pathway. This dimerization provides facile access to a conjugated *N*-heterocyclic bis-quinodimethane, which has a small singlet–triplet gap and is a potent organic electron donor. In summary, the present work describes a system that complements the repertoire of strong organic σ-donors with a representative that exhibits radical reactivity. We anticipate that the results presented here will stimulate the development of novel organic σ-donors that enable previously elusive transformations by unlocking radical pathways.

Acknowledgements

This work was supported by the German research foundation (DFG, GE 3117/1-1 and GE 3117/1-2). We thank Dr. H. Hausmann for assistance with NMR experiments and A. Danho, C. E. Campi, and S. Kunz for support with the CV measurements. Prof. P. R. Schreiner, Prof. R. Göttlich, and Prof. H. A. Wegner are acknowledged for their continuous support. Open Access funding enabled and organized by Projekt DEAL.

Conflict of Interest

The authors declare no conflict of interest.

Data Availability Statement

The data that support the findings of this study are available in the supplementary material of this article.

Keywords: DFT Computation · Dimerization · Diradical · Lewis Base · *N*-Heterocyclic Quinodimethane

[1] a) A. J. Arduengo, R. L. Harlow, M. Kline, *J. Am. Chem. Soc.* **1991**, *113*, 361; b) D. Enders, O. Niemeier, A. Henseler, *Chem. Rev.* **2007**, *107*, 5606; c) M. N. Hopkinson, C. Richter, M. Schedler, F. Glorius, *Nature* **2014**, *510*, 485.

[2] a) N. Kuhn, A. Abu-Rayyan, A. Al-Sheikh, K. Eichele, C. Maichle-Mößmer, M. Steimann, Sweidan, *Z. Naturforsch. B* **2005**, *60*, 294; b) N. Kuhn, H. Bohnen, D. Bläser, R. Boese, *Chem. Ber.* **1994**, *127*, 1405; c) N. Kuhn, H. Bohnen, J. Kreutzberg, D. Bläser, R. Boese, *J. Chem. Soc. Chem. Commun.* **1993**, 1136; d) N. Kuhna, H. Bohnena, G. Henkel, J. Kreutzberg, *Z. Naturforsch. B* **1996**, *51*, 1267.

[3] a) A. Fürstner, M. Alcarazo, R. Goddard, C. W. Lehmann, *Angew. Chem. Int. Ed.* **2008**, *47*, 3210; b) K. Powers, C. Hering-Junghans, R. McDonald, M. J. Ferguson, E. Rivard, *Polyhedron* **2016**, *108*, 8; c) B. Maji, M. Horn, H. Mayr, *Angew. Chem. Int. Ed.* **2012**, *51*, 6231.

[4] a) M. M. Hansmann, P. W. Antoni, H. Pesch, *Angew. Chem. Int. Ed.* **2020**, *59*, 5782; b) A. Eitzinger, J. Reitz, P. W. Antoni, H. Mayr, A. R. Ofial, M. M. Hansmann, *Angew. Chem. Int. Ed.* **2023**, *62*, e202309790.

[5] a) S. M. I. Al-Rafia, A. C. Malcolm, S. K. Liew, M. J. Ferguson, R. McDonald, E. Rivard, *Chem. Commun.* **2011**, *47*, 6987; b) A. Causero, H. Elsen, J. Pahl, S. Harder, *Angew. Chem. Int. Ed.* **2017**, *56*, 6906; c) Y. Wang, M. Y. Abraham, R. J. Gilliard, D. R. Sexton, P. Wei, G. H. Robinson, *Organometallics* **2013**, *32*, 6639; d) S. M. I. Al-Rafia, M. J. Ferguson, E. Rivard, *Inorg. Chem.* **2011**, *50*, 10543; e) A. Dumrath, X.-F. Wu, H. Neumann, A. Spannenberg, R. Jackstell, M. Beller, *Angew. Chem. Int. Ed.* **2010**, *49*, 8988; f) I. C. Watson, A. Schumann, H. Yu, E. C. Davy, R. McDonald, M. J. Ferguson, C. Hering-Junghans, E. Rivard, *Chem. Eur. J.* **2019**, *25*, 9678; g) A. Doddi, M. Peters, M. Tamm, *Chem. Rev.* **2019**, *119*, 6994.

[6] a) M. Blümel, R. D. Crocker, J. B. Harper, D. Enders, T. V. Nguyen, *Chem. Commun.* **2016**, *52*, 7958; b) U. Kaya, U. P. N. Tran, D. Enders, J. Ho, T. V. Nguyen, *Org. Lett.* **2017**, *19*, 1398; c) S. Naumann, A. W. Thomas, A. P. Dove, *Angew. Chem. Int. Ed.* **2015**, *54*, 9550; d) H. Wang, Q. Wang, J. He, Y. Zhang, *Polym. Chem.* **2019**, *10*, 3597; e) P. Walther, A. Krauß, S. Naumann, *Angew. Chem. Int. Ed.* **2019**, *58*, 10737.

[7] a) Y.-B. Wang, Y.-M. Wang, W.-Z. Zhang, X.-B. Lu, *J. Am. Chem. Soc.* **2013**, *135*, 11996; b) V. B. Saptal, B. M. Bhanage, *ChemSusChem* **2016**, *9*, 1980; c) W. Li, N. Yang, Y. Lyu, *J. Org. Chem.* **2016**, *81*, 5303; d) L. Y. M. Eymann, P. Varava, A. M. Shved, B. F. E. Curchod, Y. Liu, O. M. Planes, A. Sienkiewicz, R. Scopelliti, F. Fadaei Tirani, K. Severin, *J. Am. Chem. Soc.* **2019**, *141*, 17112; e) P. Varava, Z. Dong, R. Scopelliti, F. Fadaei-Tirani, K. Severin, *Nat. Chem.* **2021**, *13*, 1055; f) P. W. Antoni, C. Golz, J. J. Holstein, D. A. Pantazis, M. M. Hansmann, *Nat. Chem.* **2021**, *13*, 587.

[8] Z. Pei, N. L. Magann, M. J. Sowden, R. B. Murphy, M. G. Gardiner, M. S. Sherburn, M. L. Coote, *J. Am. Chem. Soc.* **2023**, *145*, 16037.

[9] a) D. Rottschäfer, B. Neumann, H.-G. Stammler, M. van Gastel, D. M. Andrada, R. S. Ghadwal, *Angew. Chem. Int. Ed.* **2018**, *57*, 4765; b) D. Rottschäfer, N. K. T. Ho, B. Neumann, H.-G. Stammler, M. van Gastel, D. M. Andrada, R. S. Ghadwal, *Angew. Chem. Int. Ed.* **2018**, *57*, 5838; c) R. S. Ghadwal, *Angew. Chem. Int. Ed.* **2023**, *62*, e202304665.

[10] a) J.-D. Chai, M. Head-Gordon, *J. Chem. Phys.* **2008**, *128*, 84106; b) M. Müller, A. Hansen, S. Grimme, *J. Chem. Phys.* **2023**, *158*, 14103; c) E. Caldeweyher, S. Ehlert, A. Hansen, H. Neugebauer, S. Spicher, C. Bannwarth, S. Grimme, *J. Chem. Phys.* **2019**, *150*, 154122; d) E. Caldeweyher, C. Bannwarth, S. Grimme, *J. Chem. Phys.* **2017**, *147*, 34112.

[11] S. Grimme, J. G. Brandenburg, C. Bannwarth, A. Hansen, *J. Chem. Phys.* **2015**, *143*, 54107.

[12] a) H. Song, E. Lee, *Chem. Eur. J.* **2023**, *29*, e202203364; b) K. C. Mondal, P. P. Samuel, H. W. Roesky, B. Niepötter, R. Herbst-Irmer, D. Stalke, F. Ehret, W. Kaim, B. Maity, D. Koley, *Chem. Eur. J.* **2014**, *20*, 9240; c) R. Gompper, H.-U. Wagner, E. Kutter, *Chem. Ber.* **1968**, *101*, 4144; d) F. Witte, P. Rietsch, S. Sinha, A. Krappe, J.-O. Joswig, J. P. Götze, N. Nirmalananthan-Budau, U. Resch-Genger, S. Eigler, B. Paulus, *J. Phys. Chem. B* **2021**, *125*, 4438; e) P. Srujana, T. Gera, T. P. Radhakrishnan, *J. Mater. Chem. C* **2016**, *4*, 6510.

[13] R. S. Ghadwal, S. O. Reichmann, R. Herbst-Irmer, *Chem. Eur. J.* **2015**, *21*, 4247.

[14] W. S. Trahanovsky, S. P. Lorimor, *J. Org. Chem.* **2006**, *71*, 1784.

[15] Deposition numbers 2304290 (for **6**), and 2304291 (for **8**) contain the supplementary crystallographic data for this paper. These data are provided free of charge by the joint Cambridge Crystallographic Data Centre and Fachinformationszentrum Karlsruhe Access Structures service.

[16] a) Y. Ito, S. Miyata, M. Nakatsuka, T. Saegusa, *J. Org. Chem.* **1981**, *46*, 1043; b) L. A. Errede, R. S. Gregorian, J. M. Hoyt, *J. Am. Chem. Soc.* **1960**, *82*, 5218.

[17] a) K. Oyaizu, K. Saito, E. Tsuchida, *Chem. Lett.* **2000**, *29*, 1318; b) Y. Liu, P. Varava, A. Fabrizio, L. Y. M. Eymann, A. G. Tskhovrebov, O. M. Planes, E. Solari, F. Fadaei-Tirani, R. Scopelliti, A. Sienkiewicz, C. Corminboeuf, K. Severin, *Chem. Sci.* **2019**, *10*, 5719.

[18] A. V. Marenich, C. J. Cramer, D. G. Truhlar, *J. Phys. Chem. B* **2009**, *113*, 6378.

[19] a) G. Wittig, B. Fartmann, *Justus Liebigs Ann. Chem.* **1943**, *554*, 213; b) R. Marquardt, W. Sander, T. Laue, H. Hopf, *Liebigs Ann. Recl.* **1996**, *1996*, 2039; c) D. Henseler, G. Hohlneicher, *J. Mol. Struct.* **1999**, *480–481*, 515.

[20] a) J. A. Murphy, *J. Org. Chem.* **2014**, *79*, 3731; b) H. S. Farwaha, G. Bucher, J. A. Murphy, *Org. Biomol. Chem.* **2013**, *11*, 8073; c) E. Doni, J. A. Murphy, *Chem. Commun.* **2014**, *50*, 6073.

Manuscript received: November 3, 2023
Accepted manuscript online: December 13, 2023
Version of record online: January 18, 2024

5.3 Facile (3+2) Cycloaddition between an *N*-Heterocyclic Olefin and Nitrous Oxide at Ambient Conditions

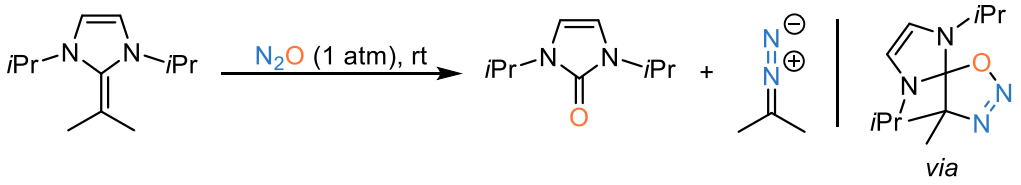

Wir berichten, dass ein *gem*-dimethyliertes *N*-heterozyklisches Olefin (NHO) mit N_2O bei Raumtemperatur reagiert und dabei ein Imidazolon sowie ein Azin bildet, welches aus dem intermediär gebildeten 2-Diazopropan entsteht. Dessen Bildung wurde indirekt durch eine Cycloaddition mit Norbornen nachgewiesen. Laut unseren Untersuchungen besteht die Reaktionsabfolge aus einer geschwindigkeitsbestimmenden 1,3-dipolarer Cycloaddition zwischen dem NHO und N_2O, gefolgt von einer Cycloreversion, die das Diazoalkan freisetzt. Der vorgeschlagene Mechanismus wird durch DFT-Berechnungen gestützt. Eine Eyring-Analyse mittels temperaturabhängiger ^{1}H-NMR-Spektroskopie ermöglichte die Bestimmung der Aktivierungsparameter der initialen 1,3-dipolaren Cycloaddition ($\Delta^{\ddagger}H$ = 11.2(4) kcal mol^{-1}, $\Delta^{\ddagger}S$ = −39.8(13) e.u., 293–308 K). Eine Analyse der Grenzorbitale zeigt, dass die Polarisation der π-Bindung des NHOs entscheidend dafür ist, dass die Cycloaddition unter milden Bedingungen abläuft.

Referenz:

J. Ariai, J. Becker, U. Gellrich, *Eur. J. Org. Chem.* **2024**, *27*, e202301252.

DOI: 10.1002/ejoc.202301252

Akzeptiertes Manuskript online: 22. Dezember 2023

Final veröffentlichte Version online: 12. Januar 2024

Check for updates

EurJOC
European Journal of Organic Chemistry

Research Article
doi.org/10.1002/ejoc.202301252

Chemistry Europe
European Chemical Societies Publishing

www.eurjoc.org

Facile (3+2) Cycloaddition between an *N*-Heterocyclic Olefin and Nitrous Oxide at Ambient Conditions

Jama Ariai,[a] Jonathan Becker,[b] and Urs Gellrich*[a]

We report that a *gem*-dimethylated *N*-heterocyclic olefin (NHO) reacts with N_2O at ambient pressure and room temperature to give an imidazolone and an azine formed from intermediately generated 2-diazopropane. The *in situ* formation of transient diazopropane was indirectly proven by its engagement in a facile cycloaddition with norbornene. According to our studies, the reaction sequence consists of a rate-determining (3+2) cycloaddition between the NHO and N_2O, followed by a cycloreversion that releases the diazoalkane. This mechanistic proposal is supported by DFT calculations. Eyring analysis using temperature-variable ^{1}H NMR spectroscopy allowed us to determine the activation parameters of the initial (3+2) cycloaddition ($\Delta^+H = 11.2(4)$ kcal/mol, $\Delta^+S = -39.8(13)$ e.u., 293–308 K). Frontier molecular orbital analysis shows that the polarization of the π-bond of the NHO decisively facilitates the cycloaddition.

Introduction

The valorization of atmospherically troublesome small molecules such as N_2O is relevant for developing sustainable synthetic methods.[1] The activation of the kinetically inert N_2O molecule by transition metal complexes[2] and, more recently, by p-block compounds such as frustrated Lewis pairs[3] and bismutidenes[4] has attracted considerable attention. Moreover, reactions of strong organic σ-donors with N_2O have been reported. Severin and co-workers showed that N_2O binds to *N*-heterocyclic carbenes (NHC) at ambient conditions to form a stable end-on adduct that decomposes at thermal or photochemical conditions.[5] Furthermore, the $AlCl_3$-mediated synthesis of azoimidazolium dyes from N_2O, NHCs, and arenes was reported.[6] In 2019, Severin and co-workers reported the formation of azo-bridged dimers of *N*-heterocyclic olefins (NHOs) upon exposure of N_2O to substituted NHOs in acetonitrile (Scheme 1).[7] In DMF or THF, however, a stable and isolable diazoalkene is formed.[8] At the same time, Hansmann and co-workers reported that exposure of the mesoionic NHO **1** to N_2O yields the diazoalkene **2**.[9] All the reported reactions between NHOs and N_2O are assumed to proceed *via* attack of the nucleophilic NHO to the *N*-terminus of N_2O. Subsequent proton migration(s) from the exocyclic CH_2 group and elimination render the azo-bridged dimer or diazoalkene.[10] Considering these results, we wondered what course the reaction of an NHO with N_2O would take if the subsequent proton migrations were not possible, for example, due to a dimethylated exocyclic methylene group.

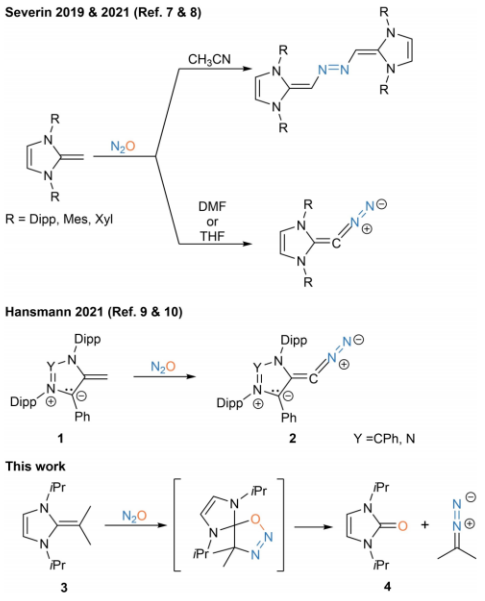

Scheme 1. Reported formation of NHO dimers and diazoalkenes upon exposure of N_2O to imidazole based NHOs bearing exocyclic CH_2 groups (Dipp = 2,6-diisopropylphenyl, Mes = 2,4,6-trimethylphenyl, Xyl = 2,6-dimethylphenyl).

[a] *J. Ariai, Dr. U. Gellrich*
Justus Liebig University
Institute of Organic Chemistry
Heinrich-Buff-Ring 17, 35392, Giessen, Germany
E-mail: urs.gellrich@org.chemie.uni-giessen.de
Homepage: https://www.uni-giessen.de/de/fbz/fb08/Inst/organische-chemie/Gellrich/

[b] *Dr. J. Becker*
Justus Liebig University
Institute of Inorganic and Analytical Chemistry
Heinrich-Buff-Ring 17, 35392, Giessen, Germany

Supporting information for this article is available on the WWW under https://doi.org/10.1002/ejoc.202301252

Research Article
doi.org/10.1002/ejoc.202301252

Results and Discussion

To address the above-mentioned question, we synthesized the *gem*-dimethylated NHO **3** and exposed a solution of it to an N_2O atmosphere. Complete conversion of **3** was observed overnight at room temperature. We monitored the reaction by ^{1}H NMR spectroscopy and observed a new set of signals that were tentatively assigned to the imidazolone **4** (Figure 1). Furthermore, two new singlets emerged at 1.83 ppm and 1.80 ppm indicating the formation of the azine **5**. After full characterization by NMR spectroscopy (^{1}H, ^{13}C, HH COSY, ^{1}H–^{13}C HMBC, ^{1}H–^{13}C HSQC, ^{1}H–^{15}N HMBC), we analyzed the reaction mixture by infrared (IR) spectroscopy (see the Supporting Information for details). Based on DFT computations of the harmonic vibrational frequencies scaled to account for anharmonicity (PBE0-D3(BJ)/def2-TZVP),[11,12,13,14,15] we simulated the IR spectra for a mixture of imidazolone **4** and acetone azine **5**.

Comparison of the computed and experimental IR spectra substantiated the formation of imidazolone **4** and azine **5**. Most significantly, we observed indicative IR bands at 1677 and 1637 cm^{-1} which we assigned to ν (C=O) of imidazolone (DFT scaled: 1715 cm^{-1}) and ν (C=N) of acetone azine (DFT scaled: 1665 cm^{-1}). The *in situ* yield, determined by quantitative ^{1}H NMR using mesitylene as internal standard, is 60% for imidazolone **4** and 27% for azine **5** (Scheme 2).

The imidazolone **4** was isolated in 53% yield after aqueous workup with HCl. However, under these conditions, acetone azine **5** is not isolable. Thus, we synthesized **5** independently following a procedure from Day and Whiting and unequivocally confirmed its formation during the reaction of NHO **3** and N_2O by NMR spiking experiments (see the Supporting Information).[16] At this point, we assumed that the reaction yields initially imidazolone **4** and 2-diazopropane, which disproportionates to acetone azine and dinitrogen under the reaction conditions (Scheme 2). The decomposition of diazoalkanes in the presence of base/nucleophiles is well documented in the literature.[17] NMR analysis of the reaction mixture also showed the formation of a by-product. While the yields of **4** and **5** are relatively insensitive to the concentration of NHO **3** (0.07–0.3 M), the formation of this by-product is favored at higher concentrations. Therefore, we performed the reaction at higher concentration, which allowed to isolate the by-product by column chromatography in 15% yield. Based on ^{1}H, ^{13}C and ^{15}N NMR spectroscopy, we were able to identify the by-product as azine **6**. Compound **6** exhibits an intense IR band at 1560 cm^{-1} assigned to the ν (C=N) of the azine moiety (DFT scaled: 1591 cm^{-1}). We were thus able to assign all IR bands appearing in the reaction mixture to compounds **4**, **5** and **6**. Screening the reaction conditions, we found that the reaction tolerates the presence of bases. This allows the formation of **3** *in situ* from the bench-stable imidazolium iodide salt **7** (Scheme 3).

Screening different bases (see the Supporting Information), we found that typical bases used for the formation of NHOs, such as KHMDS and KO*t*Bu, work well in this reaction. The 2:1 ratio, at which imidazolone **4** and azine **5** are obtained, indicates that 2-diazopropane is conserved as acetone azine. To further support the initial formation of 2-diazopropane during the reaction of **3** with N_2O, we intended to trap this diazo compound by an 1,3-dipolar cycloaddition with norbornene. Thus, we carried out the reaction in the presence of one equivalent of norbornene at the identical conditions, *i.e.*, 1 atm N_2O at room temperature (Scheme 4).

Under these conditions, the yield of the imidazolone **4** is maintained (62%) while only traces of acetone azine are present according to quantitative ^{1}H NMR. Instead, the cycloaddition product **8** is formed in moderate yield (49%).[18] The conversion of norbornene (61%) is limited by the yield of imidazolone and the associated yield of 2-diazopropane (see Scheme 2). Similar results are obtained when the NHO is formed *in situ* with KHMDS. We note that while established protocols for the

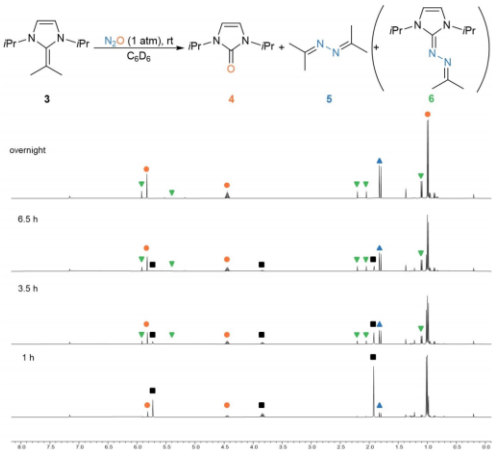

Figure 1. Reaction of NHO **3** with N_2O (1 atm) at room temperature monitored by ^{1}H NMR (400 MHz, C_6D_6). Black squares, orange circles, blue triangles pointing up, and green triangles pointing down highlight the signals assigned to NHO **3**, imidazolone **4**, azine **5**, and azine **6**, respectively. (*Vide infra* for details regarding the broadened heptet of **6** at 5.39 ppm).

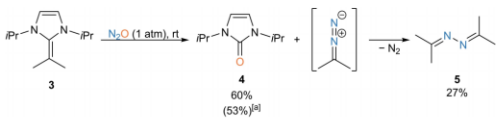

Scheme 2. Reaction of **3** with N_2O and the proposed intermediate formation of 2-diazopropane. Conversion and yields according to quantitative ^{1}H NMR unless stated otherwise.[a] Yield of isolated compound at preparative scale.

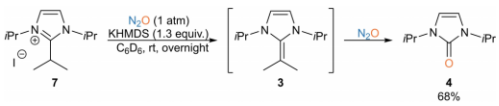

Scheme 3. *In situ* formation of the NHO by deprotonation in the presence of ambient N_2O in C_6D_6. Yield according to quantitative ^{1}H NMR.

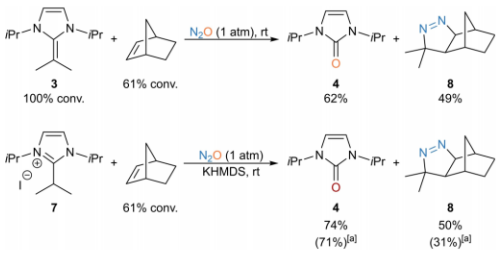

Scheme 4. Trapping of 2-diazopropane, generated by exposure of NHO **3** to N_2O, by 1,3-dipolar cycloaddition with norbornene. Conversion and yields according to quantitative ^{1}H NMR.[a] Yields of isolated products are given in parenthesis.

valorization of N_2O focus on its use as oxidant,[4,19] the reaction described herein is a rare example of the formation of a diazoalkane from N_2O.[2b,20] To gain insight into the reaction mechanism, we investigated the kinetics of the reaction of **3** with N_2O by temperature-variable ^{1}H NMR spectroscopy in C_6D_6 (Figure 2).

This study revealed a first-order dependence for the reaction rate with respect to NHO **3** and allowed us to determine the activation parameters by Eyring analysis: $\Delta^{\ddagger}H = 11.2(4)$ kcal/mol and $\Delta^{\ddagger}S = -39.8(13)$ e.u.[21] The highly negative activation entropy is indicative of an ordered transition state as in a cycloaddition reaction. Thus, we assume that the reaction of NHO **3** with N_2O commences with a (3 + 2) cycloaddition, followed by a cycloreversion that liberates the 2-diazopropane. The (3 + 2) cycloaddition between olefins and N_2O has been reported previously but requires usually harsh and technically demanding reaction conditions.[22] Even the reaction with highly reactive strained cycloalkynes requires an elevated N_2O pressure (15–75 bar).[20c] In this regard, it is remarkable that the cycloaddition between the NHO **3** and N_2O reported herein takes place already at room temperature at ambient pressure. To rationalize the facility of the 1,3-dipolar cycloaddition between NHO **3** and N_2O, we considered the frontier Kohn-Sham orbitals (Figure 3).[23,24] By inspection of the orbital levels, it is evident that the reaction proceeds by interaction of the lowest unoccupied molecular orbital (LUMO) of N_2O with the highest occupied molecular orbital (HOMO) of NHO **3**. The largest coefficient of the LUMO of N_2O is on the *N*-terminus. The HOMO of the NHO is strongly polarized towards the exocyclic carbon and thereby reflects the ylidic nature of the NHO. This is in contrast to ordinary alkene/alkyne functional groups, which lack this orbital polarization.

We further studied the reaction of **3** with N_2O computationally with the revised spin-component-scaled double-hybrid functional revDSD-PBEP86[25] in conjunction with the D4 dispersion correction[26] and the quadruple-zeta basis set def2-QZVPP (Figure 4). Solvent effects were considered implicitly using the SMD model for benzene.[27] Lowest energy conformations of all minima and transition state structures were obtained by automated exploration of conformational chemical space using CREST.[28] We assumed initial formation of the van-der-Waals complex **vdW1**. According to the computations, the end-on addition of the NHO **3** to N_2O that yields zwitterion **10** is endergonic and requires a high kinetic barrier of 28.0 kcal mol^{-1}. The (3 + 2) cycloaddition between N_2O and the double bond of **3** in which the exocyclic CMe_2 group binds to the terminal nitrogen of N_2O ($\mathbf{TS_{vdW1/9}}$) is with 23.3 kcal mol^{-1} kinetically preferred. The computed activation barrier for this initial cycloaddition is in excellent agreement with the kinetic barrier of $\Delta^{\ddagger}G_{298} = 23.0$ kcal mol^{-1} determined by Eyring analysis (Figure 2). The transition state structure shows a bent N_2O unit (143°) with the formation of the C–N bond (2.11 Å) preceding the C–O bond (2.92 Å) formation. This dominant C–N interaction is in agreement with the FMO-representation and supports the interpretation that the reaction is controlled by orbital interactions (Figure 3). The formation of the spirocyclic intermediate **9** is only slightly exergonic relative to **vdW1**. However, its fragmentation *via* a retro (3 + 2) cycloaddition

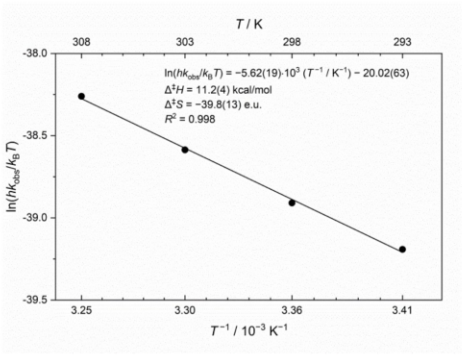

Figure 2. Determination of the activation enthalpy $\Delta^{\ddagger}H$ and activation entropy $\Delta^{\ddagger}S$ according to Eyring equation. Rate constants were obtained by variational temperature ^{1}H NMR analysis (293–308 K, C_6D_6) of the first-order decay of NHO **3** exposed to N_2O using mesitylene as internal standard.

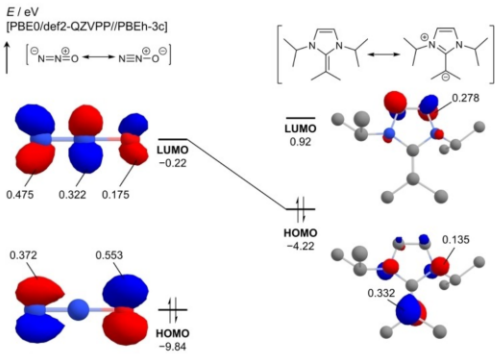

Figure 3. Canonical Kohn–Sham molecular orbitals and atomic coefficients computed at PBE0/def2-QZVPP//PBEh-3c level of theory. For brevity, degenerate orbitals of N_2O are omitted. Colour code for the depiction of the molecular structures: C in grey, N in blue, O in red, and H omitted for clarity.

Research Article
doi.org/10.1002/ejoc.202301252

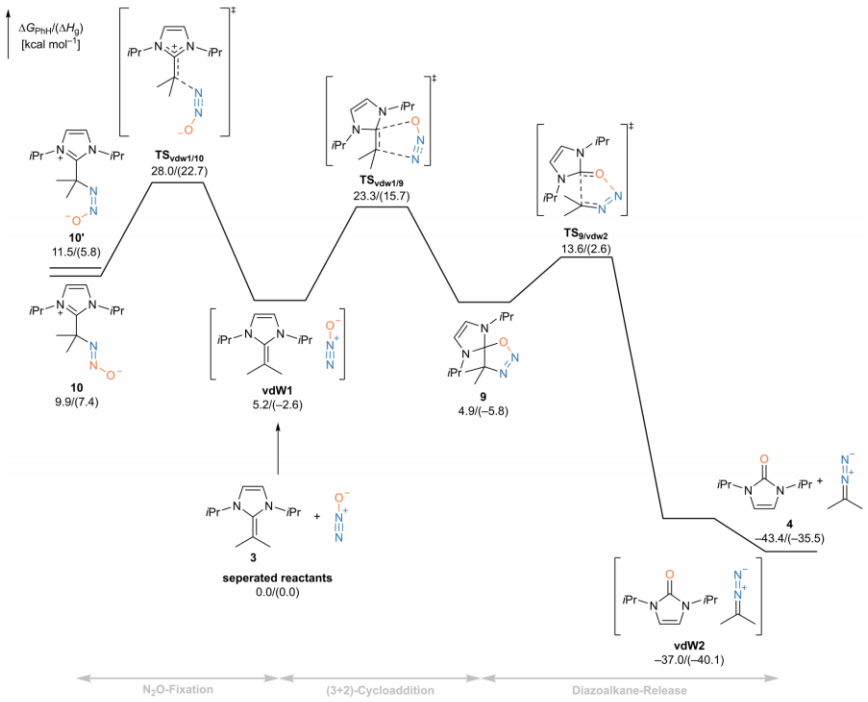

Figure 4. Gibbs free energies in benzene and gas phase enthalpies of the formation of 2-diazopropane upon exposure of **3** to N_2O computed at revDSD-PBEP86-D4/def2-QZVPP//PBEh-3c level. Solvent effects were implicitly considered with the SMD model.

requires only a moderate activation barrier of less than 10 kcal mol^{-1}. Regarding the transition state structure ($\mathbf{TS_{9/vdW2}}$), the diazoalkane moiety is bent by 133° and the scission of the N–O bond (2.10 Å) is more developed than the C–C scission (1.79 Å). Furthermore, this elementary step, that yields the imidazolone **4** and 2-diazopropane, is according to the computations highly exergonic. The overall kinetic barrier of the reaction between the separated reactants and the transition state of the (3+2) cycloaddition is computed to be 23.3 kcal mol^{-1}. Finally, we noted that the reaction described herein is sensitive regarding the substitution pattern of the NHO: When an NHO with 2,6-diisopropylphenyl instead of the isopropyl substituents at nitrogen is exposed to N_2O, no reaction is observed. The barrier of the cycloaddition of such an NHO with 2,6-diisopropylphenyl substituents at nitrogen with N_2O is 29.1 kcal/mol and therefore increased by 5.8 kcal/mol compared to the isopropyl derivative **3**. Likewise, NHOs with an imidazolidine backbone do not show any reactivity towards N_2O.

Conclusions

In summary, we have documented that NHO **3** reacts with N_2O at ambient conditions to give an imidazolone and a transient diazoalkane. According to our kinetic and computational studies, this reaction proceeds *via* a sequence of (3+2)-cycloaddition and cycloreversion. FMO analysis shows that the orbital polarization of the NHO enhances the orbital interactions with N_2O, promoting the rate-determining cycloaddition. The reaction also works when the NHO is formed *in situ* by deprotonation of a bench-stable imidazolium salt. This reaction pathway is unlocked by a *gem*-dimethyl substitution at the reactive exocyclic carbon atom, which prevents proton migration within an NHO–N_2O adduct. Complementary to established protocols for the valorization of N_2O which focus on its use as oxidant, this reaction is a rare example of the formation of a diazoalkane from N_2O. We expect this discovery to stimulate the development of synthetic protocols for the valorization of N_2O.

Experimental Section

General procedure for the activation of N_2O: In a nitrogen-filled glovebox, NHO **3** (9.5 mg, 0.05 mmol) was dissolved in 0.4 mL C_6D_6 and transferred to an NMR tube with J. Young valve. In a fume hood, the solution was degassed by three freeze-pump-thaw cycles. A balloon, connected to a vacuum line and an N_2O cylinder *via* a three-way valve, was purged multiple times with N_2O. The NMR tube, connected to the filled balloon and a vacuum line *via* three-way valve, was exposed to the N_2O atmosphere for a short duration after multiple purging. The reaction proceeded in a closed tube under a static N_2O atmosphere and full conversion was achieved overnight. For *in situ* formation of NHO **3**, 1,2,3-triisopropylimidazolium iodide **7** (16 mg, 0.05 mmol) was suspended in a KHMDS (13 mg, 1.3 equiv.) solution of 0.4 mL C_6D_6 in an NMR tube with J. Young valve.

Trapping of 2-Diazopropane with Norbornene: In a nitrogen-filled glovebox, NHO **3** (9.2 mg, 0.047 mmol), norbornene (4.5 mg, 0.049 mmol), and mesitylene (6.96 μL, 0.050 mmol) were dissolved in 0.4 mL C_6D_6 and transferred to an NMR tube with J. Young valve. In a fume hood, the solution was degassed by three freeze-pump-thaw cycles. A balloon, connected to a vacuum line and an N_2O cylinder *via* a three-way valve, was purged multiple times with N_2O. The NMR tube, connected to the filled balloon and a vacuum line *via* a three-way valve, was exposed to the N_2O atmosphere for a short duration after multiple purging. The reaction proceeded in a closed tube under a static N_2O atmosphere and full conversion was achieved overnight. The NMR data are consistent with literature reports.[18]

1,3-Diisopropyl-2-(1-methylethylidene)imidazoline 3: To a 250 mL round-bottom flask equipped with a stir bar, septum, Schlenk-frit, joined to a Schlenk flask containing a stir bar, KH (30% in mineral oil, 17.2 g, 129 mmol, 2 equiv.) was added using a Pasteur pipette. The suspension was washed four times with *n*-pentane (ca. 10 mL) to remove the mineral oil. Then, washed KH was suspended in 100 mL diethyl ether. While stirring, 1,2,3-triisopropylimidazolium iodide **7** (17.73 g, 55.0 mmol, 1.0 equiv.) was added and the reaction mixture was vigorously stirred for two days in the absence of light. Then, the solvent was removed *in vacuo* at 0 °C. The residue was suspended in *n*-pentane, filtrated, and extracted with *n*-pentane. The resulting red solution was concentrated *in vacuo* at 0 °C to remove *n*-pentane. The obtained liquid was transferred and distilled (70–71 °C/2.0 mbar) to afford 1,3-diisopropyl-2-(1-methylethylidene)imidazoline **3** (7.630 g, 71%) as a yellowish liquid, which was stored in the freezer of a glovebox in the absence of light at −36 °C. ^{1}H NMR (400 MHz, C_6D_6) δ 5.73 (s, 2H, CH=CH), 3.84 (hept, J = 6.6 Hz, 2H, N–C<u>H</u>$(CH_3)_2$), 1.93 (s, 6H, C=C$(CH_3)_2$), 1.01 (d, J = 6.7 Hz, 12H, N–CH(C<u>H</u>$_3)_2$). ^{13}C NMR (101 MHz, C_6D_6) δ 147.9 (<u>C</u>=C$(CH_3)_2$), 114.2 (CH=CH), 72.8 (C=<u>C</u>$(CH_3)_2$), 49.7 (N–<u>C</u>H$(CH_3)_2$), 21.7 (C=C(<u>C</u>H$_3)_2$), 20.5 (N–CH(<u>C</u>H$_3)_2$). HRMS (ESI): m/z $[M+H]^+$ calcd for $C_{12}H_{23}N_2$ 195.1856; found 195.1853.

1,3-Dihydro-1,3-bis(1-methylethyl)-2*H*-imidazol-2-one 4: In a nitrogen-filled glovebox, NHO **3** (104 mg, 0.535 mmol) was dissolved in 4.0 mL Et_2O and transferred to a 50 mL Schlenk tube with J. Young valve equipped with a stir bar. In a fume hood, the solution was degassed by three freeze-pump-thaw cycles. A balloon, connected to a vacuum line and an N_2O cylinder *via* a three-way valve, was purged multiple times with N_2O. The Schlenk tube, connected to the filled balloon and a vacuum line *via* a three-way valve, was exposed to the N_2O atmosphere for a short duration after multiple purging. The reaction mixture was stirred vigorously overnight in a closed tube under a static N_2O atmosphere. Then, the reaction mixture was poured onto 10 mL HCl (aq, 1 M). After phase separation, the organic phase was washed with water (3×5 mL). The combined aqueous phases were extracted with Et_2O (2×10 mL). The combined organic phases were washed with 10 mL brine (NaCl aq sat), dried over Na_2SO_4, and filtered. After the removal of all volatiles *in vacuo*, the title compound **4** was obtained as colorless/yellowish oil (47 mg, 53%). ^{1}H NMR (400 MHz, $CDCl_3$) δ 6.21 (s, 2H, CH=CH), 4.39 (hept, J = 6.7 Hz, 2H, –C<u>H</u>$(CH_3)_2$), 1.26 (d, J = 6.8 Hz, 12H, –CH(C<u>H</u>$_3)_2$). ^{13}C NMR (101 MHz, $CDCl_3$) δ 151.8 (C=O), 106.6 (CH=CH), 44.3 (–CH(<u>C</u>H$_3)_2$), 22.2 (–<u>C</u>H$(CH_3)_2$). ^{15}N NMR (41 MHz, $CDCl_3$) δ −233.5. IR (KBr, film, cm^{-1}): 3174 (w), 3137 (w), 3106 (w), 2975 (s), 2931 (s), 2876 (m), 2855 (m), 1659 (s), 1573 (w), 1461 (s), 1446 (s), 1393 (m), 1371 (m), 1329 (w) 1258 (m), 1224 (s), 1176 (w), 1162 (w), 1134 (m), 1087 (m), 1000 (m), 930 (w), 876 (m), 801 (m), 758 (w), 705 (m), 660 (m). HRMS (ESI): m/z $[M+Na]^+$ calcd for $C_9H_{16}N_2ONa^+$ 191.1155; found 191.1150.

Acetone Azine 5: The compound was synthesized according to an unmodified literature procedure.[16] ^{1}H NMR (400 MHz, C_6D_6) δ 1.83 (s, 6H), 1.80 (s, 6H).

(1,3-Dihydro-1,3,diisopropyl-2H-imidazol-2-one)-2-(1-methylethylene)-hydrazine 6: In a nitrogen-filled glovebox, NHO **3** (108 mg, 0.56 mmol) was dissolved in 1.0 mL Et_2O and transferred to a 50 mL Schlenk tube with J. Young valve equipped with a stir bar. In a fume hood, the solution was degassed by three freeze-pump-thaw cycles. A balloon, connected to a vacuum line and an N_2O cylinder *via* a three-way valve, was purged multiple times with N_2O. The Schlenk tube, connected to the filled balloon and a vacuum line *via* a three-way valve, was exposed to the N_2O atmosphere for a short duration after multiple purging. The reaction mixture was stirred vigorously overnight in a closed tube under a static N_2O atmosphere. Then, the reaction mixture was directly subjected to column chromatography (silica, first EtOAc/*n*-hexane (2 : 3, R_f 0.0) followed by EtOAc/*n*-hexane (2 : 3) + 5 vol% Et_3N (R_f 0.4)). After the removal of all volatiles *in vacuo*, the title compound **6** was obtained as a yellow oil (19 mg, 15%). ^{1}H NMR (700 MHz, $CDCl_3$) δ 6.23 (s, 2H, CH=CH), 5.14 (hept, J = 6.8 Hz, 2H, N–C<u>H</u>$(CH_3)_2$), 1.97 (s, 3H, C_q–CH_3), 1.91 (s, 3H, C_q–CH_3), 1.28 (d, J = 6.7 Hz, 12H, N–CH(C<u>H</u>$_3)_2$). ^{13}C NMR (176 MHz, $CDCl_3$) δ 149.1 (N–C_q-(N)–N), 148.9 (–N=<u>C$_q$</u>–CH_3), 108.6 (CH=CH), 46.7 (N–<u>C</u>H$(CH_3)_2$), 25.0 (C_q–<u>C</u>H_3), 22.1 (N–CH(<u>C</u>H$_3)_2$), 16.1 (C_q–<u>C</u>H_3). ^{15}N NMR (71 MHz, $CDCl_3$) δ −44.3 (–N=C_q(CH$_3)_2$), −241.7 (<u>N</u>–C_q(N)–<u>N</u>). ^{1}H NMR (600 MHz, C_6D_6) δ 5.90 (s, 2H, CH=CH), 5.39 (s br, 2H, N–C<u>H</u>$(CH_3)_2$), 2.22 (s, 3H, C_q–CH_3), 2.06 (s, 3H, C_q–CH_3), 1.10 (d, J = 6.8 Hz, 12H, N–CH(C<u>H</u>$_3)_2$). ^{13}C NMR (151 MHz, C_6D_6) δ 148.7 (N–C_q(N)–N), 147.4 (–N=<u>C$_q$</u>–CH_3), 108.3 (CH=CH), 46.7 (N–<u>C</u>H$(CH_3)_2$), 25.2 (C_q–<u>C</u>H_3), 22.0 (N–CH(<u>C</u>H$_3)_2$), 16.5 (C_q–<u>C</u>H_3). ^{15}N NMR (71 MHz, C_6D_6) δ −41.9 (–N=C_q(CH$_3)_2$), −243.9 (<u>N</u>–C_q(N)–<u>N</u>). IR (ATR, C_6D_6, cm^{-1}): 1560 ν(C=N). HRMS (ESI): m/z $[M+H]^+$ calcd for $C_{12}H_{23}N_4^+$ 223.1917; found 223.1918.

1,2,3-Triisopropylimidazolium Iodide 7: In a two-neck round-bottom flask equipped with a stir bar and a reflux condenser, 2-isopropylimidazole (9.33 g, 84.7 mmol, 1.0 equiv.) was dissolved in 120 mL acetonitrile. While stirring, K_2CO_3 (14.44 g, 104 mmol, 1.2 equiv.) and 2-iodopropane (42 mL, 420 mmol, 5.0 equiv.) were added. The suspension was refluxed at 90 °C under gentle nitrogen flow. Additional portions of 2-iodopropane (8.5 mL, 84.5 mmol, 1.0 equiv.) were added after 1.5 days and another 2.5 days, respectively. After 6 days in total full conversion was achieved according to ESI–MS. The reaction mixture was filtrated. After the removal of the volatiles, the solid residue was triturated in boiling toluene. Then, the product was dissolved in a minimum amount of acetone and precipitated by addition of ethyl acetate (7–10 fold excess). After filtration, the resulting powder was washed with ethyl acetate in several portions until the washing solution was colorless and finally with *n*-hexane once to afford 1,2,3-triisopropylimidazolium iodide **7** as a colorless powder (21.00 g, 68%). Crystals suitable for single crystal X-ray diffraction were obtained by vapor diffusion from either acetone/*n*-pentane or acetone/ether (deposition number 2099774). ^{1}H NMR (400 MHz, $CDCl_3$) δ 7.62 (s, 2H, CH=CH), 4.88

(hept, $J = 6.7$ Hz, 2H, N–C<u>H</u>$(CH_3)_2$), 3.90 (hept, $J = 7.3$ Hz, 1H, C–C<u>H</u>-$(CH_3)_2$), 1.51 (d, $J = 6.7$ Hz, 12H, N–CH$(C\underline{H}_3)_2$), 1.45 (d, $J = 7.3$ Hz, 6H, C–CH$(C\underline{H}_3)_2$). ^{13}C NMR (101 MHz, $CDCl_3$) δ 147.7 (C_q), 119.4 (CH=CH), 51.3 (N–<u>C</u>H$(CH_3)_2$), 24.6 (C–<u>C</u>H$(CH_3)_2$), 23.3 (N–CH$(\underline{C}H_3)_2$), 20.0 (C–CH$(\underline{C}H_3)_2$). HRMS (ESI): *m/z* $[M]^+$ calcd for $C_{12}H_{23}N_2$ 195.1856; found 195.1764. HRMS (ESI): *m/z* $[M]^-$ calcd for I 126.9050; found 126.9109.

Cycloaddition Product 8: In a nitrogen-filled glovebox, 1,2,3-triisopropylimidazolium iodide (425 mg, 1.3 mmol), KHMDS (345 mg, 1.3 equiv.), and norbornene (122 mg, 1.0 equiv.) were suspended in 10 mL toluene inside a Schlenk tube with J. Young valve. In a fume hood, the suspension was degassed by three freeze-pump-thaw cycles. A balloon, connected to a vacuum line and an N_2O cylinder *via* a three-way valve, was purged multiple times with N_2O. The NMR tube, connected to the filled balloon and a vacuum line *via* three-way valve, was exposed to the N_2O atmosphere for a short duration after multiple purging. The reaction proceeded with the N_2O balloon connected to the Schlenk tube overnight. Then, all volatiles were removed *in vacuo* and the solid residue was extracted with Et_2O and passed through a silica plug (5 g silica gel). The cycloaddition product **8** was eluted with 20% EtOAc/*n*-hexane (50 mL) and then imidazolone **4** was eluted with 40% EtOAc/*n*-hexane with 5 vol% Et_3N (50 mL). After removal of all volatiles *in vacuo*, imidazolone **4** was obtained as a yellowish oil (156 mg, 71%), and the cycloaddition product **8** was obtained as a colorless oil after distillation at 40–50 °C (bath)/oil pump (68 mg, 31%). The ^{1}H NMR data is consistent with literature reports.[18]

Supporting Information

Additional references cited within the Supporting Information.[29–38]

Acknowledgements

We thank the German research foundation (DFG, GE 3117/1-1), the Aventis Foundation, and the Fonds of the Chemical Industry for financial support. We thank Dr. H. Hausmann for assistance and discussions regarding NMR experiments and Dr. D. Gerbig for assistance with IR experiments. Continuous support by Prof. P. R. Schreiner, R. Göttlich, and H. A. Wegner is acknowledged. Open Access funding enabled and organized by Projekt DEAL.

Conflict of Interests

The authors declare no conflict of interest.

Data Availability Statement

The data that support the findings of this study are available in the supplementary material of this article.

Keywords: Small molecule activation · *N*-heterocyclic olefin · DFT calculations · cycloadditions · nitrous oxide

[1] a) D. J. Wuebbles, *Science* **2009**, *326*, 56–57; b) A. R. Ravishankara, J. S. Daniel, R. W. Portmann, *Science* **2009**, *326*, 123–125.
[2] a) W. B. Tolman, *Angew. Chem. Int. Ed.* **2010**, *49*, 1018–1024; b) K. Severin, *Chem. Soc. Rev.* **2015**, *44*, 6375–6386.
[3] a) E. Otten, R. C. Neu, D. W. Stephan, *J. Am. Chem. Soc.* **2009**, *131*, 9918–9919; b) D. W. Stephan, G. Erker, *Chem. Sci.* **2014**, *5*, 2625–2641; c) Z. Mo, E. L. Kolychev, A. Rit, J. Campos, H. Niu, S. Aldridge, *J. Am. Chem. Soc.* **2015**, *137*, 12227–12230.
[4] Y. Pang, M. Leutzsch, N. Nöthling, J. Cornella, *J. Am. Chem. Soc.* **2020**, *142*, 19473–19479.
[5] a) A. G. Tskhovrebov, E. Solari, M. D. Wodrich, R. Scopelliti, K. Severin, *Angew. Chem. Int. Ed.* **2012**, *51*, 232–234; b) A. G. Tskhovrebov, B. Vuichoud, E. Solari, R. Scopelliti, K. Severin, *J. Am. Chem. Soc.* **2013**, *135*, 9486–9492.
[6] A. G. Tskhovrebov, L. C. E. Naested, E. Solari, R. Scopelliti, K. Severin, *Angew. Chem. Int. Ed.* **2014**, *53*, 1–5.
[7] a) L. Y. M. Eymann, P. Varava, A. M. Shved, B. F. E. Curchod, Y. Liu, O. M. Planes, A. Sienkiewicz, R. Scopelliti, F. Fadaei Tirani, K. Severin, *J. Am. Chem. Soc.* **2019**, *141*, 17112–17116; b) L. Y. M. Eymann, P. Varava, A. M. Shved, B. F. E. Curchod, Y. Liu, O. M. Planes, A. Sienkiewicz, R. Scopelliti, F. Fadaei Tirani, K. Severin, *J. Am. Chem. Soc.* **2020**, *142*, 1112.
[8] P. Varava, Z. Dong, R. Scopelliti, F. Fadaei-Tirani, K. Severin, *Nat. Chem.* **2021**, *13*, 1055–1060.
[9] P. W. Antoni, C. Golz, J. J. Holstein, D. A. Pantazis, M. M. Hansmann, *Nat. Chem.* **2021**, *13*, 587–593.
[10] a) P. W. Antoni, J. Reitz, M. M. Hansmann, *J. Am. Chem. Soc.* **2021**, *143*, 12878–12885; b) M. M. Hansmann, *Angew. Chem. Int. Ed.* **2023**, *62*, e202304574.
[11] a) C. Adamo, V. Barone, *J. Chem. Phys.* **1999**, *110*, 6158–6170; b) M. Ernzerhof, G. E. Scuseria, *J. Chem. Phys.* **1999**, *110*, 5029–5036.
[12] a) S. Grimme, J. Antony, S. Ehrlich, H. Krieg, *J. Chem. Phys.* **2010**, *132*, 154104; b) S. Grimme, S. Ehrlich, L. Goerigk, *J. Comput. Chem.* **2011**, *32*, 1456–1465.
[13] F. Weigend, R. Ahlrichs, *Phys. Chem. Chem. Phys.* **2005**, *7*, 3297–3305.
[14] M. K. Kesharwani, B. Brauer, J. M. L. Martin, *J. Phys. Chem. A* **2015**, *119*, 1701–1714.
[15] a) F. Neese, *WIREs Comput. Mol. Sci.* **2012**, *2*, 73–78; b) F. Neese, *WIREs Comput. Mol. Sci.* **2018**, *8*, e1327.
[16] A. C. Day, M. C. Whiting, *Org. Synth.* **1970**, *50*, 3.
[17] a) M. Regitz, *Angew. Chem. Int. Ed. Engl.* **1967**, *6*, 733–749; b) L. J. McDowell, M. M. Khodaei, D. Bethell, *Org. Biomol. Chem.* **2003**, *1*, 995–1003; c) D. Bethell, A. R. Newall, G. Stevens, D. Whittaker, *J. Chem. Soc. B* **1969**, 749–754; d) G. W. Cowell, A. Ledwith, *Q. Rev. Chem. Soc.* **1970**, *24*, 119–167.
[18] a) M. Christl, E. Brunn, W. R. Roth, H.-W. Lennartz, *Tetrahedron* **1989**, *45*, 2905–2915; b) M. W. Majchrzak, J. Warkentin, *J. Phys. Org. Chem.* **1990**, *3*, 339–345.
[19] a) R. Zeng, M. Feller, Y. Diskin-Posner, L. J. W. Shimon, Y. Ben-David, D. Milstein, *J. Am. Chem. Soc.* **2018**, *140*, 7061–7064; b) H. Tanaka, K. Hashimoto, K. Suzuki, Y. Kitaichi, M. Sato, T. Ikeno, T. Yamada, *Bull. Chem. Soc. Jpn.* **2004**, *77*, 1905–1914; c) V. N. Parmon, G. I. Panov, A. Uriarte, A. S. Noskov, *Catal. Today* **2005**, *100*, 115–131.
[20] a) F. M. Beringer, J. A. Farr, JR, S. Sands, *J. Am. Chem. Soc.* **1953**, *75*, 3984–3987; b) I. R. Landman, F. Fadaei-Tirani, K. Severin, *Chem. Commun.* **2021**, *57*, 11537–11540; c) K. Banert, O. Plefka, *Angew. Chem. Int. Ed.* **2011**, *50*, 6171–6174; d) R. Monreal-Corona, E. Besalú, A. Pla-Quintana, A. Poater, *Org. Chem. Front.* **2022**, *9*, 4347–4357; e) E. Müller, W. Rundel, *Chem. Ber.* **1957**, *90*, 1302–1306; f) R. Meier, W. Frank, *Chem. Ber.* **1956**, *89*, 2747–2750.
[21] H. Eyring, *J. Chem. Phys.* **1935**, *3*, 107–115.
[22] F. S. Bridson-Jones, G. D. Buckley, *J. Chem. Soc.* **1951**, 3009–3016.
[23] M. J. Frisch, G. W. Trucks, H. B. Schlegel, G. E. Scuseria, M. A. Robb, J. R. Cheeseman, G. Scalmani, V. Barone, G. A. Petersson, H. Nakatsuji, X. Li, M. Caricato, A. V. Marenich, J. Bloino, B. G. Janesko, R. Gomperts, B. Mennucci, H. P. Hratchian, J. V. Ortiz, A. F. Izmaylov, J. L. Sonnenberg, D. Williams-Young, F. Ding, F. Lipparini, F. Egidi, J. Goings, B. Peng, A. Petrone, T. Henderson, D. Ranasinghe, V. G. Zakrzewski, J. Gao, N. Rega, G. Zheng, W. Liang, M. Hada, M. Ehara, K. Toyota, R. Fukuda, J. Hasegawa, M. Ishida, T. Nakajima, Y. Honda, O. Kitao, H. Nakai, T. Vreven, K. Throssell, J. A. Montgomery, J. E. Peralta, F. Ogliaro, M. J. Bearpark, J. J. Heyd, E. N. Brothers, K. N. Kudin, V. N. Staroverov, T. A. Keith, R. Kobayashi, J. Normand, K. Raghavachari, A. P. Rendell, J. C. Burant, S. S. Iyengar, J. Tomasi, M. Cossi, J. M. Millam, M. Klene, C. Adamo, R. Cammi, J. W. Ochterski, R. L. Martin, K. Morokuma, O. Farkas, J. B. Foresman, D. J. Fox, *Gaussian 16, Revision C.01*, Gaussian, Inc, Wallingford, CT, **2016**.

[24] S. Grimme, J. G. Brandenburg, C. Bannwarth, A. Hansen, *J. Chem. Phys.* **2015**, *143*, 54107.
[25] a) G. Santra, N. Sylvetsky, J. M. L. Martin, *J. Phys. Chem. A* **2019**, *123*, 5129–5143; b) G. Santra, J. M. L. Martin, *Isr. J. Chem.* **2020**, *60*, 787–804.
[26] a) E. Caldeweyher, C. Bannwarth, S. Grimme, *J. Chem. Phys.* **2017**, *147*, 34112; b) E. Caldeweyher, S. Ehlert, A. Hansen, H. Neugebauer, S. Spicher, C. Bannwarth, S. Grimme, *J. Chem. Phys.* **2019**, *150*, 154122.
[27] A. V. Marenich, C. J. Cramer, D. G. Truhlar, *J. Phys. Chem. B* **2009**, *113*, 6378–6396.
[28] a) S. Grimme, *J. Chem. Theory Comput.* **2019**, *15*, 2847–2862; b) P. Pracht, F. Bohle, S. Grimme, *Phys. Chem. Chem. Phys.* **2020**, *22*, 7169–7192.
[29] G. R. Fulmer, A. J. M. Miller, N. H. Sherden, H. E. Gottlieb, A. Nudelman, B. M. Stoltz, J. E. Bercaw, K. I. Goldberg, *Organometallics* **2010**, *29*, 2176–2179.
[30] a) R. K. Harris, E. D. Becker, S. M. Cabral de Menezes, R. Goodfellow, P. Granger, *Pure Appl. Chem.* **2001**, *73*, 1795–1818; b) R. K. Harris, E. D. Becker, S. M. Cabral de Menezes, P. Granger, R. E. Hoffman, K. W. Zilm, *Pure Appl. Chem.* **2008**, *80*, 59–84.
[31] S. Grimme, *Chem. Eur. J.* **2012**, *18*, 9955–9964.
[32] J. P. Perdew, K. Burke, M. Ernzerhof, *Phys. Rev. Lett.* **1996**, *77*, 3865–3868.
[33] J. P. Perdew, *Phys. Rev. B* **1986**, *33*, 8822–8824.
[34] R. Izsák, F. Neese, *J. Chem. Phys.* **2011**, *135*, 144105.
[35] L. Krause, R. Herbst-Irmer, G. M. Sheldrick, D. Stalke, *J. Appl. Crystallogr.* **2015**, *48*, 3–10.
[36] G. M. Sheldrick, *Acta Crystallogr. Sect. A* **2015**, *71*, 3–8.
[37] G. M. Sheldrick, *Acta Crystallogr. Sect. C* **2015**, *71*, 3–8.
[38] S. Parsons, H. D. Flack, T. Wagner, *Acta Crystallogr. Sect. B* **2013**, *69*, 249–259.

Manuscript received: December 15, 2023
Revised manuscript received: December 20, 2023
Accepted manuscript online: December 22, 2023
Version of record online: January 12, 2024

5.4 An Acceptor-substituted *N*-Heterocyclic *ortho*-Quinodimethane: Pushing the Boundaries of Polarization in Donor–Acceptor-substituted Polyenes

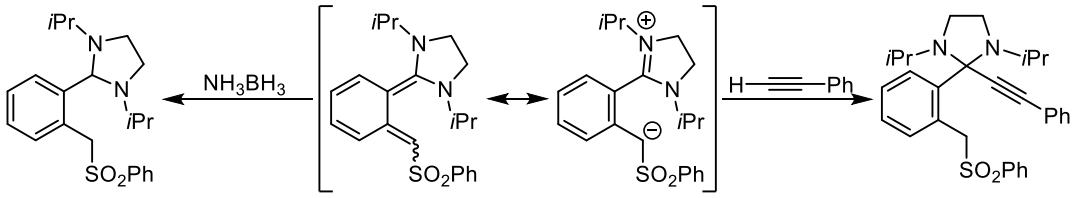

Wir berichten über die Synthese, Isolierung und Charakterisierung eines stabilen Donor–Akzeptor-substituierten *ortho*-Chinodimethans (engl. *ortho-quinodimethane*, *o*QDM). Dieses System mit einem Imidazolidin-Gerüst als Donor kann auch als Akzeptor-substituiertes *ortho-N*-heterozyklisches Chinodimethan (engl. *ortho-N-heterocyclic quinodimethane*, *o*NHQ) bezeichnet werden. Wir untersuchten das Ausmaß der Polarisation des konjugierten π-Systems mithilfe von Einkristall-Röntgenbeugung, NMR- und UV-vis-Spektroskopie, zyklischer Voltammetrie und DFT-Berechnungen. Die Bindungslängen im Phenyl-Linker weisen nicht die für *o*QDMs typische Alternation auf. Darüber hinaus deuten die ^{13}C- und ^{15}N-NMR-Verschiebungen auf eine signifikante Ladungstrennung hin, eine Interpretation, die durch den für aromatische Verbindungen typischen diatropen Ringstrom, mittels $NICS_{ZZ}(r)$-Berechnungen ermittelt, unterstützt wird. DFT-Berechnungen zeigen, dass die Polarisation primär ein elektronischer Effekt ist, der durch sterische Einflüsse verstärkt wird. Auffallend ist, dass die Oxidations- und Reduktionspotenziale des Donor–Akzeptor-substituierten *o*QDMs praktisch identisch mit denen authentischer anionischer und kationischer Derivate sind. Die Ergebnisse zeigen daher, dass eine aromatische zwitterionische Lewis-Struktur die elektronische Struktur besser wiedergibt als eine neutrale chinoide Lewis-Struktur, was darauf hindeutet, dass das Akzeptor-substituierte *o*NHQ ein seltenes Beispiel für ein organisches Zwitterion mit konjugierten Ladungszentren ist. Die ambiphile Reaktivität des Akzeptor-substituierten *o*NHQs, nachgewiesen durch die Dehydrierung von Amminboran und die Addition von Phenylacetylen unter heterolytischer C−H-Bindungsspaltung, unterstützt die Einstufung als organisches Zwitterion und erinnert an frustrierte Lewis-Paare (FLPs). Somit kann das Akzeptor-substituierte *o*NHQ hinsichtlich seiner Reaktivität als intramolekulares kohlenstoffbasiertes FLP angesehen werden.

Referenz:

J. Ariai, U. Gellrich, *J. Am. Chem. Soc.* **2024**, *im Druck*.

DOI: 10.1021/jacs.4c13783

Akzeptiertes Manuskript online: 14. November 2024

Final veröffentlichte Version online: *im Druck*

JACS
JOURNAL OF THE AMERICAN CHEMICAL SOCIETY
pubs.acs.org/JACS
Article

An Acceptor-Substituted *N*-Heterocyclic *ortho*-Quinodimethane: Pushing the Boundaries of Polarization in Donor–Acceptor-Substituted Polyenes

Jama Ariai and Urs Gellrich*

Cite This: https://doi.org/10.1021/jacs.4c13783
Read Online
ACCESS | Metrics & More | Article Recommendations | Supporting Information

ABSTRACT: We report the synthesis, isolation, and characterization of a stable donor–acceptor substituted *ortho*-quinodimethane (*o*QDM). This system with an imidazolidine scaffold as the donor can also be referred to as acceptor-substituted *ortho*-*N*-heterocyclic quinodimethane (*o*NHQ). We have examined the extent of polarization of the conjugated π-system using single-crystal X-ray diffraction, NMR and UV/vis spectroscopy, cyclic voltammetry, and DFT computations. The bond lengths in the phenyl linker do not exhibit the alternation typical of *o*QDMs. In addition, the ^{13}C and ^{15}N NMR shifts suggest significant charge separation, an interpretation supported by the diatropic ring current determined by $NICS_{ZZ}(r)$ computations, which is characteristic of aromatic compounds. DFT calculations show that polarization is an electronic effect that is amplified by steric influences. More strikingly, the oxidation and reduction potentials of the push–pull substituted *o*QDM are virtually identical to those of authenticated anionic and cationic derivatives. The results therefore indicate that an aromatic zwitterionic structure represents the electronic structure more accurately than a neutral quinoidal Lewis structure, which indicates that the acceptor-substituted *o*NHQ is a rare example of an organic zwitterion in which the centers of charge are in conjugation. The ambiphilic reactivity of the acceptor-substituted *o*NHQ, which is evidenced by the dehydrogenation of ammonia borane and the addition of phenylacetylene via heterolytic C–H bond cleavage, further supports its notation as an organic zwitterion and is reminiscent of frustrated Lewis pairs (FLPs). Thus, the acceptor-substituted *o*NHQ can be considered to be an intramolecular carbogenic FLP in terms of its reactivity.

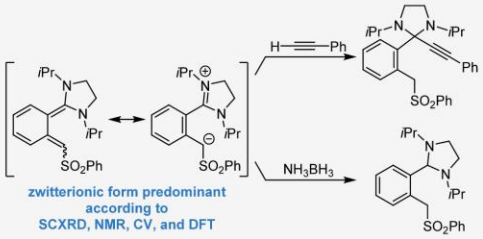

INTRODUCTION

Organic molecules featuring π-systems with unconventional electronic structures are of fundamental significance in physical organic chemistry and are also crucial for applications in molecular electronics.[1] Specifically, π-extended dimers and push–pull chromophores, in which donor and acceptor substituents induce a polarization of the π-electron density,[2] have been identified as promising building blocks for materials with attractive optoelectronic properties and potential applications in singlet fission.[3] The pronounced polarization of a π-bond also influences the chemistry of *N*-heterocyclic olefins (NHOs) reflected by the dipolar resonance structure (Scheme 1).[4] This class of organic Lewis bases is described as *N*-heterocyclic carbenes (NHCs) extended by an alkylidene group and finds broad applications in catalysis and coordination chemistry as ligands.[5] Moreover, NHOs have been employed in polymerizations,[6] CO_2 binding,[7] and N_2O activation,[8] the latter being particularly notable as it led to the first isolable diazoolefins.[9] Recently, we reported on *N*-heterocyclic quinodimethanes (NHQs), which can be described as NHOs with a phenylene linker between the imidazole core and the alkylidene linker.[10] Besides unique open-shell reactivity, our findings indicated that these systems exhibit superior proton affinity compared with analogous NHCs and NHOs, attributed to the enhanced polarization of the π-electron density due to the aromatization of the phenylene linker, as illustrated in the resonance structure in Scheme 1. We now became interested in elucidating whether the introduction of an acceptor substituent in an *ortho*-NHQ (*o*NHQ) would polarize π-electron density to such an extent that charge separation in a conjugated polyene is observed. Unlike mesoionic NHOs[11] and pyridinium ylides[12] that cannot be represented without formal charges, it is possible to formulate a neutral quinoidal resonance structure for an acceptor-substituted *o*NHQ. According to conventional understanding, the neutral quinoidal representation should be a more accurate description than a zwitterionic Lewis structure

Received: October 2, 2024
Revised: November 2, 2024
Accepted: November 5, 2024

Scheme 1. Context of This Work: Increasing π-Bond Polarization and Charge Separation in the Series *N*-Heterocyclic Olefin, *N*-Heterocyclic Quinodimethane, and Acceptor-Substituted *N*-Heterocyclic Quinodimethane

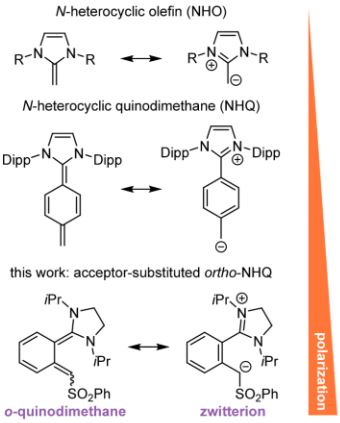

with formal charges, as the common rules for drawing Lewis structures rely on satisfying the octet rule while minimizing formal charges/charge separation.[13]

It is noteworthy that an acceptor-substituted *o*NHQ with charge separation could also be regarded as isolobal to a phenylene-linked B−N frustrated Lewis pair (FLP).[14] The question therefore arises if an acceptor-substituted *o*NHQ can be considered in terms of reactivity as a carbogenic FLP. This term was coined by Alcarazo and co-workers as they introduced the intermolecular FLP that features an electron-deficient allene paired with a sterically demanding NHC.[15] Additionally, intermolecular FLPs have been developed that combine a trityl or trioxatriangulenium cation with an NHC as the Lewis basic component.[16]

Herein, we report the synthesis of an acceptor-substituted *o*NHQ and present detailed studies of its electronic structure to address the extent of charge separation across the conjugated π-system in the solid state, in solution, and in the gas phase. For this purpose, we selected an imidazolidine-based system that is capable of stabilizing the positive charge solely by resonance instead of aromaticity. Concerning the acceptor substituent, we chose a sulfonyl group that stabilizes the negative charge by negative hyperconjugation, as opposed to resonance stabilization commonly encountered for carbonyl and nitrile groups, thereby formally maintaining a carbon-centered carbanion.[17]

RESULTS AND DISCUSSION

We began our study with the synthesis of suitable precursor **3** that would allow us to generate acceptor-substituted *o*NHQ **4** by deprotonation (Scheme 2). Starting from commercially available 2-(bromomethyl)benzonitrile, the literature known aldehyde **1** was obtained by a two-step synthesis with an overall yield of 64%.[18,19] Subsequent cyclization and oxidation afford the desired imidazolinium bromide precursor **3**.[18,19]

Treatment of **3** with KHMDS in DMSO-d_6 or CD_3CN resulted in quantitative conversion to **4** (Figure S52). Attempts to isolate **4** after deprotonation with KHMDS resulted in a

Scheme 2. Synthesis of the Acceptor-Substituted *ortho*-*N*-Heterocyclic Quinodimethane[a]

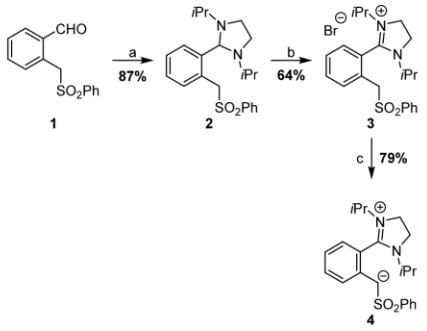

[a]Conditions: (a) *N*,*N*′-Diisopropylethylenediamine, EtOH, reflux, overnight; (b) NBS, DME, rt, 30 min; (c) *n*-BuLi, THF,−78 °C to rt, 1 h; then 0 °C, 30 min.

mixture of **3** and **4** (Figure S55, see Chapter 3.1 of the Supporting Information for further details).[20] However, deprotonation with *n*-butyllithium in THF afforded a bright yellow solid after precipitation with diethyl ether. Upon layering a DMF-solution of **4** with diethyl ether, yellow needles formed. Single-crystal X-ray diffraction (SCXRD) analysis confirmed that these crystals consist of **4**. We also obtained the LiBr-pyridine complex $[(\mathbf{4})_2\mathrm{Li(pyr)}]\mathrm{Br}$ upon crystallization of the crude product from pyridine (Figure 1). In both molecular structures, **4** adopts the same conformation. We analyzed the bond lengths in the phenylene linker and compared them to those of the DFT-optimized structure at the PBE0-D4/def2-TZVPP level (Table 1).[21] The experimental bond lengths of the individual rings show little variation and are overall in excellent agreement with the DFT-optimized bond lengths in the gas phase. The C−C bond lengths and the calculated Wiberg bond indices (WBIs) range from 1.385(3) to 1.425(3) Å and from 1.22 to 1.56, respectively. Thus, the C−C bonds in **4** are more uniform compared to *o*-xylylene (WBIs: 1.0−1.7). Furthermore, the C−C bonds to the α-sulfonyl carbon and the imidazolinium ring are 1.428(3) and 1.479(3) Å in length, respectively, suggesting C−C single bonds rather than double bonds. Compared to the starting material **3**, the C1−C1′ bond to the α-sulfonyl carbon is shortened by 0.076(5) Å, while the C2−C2′ bond length to the imidazolinium ring is identical within the margin of error (Figures S10 and Table S8). Additionally, the *N*-heterocycle is twisted by 75° with respect to the phenyl linker, while the sulfonyl unit is rotated by 15°. The absence of a pronounced bond length alternation as in *o*-xylylene and the sizable twist of the imidazolinium ring out of plane, maintaining the C2−C2′ bond length of **3**, indicate that **4** exhibits an aromatic phenyl linker that separates the formally positively charged imidazolinium ring from the formally negatively charged α-sulfonyl carbanion unit in the solid state structure (SCXRD) and in the gas phase (DFT).

While *o*-xylylene rearomatizes by forming a dimer or benzocyclobutene,[22] the C1′−C2′ distance of 2.89 Å in **4** determined by SCXRD indicates the absence of a binding interaction between the α-sulfonyl carbon and the imidazolinium ring, a feature typical for FLPs.[23] This situation is reminiscent of the extreme case of push−pull cyclopropanes,

https://doi.org/10.1021/jacs.4c13783
J. Am. Chem. Soc. XXXX, XXX, XXX−XXX

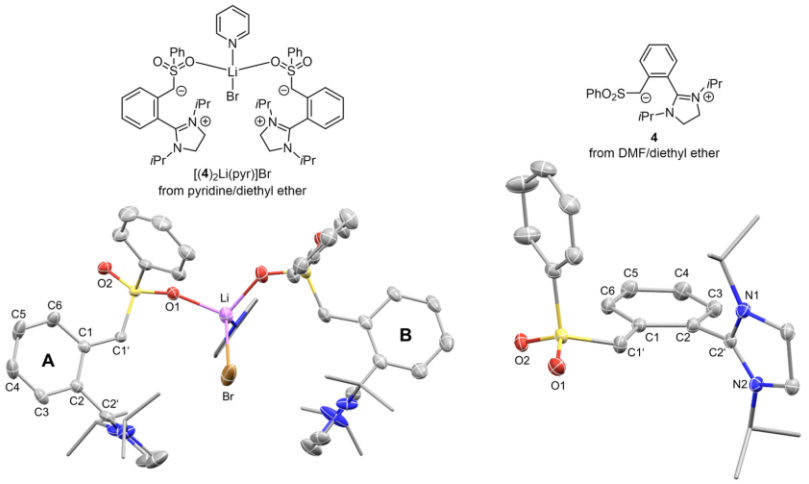

Figure 1. Molecular structure of **4** derived from SCXRD (50% probability ellipsoids, all hydrogens and residual pyridine solvent molecules are omitted, disorder of the isopropyl groups, and the pyridine are not shown). The left molecular structure shows the LiBr-pyridine-complex $[(\mathbf{4})_2\mathrm{Li(pyr)}]\mathrm{Br}$ crystallized from pyridine/diethyl ether and the right molecular structure shows the isolated species crystallized from *N*,*N*-dimethylformamide/diethyl ether. Selected bond lengths and angles (for C−C bond lengths of the phenyl linker (C1−C6) see Table 1): $[(\mathbf{4})_2\mathrm{Li(pyr)}]\mathrm{Br}$: Li−Br: 2.507(6) Å, Li−O1a: 1.949(6) Å, S−O1a: 1.459(2) Å, S−O2a: 1.451(2) Å, N1a−C2′a: 1.325(4) Å, N2a−C2′a: 1.321(4) Å, S−C1′a−C1a−C6a: 6.0(4)°, N1a−C2′a−C2a−C3a: 66.0(4)°, Li−O1b: 1.929(6) Å, S−O1b: 1.463(2) Å, S−O2b: 1.452(2) Å, N1b−C2′b: 1.307(4) Å, N2b−C2′b: 1.300(4) Å, S−C1′b−C1b−C6b: 20.5(5)°, N1b−C2′b−C2b−C6b: 86.1(4)°; **4**: S−O1: 1.4564(17) Å, S−O2: 1.4548(17) Å, N1−C2′: 1.324(3) Å, N2−C2′: 1.324(3) Å, S−C1′−C1−C6: 15.4(3)°, N2−C2′−C2−C3: 74.7(3)°.

Table 1. Selected C−C Bond Lengths of 4 Derived from SCXRD[a]

	C1−C2	C2−C3	C3−C4	C4−C5	C5−C6	C6−C1	C1−C1′	C2−C2′
$\mathbf{4}_A$−[Li]	1.425(4)	1.396(4)	1.378(5)	1.394(5)	1.366(5)	1.425(4)	1.418(4)	1.467(4)
$\mathbf{4}_B$−[Li]	1.420(5)	1.389(5)	1.373(5)	1.389(5)	1.379(5)	1.418(4)	1.424(4)	1.479(4)
4	1.425(3)	1.397(3)	1.388(3)	1.391(4)	1.385(3)	1.424(3)	1.428(3)	1.479(3)
DFT	1.428 [1.22]	1.400 [1.34]	1.373 [1.49]	1.403 [1.32]	1.370 [1.56]	1.425 [1.24]	1.402 [1.34]	1.447 [1.08]

[a]The indices A and B indicate the independent fragments within the LiBr-complex (Figure 1). DFT-optimized bond lengths refer to the PBE0-D4/def2-TZVPP level and Wiberg bond indices are given in square brackets. All bond lengths in Å.

which can be regarded as a 1,3-zwitterion.[24] In the following, we discuss if the electronic structure of **4** is best described as a nonaromatic *o*QDM or as an aromatic zwitterion (Scheme 3).

Scheme 3. Selected Resonance Structures of 4

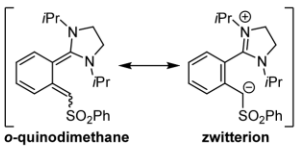

We studied **4** by nuclear magnetic resonance (NMR) spectroscopy in THF-d_8. To assess whether the heterocycle is better described as imidazolinium or imidazolidine, we determined the ^{15}N chemical shift by utilizing ^{1}H−^{15}N−HMBC NMR spectroscopy (Figure 2a). The ^{15}N shift of **4** (−247.6 ppm) is comparable to that of imidazolinium bromide **3** (−243.0 ppm), strongly suggesting the presence of a positively charged imidazolinium ring in **4**. Concerning ^{13}C NMR shifts, the carbon atoms in 1,3- and 1,5-position relative to the carbanionic center are notably shielded and resonate at 107.5−118.6 ppm. It is remarkable that exactly these carbon atoms carry a negative formal charge in the resonance structures of the zwitterion (Figure 2b). It should be noted that the σ-orbitals must be taken into account for a comprehensive analysis of the ^{13}C NMR shifts.[25] The α-sulfonyl carbon (C1′) resonates at 67.5 ppm. Furthermore, we employed nucleus-independent chemical shift (NICS) analysis to examine the ring currents in the series of *o*-xylylene, *o*NHQ **5** missing the acceptor substituent, and **4** (Figure 2c).[26] While the former two exhibit a paratropic ring current (nonaromatic phenylene moiety), **4** shows a diatropic ring current, suggesting an aromatic phenyl linker. This is in contrast to typical 1,3-benzodithiol-2-ylidene/dicyanomethylene-substituted push−pull *para*-quinodimethanes for which NICS calculations reveal a less pronounced aromatic character (Figure S20).[27] It should also be noted in this context that while this article was under review, Zhang and co-workers reported the synthesis and investigation of the zwitterionic structure of *para*-quinodimethane derivatives with a triphenylphosphine donor and a dicyanomethylene acceptor.[28] We further analyzed the stereoelectronic influences on the

https://doi.org/10.1021/jacs.4c13783
J. Am. Chem. Soc. XXXX, XXX, XXX−XXX

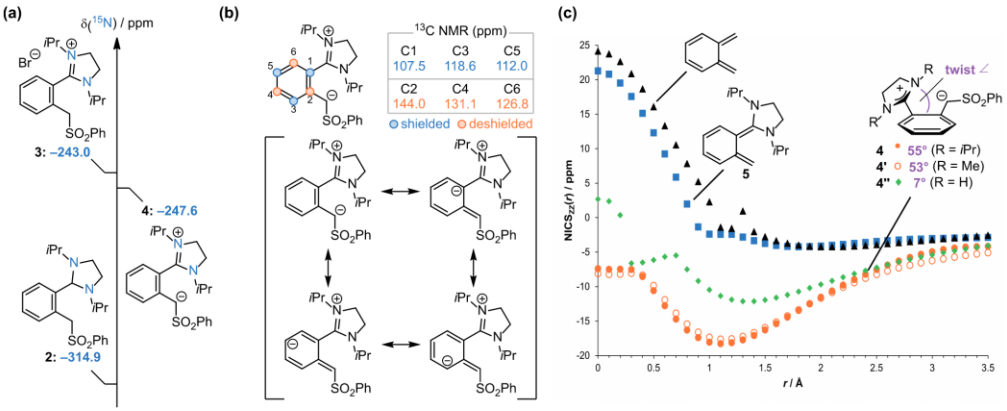

Figure 2. Probing the electronic structure of **4** by NMR spectroscopy in THF-d_8 and NICS computations. (a) Comparison of the ^{15}N chemical shifts of **4** in the series of neutral aminal **2** and cationic imidazolinium **3** referenced to CH_3NO_2 (41 MHz). (b) Selected resonance structures and assignment of the ^{13}C chemical shifts to the phenyl linker (101 MHz). (c) Computed $NICS_{ZZ}$ values at the PBE0/def2-QZVPP//PBE0-D4/def2-TZVPP level in the gas phase. Dihedral angles (in purple) refer to the twist of the imidazolinium ring with respect to the phenyl linker (N−C2′−C2−C3).

aromaticity of the covalent linker in **4** by considering different *N*-substituted derivatives. Substitution of the isopropyl group with a methyl group (**4′**) hardly causes any change in the structural parameters and the diatropic current (Table S22). However, substitution with a proton (**4″**) leads to planarization of the imidazolinium ring (Figure S14). In fact, the heterocycle in hypothetical **4″** is closer to coplanarity with respect to the phenyl linker compared to acceptorless *o*NHC **5** (twisted by 7 and 32°, respectively). Surprisingly, the ring current in the center of **4″** is paratropic ($NICS_{ZZ}(0)$ = +2.7), but the remaining profile shows a typical diatropic behavior, however, less pronounced compared to **4′** and **4**. When the sulfone group in **4″** is replaced by a sulfoxide or phenyl group, the diatropic current gradually displaces the paratropic contributions until eventually the profile of **5** is obtained (Figure S15). This emphasizes the decisive role of the acceptor strength that is required to polarize the covalent linker electronically despite having centers of charge in formal conjugation. Thus, the gas phase computations suggest that charge separation across the covalent linker while retaining its aromaticity is an intrinsic electronic effect attributed to the donor−acceptor substitution pattern. In addition, steric effects, which cause twisting of the heterocycle, prevent quenching of the separated charges by conjugation and thereby enhance the polarization. Charge delocalization across the phenyl linker is also reflected in the ^{1}H NMR spectrum, causing a high-field shift up to 6.13 ppm. The proton in the benzylic position gives a signal at 4.41 ppm. NMR studies in more polar solvents such as pyridine-d_5, CD_3CN, and DMSO-d_6 led to similar conclusions (Figure S39). In the cases of CD_3CN and DMSO-d_6, however, the ^{1}H NMR signal of the benzylic hydrogen vanishes because of the H/D exchange (Figure S1).

We further investigated the zwitterionic nature of **4** electrochemically using cyclic voltammetry (Figure 3). We observed a well separated reduction and oxidation at $E_{p/2}$ = −2.00 V and $E_{p/2}$ = −0.40 V, respectively. To interpret the potentials and thus the extent of polarization in terms of the quinoidal/zwitterionic resonance structures, we recorded CVs

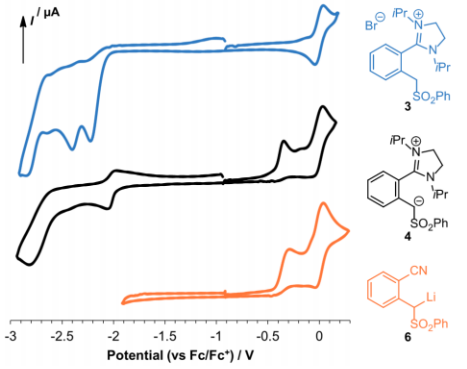

Figure 3. Cyclic voltammograms of **4** (black), imidazolinium bromide **3** (blue), and *α*-sulfonyl carbanion **6** (orange) recorded in DMF (0.1 M nBu$_4$NPF$_6$, 250 mV/s) with ferrocene as internal reference.

for the reduction of imidazolinium bromide **3**, an authenticated cation, and for the oxidation of lithiated 2-(phenylsulfonylmethyl)benzonitrile **6**, an authenticated anion. Visual inspection reveals that the reduction and oxidation potentials of **4** are comparable to those of the imidazolinium bromide **3** ($E_{p/2}$ = −2.15 V) and the *α*-sulfonyl carbanion **6** ($E_{p/2}$ = −0.37 V), respectively.

Motivated by the intense yellow color of the crystals and solutions of **4**, we recorded UV/vis spectra in THF at different concentrations. Two distinct absorption bands at 308 nm (ε = 3.1(2) × 10^3 cm^{-1} L^1 mol^{-1}) and 366 nm (ε = 1.7(1) × 10^3 cm^{-1} L^1 mol^{-1}) are observed (Figure 4). TD-DFT computations at the *ω*B97X-D4/def2-QZVPP//PBE0-D4/def2-TZVPP level of theory allowed us to assign the excitation at 366 nm to a $\pi \rightarrow \pi^*$ transition (calculated absorption at 325 nm) from the highest occupied molecular orbital (HOMO) to the lowest unoccupied molecular orbital

https://doi.org/10.1021/jacs.4c13783
J. Am. Chem. Soc. XXXX, XXX, XXX−XXX

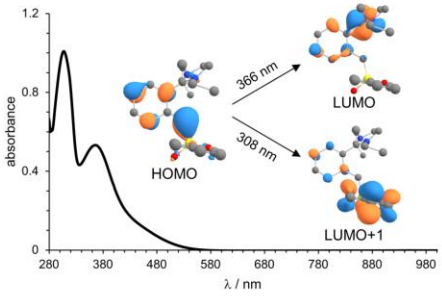

Figure 4. UV/vis spectrum of **4** in THF (4×10^{-4} mol/L). Inset shows the canonical Kohn–Sham molecular orbitals assigned to the absorption bands based on TD-DFT computations at ωB97X-D4/def2-QZVPP//PBE0-D4/def2-TZVPP level, including the CPCM model for THF to account for bulk solvation (calculated absorptions at 325 and 294 nm).

(LUMO).[29] Similarly, the second absorption at 308 nm is assigned to a $\pi \rightarrow \pi^*$ transition (calculated absorption at 294 nm) from HOMO to the LUMO+1. The absorption band of the HOMO → LUMO transition extends into the visible range (up to 570 nm), which in turn causes the yellow appearance of **4**. Furthermore, the acceptor substituent increases the singlet–triplet gap $\Delta E_{S\rightarrow T}$ from 35.8 kcal/mol (**5**) to 51.7 kcal/mol (**4**).

Regarding the weight between the neutral quinoidal and the zwitterionic resonance structures, we anticipate an influence of solvent polarity. Therefore, we systematically examined the HOMO → LUMO absorption band in the following solvents of increasing polarity (relative permittivities in parentheses): THF (7.52), pyridine (13.26), 1,2-difluorobenzene (13.38), acetonitrile (36.64), DMF (38.25), and DMSO (47.24).[30] While the absorption wavelength barely changes (360–366 nm), the molar absorption coefficient significantly increases with higher solvent permittivity from $1.7(1) \times 10^3$ to $4.5(1) \times 10^3$ cm^{-1} L^1 mol^{-1} (Table S2 and Figures S7 and S8). We further determined the contribution of intramolecular push–pull stabilization by conjugation and the amount of aromatic stabilization energy (ASE) of **4** using isodesmic equations at revDSD-PBEP86-D4/def2-QZVPP//PBEh-3c level and the SMD model to account for electrostatic solvent interactions implicitly (Scheme 4).[31]

In the gas phase, the conjugation between the imidazolinium ring and the α-sulfonyl carbanion moiety is 20.3 kcal/mol. This contribution is reduced to 15.2 kcal/mol in THF due to partially quenched charges diminishing electrostatic interactions with the solvent. The ASE is 29.4 kcal/mol in the gas phase and increases by 3.6 kcal/mol in THF which reflects the additional charge separation caused by aromatization of the covalent linker. The ASE of benzene at the same level (34.8 kcal/mol) is comparable to the amount of **4** (Scheme S2). The total intramolecular π-stabilization is 49.6 kcal/mol in the gas phase and 48.2 kcal/mol in THF.

During an exploration of the conformational space, we found a *syn* conformer ($\mathbf{4}_{syn}$) in addition to the *anti* conformer ($\mathbf{4}_{anti}$) that was found in the solid state structure (Figure 5). While $\mathbf{4}_{anti}$ is 4.7 kcal/mol more stable in THF, $\mathbf{4}_{syn}$ is 2.7 kcal/mol more stable in the gas phase. This is consistent with the computed dipole moments. The *anti* conformer with the

Scheme 4. Isodesmic Equations for the Quantification of Intramolecular Push–Pull Stabilization and Aromatic Stabilization Energy[a]

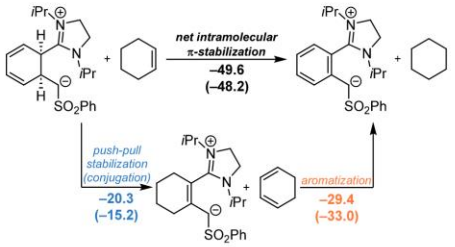

[a]Zero-point corrected electronic energies at 0 K computed at revDSD-PBEP86-D4/def2-QZVPP//PBEh-3c level in kcal/mol. Values in parentheses consider electrostatic interactions from bulk solvation implicitly (SMD model for THF).

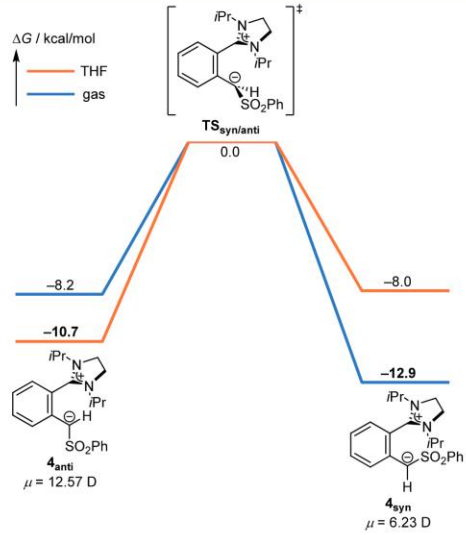

Figure 5. Potential energy surface of the rotational barrier of **4** computed at the revDSD-PBEP86-D4/def2-QZVPP//PBEh-3c level in the gas phase (blue). Bulk solvation was considered implicitly using the SMD model for THF (orange). Dipole moments μ (given in Debye) were computed at the PBE0-D4/def2-TZVPP level.

higher dipole moment (12.57 D) benefits from greater solvation energy compared to the *syn* conformer with a dipole moment of 6.23 D. Note that the dipole moments of $\mathbf{4}_{syn}$ and $\mathbf{4}_{anti}$ are particularly high, even exceeding the dipole moment of *cis*-$C_6F_6H_6$ (Scheme S4).[32] The computed barrier for the rotation around the C1–C1′ bond, interconverting $\mathbf{4}_{syn} \rightleftharpoons \mathbf{4}_{anti}$, is 10.7 kcal/mol in THF (and 12.9 kcal/mol in the gas phase). Thus, the rotational barrier is significantly lower than that of the C–N rotation in *N*,*N*-dimethylacetamide[33] but higher than that of the C–C rotation in 1,3-butadiene (*s-cis*⇌*s-trans*).[34]

In summary, the findings from SCXRD, NMR spectroscopy, CV, and DFT suggest that a zwitterionic description is the

https://doi.org/10.1021/jacs.4c13783
J. Am. Chem. Soc. XXXX, XXX, XXX–XXX

more accurate representation of the electronic structure of **4**, with ^{13}C NMR data implying some delocalization of the negative charge over the phenyl ring. Furthermore, we analyzed the charge distribution and molecular orbitals within the series *o*-xylylene, *o*NHC **5**, and zwitterion **4** at the PBE0/def2-QZVPP//PBE0-D4/def2-TZVPP level of theory. While the charge distribution within the rings is similar, it varies significantly at the exocyclic carbon atoms (Figure S18). The methylene group in *o*-xylylene exhibits a charge of −0.35. The introduction of the NHC substituent (*o*-xylylene → **5**) increases the polarization, resulting in a higher charge density of the methylene group (−0.54) and charge depletion at the C2-position of the *N*-heterocycle (+0.52). Adding the sulfone substituent to the methylene group (**5** → **4**) increases the charge density even further to −0.81, accompanied by charge depletion at the C2-position of the *N*-heterocycle (+0.64). This evaluation is based on gas phase computations, but the results are virtually identical if implicit solvation of **4** in DMF as a polar solvent is taken into account. The polarization is also clearly reflected in the shapes of the HOMO and LUMO. In the case of *o*-xylylene, both reactive centers have the same atomic coefficient in the HOMO and LUMO. Introducing the donor substituent (*o*-xylylene → **5**) raises the energy levels and polarizes the HOMO and LUMO. The donor−acceptor substitution in **4** amplifies this effect: The HOMO is now to 49% localized at the α-sulfonyl carbon, while the LUMO is to 22% localized at the C2-carbon of the imidazolinium ring (Figure S19). A comparison of the ion affinities of **4** and **5** illustrates this effect further (Table S23). We calculated the proton affinities (PAs), methyl cation affinities (MCAs), hydride ion affinities (HIAs), and fluoride ion affinities (FIAs) at the revDSD-PBEP86-D4/def2-QZVPP//PBEh-3c level. The decrease in PAs (−12.2 kcal/mol) and MCAs (−18.1 kcal/mol) by going from **5** to **4** is compensated by an increase in HIAs (+14.1 kcal/mol) and FIAs (+19.0 kcal/mol). The fact that the PA and MCA on the one hand and the FIA and HIA on the other are balanced indicates that **4**, in contrast to NHOs, is not a pure nucleophile but should show both nucleophilic and electrophilic reactivity. Despite the acceptor substituent, the PA of **4** is higher than those of typical NHOs (Scheme S3). This computational result was substantiated experimentally by using **4** as a Brønsted base to generate an NHO from its conjugate acid, demonstrating the increased basicity of acceptor-substituted NHOs compared to that of NHOs (Figure S2). In addition, ^{31}P NMR analysis of triethylphosphine oxide according to the Gutmann−Beckett method reveals deshielding of $\Delta\delta(^{31}P)$ = +9.8 ppm in case of **4**, while no changes in the ^{31}P NMR spectrum were observed for **2** (Figure S3).[35]

In order to clarify the extent to which **4** actually reacts as an ambiphile, we reacted **4** with ammonia borane. Treatment with 1.2 equiv of NH_3BH_3 results in the formation of **2**, indicating spontaneous dehydrogenation of ammonia borane at room temperature (Scheme 5). We monitored the reaction in CD_3CN using ^1H NMR spectroscopy and observed conversion from **4** → **2** with an estimated half-life of $t_{1/2} \approx 0.6$ h (Figure S66). The ^{11}B NMR spectrum shows new signals in the range of −4 to −13 ppm indicative of cyclization products of NH_2BH_2 (Figure S67).[36] The reaction also proceeds in THF-d_8 (68% yield determined by quantitative ^1H NMR spectroscopy). Upon slow evaporation of a saturated *n*-hexane solution of **2**, colorless blocks suitable for SCXRD formed and allowed us to confirm the molecular structure (Figure 6). Comparison

Scheme 5. Dehydrogenation of Ammonia Borane

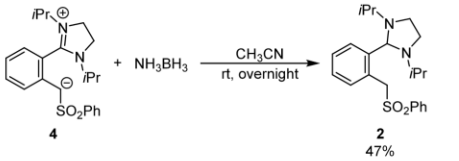

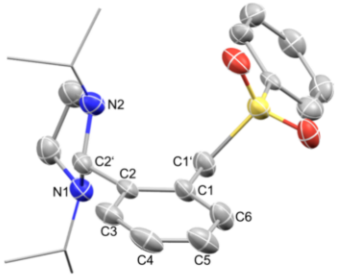

Figure 6. Molecular structure of **2** derived from SCXRD (50% probability ellipsoids, disordered parts, and hydrogens attached to carbons are omitted, and isopropyl groups are shown in stick representation for clarity). Selected bond lengths and angles: C1−C2: 1.404(4) Å, C2−C3: 1.398(5) Å, C3−C4: 1.378(5) Å, C4−C5: 1.374(6) Å, C5−C6: 1.383(5) Å, C6−C1: 1.388(4) Å, C1−C1′: 1.513(5) Å, C2−C2′: 1.512(4) Å, N1−C2′: 1.454(4) Å, N2−C2′: 1.462(4) Å. N1−C2′−C2−C1: 58.4(5)°.

of the bond lengths between **2** and **4** reveals an insignificant change of the C2−C2′ bond (≤0.03 Å difference) but considerable elongation of the N−C2′ bond (+0.13 Å). The C1−C1′ bond is elongated by 0.09 Å at a comparable C1′−C2′ distance (2.98 Å) caused by the uptake of one equivalent of H_2 by **4**. This further substantiates the aforementioned conclusion that the imidazolinium scaffold in **4** is not in conjugation, while the negative charge is partially delocalized across the π-linker.

Furthermore, phenylacetylene adds to **4** at elevated temperatures, resulting in C−H bond cleavage (Scheme 6).

Scheme 6. Addition of Phenylacetylene

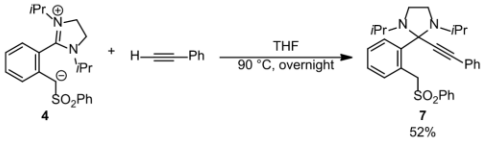

Investigation of the reaction by ^1H NMR spectroscopy shows that **4** and phenylacetylene do not react at room temperature. Upon heating, the air-stable addition product **7** is formed, while no intermediates are detected. For satisfactory yields, an excess of phenylacetylene is necessary (Table S1), resulting in the formation of **7** in 52% yield after column chromatography using Alox-B (17% of the starting material was recovered as imidazolinium salt **3**). Crystals of **7** suitable for SCXRD were grown by slow evaporation of an Et_2O/*n*-hexane solution and allowed us to confirm the molecular structure (Figure 7).

https://doi.org/10.1021/jacs.4c13783
J. Am. Chem. Soc. XXXX, XXX, XXX−XXX

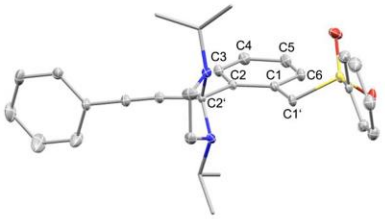

Figure 7. Molecular structure of **7** derived from SCXRD (50% probability ellipsoids, all hydrogens attached to carbons are omitted, and isopropyl groups are shown in stick representation for clarity). Selected bond lengths: C1−C2: 1.4093(12) Å, C2−C3: 1.3946(12) Å, C3−C4: 1.3908(13) Å, C4−C5: 1.3842(14) Å, C5−C6: 1.3898(14) Å, C6−C1: 1.3982(13) Å, C1−C1′: 1.5184(13) Å, C2−C2′: 1.5356(12) Å.

The addition of acetylenes to the C2-position of (benz)-imidazolinium derivatives is documented in the literature and assumed to proceed via a stepwise mechanism involving deprotonation and subsequent addition.[37] A radical mechanism is unlikely due to the increased C(sp^n)−H bond dissociation energies within the series $sp > sp^2 > sp^3$ (Figure S17). According to the calculated potential energy surface (Figure S16), the deprotonation of phenylacetylene by **4** is endergonic (+15.2 kcal/mol), and the subsequent nucleophilic addition of the acetylide is rate-determining with a barrier of 26.8 kcal/mol that is consistent with the experimental finding of a reaction at elevated temperature. This further demonstrates the ambiphilic-like reactivity of zwitterionic **4** since *o*-xylylene and its quinoidal derivatives typically participate in cycloaddition reactions.[22,38] Both the ability of **4** to dehydrogenate ammonia borane and the observed C−H bond cleavage of terminal alkynes indeed recall the reactivity exhibited by phosphine−borane-based FLPs toward terminal alkynes and ammonia borane.[39] Therefore, it seems justified to describe **4** in terms of its reactivity as an intramolecular carbogenic FLP.

CONCLUSIONS

We report the synthesis and isolation of the stable acceptor-substituted *o*NHQ **4**. The detailed analysis of its electronic structure by SCXRD, NMR and UV/vis spectroscopy, CV, and DFT calculations shows that a zwitterionic Lewis structure is a better representation of the electronic structure than a neutral quinoidal resonance structure. According to DFT, the polarization of the π-system is an electronic effect caused by donor−acceptor substitution that stabilizes the charge-separated aromatic state. This effect is further amplified by steric influences. Thus, **4** is a rare example of an organic zwitterion in which the centers of charge are in conjugation.[40] The zwitterionic character of **4** is also reflected in its ambiphilic reactivity, as shown by the dehydrogenation of ammonia borane and the addition of phenylacetylene via C−H bond cleavage. In terms of its reactivity, **4** can therefore be regarded as a carbon-based intramolecular FLP that expands the repertoire of possibilities for bond activation by purely organic compounds. Furthermore, the ambiphilic reactivity of **4** could be a starting point for the development of a new class of organocatalysts that exhibit FLP-like reactivity.

ASSOCIATED CONTENT

Supporting Information

The Supporting Information is available free of charge at https://pubs.acs.org/doi/10.1021/jacs.4c13783.

Experimental procedures, analytical data (NMR, MS, CV, UV/vis, SCXRD), and Cartesian coordinates and energies of computed structures (PDF)

Accession Codes

Deposition Numbers 2369439, 2369515, 2369529, 2369531, and 2369533 contain the supplementary crystallographic data for this paper. These data can be obtained free of charge via the joint Cambridge Crystallographic Data Centre (CCDC) and Fachinformationszentrum Karlsruhe Access Structures service.

AUTHOR INFORMATION

Corresponding Author

Urs Gellrich − *Institut für Organische Chemie, Justus-Liebig-Universität Gießen, 35392 Gießen, Germany; Fachgebiet Organische Chemie, Universität Hohenheim, 70599 Stuttgart, Germany;* orcid.org/0000-0002-8119-9626; Email: urs.gellrich@uni-hohenheim.de

Author

Jama Ariai − *Institut für Organische Chemie, Justus-Liebig-Universität Gießen, 35392 Gießen, Germany;* orcid.org/0000-0003-3083-3663

Complete contact information is available at: https://pubs.acs.org/10.1021/jacs.4c13783

Author Contributions

The manuscript was written through contributions of all authors. All authors have given approval to the final version of the manuscript.

Funding

German research foundation (DFG, GE 3117/1-1 and GE 3117/1-2).

Notes

The authors declare no competing financial interest.

ACKNOWLEDGMENTS

This work was supported by the German research foundation (Emmy−Noether program, GE 3117/1-1 and GE 3117/1-2). We further thank the Aventis Foundation and the Fonds of the Chemical Industry in Germany for supporting preliminary studies on this project with a Hoechst-fellowship to J.A. The authors thank Dr. H. Hausmann for assistance with NMR experiments and Dr. C. Würtele for his support with the SCXRD refinements. Prof. P. R. Schreiner, Prof. R. Göttlich, and Prof. H. A. Wegner are acknowledged for their continuous support.

REFERENCES

(1) (a) Chen, Z. X.; Li, Y.; Huang, F. Persistent and Stable Organic Radicals: Design, Synthesis, and Applications. *Chem.* **2021**, *7* (2), 288−332. (b) Zeng, Z.; Shi, X.; Chi, C.; López Navarrete, J. T.; Casado, J.; Wu, J. Pro-aromatic and anti-aromatic π-conjugated molecules: an irresistible wish to be diradicals. *Chem. Soc. Rev.* **2015**, *44* (18), 6578−6596. (c) Liu, Q.; Onishi, K.; Miyazawa, Y.; Wang, Z.; Hatano, S.; Abe, M. Energetically More Stable Singlet Cyclopentane-1,3-diyl Diradical with π-Single Bonding Character than the Corresponding σ-Single Bonded Compound. *J. Am. Chem. Soc.*

2023, *145* (49), 27089−27094. (d) Abe, M.; Ye, J.; Mishima, M. The chemistry of localized singlet 1,3-diradicals (biradicals): from putative intermediates to persistent species and unusual molecules with a π-single bonded character. *Chem. Soc. Rev.* **2012**, *41* (10), 3808−3820. (e) Sun, Z.; Ye, Q.; Chi, C.; Wu, J. Low band gap polycyclic hydrocarbons: from closed-shell near infrared dyes and semiconductors to open-shell radicals. *Chem. Soc. Rev.* **2012**, *41* (23), 7857−7889.

(2) (a) Messelberger, J.; Grünwald, A.; Pinter, P.; Hansmann, M. M.; Munz, D. Carbene derived diradicaloids−building blocks for singlet fission? *Chem. Sci.* **2018**, *9* (28), 6107−6117. (b) Xia, D.; Keerthi, A.; An, C.; Baumgarten, M. Synthesis of a quinoidal dithieno[2,3-d;2′,3′-d]benzo[2,1-b;3,4-b′]-dithiophene based open-shell singlet biradicaloid. *Org. Chem. Front.* **2017**, *4* (1), 18−21. (c) Wilbuer, J.; Grenz, D. C.; Schnakenburg, G.; Esser, B. Donor- and acceptor-functionalized dibenzo[a,e]pentalenes: modulation of the electronic band gap. *Org. Chem. Front.* **2017**, *4* (5), 658−663. (d) Meyers, F.; Bredas, J. L.; Zyss, J. Electronic structure and nonlinear optical properties of push-pull polyenes: theoretical investigation of benzodithia polyenals and dithiolene polyenals. *J. Am. Chem. Soc.* **1992**, *114* (8), 2914−2921. (e) Dar, A. H.; Gowri, V.; Gopal, A.; Muthukrishnan, A.; Bajaj, A.; Sartaliya, S.; Selim, A.; Ali, M. E.; Jayamurugan, G. Designing of Push−Pull Chromophores with Tunable Electronic and Luminescent Properties Using Urea as the Electron Donor. *J. Org. Chem.* **2019**, *84* (14), 8941−8947. (f) Ullrich, T.; Munz, D.; Guldi, D. M. Unconventional singlet fission materials. *Chem. Soc. Rev.* **2021**, *50* (5), 3485−3518. (g) Casanova, D. Theoretical Modeling of Singlet Fission. *Chem. Rev.* **2018**, *118* (15), 7164−7207. (h) Smith, M. B.; Michl, J. Singlet Fission. *Chem. Rev.* **2010**, *110* (11), 6891−6936.

(3) (a) Busby, E.; Xia, J.; Wu, Q.; Low, J. Z.; Song, R.; Miller, J. R.; Zhu, X.-Y.; Campos, L. M.; Sfeir, M. Y. A design strategy for intramolecular singlet fission mediated by charge-transfer states in donor−acceptor organic materials. *Nat. Mater.* **2015**, *14* (4), 426−433. (b) Margulies, E. A.; Miller, C. E.; Wu, Y.; Ma, L.; Schatz, G. C.; Young, R. M.; Wasielewski, M. R. Enabling singlet fission by controlling intramolecular charge transfer in π-stacked covalent terrylenediimide dimers. *Nat. Chem.* **2016**, *8* (12), 1120−1125. (c) Alvertis, A. M.; Lukman, S.; Hele, T. J. H.; Fuemmeler, E. G.; Feng, J.; Wu, J.; Greenham, N. C.; Chin, A. W.; Musser, A. J. Switching between Coherent and Incoherent Singlet Fission via Solvent-Induced Symmetry Breaking. *J. Am. Chem. Soc.* **2019**, *141* (44), 17558−17570. (d) Berkelbach, T. C.; Hybertsen, M. S.; Reichman, D. R. Microscopic theory of singlet exciton fission. II. Application to pentacene dimers and the role of superexchange. *J. Chem. Phys.* **2013**, *138* (11), 114103. (e) Neef, A.; Beaulieu, S.; Hammer, S.; Dong, S.; Maklar, J.; Pincelli, T.; Xian, R. P.; Wolf, M.; Rettig, L.; Pflaum, J.; Ernstorfer, R. Orbital-resolved observation of singlet fission. *Nature* **2023**, *616* (7956), 275−279. (f) Majdecki, M.; Hsu, C.-H.; Wang, C.-H.; Shi, E. H.-C.; Zakrocka, M.; Wei, Y.-C.; Chen, B.-H.; Lu, C.-H.; Yang, S.-D.; Chou, P.-T.; Gawel, P. Singlet Fission in a New Series of Systematically Designed Through-space Coupled Tetracene Oligomers. *Angew. Chem., Int. Ed.* **2024**, *63* (16), No. e202401103. (g) Zirzlmeier, J.; Lehnherr, D.; Coto, P. B.; Chernick, E. T.; Casillas, R.; Basel, B. S.; Thoss, M.; Tykwinski, R. R.; Guldi, D. M. Singlet fission in pentacene dimers. *Proc. Natl. Acad. Sci. U.S.A.* **2015**, *112* (17), 5325−5330. (h) Majumder, K.; Mukherjee, S.; Panjwani, N. A.; Lee, J.; Bittl, R.; Kim, W.; Patil, S.; Musser, A. J. Controlling Intramolecular Singlet Fission Dynamics via Torsional Modulation of Through-Bond versus Through-Space Couplings. *J. Am. Chem. Soc.* **2023**, *145* (38), 20883−20896. (i) Ito, S.; Nagami, T.; Nakano, M. Design Principles of Electronic Couplings for Intramolecular Singlet Fission in Covalently-Linked Systems. *J. Phys. Chem. A* **2016**, *120* (31), 6236−6241. (j) Korovina, N. V.; Pompetti, N. F.; Johnson, J. C. Lessons from intramolecular singlet fission with covalently bound chromophores. *J. Chem. Phys.* **2020**, *152* (4), 40904. (k) Blaskovits, J. T.; Fumanal, M.; Vela, S.; Corminboeuf, C. Designing Singlet Fission Candidates from Donor−Acceptor Copolymers. *Chem. Mater.* **2020**, *32* (15), 6515−6524. (l) Wang, T.; Liu, H.; Wang, X.; Tang, L.; Zhou, J.; Song, X.; Lv, L.; Chen, W.; Chen, Y.; Li, X. Intramolecular singlet fission and triplet exciton harvesting in tetracene oligomers for solar energy conversion. *J. Mater. Chem. A* **2023**, *11* (16), 8515−8539. (m) Sanders, S. N.; Kumarasamy, E.; Pun, A. B.; Steigerwald, M. L.; Sfeir, M. Y.; Campos, L. M. Intramolecular Singlet Fission in Oligoacene Heterodimers. *Angew. Chem., Int. Ed.* **2016**, *55* (10), 3373−3377. (n) Ito, S.; Nagami, T.; Nakano, M. Correction to "Design Principles of Electronic Couplings for Intramolecular Singlet Fission in Covalently-Linked Systems. *J. Phys. Chem. A* **2017**, *121* (38), 7307.

(4) (a) Kuhn, N.; Bohnen, H.; Kreutzberg, J.; Bläser, D.; Boese, R. 1,3,4,5-Tetramethyl-2-methyleneimidazoline—an Ylidic Olefin. *J. Chem. Soc., Chem. Commun.* **1993**, *14*, 1136−1137. (b) Gruseck, U.; Heuschmann, M. 2-Alkylidenimidazolidine−Synthese, Basizität, ^{1}H- und ^{13}C-NMR-Spektren. *Chem. Ber.* **1987**, *120* (12), 2053−2064. (c) Quast, H.; Ach, M.; Kindermann, M. K.; Rademacher, P.; Schindler, M. Synthese, NMR-Spektren und Photoelektronen-Spektren von cyclischen Keten-N,X1-acetalen (2-Alkyliden-N-heterocyclen). *Chem. Ber.* **1993**, *126* (2), 503−516. (d) Schuldt, R.; Kästner, J.; Naumann, S. Proton Affinities of N-Heterocyclic Olefins and Their Implications for Organocatalyst Design. *J. Org. Chem.* **2019**, *84* (4), 2209−2218. (e) Li, Z.; Ji, P.; Cheng, J.-P. Brönsted Basicities and Nucleophilicities of N-Heterocyclic Olefins in Solution: N-Heterocyclic Carbene versus N-Heterocyclic Olefin. Which Is More Basic, and Which Is More Nucleophilic? *J. Org. Chem.* **2021**, *86* (3), 2974−2985.

(5) (a) Naumann, S. Synthesis, properties & applications of N-heterocyclic olefins in catalysis. *Chem. Commun.* **2019**, *55* (78), 11658−11670. (b) Roy, M. M. D.; Rivard, E. Pushing Chemical Boundaries with N-Heterocyclic Olefins (NHOs): From Catalysis to Main Group Element Chemistry. *Acc. Chem. Res.* **2017**, *50* (8), 2017−2025. (c) Fürstner, A.; Alcarazo, M.; Goddard, R.; Lehmann, C. W. Coordination Chemistry of Ene-1,1-diamines and a Prototype "Carbodicarbene. *Angew. Chem., Int. Ed.* **2008**, *47* (17), 3210−3214. (d) Kronig, S.; Jones, P. G.; Tamm, M. Preparation of 2-Alkylidene-Substituted 1,3,4,5-Tetramethylimidazolines and Their Reactivity Towards Rh^{I} Complexes and $B(C_6F_5)_3$. *Eur. J. Inorg. Chem.* **2013**, *2013* (13), 2301−2314. (e) Rottschäfer, D.; Sharma, M. K.; Neumann, B.; Stammler, H.-G.; Andrada, D. M.; Ghadwal, R. S. A Modular Access to Divinyldiphosphenes with a Strikingly Small HOMO−LUMO Energy Gap. *Chem.—Eur. J.* **2019**, *25* (34), 8127−8134. (f) Powers, K.; Hering-Junghans, C.; McDonald, R.; Ferguson, M. J.; Rivard, E. Improved synthesis of N-heterocyclic olefins and evaluation of their donor strengths. *Polyhedron* **2016**, *108*, 8−14. (g) Ibrahim Al-Rafia, S. M.; Malcolm, A. C.; Liew, S. K.; Ferguson, M. J.; McDonald, R.; Rivard, E. Intercepting low oxidation state main group hydrides with a nucleophilic N-heterocyclic olefin. *Chem. Commun.* **2011**, *47* (24), 6987−6989. (h) Buchmeiser, M. R.; Imbrich, D.; Wang, D.; Naumann, S. Betainic and ionic tungsten (VI) imido alkylidene N-heterocyclic olefin complexes. *J. Organomet. Chem.* **2023**, *991*, No. 122674. (i) Kooij, B.; Dong, Z.; Fadaei-Tirani, F.; Scopelliti, R.; Severin, K. Synthesis and Reactivity of an Anionic Diazoolefin. *Angew. Chem., Int. Ed.* **2023**, *62* (34), No. e202308625. (j) Kooij, B.; Varava, P.; Fadaei-Tirani, F.; Scopelliti, R.; Pantazis, D. A.; van Trieste, G. P., III; Powers, D. C.; Severin, K. Copper Complexes with Diazoolefin Ligands and their Photochemical Conversion into Alkenylidene Complexes. *Angew. Chem., Int. Ed.* **2023**, *62* (4), No. e202214899. (k) Kooij, B.; Dong, Z.; Varava, P.; Fadaei-Tirani, F.; Scopelliti, R.; Piveteau, L.; Severin, K. Vanadium complexes with N-heterocyclic vinylidene ligands. *Chem. Commun.* **2022**, *58* (26), 4204−4207. (l) Feuerstein, W.; Varava, P.; Fadaei-Tirani, F.; Scopelliti, R.; Severin, K. Synthesis, structural characterization, and coordination chemistry of imidazole-based alkylidene ketenes. *Chem. Commun.* **2021**, *57* (87), 11509−11512. (m) Iturmendi, A.; García, N.; Jaseer, E. A.; Munárriz, J.; Sanz Miguel, P. J.; Polo, V.; Iglesias, M.; Oro, L. A. N-Heterocyclic olefins as ancillary ligands in catalysis: a study of their behaviour in transfer hydrogenation reactions. *Dalton Trans.* **2016**, *45* (32), 12835−12845. (n) Watson, I. C.; Schumann, A.; Yu, H.; Davy, E. C.; McDonald, R.; Ferguson, M.

https://doi.org/10.1021/jacs.4c13783
J. Am. Chem. Soc. XXXX, XXX, XXX−XXX

J.; Hering-Junghans, C.; Rivard, E. N-Heterocyclic Olefin-Ligated Palladium(II) Complexes as Pre-Catalysts for Buchwald−Hartwig Aminations. *Chem.—Eur. J.* **2019**, *25* (41), 9678−9690. (o) Schumann, A.; Hering-Junghans, C. NHO to aNHC Isomerization at a Pd^0-Center. *Eur. J. Inorg. Chem.* **2018**, *2018* (22), 2584−2588.

(6) (a) Naumann, S.; Thomas, A. W.; Dove, A. P. N-Heterocyclic Olefins as Organocatalysts for Polymerization: Preparation of Well-Defined Poly(propylene oxide). *Angew. Chem., Int. Ed.* **2015**, *54* (33), 9550−9554. (b) Naumann, S.; Thomas, A. W.; Dove, A. P. Highly Polarized Alkenes as Organocatalysts for the Polymerization of Lactones and Trimethylene Carbonate. *ACS Macro Lett.* **2016**, *5* (1), 134−138. (c) Walther, P.; Frey, W.; Naumann, S. Polarized olefins as enabling (co)catalysts for the polymerization of γ-butyrolactone. *Polym. Chem.* **2018**, *9* (26), 3674−3683. (d) Walther, P.; Krauß, A.; Naumann, S. Lewis Pair Polymerization of Epoxides via Zwitterionic Species as a Route to High-Molar-Mass Polyethers. *Angew. Chem., Int. Ed.* **2019**, *58* (31), 10737−10741.

(7) (a) Wang, Y.-B.; Wang, Y.-M.; Zhang, W.-Z.; Lu, X.-B. Fast CO_2 Sequestration, Activation, and Catalytic Transformation Using N-Heterocyclic Olefins. *J. Am. Chem. Soc.* **2013**, *135* (32), 11996−12003. (b) Saptal, V. B.; Bhanage, B. M. N-Heterocyclic Olefins as Robust Organocatalyst for the Chemical Conversion of Carbon Dioxide to Value-Added Chemicals. *ChemSusChem* **2016**, *9* (15), 1980−1985. (c) Maji, S.; Das, A.; Bhatt, M. M.; Mandal, S. K. Metal-free organocatalytic S-formylation of thiols using CO_2. *Nat. Catal.* **2024**, *7* (4), 375−385. (d) Wang, Z.; Niu, Q.-H.; Xue, X.-S.; Ji, P. The Brönsted Basicities of N-Heterocyclic Olefins in DMSO: An Effective Way to Evaluate the Stability of NHO−CO_2 Adducts. *J. Org. Chem.* **2020**, *85* (20), 13204−13210.

(8) (a) Landman, I. R.; Fadaei-Tirani, F.; Severin, K. Nitrous oxide as a diazo transfer reagent: the synthesis of triazolopyridines. *Chem. Commun.* **2021**, *57*, 11537−11540. (b) Eymann, L. Y. M.; Varava, P.; Shved, A. M.; Curchod, B. F. E.; Liu, Y.; Planes, O. M.; Sienkiewicz, A.; Scopelliti, R.; Fadaei Tirani, F.; Severin, K. Synthesis of Organic Super-Electron-Donors by Reaction of Nitrous Oxide with N-Heterocyclic Olefins. *J. Am. Chem. Soc.* **2019**, *141* (43), 17112−17116. (c) Ariai, J.; Becker, J.; Gellrich, U. Facile (3 + 2) Cycloaddition between an N-Heterocyclic Olefin and Nitrous Oxide at Ambient Conditions. *Eur. J. Org. Chem.* **2024**, *27* (5), No. e202301252. (d) Eymann, L. Y. M.; Varava, P.; Shved, A. M.; Curchod, B. F. E.; Liu, Y.; Planes, O. M.; Sienkiewicz, A.; Scopelliti, R.; Fadaei Tirani, F.; Severin, K. Synthesis of Organic Super-Electron-Donors by Reaction of Nitrous Oxide with N-Heterocyclic Olefins. *J. Am. Chem. Soc.* **2020**, *142* (2), 1112.

(9) (a) Hansmann, M. M. Diazoalkenes: From an Elusive Intermediate to a Stable Substance Class in Organic Chemistry. *Angew. Chem., Int. Ed.* **2023**, *62* (35), No. e202304574. (b) Antoni, P. W.; Reitz, J.; Hansmann, M. M. N_2/CO Exchange at a Vinylidene Carbon Center: Stable Alkylidene Ketenes and Alkylidene Thioketenes from 1,2,3-Triazole Derived Diazoalkenes. *J. Am. Chem. Soc.* **2021**, *143* (32), 12878−12885. (c) Antoni, P. W.; Golz, C.; Holstein, J. J.; Pantazis, D. A.; Hansmann, M. M. Isolation and reactivity of an elusive diazoalkene. *Nat. Chem.* **2021**, *13* (6), 587−593. (d) Varava, P.; Dong, Z.; Scopelliti, R.; Fadaei-Tirani, F.; Severin, K. Isolation and characterization of diazoolefins. *Nat. Chem.* **2021**, *13*, 1055−1060.

(10) Ariai, J.; Ziegler, M.; Würtele, C.; Gellrich, U. An N-Heterocyclic Quinodimethane: A Strong Organic Lewis Base Exhibiting Diradical Reactivity. *Angew. Chem., Int. Ed.* **2024**, *63* (16), No. e202316720.

(11) (a) Hansmann, M. M.; Antoni, P. W.; Pesch, H. Stable Mesoionic N-Heterocyclic Olefins (mNHOs). *Angew. Chem., Int. Ed.* **2020**, *59* (14), 5782−5787. (b) Sun, Q.; Eitzinger, A.; Esken, R.; Antoni, P. W.; Mayer, R. J.; Ofial, A. R.; Hansmann, M. M. Pyridinium-Derived Mesoionic N-Heterocyclic Olefins (py-mNHOs). *Angew. Chem., Int. Ed.* **2024**, *63* (10), No. e202318283. (c) Eitzinger, A.; Reitz, J.; Antoni, P. W.; Mayr, H.; Ofial, A. R.; Hansmann, M. M. Pushing the Upper Limit of Nucleophilicity Scales by Mesoionic N-Heterocyclic Olefins. *Angew. Chem., Int. Ed.* **2023**, *62* (40), No. e202309790.

(12) Allgäuer, D. S.; Mayer, P.; Mayr, H. Nucleophilicity Parameters of Pyridinium Ylides and Their Use in Mechanistic Analyses. *J. Am. Chem. Soc.* **2013**, *135* (40), 15216−15224.

(13) (a) Ahmad, W.-Y.; Omar, S. Drawing Lewis structures: A Step-by-Step Approach. *J. Chem. Educ.* **1992**, *69* (10), 791−792. (b) Kaufmann, I.; Hamza, K. M.; Rundgren, C.-J.; Eriksson, L. Developing an approach for teaching and learning about Lewis structures. *Int. J. Sci. Educ.* **2017**, *39* (12), 1601−1624. (c) Pardo, J. Q. Teaching a Model for Writing Lewis Structures. *J. Chem. Educ.* **1989**, *66* (6), 456−458. (d) Suidan, L.; Badenhoop, J. K.; Glendening, E. D.; Weinhold, F. Common Textbook and Teaching Misrepresentations of Lewis Structures. *J. Chem. Educ.* **1995**, *72* (7), 583−586. (e) Lever, A. B. P. Lewis Structures and the Octet Rule. An automatic procedure for writing canonical forms. *J. Chem. Educ.* **1972**, *49* (12), 819−821.

(14) (a) Chernichenko, K.; Nieger, M.; Leskelä, M.; Repo, T. Hydrogen activation by 2-boryl-N,N-dialkylanilines: a revision of Piers' ansa-aminoborane. *Dalton Trans.* **2012**, *41* (30), 9029−9032. (b) Chernichenko, K.; Madarász, Á.; Pápai, I.; Nieger, M.; Leskelä, M.; Repo, T. A frustrated-Lewis-pair approach to catalytic reduction of alkynes to cis-alkenes. *Nat. Chem.* **2013**, *5*, 718−723.

(15) Inés, B.; Holle, S.; Goddard, R.; Alcarazo, M. Heterolytic S−S Bond Cleavage by a Purely Carbogenic Frustrated Lewis Pair. *Angew. Chem., Int. Ed.* **2010**, *49* (45), 8389−8391.

(16) (a) Runyon, J. W.; Steinhof, O.; Dias, H. V. R.; Calabrese, J. C.; Marshall, W. J.; Arduengo, A. J. Carbene-Based Lewis Pairs for Hydrogen Activation. *Aust. J. Chem.* **2011**, *64* (8), 1165−1172. (b) Shaikh, A. C.; Veleta, J. M.; Moutet, J.; Gianetti, T. L. Trioxatriangulenium (TOTA$^+$) as a robust carbon-based Lewis acid in frustrated Lewis pair chemistry. *Chem. Sci.* **2021**, *12* (13), 4841−4849. (c) Weicker, S. A.; Stephan, D. W. Main Group Lewis Acids in Frustrated Lewis Pair Chemistry: Beyond Electrophilic Boranes. *Bull. Chem. Soc. Jpn.* **2015**, *88* (8), 1003−1016.

(17) (a) Raabe, G.; Gais, H.-J.; Fleischhauer, J. Ab Initio Study of the Effect of Fluorination upon the Structure and Configurational Stability of α-Sulfonyl Carbanions: The Role of Negative Hyperconjugation. *J. Am. Chem. Soc.* **1996**, *118* (19), 4622−4630. (b) Wolfe, S.; Rauk, A.; Csizmadia, I. G. Structure of an.alpha.-sulfonyl carbanion. *J. Am. Chem. Soc.* **1969**, *91* (6), 1567−1569. (c) Grossert, J. S.; Hoyle, J.; Cameron, T. S.; Roe, S. P.; Vincent, B. R. The structures of some sulphur-stabilized carbanions and stereoelectronic requirements for the formation of α-sulphonyl carbanions. *Can. J. Chem.* **1987**, *65* (6), 1407−1415. (d) Alabugin, I. V.; Gilmore, K. M.; Peterson, P. W. Hyperconjugation. *WIREs Comput. Mol. Sci.* **2011**, *1* (1), 109−141.

(18) Orita, A.; Hasegawa, D.; Nakano, T.; Otera, J. Double Elimination Protocol for Synthesis of 5,6,11,12-Tetradehydrodibenzo-[a,e]cyclooctene. *Chem.—Eur. J.* **2002**, *8* (9), 2000−2004.

(19) Salerno, A.; Caterina, C.; Perillo, I. A. Synthesis of Substituted 1H,5-Dihydroimidazolium Salts by Dehydrogenation of Imidazolidines. *Synth. Commun.* **2000**, *30* (18), 3369−3382.

(20) Song, H.; Lee, E. Revisiting the Reaction of IPr with Tritylium: An Alternative Mechanistic Pathway**. *Chem.—Eur. J.* **2023**, *29* (12), No. e202203364.

(21) (a) Adamo, C.; Barone, V. Toward reliable density functional methods without adjustable parameters: The PBE0 model. *J. Chem. Phys.* **1999**, *110* (13), 6158−6170. (b) Weigend, F.; Ahlrichs, R. Balanced basis sets of split valence, triple zeta valence and quadruple zeta valence quality for H to Rn: Design and assessment of accuracy. *Phys. Chem. Chem. Phys.* **2005**, *7* (18), 3297−3305. (c) Caldeweyher, E.; Bannwarth, C.; Grimme, S. Extension of the D3 dispersion coefficient model. *J. Chem. Phys.* **2017**, *147* (3), 34112. (d) Caldeweyher, E.; Ehlert, S.; Hansen, A.; Neugebauer, H.; Spicher, S.; Bannwarth, C.; Grimme, S. A generally applicable atomic-charge dependent London dispersion correction. *J. Chem. Phys.* **2019**, *150* (15), 154122.

(22) Segura, J. L.; Martín, N. o-Quinodimethanes: Efficient Intermediates in Organic Synthesis. *Chem. Rev.* **1999**, *99* (11), 3199−3246.

https://doi.org/10.1021/jacs.4c13783
J. Am. Chem. Soc. XXXX, XXX, XXX−XXX

(23) (a) Zeonjuk, L. L.; Vankova, N.; Mavrandonakis, A.; Heine, T.; Röschenthaler, G.-V.; Eicher, J. On the Mechanism of Hydrogen Activation by Frustrated Lewis Pairs. *Chem.—Eur. J.* **2013**, *19* (51), 17413−17424. (b) Sieland, B.; Stahn, M.; Schoch, R.; Daniliuc, C.; Spicher, S.; Grimme, S.; Hansen, A.; Paradies, J. Dispersion Energy-Stabilized Boron and Phosphorus Lewis Pairs. *Angew. Chem., Int. Ed.* **2023**, *62* (35), No. e202308752.

(24) (a) Schneider, T. F.; Werz, D. B. Ring-Enlargement Reactions of Donor−Acceptor-Substituted Cyclopropanes: Which Combinations are Most Efficient? *Org. Lett.* **2011**, *13* (7), 1848−1851. (b) Kreft, A.; Lücht, A.; Grunenberg, J.; Jones, P. G.; Werz, D. B. Kinetic Studies of Donor−Acceptor Cyclopropanes: The Influence of Structural and Electronic Properties on the Reactivity. *Angew. Chem., Int. Ed.* **2019**, *58* (7), 1955−1959. (c) Schneider, T. F.; Kaschel, J.; Werz, D. B. A New Golden Age for Donor−Acceptor Cyclopropanes. *Angew. Chem., Int. Ed.* **2014**, *53* (22), 5504−5523. (d) Werz, D. B.; Biju, A. T. Uncovering the Neglected Similarities of Arynes and Donor−Acceptor Cyclopropanes. *Angew. Chem., Int. Ed.* **2020**, *59* (9), 3385−3398. (e) Ahlburg, N. L.; Hergert, O.; Jones, P. G.; Werz, D. B. Donor-Acceptor Cyclopropanes: Activation Enabled by a Single, Vinylogous Acceptor. *Angew. Chem., Int. Ed.* **2023**, *62* (1), No. e202214390. (f) von Köller, H. F.; Jones, P. G.; Werz, D. B. A Widely Applicable and Versatile Method for the Ring-Opening 1,3-Carbocarbonation of Donor-Acceptor Cyclopropanes. *Chem.—Eur. J.* **2023**, *29* (20), No. e202203986. (g) Kolb, S.; Petzold, M.; Brandt, F.; Jones, P. G.; Jacob, C. R.; Werz, D. B. Electrocatalytic Activation of Donor−Acceptor Cyclopropanes and Cyclobutanes: An Alternative $C(sp^3)$−$C(sp^3)$ Cleavage Mode. *Angew. Chem., Int. Ed.* **2021**, *60* (29), 15928−15934.

(25) Viesser, R. V.; Ducati, L. C.; Tormena, C. F.; Autschbach, J. The unexpected roles of σ and π orbitals in electron donor and acceptor group effects on the ^{13}C NMR chemical shifts in substituted benzenes. *Chem. Sci.* **2017**, *8* (9), 6570−6576.

(26) (a) Elser, V.; Haddon, R. C. Icosahedral C_{60}: an aromatic molecule with a vanishingly small ring current magnetic susceptibility. *Nature* **1987**, *325* (6107), 792−794. (b) Saunders, M.; Jiménez-Vázquez, H. A.; Cross, R. J.; Mroczkowski, S.; Freedberg, D. I.; Anet, F. A. L. Probing the interior of fullerenes by ^3He NMR spectroscopy of endohedral $^3He@C_{60}$ and $^3He@C_{70}$. *Nature* **1994**, *367* (6460), 256−258. (c) Saunders, M.; Cross, R. J.; Jiménez-Vázquez, H. A.; Shimshi, R.; Khong, A. Noble Gas Atoms Inside Fullerenes. *Science* **1996**, *271* (5256), 1693−1697. (d) Schleyer, P. v. R.; Maerker, C.; Dransfeld, A.; Jiao, H.; van Eikema Hommes, N. J. R. Nucleus-Independent Chemical Shifts: A Simple and Efficient Aromaticity Probe. *J. Am. Chem. Soc.* **1996**, *118* (26), 6317−6318. (e) Chen, Z.; Wannere, C. S.; Corminboeuf, C.; Puchta, R.; Schleyer, P. V. R. Nucleus-Independent Chemical Shifts (NICS) as an Aromaticity Criterion. *Chem. Rev.* **2005**, *105* (10), 3842−3888. (f) Stanger, A. NICS−Past and Present. *Eur. J. Org. Chem.* **2020**, *2020* (21), 3120−3127.

(27) (a) Gompper, R.; Wagner, H.-U.; Kutter, E. Ketenderivate, XIII. Stabile p-Chinodimethane, I: Synthesen und Eigenschaften. *Chem. Ber.* **1968**, *101* (12), 4123−4143. (b) Gompper, R.; Wagner, H.-U. Dereinfluss der anellierung auf die farbe von chinonmethiden, chinodimethanen und arylcarboniumionen. *Tetrahedron Lett.* **1968**, *9* (2), 165−169. (c) Zeng, Z.; Lee, S.; Son, M.; Fukuda, K.; Burrezo, P. M.; Zhu, X.; Qi, Q.; Li, R.-W.; Navarrete, J. T. L.; Ding, J.; Casado, J.; Nakano, M.; Kim, D.; Wu, J. Push−Pull Type Oligo(N-annulated perylene)quinodimethanes: Chain Length and Solvent-Dependent Ground States and Physical Properties. *J. Am. Chem. Soc.* **2015**, *137* (26), 8572−8583. (d) Smith, M. J.; Clegg, W.; Nguyen, K. A.; Rogers, J. E.; Pachter, R.; Fleitz, P. A.; Anderson, H. L. Synthesis and crystal structure of a push−pull quinoidal porphyrin: a nanoporous framework assembled from cyclic trimer aggregates. *Chem. Commun.* **2005**, *19*, 2433−2435. (e) Takahashi, T.; Takimiya, K.; Otsubo, T.; Aso, Y. Synthesis and Spectral Properties of a Highly Soluble Push−Pull Type of Quinoidal Thiophenes. *Org. Lett.* **2005**, *7* (20), 4313−4316. (f) Inoue, S.; Aso, Y.; Otsubo, T. Push-pull type of diphenoquinoid chromophores as novel near-infrared dyes. *Chem. Commun.* **1997**, *12*, 1105−1106.

(28) Shang, W.; Meng, W.; Chen, L.; Shangguan, Z.; Huang, Y.; Zhang, X.-S.; Li, C.; Bai, S.; Zhang, G.; Zhang, D. Novel Dissymmetric Formal Quinoidal Molecules End-Capped by Dicyanomethylene and Triphenylphosphonium. *Angew. Chem., Int. Ed.* **2024**, *63* (46), No. e202412704.

(29) (a) Chai, J.-D.; Head-Gordon, M. Systematic optimization of long-range corrected hybrid density functionals. *J. Chem. Phys.* **2008**, *128* (8), 84106. (b) Mardirossian, N.; Head-Gordon, M. ωB97X-V: A 10-parameter, range-separated hybrid, generalized gradient approximation density functional with nonlocal correlation, designed by a survival-of-the-fittest strategy. *Phys. Chem. Chem. Phys.* **2014**, *16* (21), 9904−9924. (c) Müller, M.; Hansen, A.; Grimme, S. ωB97X-3c: A composite range-separated hybrid DFT method with a molecule-optimized polarized valence double-ζ basis set. *J. Chem. Phys.* **2023**, *158* (1), 14103.

(30) Lide, D. R. *CRC Handbook of Chemistry and Physics, Internet Version 2005*; CRC Press, 2005.

(31) (a) Santra, G.; Sylvetsky, N.; Martin, J. M. L. Minimally Empirical Double-Hybrid Functionals Trained against the GMTKN55 Database: revDSD-PBEP86-D4, revDOD-PBE-D4, and DOD-SCAN-D4. *J. Phys. Chem. A* **2019**, *123* (24), 5129−5143. (b) Santra, G.; Martin, J. M. L. Empirical Double-Hybrid Density Functional Theory: A 'Third Way' In Between WFT and DFT. *Isr. J. Chem.* **2020**, *60* (8−9), 787−804. (c) Grimme, S.; Brandenburg, J. G.; Bannwarth, C.; Hansen, A. Consistent structures and interactions by density functional theory with small atomic orbital basis sets. *J. Chem. Phys.* **2015**, *143* (5), 54107. (d) Marenich, A. V.; Cramer, C. J.; Truhlar, D. G. Universal Solvation Model Based on Solute Electron Density and on a Continuum Model of the Solvent Defined by the Bulk Dielectric Constant and Atomic Surface Tensions. *J. Phys. Chem. B* **2009**, *113* (18), 6378−6396.

(32) Keddie, N. S.; Slawin, A. M. Z.; Lebl, T.; Philp, D.; O'Hagan, D. All-cis 1,2,3,4,5,6-hexafluorocyclohexane is a facially polarized cyclohexane. *Nat. Chem.* **2015**, *7* (6), 483−488.

(33) (a) Carreira, L. A. Determination of the torsional potential function of 1,3-butadiene. *J. Chem. Phys.* **1975**, *62* (10), 3851−3854. (b) Gasparro, F. P.; Kolodny, N. H. NMR Determination of the Rotational Barrier in N,N-dimethylacetamide. A physical chemistry experiment. *J. Chem. Educ.* **1977**, *54* (4), 258−261. (c) Ross, B. D.; True, N. S.; Matson, G. B. Gas-phase Nuclear Magnetic Resonance Investigation of Chemical Exchange in N,N-Dimethylacetamide. Medium Effects on Kinetic Parameters. *J. Phys. Chem.* **1984**, *88* (12), 2675−2678. (d) Wiberg, K. B.; Rablen, P. R.; Rush, D. J.; Keith, T. A. Amides. 3. Experimental and Theoretical Studies of the Effect of the Medium on the Rotational Barriers for N,N-Dimethylformamide and N,N-Dimethylacetamide. *J. Am. Chem. Soc.* **1995**, *117* (15), 4261−4270.

(34) Murcko, M. A.; Castejon, H.; Wiberg, K. B. Carbon−Carbon Rotational Barriers in Butane, 1-Butene, and 1,3-Butadiene. *J. Phys. Chem.* **1996**, *100* (40), 16162−16168.

(35) (a) Mayer, U.; Gutmann, V.; Gerger, W. The acceptor number — A quantitative empirical parameter for the electrophilic properties of solvents. *Monatsh. Chem.* **1975**, *106* (6), 1235−1257. (b) Beckett, M. A.; Strickland, G. C.; Holland, J. R.; Sukumar Varma, K. A convenient n.m.r. method for the measurement of Lewis acidity at boron centres: correlation of reaction rates of Lewis acid initiated epoxide polymerizations with Lewis acidity. *Polymer* **1996**, *37* (20), 4629−4631.

(36) (a) Al-Kukhun, A.; Hwang, H. T.; Varma, A. Mechanistic studies of ammonia borane dehydrogenation. *Int. J. Hydrogen Energy* **2013**, *38* (1), 169−179. (b) Yang, X.; Zhao, L.; Fox, T.; Wang, Z.-X.; Berke, H. Transfer Hydrogenation of Imines with Ammonia−Borane: A Concerted Double-Hydrogen-Transfer Reaction. *Angew. Chem., Int. Ed.* **2010**, *49* (11), 2058−2062.

(37) (a) Chen, W.-C.; Shih, W.-C.; Jurca, T.; Zhao, L.; Andrada, D. M.; Peng, C.-J.; Chang, C.-C.; Liu, S.-k.; Wang, Y.-P.; Wen, Y.-S.; Yap, G. P. A.; Hsu, C.-P.; Frenking, G.; Ong, T.-G. Carbodicarbenes:

https://doi.org/10.1021/jacs.4c13783
J. Am. Chem. Soc. XXXX, XXX, XXX−XXX

Unexpected π-Accepting Ability during Reactivity with Small Molecules. *J. Am. Chem. Soc.* **2017**, *139* (36), 12830−12836. (b) Golantsov, N. E.; Golubenkova, A. S.; Festa, A. A.; Varlamov, A. V.; Voskressensky, L. G. A Domino Route toward Polysubstituted Pyrroles from 2-Imidazolines and Electron-Deficient Alkynes. *Org. Lett.* **2020**, *22* (12), 4726−4731.

(38) (a) Adachi, K.; Hirose, S.; Ueda, Y.; Uekusa, H.; Hamura, T. Thermodynamically Stable o-Quinodimethane: Synthesis, Structure, and Reactivity. *Chem.—Eur. J.* **2021**, *27* (11), 3665−3669. (b) Inagaki, K.; Onozawa, Y.; Fukuhara, Y.; Yokogawa, D.; Muto, K.; Yamaguchi, J. Facile Generation of ortho-Quinodimethanes Toward Polycyclic Compounds. *ChemRxiv (Organic Chemistry)*. **2024**. DOI: (accessed 2024-11-02). (c) Sano, H.; Ohtsuka, H.; Migita, T. A convenient method for the generation of o-quinodimethanes by proton induced 1,4-elimination of o-(1-hydroxyalkyl)benzyltributylstannanes. *J. Am. Chem. Soc.* **1988**, *110* (6), 2014−2015.

(39) (a) Dureen, M. A.; Stephan, D. W. Terminal Alkyne Activation by Frustrated and Classical Lewis Acid/Phosphine Pairs. *J. Am. Chem. Soc.* **2009**, *131* (24), 8396−8397. (b) Mo, Z.; Rit, A.; Campos, J.; Kolychev, E. L.; Aldridge, S. Catalytic B−N Dehydrogenation Using Frustrated Lewis Pairs: Evidence for a Chain-Growth Coupling Mechanism. *J. Am. Chem. Soc.* **2016**, *138* (10), 3306−3309. (c) Boom, D. H. A.; de Boed, E. J. J.; Nicolas, E.; Nieger, M.; Ehlers, A. W.; Jupp, A. R.; Slootweg, J. C. Catalytic Dehydrogenation of Amine-Boranes using Geminal Phosphino-Boranes. *Z. Anorg. Allg. Chem.* **2020**, *646* (13), 586−592. (d) Stephan, D. W. The broadening reach of frustrated Lewis pair chemistry. *Science* **2016**, *354* (6317), aaf7229. (e) Stephan, D. W.; Erker, G. Frustrated Lewis Pair Chemistry: Development and Perspectives. *Angew. Chem., Int. Ed.* **2015**, *54* (22), 6400−6441.

(40) Chrysochos, N.; Pätsch, S.; Elvers, B. J.; Krummenacher, I.; Nandeshwar, M.; Prabusankar, G.; Braunschweig, H.; Schulzke, C.; Ravat, P.; Jana, A. Introducing an orthogonally polarized electron-rich alkene: synthesis of a zwitterionic boron-containing π-conjugated system. *Chem. Commun.* **2023**, *59* (82), 12350−12353.

https://doi.org/10.1021/jacs.4c13783
J. Am. Chem. Soc. XXXX, XXX, XXX−XXX

6 Publikationen in Kooperation

6.1 Synthesis and characterization of a formal 21-electron cobaltocene derivative

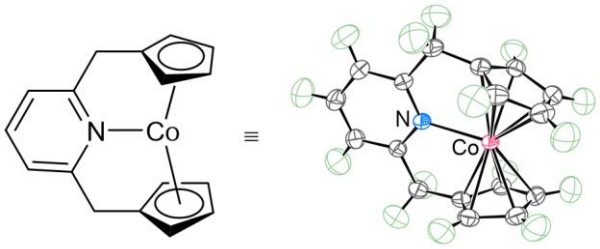

Metallocene sind äußerst vielseitige metallorganische Verbindungen und können in ihren Komplexen eine diverse Anzahl formaler Valenzelektronen stabilisieren. Bislang wurden *d*-Block-Metallocene mit einer Elektronenzahl von bis zu 20 synthetisiert und in der Katalyse, der Sensorik und anderen Bereichen eingesetzt. Metallocene mit mehr als 20 Elektronen sind jedoch bislang nur schwer zugänglich. Die Synthese und Isolierung solcher Komplexe stellt eine Herausforderung dar, weil die Metall−Kohlenstoff-Bindungen in *d*-Block-Metallocenen mit zunehmender Abweichung von der stabilen 18-Elektronen-Konfiguration schwächer werden. Wir berichten hier über die Synthese, Isolierung und Charakterisierung eines 21-Elektronen-Cobaltocen-Derivats. Diese Entdeckung basiert auf einem Ligandendesign, das die Koordination eines Elektronenpaardonors an ein 19-Elektronen-Cobaltocen-Derivat unter Beibehaltung der Cobalt−Kohlenstoff-Bindungen ermöglicht – ein bisher unerforschter synthetischer Ansatz. Weiterhin klären wir den Ursprung der Stabilität, die Redoxchemie und den Spin-Zustand des 21-Elektronen-Komplexes auf. Diese Studie zeigt eine synthetische Methode, die Struktur, die chemische Bindung und die Eigenschaften des 21-Elektronen-Metallocen-Derivats auf, die unser konzeptionelles Verständnis der Chemie der *d*-Block-Metallocene erweitert. Wir erwarten, dass dieser Bericht neuartige synthetische Möglichkeiten in der Chemie der *d*-Block-Übergangsmetalle, einschließlich der Bereiche Katalyse und Materialchemie, eröffnen wird.

Referenz:

S. Takebayashi, J. Ariai, U. Gellrich, S. V. Kartashov, R. R. Fayzullin, H.-B. Kang, T. Yamane, K. Sugisaki, K. Sato, *Nat. Commun.* **2023**, *14*, 4979.

DOI: 10.1038/s41467-023-40557-7

Akzeptiertes Manuskript online: 1. August 2023

Final veröffentlichte Version online: 5. September 2023

nature communications

Article

https://doi.org/10.1038/s41467-023-40557-7

Synthesis and characterization of a formal 21-electron cobaltocene derivative

Received: 26 April 2023

Accepted: 1 August 2023

Published online: 05 September 2023

Check for updates

Satoshi Takebayashi[1] ✉, Jama Ariai[2], Urs Gellrich[2] ✉, Sergey V. Kartashov[3], Robert R. Fayzullin[3] ✉, Hyung-Been Kang[4], Takeshi Yamane[5], Kenji Sugisaki[5,6,7,8] & Kazunobu Sato[5]

Metallocenes are highly versatile organometallic compounds. The versatility of the metallocenes stems from their ability to stabilize a wide range of formal electron counts. To date, *d*-block metallocenes with an electron count of up to 20 have been synthesized and utilized in catalysis, sensing, and other fields. However, *d*-block metallocenes with more than formal 20-electron counts have remained elusive. The synthesis and isolation of such complexes are challenging because the metal–carbon bonds in *d*-block metallocenes become weaker with increasing deviation from the stable 18-electron configuration. Here, we report the synthesis, isolation, and characterization of a 21-electron cobaltocene derivative. This discovery is based on the ligand design that allows the coordination of an electron pair donor to a 19-electron cobaltocene derivative while maintaining the cobalt–carbon bonds, a previously unexplored synthetic approach. Furthermore, we elucidate the origin of the stability, redox chemistry, and spin state of the 21-electron complex. This study reveals a synthetic method, structure, chemical bonding, and properties of the 21-electron metallocene derivative that expands our conceptual understanding of *d*-block metallocene chemistry. We expect that this report will open up previously unexplored synthetic possibilities in *d*-block transition metal chemistry, including the fields of catalysis and materials chemistry.

Since the discovery of ferrocene in the 1950s by Kealy and Pauson, as well as Miller et al.[1], and the Nobel Prize-winning work of Fischer and Wilkinson[2,3], various derivatives of metallocenes have been synthesized and have played pivotal roles in important discoveries in a variety of fields, including catalysis[4,5], materials[6–9], energy[10], and medical[11,12] sciences (Fig. 1a). The versatility of metallocenes stems from the ability of the cyclopentadienyl ligand (Cp) and its derivatives to stabilize metals with a wide range of valence electron counts. To date, *d*-block metallocenes and their derivatives with a formal electron count in the range from 14 to 20, including recently synthesized 16-electron ferrocene dication[13] and 20-electron cobaltocene anion[14], have been isolated. Wilkinson and Hursthouse et al. reported a possible formal 21-electron manganocene derivative, $MnCp_2(dmpe)$ [dmpe: 1,2-bis(dimethylphosphino)ethane] (Fig. 1b)[15]. However, as noted by the

[1]Science and Technology Group, Okinawa Institute of Science and Technology Graduate University, 1919-1 Tancha, Onna-son, Okinawa 904-0495, Japan. [2]Institute of Organic Chemistry, Justus Liebig University Giessen, Heinrich-Buff-Ring 17, Giessen D-35392, Germany. [3]Arbuzov Institute of Organic and Physical Chemistry, FRC Kazan Scientific Center, Russian Academy of Sciences, 8 Arbuzov Street, Kazan 420088, Russian Federation. [4]Engineering Section, Okinawa Institute of Science and Technology Graduate University, 1919-1 Tancha, Onna-son, Okinawa 904-0495, Japan. [5]Department of Chemistry, Graduate School of Science, Osaka Metropolitan University, 3-3-138 Sugimoto, Sumiyoshi-ku, Osaka 558-8585, Japan. [6]JST PRESTO, 4-1-8 Honcho, Kawaguchi, Saitama 332-0012, Japan. [7]Present address: Graduate School of Science and Technology, Keio University, 7-1 Shinkawasaki, Saiwai-ku, Kawasaki, Kanagawa 212-0032, Japan. [8]Present address: Quantum Computing Center, Keio University, 3-14-1 Hiyoshi, Kohoku-ku, Yokohama, Kanagawa 223-8522, Japan.
✉e-mail: satoshi.takebayashi@oist.jp; urs.gellrich@org.chemie.uni-giessen.de; robert.fayzullin@gmail.com

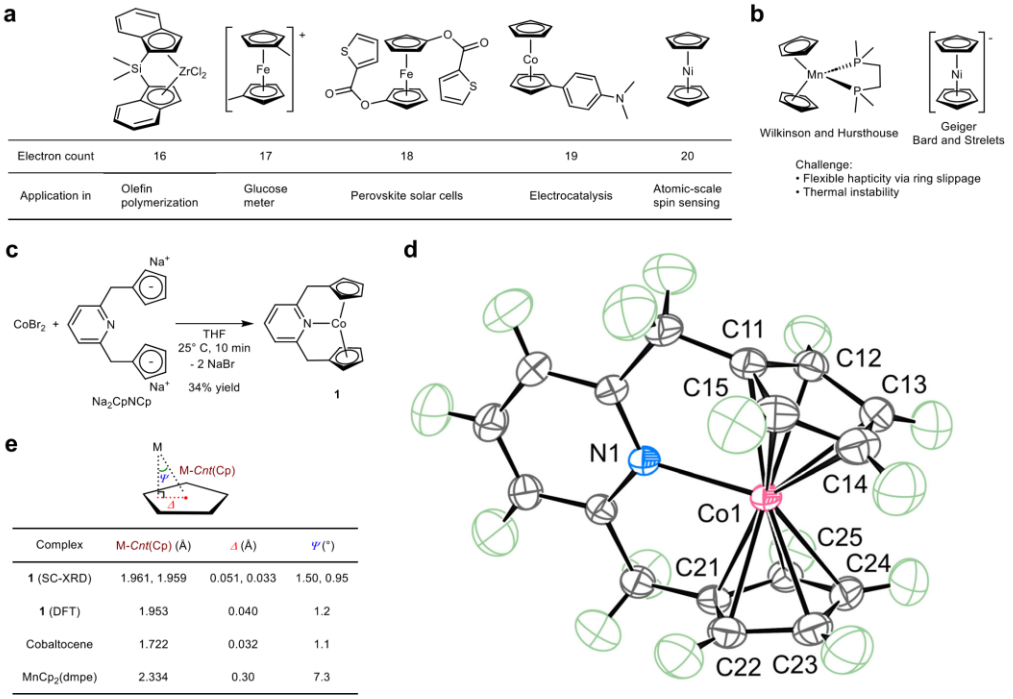

Complex	M-*Cnt*(Cp) (Å)	Δ (Å)	Ψ (°)
1 (SC-XRD)	1.961, 1.959	0.051, 0.033	1.50, 0.95
1 (DFT)	1.953	0.040	1.2
Cobaltocene	1.722	0.032	1.1
$MnCp_2$(dmpe)	2.334	0.30	7.3

Fig. 1 | Preparation of 21-electron metallocene derivatives. a Selected examples of metallocenes and their applications. **b** Previously proposed 21-electron metallocene derivatives. **c** Synthetic route to the 21-electron cobaltocene derivative, complex **1**. THF: tetrahydrofuran. **d** Oak Ridge Thermal Ellipsoid Plot (ORTEP) of **1** at the 80% probability level according to high-resolution single-crystal X-ray diffraction (SC-XRD). Green ellipsoids: hydrogen atoms. **e** Comparison of M–*Cnt*(Cp), Δ, and Ψ values. M: metal. DFT: density functional theory. dmpe: 1,2-bis(dimethylphosphino)ethane. Cp: cyclopentadienyl.

authors, the formation of this complex does not follow the expected trend of other metallocenes[16]. Furthermore, as with other manganocene complexes, the coordination mode of the Cp ligands in this complex deviates from the ideal η^5-coordination because of ring slippage[15,17–22]. This anomalous behavior of manganocene complexes is attributed to the primarily electrostatic character of the Mn–C(Cp) interactions, and the observed coordination modes are mainly controlled by the steric factor of the ligands[22–24]. The solid-state zigzag chain structure of $MnCp_2$ is a vivid example of the anomalous coordination chemistry of manganocene complexes[23]. Therefore, according to the available literature data, the formal electron count of $MnCp_2$(dmpe) cannot be conclusively described. Geiger et al.[25] and later Bard and Strelets et al.[26] reported the electrochemical reduction of $NiCp_2$ and proposed the formation of formal 21-electron $NiCp_2^-$ based on cyclic voltammetry (CV) (Fig. 1b). However, since this complex is thermally unstable and cannot be isolated, the possibilities for its characterization are limited.

The 18-electron rule works best for the complexes with strong π-accepting ligands[27] and the existence of formal 14- to 20-electron metallocenes clearly shows that the 18-electron rule is only loosely applicable to metallocene complexes, especially paramagnetic ones. Furthermore, it is worth nothing to point out that a bonding model based on sd^n hybridization and 3c–4e hypervalent bonding[28–30] indicates the possible formation of formal 21-electron metallocene derivatives by exploiting weaker attractive interactions such as higher multi-center donor–acceptor interactions, long-range electrostatics, London dispersion, and/or entropically favorable interstitial vacancies[31]. Nevertheless, the isolation of well-defined *d*-block metallocenes or their derivatives with more than a formal 20-electron count has remained elusive. The difficulty in synthesizing formal 21-electron complexes lies in the fact that increasing deviation from the stable 18-electron configuration destabilizes metal–C(Cp) interactions and promotes the change of hapticity of Cp ligands[32–37] or decomposition of the complexes[25,26]. Here, we report the synthesis, isolation, and detailed theoretical and experimental characterization of a new cobaltocene derivative with a formal electron count of 21 (Fig. 1c).

Results and Discussion

Synthesis and spectroscopic characterization

Inspired by the coordination chemistry of Cp_2Ni[32], we envisioned that the incorporation of two Cp ligands into a pyridine-based pincer ligand motif might allow the *N*-coordination of the pyridine ligand to the metal center while maintaining the η^5-coordination mode of the two Cp groups. For this reason, the Na_2CpNCp ligand (Fig. 1c)[38] was chosen for the synthesis of metallocene derivatives with formal valence electron counts of more than 20. Prior to this work, the coordination chemistry of *d*-block metals and Na_2CpNCp was known only with metals with a formal *d*-electron count of less than four[39–41]. Portionwise addition of Na_2CpNCp to a tetrahydrofuran (THF) solution of $CoBr_2$ at room temperature resulted in the formation of a NaBr precipitate. Following the workup, an orange crystalline solid of 2,6-bis(methylenecyclopentadienyl)pyridinecobalt (**1**) was isolated in 34% yield (average of two experiments) (Fig. 1c). Unlike $NiCp_2^-$, complex **1** was

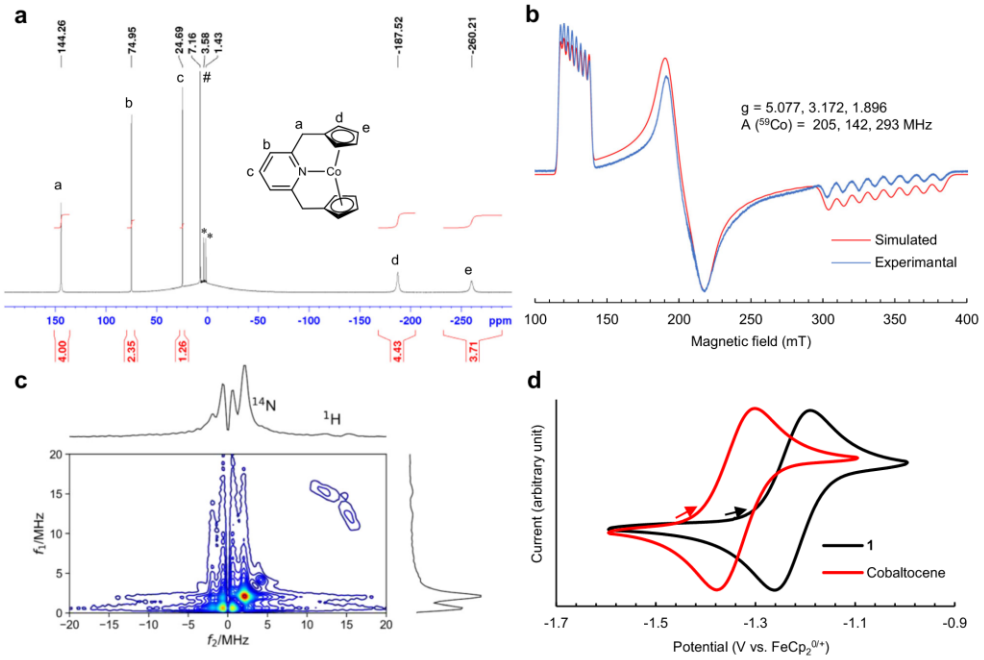

Fig. 2 | Characterization of complex 1. a ^{1}H NMR (400.15 MHz, 298 K, in C_6D_6) spectrum of **1** and signal assignments (a-e). *: signals from residual THF. #: a signal from residual C_6D_5H. **b** Experimental (4.2 K, toluene glass) and simulated X-band EPR spectra of **1** using fictitious $S = 1/2$. g: effective g-values. A(^{59}Co): ^{59}Co hyperfine coupling constants. **c** Four-pulse HYSCORE spectrum of **1** observed at 320 mT (4 K, toluene-d_8 glass). **d** CV of **1** and cobaltocene recorded with a glassy carbon electrode (3 mm diameter) from −1.6 to −1 V range with a scan rate of 0.01 V s^{-1}, in 0.1 M $[Bu_4N]PF_6$ THF at 25 °C, and reported vs. $FeCp_2^{+/0}$. The starting point (open circuit potential) and direction of scans are indicated by arrows.

stable as a solid or as a solution under nitrogen at ambient temperature.

In order to unambiguously show the bonding situation and formal electron count of **1**, the paramagnetic complex **1** was characterized by a number of methods, including high-resolution single-crystal X-ray diffraction (SC-XRD), ^{1}H, ^{13}C, and ^{2}H nuclear magnetic resonance (NMR) spectroscopies, electron paramagnetic resonance (EPR) spectroscopy, vibrating sample magnetometry (VSM), electrospray ionization mass spectrometry (ESI-MS), elemental analysis, and density functional theory (DFT) calculations at the TPSSh-D4/def2-QZVPP//TPSS-D4/def2-TZVPP level of theory. The molecular structure of **1** in the crystal, obtained by precision high-resolution SC-XRD at 100 K with a reciprocal resolution $\sin(\theta_{max}/\lambda)$ of 1.26 Å^{-1} and following multipole refinement[42], supports the *N*-coordination of a pyridine moiety and η^5-coordination mode of two Cp groups (Fig. 1d). More specifically, the Co–N bond distance of 2.1998(3) Å is within the internuclear Co^{II}–N_{Py} distances in the neutral Co^{II}PNP pincer complexes, which are in the range from 1.974 to 2.343 Å with an average distance of 2.144 Å (Supplementary Table 2). The Co–C(Cp) distances are in the range from 2.2783(3) to 2.3292(2) Å with an average distance of 2.302 Å, and the Co–Cp centroid (Co–*Cnt*(Cp)) distances are 1.9607(2) and 1.9593(2) Å. These distances are significantly longer than those of cobaltocene (2.112 Å for the average of the libration-corrected Co–C(Cp) distances and ca. 1.722 Å for Co–*Cnt*(Cp))[43] and may indicate a weakening of the Co–C(Cp) interactions. The differences between the maximum and minimum Co–C(Cp) distances of 0.051 and 0.035 Å for the two Cp groups are similar to those of cobaltocene (0.033 Å)[43]. The coordination mode of the Cp groups was further analyzed by the Cp ring slip parameters Δ and Ψ (Fig. 1e)[44]. The Δ and Ψ values of complex **1** are among the smallest reported for Δ and Ψ[35,44] and strongly support the η^5-coordination mode of the two Cp groups. In comparison, the proposed 21-electron manganocene derivative, $MnCp_2$(dmpe), has a significantly larger deviation from the ideal η^5-coordination mode (Fig. 1e). The Δ and Ψ values derived from the gas-phase DFT calculations are in agreement with the experimental values, supporting that crystal packing effects are not essential for the η^5-coordination (Fig. 1e). The DFT optimized structure reproduces the equidistance of the Co–C(Cp) bonds with an average distance of 2.297(21) Å and a short Co–N distance of 2.2176 Å. Furthermore, the average Wiberg bond index for the Co–C(Cp) bonds of 0.15(2) is similar to that of cobaltocene (0.22(5)) as calculated at the same level of theory, and a practically uniform distribution of negative charges on the Cp rings was observed by the calculations (Supplementary Table 3).

In solution, the ^{1}H NMR spectrum of **1** showed five signals between −260 and +144 ppm (Fig. 2a). All the ^{1}H NMR signals were assigned based on selective deuteration of the Cp groups and two-dimensional NMR experiments (Supplementary Figs. 6, 7, and 12). The two broader signals at the higher field are from the Cp rings, and the three sharper signals at the lower field are from the pyridine ring and CH_2 groups of the CpNCp ligand. The ^{13}C NMR spectrum shows four signals between −504 and +410 ppm (Supplementary Fig. 5), and the signals are partially assigned based on two-dimensional NMR and the splitting pattern of the signals. Three ^{13}C NMR signals are missing, most likely due to the close proximity of the Cp groups to the paramagnetic Co center. Magnetic measurements conducted by the Evans NMR method (298 K,

in C_6D_6) and VSM (298 K, bulk solid) showed that **1** has an effective magnetic moment μ_{eff} of 4.3 and 3.99 μ_B (μ_B: Bohr magneton) in solution and solid state, respectively, which indicates that **1** has the $S = 3/2$ ground electron spin state. The $S = 3/2$ ground electron spin state was further supported by continuous wave (cw)-EPR, where a large deviation of effective g-values from that of a free electron was observed due to the sizable zero-field splitting of the $S = 3/2$ complex (Fig. 2b). The EPR spectrum also clearly shows the presence of large ^{59}Co hyperfine splitting, which supports the presence of a cobalt-centered radical.

The presence of the Co–N bond in the frozen solution was supported by pulse-EPR measurements, which observed the electron spin echo envelope modulation (ESEEM) effects[45]. The two-dimensional field-swept two-pulse and three-pulse ESEEM spectra observed at 4 K (Supplementary Figs. 30 and 31) showed the nuclear modulation effects due to the N atom coupled with the Co atom, indicating the presence of bonding interaction between them. Furthermore, we applied four-pulse hyperfine sublevel correlation (HYSCORE) spectroscopy[46] to measure the nuclear spins coupled with the Co atom. The HYSCORE spectrum (Fig. 2c) showed the correlation peaks due to the ^{1}H and ^{14}N atoms. The ^{1}H-HYSCORE signals spreading over a frequency range of 3–4 MHz in the angular selective spectra were assigned to the protons belonging to the Cp groups. Based on the cw-EPR spectrum and the modulation effects, we determined spin-Hamiltonian parameters of **1** with $S = 3/2$[47](Supplementary Fig. 33, Supplementary Table 1) as well as fictitious $S = 1/2$ (Fig. 2b). The experimental tensors showed that the principal axis with the largest principal value of the ^{14}N-hyperfine coupling (A) tensor coincides with that of the ^{59}Co-A tensor. This observation indicates the presence of electronic interaction between the Co and N atoms in the frozen solution.

The cyclic voltammogram of **1** showed reversible $Co^{3+/2+}$ half-wave potential at −1.23 V (vs. $FeCp_2^{+/0}$ in MeCN), which is 0.11 V higher or less negative than that of cobaltocene (Fig. 2d). This change in the $Co^{3+/2+}$ half-wave potential is not due to the introduction of the pyridinylmethyl group on each Cp ring, since such a substitution is expected to decrease the reduction potential by about 0.02 V[48]. Thus, the *N*-coordination of the pyridine group unexpectedly increases the reduction potential of **1** despite the increase in formal electron count.

Examination of the interatomic interactions

The bonding situation in **1** was further investigated by the quantum topological analysis of the experimental electron density $\rho(\mathbf{r})$[49] and electrostatic potential $\varphi_{es}(\mathbf{r})$[50] in the crystal. The analysis identified six bond critical points (BCPs) with negative near-zero values of the electronic energy density $h(\mathbf{r})$ corresponding to the Co–N and Co–C(Cp) coordinate bonds (Supplementary Fig. 34)[51]. In comparison, the analysis of $\rho(\mathbf{r})$ derived from DFT calculations resulted in a different set of Co–C(Cp) coordinate bonds (Supplementary Figs. 34 and 35), while Co–N was still present. It is known that the location of BCPs alone is not sufficient to correctly describe metal···Cp hapticity[52]. Therefore, the distribution of the Laplacian of electron density $\nabla^2\rho(\mathbf{r})$ (Fig. 3a and Supplementary Fig. 36) was studied. Examination of the $\nabla^2\rho(\mathbf{r})$ maps reveals that the charge concentration lobes associated with the N atom and each C atom of the Cp rings (lobes of red contour in Fig. 3a) are directed toward the Co atom in the electron depletion region (blue contours) approximately along the internuclear lines. Moreover, the N-atom lobe is directed into the furcation region between the valence shell charge concentrations of the Co atom, supporting the donor–acceptor nature of the coordinate Co–N bond. These observations suggest the η^5-coordination of both Cp groups as well as the *N*-coordination of the pyridine group. The experimental and theoretical values of $\rho(\mathbf{r})$, $\nabla^2\rho(\mathbf{r})$, and $h(\mathbf{r})$ at the BCP for Co–N: 0.057, 0.220, and −0.006 a.u. and 0.055, 0.218, and −0.011 a.u., respectively, showed good agreement. An approximate Co–N delocalization index

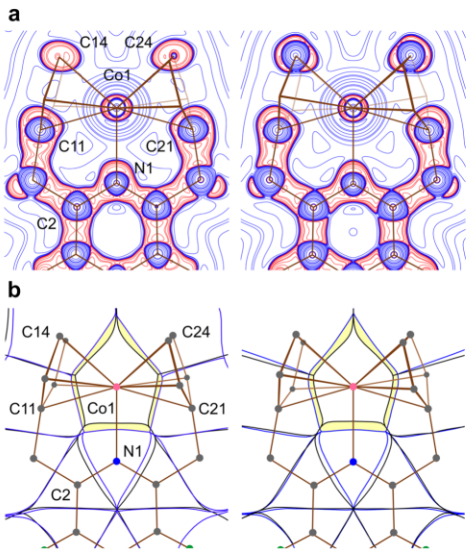

Fig. 3 | Quantum chemical topology of 1. Experimental maps based on SC-XRD data (left) and theoretical maps based on gas-phase DFT calculations (right) are compared. Map planes pass through the atoms Co1, N1, and C2. **a** Contour maps of $\nabla^2\rho(\mathbf{r})$; the logarithmic scale in the form of $\pm 1, 2, 4, 8 \cdot 10^n$ ($-2 \le n \le 3$) e Å^{-5} is adopted; blue and red colors correspond to positive and negative function values, respectively. **b** Superposition of the zero-flux boundaries of ρ-basins (black) and φ_{es}-basins (blue) in the gradient vector fields $\nabla\rho(\mathbf{r})$ and $\nabla\varphi_{es}(\mathbf{r})$.

(DI) of 0.78 and an average Co–C(Cp) DI of 0.52(5), obtained from DFT calculations, further support the presence of interactions between Co and N, as well as all C(Cp) atoms[52,53].

The Coulombic attraction between Co and N as well as C(Cp) atoms was examined by superposing trajectory maps of the gradient vector fields of charge density and electrostatic potential, $\nabla\rho(\mathbf{r})$ and $\nabla\varphi_{es}(\mathbf{r})$ (Fig. 3b)[50,54]. The electrons within the volumetric overlapping area of $\nabla\rho(\mathbf{r})$ and $\nabla\varphi_{es}(\mathbf{r})$ (colored yellow in Fig. 3b) belong to the atomic ρ-basins of N and all C(Cp) but simultaneously fall into the neighboring pseudoatomic φ_{es}-basin of Co; therefore, these captured electrons are drawn toward the Co nucleus by the electrostatic force $\mathbf{F}_{es}(\mathbf{r}) = \nabla\varphi_{es}(\mathbf{r})$. This area represents the trace of the expansion of the ligand atoms of the first coordination sphere, capturing electrons, and the compression of the Co atom losing electrons as a result of the chemical bond formation starting from free neutral atoms. The electron transfer thus defined is estimated to be 0.90 and 0.98 e for **1** in the crystal according to experimental diffraction data and for the free molecule from DFT calculations, respectively. The action of the electric field generated by the cobalt atom inside the nearest 11 atoms of the ligand, as well as the joint total interatomic charge transfer from Co to N and C(Cp), indicates that all 10 C(Cp), as well as the N-atom, form a "ligand binding field" around the Co-coordination center. The experimental and computational studies strongly support the presence of the Co–N bond and two η^5-coordinated Cp ligands, and together show that complex **1** is a formal 21-electron cobaltocene derivative.

Attempted synthesis of 22-, 20-, and 19-electron analogs

Aiming at the formation of a 22-electron analog, we attempted to synthesize the analogous Ni(CpNCp) complex. However, the reaction between Na_2CpNCp and $NiCl_2$(DME) (DME: 1,2-dimethoxyethane) resulted in the formation of a dimeric nickel complex **2** that lacked

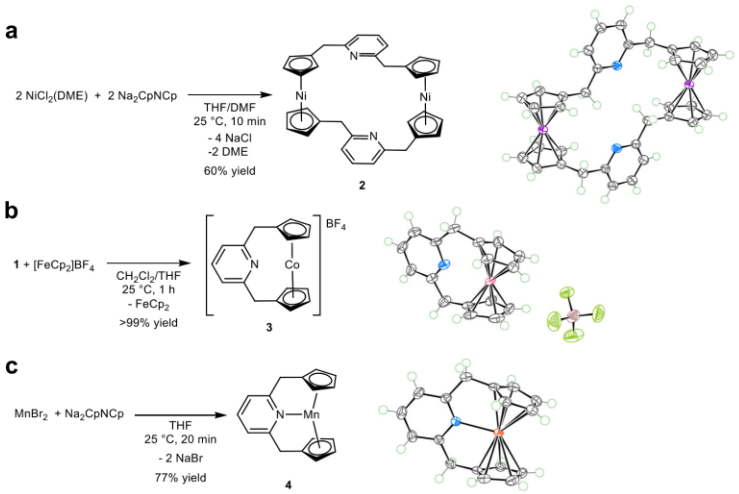

Fig. 4 | Attempted formation of formal 22-, 20-, and 19-electron analogs. **a** Synthetic route to the dimeric Ni^{II} complex **2**. THF: tetrahydrofuran. DMF: dimethylformamide. DME: 1,2-dimethoxyethane. **b** Oxidation of **1** with $[FeCp_2]BF_4$ to generate Co^{III} complex **3**. **c** Synthetic route to the Mn^{II} complex **4**. Insert: Molecular structure of corresponding complexes at the 80 % probability level for non-hydrogen atoms according to SC-XRD.

Ni–N bonds (Fig. 4a). Therefore, the addition of one more electron cancels out the stability of the complex gained by the formation of the metal–N bond. The one-electron oxidation of **1** was also investigated to elucidate if a formal 20-electron analog could be prepared. Oxidation of **1** by $[FeCp_2]BF_4$ resulted in the quantitative formation of a diamagnetic cobaltocenium complex **3** (Fig. 4b). The SC-XRD analysis of **3** revealed long Co···N internuclear distances of 2.745(4) and 2.790(5) Å, which vary significantly for two molecules in the asymmetric cell. Furthermore, the average Co–C(Cp) bond length is significantly shortened from 2.302 to 2.084 Å and close to that of $[CoCp_2]BF_4$ (2.041 Å)[55]. The variable temperature (from −40 to 80 °C) NMR measurements showed no sign of reversible coordination of the pyridine group, and the ^{15}N NMR chemical shift of **3** is close to that of Na_2CpNCp. Therefore, **3** is best described as a formal 18-electron complex without Co–N bonding. The absence of Co–N bonding is likely due to the formation of a stronger attractive interaction between the anionic Cp groups and the Co^{3+} center, as evidenced by the shortening of the Co–C(Cp) bonds, which increases the energy penalty required to form a Co–N bond. To further investigate the coordination chemistry of the CpNCp ligand, we synthesized the Mn complex **4** (Fig. 4c). A μ_{eff} of 6.2 (in C_6D_6, at 298 K) and the cw-EPR spectrum and its simulation with $S = 5/2$ spin state supports an $S = 5/2$ ground electron spin state of **4** (Supplementary Fig. 27). The SC-XRD analysis of **4** showed that the Mn–N distance is 2.2709(14) Å, which is within the Mn–N distance of other N-donor-ligated manganocene derivatives[24]. The Cp ring slip parameters Δ of 0.213 and 0.105 Å as well as Ψ of 5.7° and 2.8° are relatively small but significantly larger than those of **1** (Fig. 1e). Thus, like other manganocene derivatives, the coordination chemistry of **4** is more strongly influenced by the ligand steric factor[24]. These studies of the Ni, Co, and Mn complexes led us to further investigate the origin of the stability of complex **1** and the instability of the metal–N bonds in complexes **2** and **3** by computational methods.

Origin of the stability

The origin of the stability of **1** and the unexpected increase in the $Co^{3+/2+}$ reduction potential were investigated by computational methods. Using DFT calculations, we were able to locate an isomer of **1** with an $S = 1/2$ spin state in which the coordinate Co–N bond is broken, as a local minimum energy structure (**1′**, Fig. 5).

The relaxed potential energy surface scans of the Co–N distance reveal that upon decreasing the Co–N distance, the 21-electron configuration with a spin state of $S = 3/2$ is more stabilized than the 19-electron configuration with $S = 1/2$ (Supplementary Fig. 41), with **1** being 5 kcal mol^{-1} (Gibbs free energy at 298 K) more stable than **1′**. Thus, the coordination of nitrogen significantly stabilizes complex **1**. Figure 5 shows the frontier molecular orbital (MO) diagrams of cobaltocene, **1′**, and **1**, derived canonically from Kohn–Sham quasi-restricted orbitals (KS-QROs)[56]. As expected, the MO diagrams of cobaltocene and **1′** are similar, and no significant change in the energy of the singly occupied molecular orbital (SOMO) was observed. Examination of the canonical KS-QROs of **1** revealed that the Co–N bond in **1** results from the σ-type interaction between the metal *d*-orbital and the nitrogen lone pair. The formation of the Co–N bond has two consequences. First, it generates the Co–N antibonding orbital, which is singly occupied (Fig. 5, SOMO1). Thus, the Co–N bond formally has a bond order of 0.5. This situation is reminiscent of the formation of 19-electron adducts from the 17-electron complexes, where the formation of one-half of a metal-ligand bond stabilizes the 19-electron complex[57]. Second, the formation of the Co–N bond significantly lowers the energy level of the SOMO and the lowest unoccupied molecular orbital (LUMO) of **1′**, and both can be singly occupied to form an $S = 3/2$ ground electron spin state (Fig. 5, SOMO2 and SOMO3). These two orbitals are Co···Cp antibonding, and their partial occupation explains the significant elongation of the Co–C(Cp) internuclear distances in **1**. The decrease in the energy of the highest SOMO3 explains the observed increase in the $Co^{3+/2+}$ reduction potential. These half-filled Co···Cp antibonding orbitals allow the Cp ligands to maintain the η^5-coordination mode. Therefore, the stability of **1** is a product of the formation of one-half of a Co–N bond and the half-filled two Co···Cp antibonding orbitals, and the pincer ligand motif that holds all these weak Co–N and Co–C(Cp) bonds together. Indeed, a control experiment showed that coordination of pyridine to cobaltocene does not occur without the chelate effect provided by the pincer motif (see the Supplememntary Information for details). This

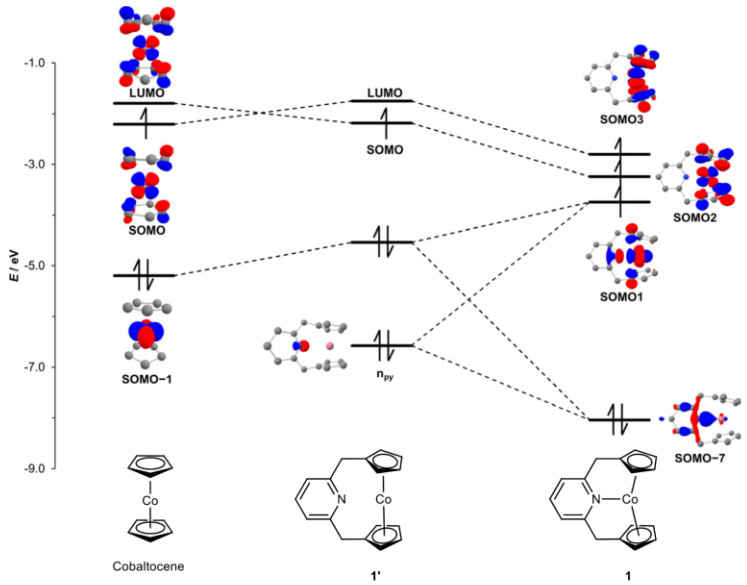

Fig. 5 | Comparison of MO diagram of cobaltocene, 1', and 1. Inset: canonical KS-QROs (isovalues at 0.05-0.13 a.u.), blue lobes: positive phases, red lobes: negative phases. For a detailed MO diagram and KS-QROs, please see Supplementary Figs. 43-46. LUMO: lowest unoccupied molecular orbital. SOMO: singly occupied molecular orbital. SOMO−1: a molecular orbital at one energy level below SOMO. SOMO−7: a molecular orbital at seven energy level below SOMO1. n_{py}: nitrogen lone pair electrons.

type of complex stabilization by half-filled metal–ligand antibonding orbitals contrasts with the way formal 20-electron $M(CO)_8$ (M = Zr, Hf)[58] and $[M(CO)_8]^-$ (M = Sc, Y, La)[59] species are stabilized by the presence of a filled purely ligand based MO. Our MO analysis also qualitatively explains the formation of **2** and **3**. The hypothetical formal 22-electron Ni(CpNCp) complex should have a fully occupied Ni–N antibonding orbital, leading to the cleavage of a Ni–N bond and the formation of **2**. The removal of one electron from **1** should lead to the pairing of the remaining two unpaired electrons in **1** to achieve a more stable low-spin configuration, in which the Co–N bond does not exist.

In summary, we have synthesized the formal 21-electron cobaltocene derivative **1** by utilizing the chelate effect of the CpNCp pincer ligand, which enables the coordination of the nitrogen lone pair donor while maintaining the η^5-coordination mode of two Cp groups. The structural analysis, quantum-chemical topological studies, and DFT calculations strongly support the presence of the Co–N bond and two η^5-coordinated Cp ligands, and thus the formation of the 21-electron cobaltocene derivative. The stability and unexpected redox property of the 21-electron complex **1** originate from the half-filled Co–N and Co···Cp antibonding orbitals, and the chelation effect of the pincer ligand. The formal 21-electron metallocene presented here expands our understanding and perception of metallocene and organometallic chemistry, as well as chemical bond theory. It is anticipated that this discovery will open up unexplored possibilities in transition metal chemistry, especially in the field of catalysis and materials science.

Methods

General considerations and materials for the synthetic study

All reactions were carried out under an N_2 atmosphere using an MBRAUN glovebox, UNILAB Plus SP, equipped with an MB-20-G gas purifier, an MB-LMF-2/40-REG regenerable solvent trap, and an MB-GS-35 -35 °C freezer. All glasswares were dried overnight at 170 °C and cooled down under vacuum in the glovebox antechamber. All solvents were reagent grade or higher. *n*-Pentane (≥ 99.0%), hexane (≥ 95.0%, *n*-hexane with minor amounts of isomers of methylpentane and methylcyclopentane), *n*-heptane (≥ 99.0%), dichloromethane (≥ 99.5%), benzene (≥ 99.7%), toluene (≥ 99.8%), acetonitrile (≥ 99.8%), methanol (≥ 99.8%), tetrahydrofuran (Sigma-Aldrich 401757-1 L, anhydrous, ≥99.9%, inhibitor-free), diethyl ether (≥ 99.8%, inhibitor-free), hexamethyldisiloxane (Sigma-Aldrich 205389-500 ML, ≥98%), and dimethylformamide (DMF, ≥99.0%) were dried over MS3A (dried overnight in a 200 °C oven and cooled overnight under vacuum in the glovebox antechamber) in the glovebox for more than 2 days and stored in the glovebox. Common chemicals were purchased, kept in the glovebox, and used as received unless stated otherwise. Anhydrous $CoBr_2$ (green powder, >97%) was purchased from Fujifilm Wako Chemicals. $NiCl_2$(DME) (yellow powder, 98%) was purchased from Sigma Aldrich. $MnBr_2$ (pink powder, 99%) was purchased from Acros Organics. Celite filtration was carried out using a pipet, cotton wool, and Celite®545, which was dried overnight in a 170 °C oven, cooled down overnight under vacuum in the glovebox antechamber, and kept in the glovebox. The dimensions of the 20 mL vial are 60 mm in height, 28 mm in outer diameter, and the Teflon-coated stirring bar is 15 mm long and 5 mm in diameter.

Instrumental analysis methods

NMR spectroscopy. All deuterated solvents were purchased and dried over MS3A in the glovebox for more than 2 days and kept in the glovebox. NMR spectra were recorded using a Bruker Avance III-400N spectrometer and an Avance III NEO 500 spectrometer equipped with a cryoprobe. ^1H and ^{13}C NMR chemical shifts are reported in parts per million (δ) relative to TMS (0 ppm) with the residual solvent signal ($CDCl_3$: 7.26 (^1H) and 77.16 (^{13}C) ppm, C_6D_6: 7.16 (^1H) and 128.06 (^{13}C) ppm, THF-d_8: 1.72 (^1H) and 25.31 (^{13}C) ppm, toluene-d_8: 2.08 (^1H) and

20.43 (^{13}C) ppm, DMSO-d_6: 2.50 (^{1}H) and 39.52 (^{13}C) ppm, methanol-d_4: 3.31 (^{1}H) and 49.00 (^{13}C) ppm, CD_3CN: 1.94 (^{1}H) and 118.26 (^{13}C) ppm) as the internal references ^{2}H NMR chemical shifts are reported in parts per million (δ) relative to residual solvent signal as the internal reference. ^{11}B, ^{15}N, and ^{19}F NMR chemical shifts are reported in parts per million (δ) relative to $BF_3{\cdot}OEt_2$ in $CDCl_3$ (0 ppm), NH_3(liquid) (0 ppm), and $CFCl_3$ (0 ppm), respectively, as external references.

NMR peak assignments of diamagnetic compounds were made using ^{1}H-^{1}H-gCOSY, ^{1}H-^{13}C-HSQC, and ^{1}H-^{13}C-HMBC NMR experiments. Abbreviations for NMR spectra are s (singlet), d (doublet), t (triplet), q (quartet), quint (quintet), sep (septet), dd (doublet of doublet), td (doublet of triplet), dq (doublet of quartet), m (multiplet), and br (broad). ^{1}H NMR signals of paramagnetic complexes are reported with chemical shift (δ) and line width at half-height ($\Delta\nu^{1/2}$). Air-sensitive NMR samples were prepared in the nitrogen glovebox using a J. Young NMR tube or a standard NMR tube sealed with a septa and parafilm.

NMR measurement of paramagnetic complexes. ^{1}H NMR of paramagnetic complexes (typically 20 mM solution) was measured with delay time (d1) of 0.1 s, time domain data points (td) of 128k, and scan number (ns) of 1 to 128, and spectral width (sw) of 200 to 600 ppm. Proton-coupled ^{13}C NMR experiments were carried out using an Avance III NEO 500 spectrometer equipped with a cryoprobe. For proton coupled ^{13}C NMR experiments, a delay time (d1) of 0.1 s, a time domain data points (td) of 64k, a scan number (ns) of 64k, and a spectral width (sw) of 1100 ppm were used.

Measurement of effective magnetic moment by Evans' method. Measurement of the effective magnetic moment by Evans' method was carried out using glass capillaries containing C_6D_6 (measurement in C_6D_6) as external standards.

Single-crystal X-ray diffraction (SC-XRD). The X-ray diffraction experiments for **1**-**3** were performed on a Bruker D8 Venture diffractometer equipped with a PHOTON II CPAD detector and an IμS 3.0 microfocus X-ray source (Mo *K*α radiation). The X-ray diffraction data for the single crystal **4** were collected on a Rigaku XtaLab PRO instrument equipped with a PILATUS3 R 200 K hybrid pixel array detector and a MicroMax™-003 microfocus X-ray tube (Mo *K*α). Data were collected at 100 K according to recommended strategies, then processed and corrected. All structures were solved using SHELXT[60]. Structures **2**-**4** were refined by the full-matrix least-squares using SHELXL[61]. Non-hydrogen atoms were refined anisotropically.

VSM measurement. The VSM measurement was carried out using the Quantum Design PPMS DynaCool VSM module. VSM powder sample holders (part #: 4096-388) were weighed outside the glovebox using a microbalance and placed inside in the glovebox. All powdered samples were packed and sealed in the sample holders in the nitrogen glovebox. The sealed samples were weighed outside the glovebox using microbalance to calculate the weight of the samples.

FTIR spectroscopy. IR spectra were recorded using a Nicolet iS5 FT-IR spectrophotometer and are reported in absorption frequency (cm^{-1}). Abbreviations for FT-IR spectra are s (strong), m (medium), and w (weak).

High-resolution mass spectrometry (HRMS). HRMS data were recorded on a Thermo Scientific LTQ-Orbitrap mass spectrometer, using electrospray ionization (ESI) mode.

Elemental analyses. Elemental analyses were conducted using an Exeter Analytical CE-440 elemental analyzer. Empty tin cups were weighed outside the glovebox using a microbalance and brought in the glovebox. All samples were weighed and sealed in the tin cups in the nitrogen glovebox. The sealed samples were weighed outside the glovebox using microbalance to calculate weight of the samples. The N_2 gas in the tin cups was replaced by argon through three vacuum-argon refill cycles. All the samples were analyzed using an autosampler under a He atmosphere.

Cyclic voltammetry (CV). CV was measured inside the nitrogen glovebox using an ECstat-301WL potentiostat equipped with a glassy carbon working electrode (3.0 mm diameter), a platinum wire counter electrode (0.5 mm diameter), and an Ag/Ag^+ reference electrode (Ag wire in 0.01 M $AgNO_3$ in 0.1 M $[Bu_4N]PF_6$ MeCN solution). The sample solution was prepared by dissolving an appropriate sample in 0.1 M $[Bu_4N]NPF_6$ THF solution. All potentials are reported using the $FeCp_2^{0/+}$ couple (0 mV) as an external reference.

Computational Methods

DFT computations were performed with the ORCA software package (versions 5.0.0, 5.0.1, 5.0.3) unless otherwise noted[62–64]. For structure optimizations and harmonic vibrational frequencies, we employed the TPSS meta-GGA functional[65–67]. Additionally, we utilized Grimme's latest additive dispersion correction D4[68,69] and an Ahlrichs-type basis set with triple-zeta quality (def2-TZVPP)[70]. Minima on the potential energy surface were confirmed by the absence of imaginary frequencies. For accurate electronic energies and quasi-restricted orbitals (QROs)[56] we used the hybrid variant of this functional, i.e., TPSSh, together with the quadruple-zeta quality basis set (def2-QZVPP)[70]. We tested the influence of relativistic effects by incorporating the zeroth-order regular approximation (ZORA) at the scalar spin-free level of the theory[71]. As recommended, these calculations use a relativistically recontracted basis set (ZORA-def2-*X*VP) and a decontracted auxiliary basis set (SARC/J)[72]. Unless noted otherwise, the resolution of identity (RI) and chain-of-spheres (RIJCOSX) approximations, as implemented in ORCA, were used for (meta)-GGA and hybrid functionals, respectively, together with the appropriate auxiliary basis set (def2/J)[72,73]. All computations performed with ORCA utilized the tight SCF convergence criteria and the default integration grid (defgrid2).

Wiberg bond indices were determined in the framework of natural bond orbital (NBO 7.0.10) analysis[74]. The topological analysis of the theoretical electron density $\rho(\mathbf{r})$ and electrostatic potential $\varphi_{es}(\mathbf{r})$ was performed with Multiwfn 3.8(dev)[75]. For this purpose, we carried out single-point energy computations at TPSSh/def2-QZVPP level using the Gaussian16 software package (revision C.01) to generate a Gaussian checkpoint file as input (tight SCF convergence criteria, ultrafine integration grid)[76]. The electrostatic potential $\varphi_{es}(\mathbf{r})$ was evaluated using the built-in code[77]. The protocol for generating superposition maps of the zero-flux surfaces defined in the gradient vector fields $\nabla\rho(\mathbf{r})$ and $\nabla\varphi_{es}(\mathbf{r})$ was described in detail earlier[78].

Quantum crystallography

The X-ray diffraction data of **1** were collected at 100 K with a reciprocal resolution $\sin(\theta_{max}/\lambda)$ of 1.26 $Å^{-1}$. The multipole refinement of **1** was performed within the Hansen–Coppens formalism as implemented in MoPro[79]. The anharmonic atomic motion of Co was modeled using the Gram–Charlier expansion of the temperature factors. A block refinement of the charge density parameters and the Gram–Charlier coefficients was applied analogously to the procedure described earlier[80].

The analysis of the multipole-derived electron density $\rho(\mathbf{r})$ and electrostatic potential $\varphi_{es}(\mathbf{r})$ was performed in WinXPRO[81] analogous to the published procedures[82]. The energy density $h(\mathbf{r})$ was approximated according to Kirzhnits[83].

Data availability

All data are available in the main text or the supplementary information. Additional data are available from the corresponding authors upon request. Crystallographic data for the structures reported in this

article and its supplementary information were deposited at the Cambridge Crystallographic Data Centre under deposition numbers CCDC 2220152 (**1**), 2220153 (**1**, multipole model), 2220154 (**2**), 2220155 (**3**), and 2220156 (**4**). Copies of the data can be obtained free of charge via https://www.ccdc.cam.ac.uk/structures/.

References

1. Pauson, P. L. Ferrocene—how it all began. *J. Organomet. Chem.* **637–639**, 3–6 (2001).
2. Fischer, E. O. & Jira, R. How metallocene chemistry and research began in Munich. *J. Organomet. Chem.* **637–639**, 7–12 (2001).
3. Cotton, F. A. Cyclopentadienyl–metal chemistry in the Wilkinson Group, Harvard, 1952–1955. *J. Organomet. Chem.* **637–639**, 18–26 (2001).
4. Kaminsky, W. Highly active metallocene catalysts for olefin polymerization. *J. Chem. Soc. Dalton Trans*. 1413–1418 (1998).
5. Garrido-Barros, P., Derosa, J., Chalkley, M. J. & Peters, J. C. Tandem electrocatalytic N_2 fixation via proton-coupled electron transfer. *Nature* **609**, 71–76 (2022).
6. Fukino, T. et al. Manipulation of Discrete Nanostructures by Selective Modulation of Noncovalent Forces. *Science* **344**, 499–504 (2014).
7. Verlhac, B. et al. Atomic-scale spin sensing with a single molecule at the apex of a scanning tunneling microscope. *Science* **366**, 623–627 (2019).
8. Pal, A. N. et al. Nonmagnetic single-molecule spin-filter based on quantum interference. *Nat. Commun.* **10**, 5565 (2019).
9. Zhang, Y. et al. Distal conformational locks on ferrocene mechanophores guide reaction pathways for increased mechanochemical reactivity. *Nat. Chem.* **13**, 56–62 (2021).
10. Li, Z. et al. Organometallic-functionalized interfaces for highly efficient inverted perovskite solar cells. *Science* **376**, 416–420 (2022).
11. Cass, A. E. G. et al. Ferrocene-mediated enzyme electrode for amperometric determination of glucose. *Anal. Chem.* **56**, 667–671 (1984).
12. Patra, M. & Gasser, G. The medicinal chemistry of ferrocene and its derivatives. *Nat. Rev. Chem.* **1**, 0066 (2017).
13. Malischewski, M., Adelhardt, M., Sutter, J., Meyer, K. & Seppelt, K. Isolation and structural and electronic characterization of salts of the decamethylferrocene dication. *Science* **353**, 678–682 (2016).
14. Goodwin, C. A. P. et al. Isolation and electronic structures of derivatized manganocene, ferrocene and cobaltocene anions. *Nat. Chem.* **13**, 243–248 (2021).
15. Howard, C. G., Girolami, G. S., Wilkinson, G., Thornton-Pett, M. & Hursthouse, M. B. Tertiary phosphine adducts of manganese(II) dicyclopentadienide. Magnetic studies and structural characterization of tilted cyclopentadienyl rings. *J. Am. Chem. Soc.* **106**, 2033–2040 (1984).
16. Girolami, G. S., Wilkinson, G., Thornton-Pett, M. & Hursthouse, M. B. η^5-Cyclopentadienyl and η^5-methylcyclopentadienyl 1,2-bis(dimethylphosphino)ethane complexes of titanium(II). The crystal structure of $Ti(C_5H_4Me)_2$(dmpe). *J. Chem. Soc. Dalton Trans*. 2347–2350 (1984).
17. Heck, J., Massa, W. & Weinig, P. TMEDA Adducts of CpMnCl and Manganocene. *Angew. Chem. Int. Ed. Engl.* **23**, 722–723 (1984).
18. Abernethy, C. D. et al. Nucleophilic Carbene Complexes of Manganocene. *Organometallics* **20**, 3629–3631 (2001).
19. Soria Alvarez, C. et al. Applications of manganocene in the synthesis of Mn(II) amide and imide cages. *Dalton Trans*. 3002–3008 (2003).
20. Soria Alvarez, C. et al. Syntheses, structures and magnetic properties of Mn(II) dimers $[CpMn(\mu\text{-}X)]_2$ (Cp = C_5H_5; X = RNH, R^1R^2N, C≡CR). *Dalton Trans*. 3481–3487 (2004).
21. Walter, M. D., Baabe, D., Freytag, M. & Jones, P. G. *N*-Heterocyclic Carbene (NHC) Adducts of $[(C_5H_5)_2Mn]$ Revisited: Nothing More, Nothing Less than High-Spin (*S* = 5/2) Molecules! *Z. Anorg. Allg. Chem.* **642**, 1259–1263 (2016).
22. Bottomley, F., Keizer, P. N. & White, P. S. Steric versus electronic effects on the tilt of the cyclopentadienyl rings in adducts of manganese dicyclopentadienide. Molecular and electronic structure of dicyclopentadienide manganese tetrahydrofuran. *J. Am. Chem. Soc.* **110**, 137–140 (1988).
23. Layfield, R. A. Manganese(II): the black sheep of the organometallic family. *Chem. Soc. Rev.* **37**, 1098–1107 (2008).
24. Cannella, A. F., Dey, S. K., MacMillan, S. N. & Lacy, D. C. Structural diversity in pyridine and polypyridine adducts of ring slipped manganocene: correlating ligand steric bulk with quantified deviation from ideal hapticity. *Dalton Trans.* **47**, 5171–5180 (2018).
25. Holloway, J. D. L. & Geiger, W. E. Electron-transfer reactions of metallocenes. Influence of metal oxidation state on structure and reactivity. *J. Am. Chem. Soc.* **101**, 2038–2044 (1979).
26. Bard, A. J., Garcia, E., Kukharenko, S. & Strelets, V. V. Electrochemistry of metallocenes at very negative and very positive potentials. Electrogeneration of 17-electron Cp_2Co^{2+}, 21-electron Cp_2Co^{2-}, and 22-electron Cp_2Ni^{2-} species. *Inorg. Chem.* **32**, 3528–3531 (1993).
27. Rasmussen, S. C. The 18-electron rule and electron counting in transition metal compounds: theory and application. *ChemTexts* **1**, 10 (2015).
28. Landis, C. R., Cleveland, T. & Firman, T. K. Making Sense of the Shapes of Simple Metal Hydrides. *J. Am. Chem. Soc.* **117**, 1859–1860 (1995).
29. Landis, C. R., Firman, T. K., Root, D. M. & Cleveland, T. A Valence Bond Perspective on the Molecular Shapes of Simple Metal Alkyls and Hydrides. *J. Am. Chem. Soc.* **120**, 1842–1854 (1998).
30. Frenking, G. & Fröhlich, N. The Nature of the Bonding in Transition-Metal Compounds. *Chem. Rev.* **100**, 717–774 (2000).
31. Landis, C. R. & Weinhold, F. 18-electron rule and the 3c/4e hyperbonding saturation limit. *J. Comput. Chem.* **37**, 237–241 (2016).
32. Abernethy, C. D., Clyburne, J. A. C., Cowley, A. H. & Jones, R. A. Reactions of Transition-Metal Metallocenes with Stable Carbenes. *J. Am. Chem. Soc.* **121**, 2329–2330 (1999).
33. Baljak, S. et al. Ring-Opening Polymerization of a Strained [3]Nickelocenophane: A Route to Polynickelocenes, a Class of *S* = 1 Metallopolymers. *J. Am. Chem. Soc.* **136**, 5864–5867 (2014).
34. Huttner, G. et al. The structure of $(C_5H_5)_2W(CO)_2$ a compound containing a bent trihapto-cyclopentadienyl ligand. *J. Organomet. Chem.* **145**, 329–333 (1978).
35. Jordan, M., Saak, W., Haase, D. & Beckhaus, R. Ring-Slipped (2,2′-Bipyridine)(η^3-cyclopentadienyl)(η^5-cyclopentadienyl)vanadium(II) and Its Oxidation to (2,2′-Bipyridine)bis(η^5-cyclopentadienyl)vanadium(III) Tetraphenylborate. *Eur. J. Inorg. Chem.* **2007**, 5168–5172 (2007).
36. O'Connor, J. M. & Casey, C. P. Ring-slippage chemistry of transition metal cyclopentadienyl and indenyl complexes. *Chem. Rev.* **87**, 307–318 (1987).
37. Haaland, A. et al. The molecular structure of dicyclopentadienylzinc (zincocene) determined by gas electron diffraction and density functional theory calculations: η^5,η^5, η^3,η^3 or η^5,η^1 coordination of the ligand rings? *J. Organomet. Chem.* **684**, 351–358 (2003).
38. Paolucci, G., Fischer, R. D., Benetollo, F., Seraglia, R. & Bombieri, G. Synthesis, spectroscopy, and crystal structure of a new stable bis-cyclopentadienyl uranium(IV) dichloride containing two C_5H_4-rings interlinked by a metal-coordinated 2,6-bis(methylene)pyridyl unit. *J. Organomet. Chem.* **412**, 327–342 (1991).
39. Paolucci, G. et al. Bent Metallocenes Containing Ancillary Ligands in Ring-Bridging Chains. Synthesis, Spectroscopy, and X-ray Crystal

Structure of [2,6-Bis(methylenecyclopentadienyl)pyridine]chromium(II). *Organometallics* **13**, 1746–1750 (1994).
40. Qian, C., Guo, J., Ye, C., Sun, J. & Zheng, P. Synthesis of 5-*ansa*-zirconocene complexes and crystal structure of [Zr{$C_6H_4(CH_2C_5H_4)_2$-1,3}Cl_2]. *J. Chem. Soc. Dalton Trans.* 3441–3445 (1993).
41. Paolucci, G., Pojana, G., Zanon, J., Lucchini, V. & Avtomonov, E. New Trigonal-Bipyramidal 5-*ansa*-Zirconocene Derivatives. 1. {2,6-Bis(-methylcyclopentadienyl)- pyridine}zirconium(IV) Monochloride Monoalkyls and Dialkyls. Crystal Structure of [Zr{$C_5H_3N(CH_2C_5H_4)_2$-2,6}(*n*-$C_4H_9)_2$], the First Thermally Stable Dialkylzirconocene Containing β-Hydrogens. *Organometallics* **16**, 5312–5320 (1997).
42. Hansen, N. K. & Coppens, P. Testing aspherical atom refinements on small-molecule data sets. *Acta Crystallogr. A* **34**, 909–921 (1978).
43. Antipin, M. Y., Boese, R., Augart, N. & Schmid, G. Redetermination of the cobaltocene crystal structure at 100 K and 297 K: Comparison with ferrocene and nickelocene. *Struct. Chem.* **4**, 91–101 (1993).
44. Faller, J. W., Crabtree, R. H. & Habib, A. Control of slippage and conformation in indenyl complexes. *Organometallics* **4**, 929–935 (1985).
45. Mims, W. B. Envelope Modulation in Spin-Echo Experiments. *Phys. Rev. B* **5**, 2409–2419 (1972).
46. Höfer, P., Grupp, A., Nebenführ, H. & Mehring, M. Hyperfine sublevel correlation (hyscore) spectroscopy: a 2D ESR investigation of the squaric acid radical. *Chem. Phys. Lett.* **132**, 279–282 (1986).
47. Yamane, T. et al. ESR analyses of picket fence Mn^{II} and 6th ligand coordinated Fe^{III} porphyrins ($S = 5/2$) and a Co^{II}(hfac) complex ($S = 3/2$) with sizable ZFS parameters revisited: a full spin Hamiltonian approach and quantum chemical calculations. *Dalton Trans.* **47**, 16429–16444 (2018).
48. Khobragade, D. A. et al. Acceptor-Substituted Ferrocenium Salts as Strong, Single-Electron Oxidants: Synthesis, Electrochemistry, Theoretical Investigations, and Initial Synthetic Application. *Chem. Eur. J.* **18**, 12267–12277 (2012).
49. Bader, R. F. W. A quantum theory of molecular structure and its applications. *Chem. Rev.* **91**, 893–928 (1991).
50. Shteingolts, S. A., Stash, A. I., Tsirelson, V. G. & Fayzullin, R. R. Real-Space Interpretation of Interatomic Charge Transfer and Electron Exchange Effects by Combining Static and Kinetic Potentials and Associated Vector Fields. *Chem. Eur. J.* **28**, e202200985 (2022).
51. Cremer, D. & Kraka, E. A description of the chemical bond in terms of local properties of electron density and energy. *Croat. Chem. Acta* **57**, 1259–1281 (1984).
52. Farrugia, L. J., Evans, C., Lentz, D. & Roemer, M. The QTAIM Approach to Chemical Bonding Between Transition Metals and Carbocyclic Rings: A Combined Experimental and Theoretical Study of (η^5-C_5H_5)$Mn(CO)_3$, (η^6-C_6H_6)$Cr(CO)_3$, and (*E*)-{(η^5-C_5H_4)CF═CF(η^5-C_5H_4)}(η^5-C_5H_5)$_2Fe_2$. *J. Am. Chem. Soc.* **131**, 1251–1268 (2009).
53. Outeiral, C., Vincent, M. A., Martín Pendás, Á. & Popelier, P. L. A. Revitalizing the concept of bond order through delocalization measures in real space. *Chem. Sci.* **9**, 5517–5529 (2018).
54. Saifina, A. F., Kartashov, S. V., Stash, A. I., Tsirelson, V. G. & Fayzullin, R. R. Unified Picture of Interatomic Interactions, Structures, and Chemical Reactions by Means of Electrostatic and Kinetic Force Density Fields: Appel's Salt and Its Ion Pairs. *Cryst. Growth Des.* **23**, 3002–3018 (2023).
55. Mochida, T. et al. Crystal Structures and Phase Sequences of Metallocenium Salts with Fluorinated Anions: Effects of Molecular Size and Symmetry on Phase Transitions to Ionic Plastic Crystals. *Chem. Eur. J.* **22**, 15725–15732 (2016).
56. Neese, F. Importance of Direct Spin–Spin Coupling and Spin-Flip Excitations for the Zero-Field Splittings of Transition Metal Complexes: A Case Study. *J. Am. Chem. Soc.* **128**, 10213–10222 (2006).
57. Tyler, D. R. 19-Electron organometallic adducts. *Acc. Chem. Res.* **24**, 325–331 (1991).
58. Deng, G. et al. Filling a Gap: The Coordinatively Saturated Group 4 Carbonyl Complexes $TM(CO)_8$ (TM=Zr, Hf) and $Ti(CO)_7$. *Chem. Eur. J.* **26**, 10487–10500 (2020).
59. Jin, J. et al. Octacarbonyl Anion Complexes of Group Three Transition Metals $[TM(CO)_8]^-$ (TM=Sc, Y, La) and the 18-Electron Rule. *Angew. Chem. Int. Ed.* **57**, 6236–6241 (2018).
60. Sheldrick, G. *SHELXT* – Integrated space-group and crystal-structure determination. *Acta Crystallogr. A* **71**, 3–8 (2015).
61. Sheldrick, G. Crystal structure refinement with *SHELXL*. *Acta Crystallogr. C.* **71**, 3–8 (2015).
62. Neese, F. The ORCA program system. *WIREs Comput. Mol. Sci.* **2**, 73–78 (2012).
63. Neese, F. Software update: the ORCA program system, version 4.0. *WIREs Comput. Mol. Sci.* **8**, e1327 (2018).
64. Neese, F. Software update: The ORCA program system—Version 5.0. *WIREs Comput. Mol. Sci.* **12**, e1606 (2022).
65. Tao, J., Perdew, J. P., Staroverov, V. N. & Scuseria, G. E. Climbing the Density Functional Ladder: Nonempirical Meta-Generalized Gradient Approximation Designed for Molecules and Solids. *Phys. Rev. Lett.* **91**, 146401 (2003).
66. Staroverov, V. N., Scuseria, G. E., Tao, J. & Perdew, J. P. Comparative assessment of a new nonempirical density functional: Molecules and hydrogen-bonded complexes. *J. Chem. Phys.* **119**, 12129–12137 (2003).
67. Staroverov, V. N., Scuseria, G. E., Tao, J. & Perdew, J. P. Erratum: "Comparative assessment of a new nonempirical density functional: Molecules and hydrogen-bonded complexes" [J. Chem. Phys. 119, 12129 (2003)]. *J. Chem. Phys.* **121**, 11507–11507 (2004).
68. Caldeweyher, E., Bannwarth, C. & Grimme, S. Extension of the D3 dispersion coefficient model. *J. Chem. Phys.* **147**, 034112 (2017).
69. Caldeweyher, E. et al. A generally applicable atomic-charge dependent London dispersion correction. *J. Chem. Phys.* **150**, 154122 (2019).
70. Weigend, F. & Ahlrichs, R. Balanced basis sets of split valence, triple zeta valence and quadruple zeta valence quality for H to Rn: Design and assessment of accuracy. *Phys. Chem. Chem. Phys.* **7**, 3297–3305 (2005).
71. van Lenthe, E., Ehlers, A. & Baerends, E.-J. Geometry optimizations in the zero order regular approximation for relativistic effects. *J. Chem. Phys.* **110**, 8943–8953 (1999).
72. Weigend, F. Accurate Coulomb-fitting basis sets for H to Rn. *Phys. Chem. Chem. Phys.* **8**, 1057–1065 (2006).
73. Helmich-Paris, B., de Souza, B., Neese, F. & Izsák, R. An improved chain of spheres for exchange algorithm. *J. Chem. Phys.* **155**, 104109 (2021).
74. Glendening, E. D. et al. *NBO 7.0* (Theoretical Chemistry Institute, University of Wisconsin, Madison, 2018).
75. Lu, T. & Chen, F. Multiwfn: A multifunctional wavefunction analyzer. *J. Comput. Chem.* **33**, 580–592 (2012).
76. Frisch, M. J. et al. Gaussian 16, Revision C.01 (Gaussian, Inc., Wallingford, CT, 2016).
77. Zhang, J. & Lu, T. Efficient evaluation of electrostatic potential with computerized optimized code. *Phys. Chem. Chem. Phys.* **23**, 20323–20328 (2021).
78. Kartashov, S. V., Shteingolts, S. A., Stash, A. I., Tsirelson, V. G. & Fayzullin, R. R. Electronic and Crystal Packing Effects in Terms of Static and Kinetic Force Field Features: Picolinic Acid *N*-Oxide and Methimazole. *Cryst. Growth Des.* **23**, 1726–1742 (2023).
79. Jelsch, C., Guillot, B., Lagoutte, A. & Lecomte, C. Advances in protein and small-molecule charge-density refinement methods using *MoPro*. *J. Appl. Crystallogr.* **38**, 38–54 (2005).

80. Shteingolts, S. A. et al. On the transfer of theoretical multipole parameters for restoring static electron density and revealing and treating atomic anharmonic motion. Features of chemical bonding in crystals of an isocyanuric acid derivative. *Acta Crystallogr. B* **77**, 871–891 (2021).
81. Stash, A. I. & Tsirelson, V. G. *WinXPRO*, *3DPlot* and *TrajPlot* computer software: new options for orbital-free quantum crystallography studies. *J. Appl. Crystallogr.* **55**, 420–424 (2022).
82. Shteingolts, S. A., Stash, A. I., Tsirelson, V. G. & Fayzullin, R. R. Orbital-Free Quantum Crystallographic View on Noncovalent Bonding: Insights into Hydrogen Bonds, π···π and Reverse Electron Lone Pair···π Interactions. *Chem. Eur. J.* **27**, 7789–7809 (2021).
83. Kirzhnits, D. A. Quantum Corrections to the Thomas–Fermi Equation. *Sov. Phys. JETP* **5**, 64–71 (1957).

Acknowledgements

Funding for this work was provided by the Okinawa Institute of Science and Technology Graduate University (OIST), the Japan Society for the Promotion of Science (22K05134 (S.T.), 19H05621 (K.Sa.)), the German Research Foundation (DFG, GE_3117-1-1 (U.G.)), and the Russian Science Foundation (grant No. 21-73-10191 in part of the quantum topological study (S.V.K. and R.R.F.)). This work was supported by the OIST instrumental analysis and engineering sections.

Author contributions

S.T. designed the study, organized collaborations, synthesized and characterized complexes, conducted cw-EPR and SC-XRD measurements, and prepared VSM samples. J.A. and U.G. conducted DFT calculations for structure optimization study, MO analysis, and chemical topology study. R.R.F. and S.V.K. analyzed SC-XRD data and conducted quantum crystallography and chemical topology studies. H.-B.K. conducted VSM measurements. T.Y. and K.Sa. conducted the EPR study. K.Su. conducted DFT calculations for the EPR study. For the preparation of manuscript, R.R.F. wrote the part describing the quantum topological study, and K.Sa. wrote the part describing the pulse-EPR study. S.T. combined these parts and wrote the original manuscript. S.T., J.A., U.G., R.R.F., K.Sa., and H.-B.K. revised and edited the original manuscript.

Competing interests

The authors declare no competing interests.

Additional information

Supplementary information The online version contains supplementary material available at https://doi.org/10.1038/s41467-023-40557-7.

Correspondence and requests for materials should be addressed to Satoshi Takebayashi, Urs Gellrich or Robert R. Fayzullin.

Peer review information *Nature Communications* thanks Zhong-Ming Sun, and the other, anonymous, reviewer(s) for their contribution to the peer review of this work. A peer review file is available.

7 Zusammenfassung und Schlussfolgerung

NHOs reagieren mit N_2O unter Bildung von SEDs oder Diazoalkenen über einen Additions–Eliminierungs-Mechanismus. Anhand des *gem*-dimethylierten NHOs **5** wurde gezeigt, dass die Reaktion mit N_2O nicht auf unsubstituierte NHOs beschränkt ist. Die C=C-Doppelbindung ist ausreichend polarisiert, um bereits bei Raumtemperatur eine 1,3-dipolare Cycloaddition mit N_2O einzugehen. In einem nächsten Schritt wird ein Diazoalkan durch eine Cycloreversion des Intermediats freigesetzt. DFT-Berechnungen und kinetische Untersuchungen deuten darauf hin, dass die initiale Cycloaddition mit N_2O, gekennzeichnet durch eine stark negative Aktivierungsentropie ($\Delta^{\ddagger}S = -40(1)$ e.u.), geschwindigkeitsbestimmend für die Reaktionssequenz ist.

NHQs mit einem C_6H_4-Linker zwischen einem NHC-Fragment und einer Methylidengruppe erweitern das Repertoire von NHOs und stellen eine neue Verbindungsklasse starker σ-Donoren mit dualer Reaktivität dar. Wie anhand von **1** veranschaulicht, zeichnen sich NHQs bezüglich ihrer geschlossenschaligen Reaktivität durch ihre hohe Basizität und Protonenaffinität aus, die die von herkömmlichen NHOs und NHCs übersteigt. Gleichzeitig weisen sie eine diradikalische Reaktivität auf, die zur dehydrogenativen Kopf–Kopf-Dimerisierung führt, wobei sich über einen offenschaligen Singulett-Reaktionspfad ein SED **2** mit einem Reduktionspotential von $E_{1/2} = -1.71$ V (vs. Fc/Fc^+) bildet. Weitere Merkmale des konjugierten Bis-Chinodimethans **2** sind eine kleine Singulett–Triplett-Lücke von 4.4 kcal mol^{-1} und ein breites Absorptionsmaximum bei $\lambda_{max} = 650$ nm, welches sich über den gesamten sichtbaren Bereich (400−800 nm) erstreckt.

Wird zusätzlich noch ein Akzeptor-Substituent eingeführt, entsteht ein Donor–Akzeptor-substituiertes Chinodimethan. Anhand des *ortho*-Akzeptor-substituierten NHQs **3** wurde gezeigt, dass entgegen der gängigen Regeln zur Formulierung von Lewis-Strukturen die elektronische Struktur am besten als organisches Zwitterion beschrieben ist. Die Kombination aus Aromatizität des Linkers und dessen Donor–Akzeptor-Substitution verursacht Ladungstrennung trotz formaler Konjugation, wie aus Analysen der Strukturparameter im Festkörper (SCXRD), spektroskopischen/elektrochemischen Untersuchungen in Lösung (NMR, UV-vis, CV) und DFT-Berechnungen in der Gasphase hervorgeht. Wie aus $NICS_{ZZ}(r)$-Berechnungen von Derivaten hervorgeht, ist die Polarisation primär ein elektronischer Effekt, der sich durch sterische Einflüsse zusätzlich verstärken lässt. Eine Konsequenz der zwitterionischen Struktur ist die ambiphile Reaktivität als Carbokation/Carbanion-Paar, das sich isolobal zu FLPs verhält. Entsprechend eignet sich **3** zur Dehydrierung von Amminboran und der Addition von Phenylacetylen unter Spaltung der C−H-Bindung, sodass **3** als intramolekulares kohlenstoffbasiertes FLP betrachtet werden kann.

Außerdem konnte in einer theoretischen Arbeit gezeigt werden, dass gängige WFT- und DFT-Protokolle zu einer Überschätzung der Gibbs-Energien für assoziative Reaktionen führen. Dieser sogenannte „Entropie-Fehler“ für bimolekulare Reaktionen resultiert aus einer unzureichenden Behandlung von Entropie-Effekten in Lösung, was zur Überschätzung der Beiträge der Gasphase führt. Davon betroffen sind Aktivierungsbarrieren und vor allem Reaktionsenergien. Ein physikalisch fundierter Formalismus der Entropie in Lösung, der von Garza präsentiert wurde, eignet sich als additive Korrektur für Routineanwendungen ohne erheblichen Rechenaufwand.

8 Danksagung

An dieser Stelle möchte ich all denjenigen danken, die mich auf dem Weg zu dieser Dissertation, unfreiwillig inklusive #JLUoffline und einer Corona-Pandemie, begleitet und unterstützt haben. Herzlich bedanken möchte ich mich bei:

Prof. Dr. Urs Gellrich für die fachlichen Diskussionen und der engagierten Betreuung meiner Doktorarbeit. Ich habe in den Jahren unserer Zusammenarbeit viel gelernt und freue mich auf die nächsten chemischen Herausforderungen.

Prof. Dr. Peter R. Schreiner, PhD für das Anfertigen des Zweitgutachtens und für die Möglichkeit zur Teilnahme an den Arbeitsgruppenseminaren.

allen Mitgliedern der **Gellrich-Gruppe**: **Dr. Max Hasenbeck**, **Dr. Tizian Müller**, **Dr. Sebastian Ahles, Dr. Ravindra Phatake, Dr. Felix Wech, Arthur Averdunk** und **Niklas Koch** Es war mir eine große Freude, mit euch gemeinsam das Labor einzurichten, Nussecken zu essen (danke **Bäcker Braun**), und den Spaß während der unzähligen Stunden am Abzug und an der Glovebox nicht zu verlieren. Danke für die fachlichen Diskussionen, den unterhaltsamen Gesprächen und der abwechslungsreichen Musik (danke **Sebastian** für die Bluetooth-Boxen). Genauso möchte ich mich bei **Dr. Henrik F. König, Michael Kirchner, John G. Liebig, Dietmar König, Maya Ziegler** und **Morena Khajo** für die Zusammenarbeit bedanken. Es war mir eine Freude, euch durch Bachelor- und Master-Projekte zu begleiten.

dem gesamten OC-Institut (**Göttlich-, PRS-** und **Wegner-Gruppe**) und der **Schindler-Gruppe** für das konstruktive Miteinander und der Unterstützung mit Chemikalien/Gerätschaften und sonstigen Gebrauchsmaterialien. Besonderer Dank gilt der **Göttlich-Gruppe** für die Mitnutzung der Kaffee-Küche.

Finn, **Oli**, **Jan**, **Bastian**, **Lucia**, **Nadine**, **Max**, und **Luciano** für die schöne gemeinsame Zeit an der JLU und in Gießen.

Dr. Satoshi Takebayashi und **Dr. Robert R. Fayzullin** für die schöne und andauernde internationale Zusammenarbeit.

Dr. Heike Hausmann, Anika Bernhardt, Inna Klein und **Anja Platt** für Messung unzähliger NMR-Proben und der andauernden Unterstützung, wenn es mal wieder schnell gehen musste, weil meine Probe instabil ist.

Eike Santowski und **Mario Daubner** für die Arbeit in der Chemikalienausgabe, besonders für eure Unterstützung, wenn ich mal wieder ungeduldig war und es schnell gehen sollte.

Anja Beneckenstein für die Arbeit in der Glasbläserei und der Gerätеausgabe.

Dr. Jonathan Becker für den Crash-Kurs in SCXRD-Strukturverfeinerungen und zusammen mit **Dr. Christian Würtele** und **Lisa-Marie Wagner** für die Messung/Auswertung etlicher Kristallstrukturen.

Dr. Dennis Gerbig für die Einführung in die „Computerchemie“ und der Administration der Rechencluster, damit ich mich einzig um die quantenmechanischen Probleme kümmern konnte.

Edgar Reitz dafür, dass jedes IT-Problem umgehend gelöst und jedes defekte Elektrogerät wieder funktionsfähig ist, sobald man anruft. Ein riesiges Dankeschön für die bestmögliche Unterstützung während #JLUoffline zum Erhalt des Forschungsbetriebes.

Michaela Richter, Maurice Monnard und **Annika Jäger** dafür, dass ich mich kaum um bürokratische Angelegenheiten kümmern musste.

der **Aventis Foundation** und dem **Fonds des Verbandes der Chemischen Industrie (VCI)** für die finanzielle Unterstützung in Form des Hoechst Doktorandenstipendiums. Ich bin dankbar für die Unterstützung während #JLUoffline und der Möglichkeit, internationale Konferenzen zu besuchen.

meiner ehemaligen Chemie-Lehrerin **Ina Preis** dafür, dass sie mich als die erste Person für Chemie begeistert hat, obwohl ich Chemie während vorheriger Schuljahre uninteressant fande. Ich war mir sicher, ich würde eines Tages Mathematik oder Informatik studieren, und ich bin froh, dass es Chemie geworden ist.

all meinen **Freunden** und meiner **Familie** dafür, dass sie immer an mich geglaubt haben und in herausfordernden Zeiten mit Kraft und Zuversicht meinen Rücken gestärkt haben. Danke! ♥